



UNIVERSIDAD MICHOACANA DE SAN NICOLÁS DE HIDALGO

INSTITUTO DE INVESTIGACIÓN EN
METALURGIA Y MATERIALES

Effect of Salinity and Overgrinding on the Flotation of Malachite

Tesis para obtener Doctorado en ciencias en metalurgia y ciencias de los
materiales

PRESENTA:
M.C. Zhili Li

ASESOR:
Dr. Feng Rao Wu

COASESOR:
Dr. Shaoxian Song Hu



Morelia, Michoacán, México, Febrero 2019



Instituto de Investigación
en Metalurgia y Materiales

Of. Núm. IIM-ST-010-2019.

Morelia, Mich., Enero 10 del 2019.

M. C. ZHILI LI
Presente

Por medio de la presente, esta dirección del Instituto de Investigación en Metalurgia y Materiales de la Universidad Michoacana de San Nicolás de Hidalgo, tiene a bien informarle que para presentar su examen de grado de Doctor en Ciencias en Metalurgia y Ciencias de los Materiales, con la tesis titulada ***"EFECT OF SALINITY AND OVERGRINDING ON THE FLOTATION OF MALACHITE"***, le ha sido asignada la siguiente mesa sinodal:


1501005-5	DR. FENG RAO WU	(Presidente)
0200161-6	DR. CARLOS ALBERTO LEON PATIÑO	(Vocal)
9900237-0	DR. RAMIRO ESCUDERO GARCIA	(Vocal)
1501007-7	DR. DIANA CHOLICO GONZALEZ	(Vocal)
1501007-3	DR. NOEMÍ ORTIZ LARA	(Vocal)
0400318-7	DR. RICARDO MORALES ESTRELLA	(Suplente)

Agradeciendo de antemano las atenciones que se sirva prestar a la presente, aprovecho para enviarle un cordial saludo.

U. M. S. N. H.

Atentamente


Dr. Alberto Ruíz Marines
Director


Instituto de Investigación
en Metalurgia y Materiales

Instituto de Investigación en Metalurgia y Materiales
Universidad Michoacana de San Nicolás de Hidalgo

ARM/cea

Acknowledgement

The financial supports from the Consejo Nacional de Ciencia y Tecnología (CONACyT) of Mexico under the grant No. 270186, the Natural Science Foundation of Hubei Province of China under the grant No. 2016CFA013 and the Wuhan Science and Technology Bureau of China under the project No. 2016070204020156 are gratefully acknowledged. I would like to thank CONACyT for granting the scholarship NO. 717627 during my PhD study. I appreciate Universidad Michoacana de San Nicolás de Hidalgo (UMSNH) and the Instituto de Investigación en Metalurgia y Materiales (IIMM) providing an enjoyable study and working environment.

Next, I would like to express my sincere gratitude to my advisor Dr. Feng Rao Wu for the continuous support of my Ph.D study and related research, for his patience, motivation, and immense knowledge. His guidance helped me in all the time of research and writing of the thesis. I also want to give my great gratitude to my co-supervisor, Dr. Shaoxian Song. His fund of knowledge and serious attitude in work are worthy of my learning. And he always steers me in the right direction both in my research work and my life.

Besides my advisor, I would like to thank the rest of my thesis committee: Dr. Ramiro Escudero, Dr. Carlos Leon Patiño, Dr. Diana Cholico González, and Dr. Noemi Ortiz, for their insightful comments and encouragement, but also for the hard question which incited me to widen my research from various perspectives. I also want to thank all my friends in IIMM, M.C. Carlos Arreola, Ing. Alma Gallegos, M.C. Qian Wan, M.C. Xing Li, M.C. Xiang Tian. Thanks for your help and support in my work and life. Thanks to all my friends at Wuhan University of Technology.

I would like to thank my family: my parents, my brother and sister for supporting me spiritually throughout my PhD study. Without their support and encouragement, I would not concentrate on my study and research work.

Content

Index of Figures.....	i
Index of Tables.....	v
Abstract.....	vi
Introduction.....	ix
Justification.....	x
Hypothesis.....	x
General Objective.....	x
Goals.....	x
Chapter 1. Literature Review.....	1
1.1. Malachite flotation.....	2
1.2. The effects of salinity on flotation.....	4
1.2.1 Negative effects.....	4
1.2.2 Positive effects.....	6
1.3. Flotation of overground mineral particles.....	7
1.3.1. Difficulties in overground mineral flotation.....	7
1.3.2 Approaches for overground mineral flotation.....	7
Chapter 2. Experimental.....	10
2.1 Research line.....	11
2.2 Materials.....	11
2.3 Reagents.....	14
2.4 Methods.....	15
Chapter 3. Results and Discussion.....	20
3.1. Comparison of adsorption of phenol O-O and N-O chelating collectors at the malachite/water interface in flotation.....	21
3.2. Partially replacing sodium oleate by alcohols of different chain structures in malachite flotation.....	26
3.3 Comminution effect on surface roughness and flotation behavior of malachite surface.....	34
3.4. An example of salinity in flotation: Slime coating of kaolinite on chalcopyrite.....	39
3.5 Reexamining the adsorption of octyl hydroxamate on malachite surface: forms of molecules and anions.....	49
3.6 Effects of the common ions on the adsorption and flotation of malachite with salicylaldehyde.....	58
3.7. The effect of calcium ions in the flotation of malachite with octyl hydroxamate.....	67
3.8 Using octyl hydroxamate as emulsifier of kerosene and collector in the floc flotation of malachite fines.....	75

Chapter 4. Conclusions.....	84
Recommendations for future work.....	86
Reference.....	87
APPENDIX	99
List of Articles Published and Submitted During the P.h.D Study	99

Index of Figures

Figure 2.1. Schematic presentation of the research line.....	11
Figure 2.2. XRD pattern of malachite sample.....	13
Figure 2.3. XRD pattern of chalcopyrite sample.....	13
Figure 2.4. XRD pattern of kaolinite sample.....	14
Figure 2.5. Reagents used in the experiments (a) Salicylaldoxime; (b) Salicylhydroxamic acid; (c) potassium ethyl xanthate; (d) Sodium oleate; (e) Octyl hydroxamate; (f) α -terpineol; (g) MIBC; (h) 2-Ethylhexanol; (i) 1-octanol.....	15
Figure 3.1.1. Effect of salicyl hydroxamate and salicylaldoxime on the zeta potential of malachite as a function of pH.....	21
Figure 3.1.2. The depletion of salicyl hydroxamate and salicylaldoxime in malachite slurry as a function of pH.....	22
Figure 3.1.3. Schematic illustration of the adsorption of salicyl hydroxamate and salicylaldoxime on the malachite surface.....	23
Figure 3.1.4. Intermediate (a) and far (b) Fourier transform infrared (FTIR) spectra of malachite, malachite with salicylaldoxime and salicyl hydroxamate.....	24
Figure 3.1.5. Flotation of malachite as a function of salicylaldoxime and salicyl hydroxamate concentrations.....	25
Figure 3.1.6. Effect of pH on the flotation of malachite with salicylaldoxime and salicyl hydroxamate collectors.....	24
Figure 3.2.1. Malachite flotation with sodium oleate as a function of pH.....	25
Figure 3.2.2. Equilibrium diagram of oleate species as a function of pH in aqueous solution.....	27
Figure 3.2.3. Malachite flotation at different concentrations of sodium oleate and alcohols....	28
Figure 3.2.4. Malachite flotation with sodium oleate and alcohol mixture.....	29
Figure 3.2.5. Micro-flotation of mixed minerals (malachite:calcite=1:1) with sodium oleate alone and 2-ethylhexanol-oleate.....	30
Figure 3.2.6. Contact angle images and results of malachite treated with sodium oleate of different concentrations at pH 9.....	30
Figure 3.2.7. Contact angle results of malachite treated with sole sodium oleate and mixture of sodium oleate and alcohols.....	31
Figure 3.2.8. Zeta potentials of malachite in the presence of various concentrations of sodium oleate, alcohols, and their mixture.....	33
Figure 3.2.9. Schematic presentation of the co-adsorption of sodium oleate and alcohols on malachite surface.....	34
Figure 3.3.1. Profile of malachite surface A: (a) profile height; (b) section analysis.....	35
Figure 3.3.2. Profile of malachite surface B: (a) profile height; (b) section analysis.....	35
Figure 3.3.3. Profile of malachite surface C: (a) profile height; (b) section analysis.....	36
Figure 3.3.4. Contact angle of surface A.....	37
Figure 3.3.5. Wetting state on smooth surface (a) and rough surface (b) with hydrophilic materials (Wenzel model).....	37
Figure 3.3.6. Contact angle of malachite surface A, B, and C after treatment of 5×10^{-5} mol/L sodium oleate at pH 9.....	38
Figure 3.3.7. Wetting state on (a) smooth surface, (b) rough surface (Wenzel model) and (c) rough surface (Cassie model).....	38
Figure 3.3.8. Recovery of malachite ground with quartz and montmorillonite in the presence of	

2×10^{-5} mol/L sodium oleate.....	39
Figure 3.4.1. Flotation of chalcopyrite in tap water with and without kaolinite.....	40
Figure 3.4.2. Sedimentation of chalcopyrite and kaolinite particles in tap water solutions as a function of pH.....	41
Figure 3.4.3. Zeta potential distribution of kaolinite, chalcopyrite and their mixture as a function of pH.....	44
Figure 3.4.4. Flotation of chalcopyrite in seawater without and with kaolinite.....	44
Figure 3.4.5. Sedimentation of chalcopyrite and kaolinite particles in seawater solutions as a function of pH.....	45
Figure 3.4.6. Flotation of chalcopyrite in gypsum saturated water with and without kaolinite.....	46
Figure 3.4.7. Sedimentation of chalcopyrite and kaolinite particles in gypsum saturated solutions as a function of pH.....	47
Figure 3.4.8. SEM images of a chalcopyrite particle (a), concentrate (b), and tailing (c) in chalcopyrite flotation in tap water with 0.24 wt% of kaolinite.....	48
Figure 3.5.1. Depletion amount of K-octyl hydroxamate as a function of pH at concentration of 4×10^{-4} mol/L.....	50
Figure 3.5.2. Logarithmic diagram of K-octyl hydroxamate hydrolysis components.....	50
Figure 3.5.3. Solubility diagram of malachite showing the logarithmic concentration distribution of copper and carbonate species as a function of pH, in equilibrium with the atmosphere (activity of CO_2 (g) equal to $1 \times 10^{-3.5}$ atm).....	51
Figure 3.5.4. Adsorption isotherm of K-octyl hydroxamate on malachite at pH 9 (ambient temperature).....	51
Figure 3.5.5. Zeta potential of malachite as function of pH in the presence and absence of octyl hydroxamate. The zeta potential of copper hydroxamate precipitates is also shown.....	52
Figure 3.5.6. The XPS survey spectra of malachite (a), synthesized copper hydroxamate precipitates (b), and malachite conditioned with octyl hydroxamate at pH 7 (c) and 9 (d).....	53
Figure 3.5.7. High-resolution XPS Cu $2p_{3/2}$ spectra of malachite (a), synthesized copper hydroxamate precipitates (b), malachite after conditioning with octyl hydroxamate at pH 7 (c), and 9 (d).....	54
Figure 3.5.8. High-resolution XPS N 1s spectra of potassium octyl hydroxamate (a), synthesized copper hydroxamate precipitates (b), and malachite after conditioning with octyl hydroxamate at pH 7 (c) and 9 (d).....	55
Figure 3.5.9. Proposed interaction model of K-octyl hydroxamate with malachite.....	56
Figure 3.5.10. Flotation recovery of malachite as a function of pH at different concentration of K-octyl hydroxamate.....	57
Figure 3.6.1. Solubility of malachite and logarithmic concentration distribution of copper and carbonate species as a function of pH, in equilibrium with the atmosphere (activity of CO_2 (g) equal to $1 \times 10^{-3.5}$ atm).....	59
Figure 3.6.2. Solubility of malachite as a function of pH in aqueous solutions containing 0, 1×10^{-4} mol/L, and 1×10^{-3} mol/L Na_2CO_3	59
Figure 3.6.3. Flotation recovery of malachite with salicylaldehyde as a function of pH; malachite was previously conditioned in the presence and absence of sodium carbonate.....	60
Figure 3.6.4. Recovery of malachite conditioned under different Na_2CO_3 concentrations with 1×10^{-3} mol/L salicylaldehyde at pH 8.....	61

Figure 3.6.5. Zeta potential of malachite and malachite conditioned with different concentration of salicylaldoxime. The zeta potential of synthesized copper salicylaldoxime is also shown.....	62
Figure 3.6.6. Infrared spectra of malachite (a), salicylaldoxime (b), synthesized copper salicylaldoxime (c), and malachite conditioned with salicylaldoxime at pH 8 (d).....	63
Figure 3.6.7. The XPS survey spectra of malachite (a), copper-salicylaldoxime precipitates (b), and malachite conditioned with salicylaldoxime (c).....	63
Figure 3.6.8. High-resolution XPS Cu 2p _{3/2} spectra of malachite (a), synthesized copper salicylaldoxime (b), and malachite after conditioning with salicylaldoxime (c).....	64
Figure 3.6.9. High-resolution XPS O 1s spectra of salicylaldoxime (a), copper salicylaldoxime (b), and malachite conditioned with salicylaldoxime (c).....	65
Figure 3.6.10. High-resolution XPS N 1s spectra of salicylaldoxime (a), synthesized copper salicylaldoxime (b), and malachite after conditioning with salicylaldoxime (c).....	66
Figure 3.6.11. A schematic presentation of interaction between salicylaldoxime and malachite surface.....	67
Figure 3.7.1. Flotation recovery of malachite at different CaCl ₂ concentrations at pH 9....	67
Figure 3.7.2. Flotation recovery of malachite as a function of pH in the presence and absence of 1×10 ⁻² mol/L CaCl ₂	68
Figure 3.7.3. Zeta potential of malachite at different CaCl ₂ concentrations.....	69
Figure 3.7.4. Calculations of the concentration of each calcium species as a function of pH at a total calcium concentration of 1×10 ⁻² mol/L.....	70
Figure 3.7.5. Zeta potential of malachite in the presence of CaCl ₂ or/and hydroxamate.....	71
Figure 3.7.6. Adsorption of octyl hydroxamate in the presence of different concentration of CaCl ₂	71
Figure 3.7.7. Contact angle of malachite in the presence and absence of 1×10 ⁻² mol/L CaCl ₂ with the addition of 8×10 ⁻⁴ mol/L octyl hydroxamate at pH 9.....	72
Figure 3.7.8. Images of malachite suspension after 15 s settling with the addition of different reagents at pH 9, (a) no reagent addition, (b) 8×10 ⁻⁴ mol/L octyl hydroxamate, (c) 1×10 ⁻² mol/L CaCl ₂ and 8×10 ⁻⁴ mol/L octyl hydroxamate.....	73
Figure 3.7.9. Malachite particle size distribution with the addition of different reagents at pH 9.....	73
Figure 3.7.10. The schematic diagrams of the influence of calcium on malachite fines flotation with the addition of octyl hydroxamate at pH 9.....	75
Figure 3.8.1. Flotation recovery of malachite with the addition of two kinds of kerosene emulsions as a function of octyl hydroxamate concentration.....	76
Figure 3.8.2. Flotation recovery of malachite with the addition of two kinds of kerosene emulsions as a function of kerosene dosage.....	77
Figure 3.8.3. Optical microscopy images of the kerosene emulsions prepared by ultrasonic processor (a) without the addition of octyl hydroxamate (b) with the addition of 0.05 wt% octyl hydroxamate.....	77
Figure 3.8.4. Spreading of kerosene droplets on malachite surface measured with the captive bubble method.....	78
Figure 3.8.5. Optical microscopy images of the malachite aggregates (a) with the addition of kerosene emulsion; (b) with addition of 0.05 wt% octyl hydroxamate treated kerosene emulsion.....	79
Figure 3.8.6. Zeta potential of malachite in the presence and absence of 2×10 ⁻⁴ mol/L octyl	

hydroxamate.....79

Figure 3.8.7. Zeta potential of kerosene emulsion and 0.05 wt% octyl hydroxamate treated kerosene emulsion.....80

Figure 3.8.8. The interaction energy between malachite particles and emulsified kerosene droplets as a function of separation distance, malachite radius: 2.10 μm and kerosene radius: 1.07 μm82

Figure 3.8.9. The interaction energy between malachite particles and 0.05 wt% octyl hydroxamate treated kerosene droplets as a function of separation distance, malachite radius: 2.10 μm and kerosene radius: 0.27 μm83

Figure 3.8.10. Schematic representation of enhancement of kerosene spreading on malachite surface by using octyl hydroxamate as an emulsifier.....83

Index of Tables

Table 3.3.1. Roughness parameters of surfaces.....	36
Table 3.3.2. Specific surface area of malachite.....	39
Table 3.5.1. Atomic concentration of N, O, and Cu in malachite, copper hydroxamate precipitate, and malachite conditioned with octyl hydroxamate at pH 7 and 9.....	54
Table 3.6.1. Atomic concentration of C, N, O, and Cu in malachite, copper salicylaldoxime precipitate, and malachite conditioned with salicylaldoxime at pH 8.....	65

Abstract

In the present work, the effects of salinity and overgrinding on the flotation of malachite were investigated. First, malachite flotation behaviors were studied with different collectors, namely, salicylaldehyde, salicylhydroxamic acid, sodium oleate, combination of sodium oleate and alcohols, and octyl hydroxamate. Then, the comminution effect on the flotation of malachite was studied and an example of salinity flotation was given. After that, the flotation behavior of malachite fines in the presence of CO_3^{2-} , OH^- , and Ca^{2+} was studied. Finally, the floc flotation of overground malachite was investigated.

In these experiments, micro-flotation tests were performed to assess the flotation performance. Zeta potential measurements were used to get the qualitative adsorption information of collectors and ions on malachite surface as well as to study the aggregation of particles. Adsorption tests were conducted to acquire the quantitative adsorption information of collectors and ions on malachite surface. Contact angle measurements were utilized to quantify the hydrophobicity of malachite in the presence and absence of different reagents. Fourier-transform infrared spectroscopy (FTIR) and X-ray photoelectron spectroscopy (XPS) were employed to identify the chemicals formed after the adsorption of collectors. Flotation solution calculation analyses were used to explain the flotation results under different conditions. BET was used to measure the specific area of malachite particles. Surface topography was used to characterize the surface roughness of malachite.

Through studying malachite flotation behavior with different collectors, it is concluded that 1) salicylaldehyde and salicylhydroxamic acid are of molecular structures that resemble each other, but with different bond distances in the ligand atoms which result in their unusual adsorption behavior and collecting ability; 2) by partially replacing sodium oleate with alcohols, the selectivity of malachite flotation can be increased with high flotation recovery; 3) octyl hydroxamate functions differently in different pH range in malachite flotation. Through investigating comminution effect on malachite flotation, it is found that grinding media can influence minerals surface roughness, thus affecting the wettability of their surface and, consequently, the flotation performance. Through an example of salinity flotation, it is concluded that salinity in seawater and gypsum-saturated water compressed the electrical double layers and resulted in extensive slime coating of kaolinite on chalcopyrite and the phenomenon is more evident in alkaline pH range. Through investigation of malachite flotation in the presence of ions, it is found that calcium adsorbed onto malachite surface in the form of $\text{Ca}(\text{OH})^+$ and the adsorption of $\text{Ca}(\text{OH})^+$ promoted the aggregation of malachite fines and lowered the energy barrier between bubbles and malachite particles, resulting in increased malachite flotation recovery. Through studying the floc flotation of malachite, it is found that with the addition of octyl hydroxamate in the emulsification process, kerosene droplets were smaller and much uniform in size, and the kerosene droplets spread more readily on malachite surface, resulting in higher coverage of kerosene on malachite surface, and therefore, enhanced hydrophobic aggregation and malachite flotation recovery.

Keywords: Malachite flotation; Chelating reagent; Adsorption; Aggregation; Salinity; Overgrinding; Slime coating.

Resumen

En el presente trabajo, los efectos de la salinidad y sobremolienda en la flotación de malaquita fueron investigados. En primer lugar, el comportamiento de la flotación de malaquita fue estudiado con diferentes colectores, los cuales fueron: salicilaldoxima, salicilhidroxámico, oleato de sodio, combinación de oleato de sodio y alcoholes, y octil hidroxamato. Posteriormente, el efecto de la pulverización en la flotación de malaquita fue estudiado y se realizó ejemplo de flotación salina. Después de eso, se estudió el comportamiento de la flotación de malaquita en presencia de CO_3^{2-} , OH^- y Ca^{2+} . Finalmente, se investigó la floc flotación superficial de malaquita.

En estos experimentos, se realizaron pruebas de microflotación para evaluar el desempeño de la flotación. Se realizaron mediciones de potencial Z para obtener información de la adsorción cualitativa de los colectores y los iones en la superficie de la malaquita, así como estudiar la aglomeración de partículas. Se condujeron pruebas de adsorción para obtener información de la adsorción cuantitativa de los colectores y los iones en la superficie de la malaquita. Se utilizaron mediciones de ángulo de contacto para cuantificar la hidrofobicidad de la malaquita en presencia y ausencia de los diferentes reactivos. Se emplearon la espectroscopía infrarroja por transformada de Fourier (FTIR) y la espectroscopía fotoelectrónica de rayos X (XPS) para identificar los compuestos químicos formados después de la adsorción de los colectores. Se usaron cálculo análisis de la solución de flotación para explicar los resultados de la flotación bajo diferentes condiciones. BET fue usado para medir el área específica de las partículas de malaquita. La topografía superficial se utilizó para caracterizar la rugosidad superficial de la malaquita.

A través del estudio del comportamiento de la malaquita durante la flotación con diferentes colectores, se ha que concluido que 1) Tanto la salicilaldoxima como el salicilhidroxámico tienen estructuras moleculares semejantes, pero con diferentes distancias de enlace en los átomos del ligando, lo que resulta en su inusual comportamiento de adsorción y habilidad de colección, 2) al reemplazar parcialmente el oleato de sodio con alcoholes, la selectividad de la flotación de malaquita puede ser incrementada con una alta recuperación por flotación, 3) las funciones del octil hidroxamato son diferentes a distinto rango de pH en la flotación de malaquita. Investigando el efecto de la pulverización en la flotación de malaquita, se encontró que el medio de molienda puede influenciar la rugosidad superficial del mineral, afectando así la mojabilidad de su superficie y, por consecuencia, el desempeño de la flotación. A través de un ejemplo de flotación salina, se concluye que la salinidad del agua de mar y agua saturada de yeso comprime la doble capa eléctrica y resulta en un revestimiento fino de caolinita sobre calcopirita y el fenómeno es más evidente a un rango de pH alcalino. A través de la investigación de la flotación de malaquita en presencia de iones, se encontró que el calcio se adsorbe en la superficie de la malaquita en la forma de $\text{Ca}(\text{OH})^+$ y la adsorción de $\text{Ca}(\text{OH})^+$ promueve la agregación de finos de malaquita y baja la barrera de energía entre burbujas y partículas de ésta, resultando en un incremento en la recuperación por flotación. A través del estudio de floc flotación de malaquita, se encontró que con la adición de octil hidroxamato en el proceso de emulsificación, las gotas de queroseno son más pequeñas y con un tamaño más uniforme, y también se esparcen más rápidamente en la superficie de la malaquita, resultando en un alto recubrimiento de queroseno en la superficie de la malaquita y, por lo tanto, una aglomeración hidrofóbica mejorada al igual que la recuperación por flotación de la malaquita.

Palabras clave: Flotación de Malaquita, Reactivo Quelante, Adsorción, Aglomeración, Salinidad, Sobremolienda, Revestimiento Fino.

Introduction

Copper is one of the indispensable non-ferrous metals in modern society. The majority of copper is extracted from copper sulfide minerals, however, copper oxide minerals do account for a significant portion of copper production (Marion et al., 2017). L-SX-EW (leaching-solvent extraction-electrowinning) and flotation are two commercial approaches for processing copper oxide ores (Lee et al., 1998). For the copper oxide ores with low copper content or high basic gangue such as carbonate minerals, froth flotation becomes the most economic method for concentration and recovery of copper.

Since it is hard to control the sulfidization process, direct flotation of malachite has attracted increasingly interest. In direct flotation, much work so far has focused on the performance and adsorption mechanisms of collectors. For example, fatty acids, fatty amines, hydroxamate acid, phosphinic acids were used as collectors in malachite direct flotation. However, there are relatively few studies devoted to effects of salinity and overgrinding on the direct flotation of malachite.

Malachite, a sparingly soluble mineral, coupled with its gangue mineral, calcite, dissolves a plenty of ions into the flotation pulp. These ions affect the surface chemistry of malachite, and therefore, their flotation performance. Concerning the influence of ions on minerals flotation, some positive effects are the formation of smaller stable bubbles, compressing of the electrical double layer of minerals, activation and beneficial coagulation. Oppositely, negative effects can be the formation of metal hydroxides precipitates barriers, inadvertent activation, heterocoagulation, consumption of flotation reagents, etc.

Since malachite is a relatively soft mineral, with the Moh's hardness of 3.5-4 (Petrov et al., 2013), fines are easy to be produced in the grinding process due to overgrinding. Froth flotation poorly responds to fine mineral particles mainly due to that the collision efficiencies of fine particles with bubbles are low because of their low momentum in the flotation pulp, resulting in a low rate of flotation recovery (Sivamohan, 1990). In order to enhance the collision and attachment efficiency of particles and bubbles in the flotation of fine minerals, two main methods, namely increasing the apparent sizes of the fine particles, and decreasing the sizes of the collecting bubbles, have been utilized (Ahmadi et al., 2014; Li et al., 2017a; Song et al., 2000). Hydrophobic agglomeration is one of the effective methods to increase the apparent sizes of the fine particles, which can be used before flotation to improve the beneficiation of valuable minerals in fine particle size (Song et al., 2001a; Song et al., 2012). Floc-flotation has been widely investigated in mineral processing, including floc-flotation of galena (Song et al., 2001a; Song et al., 2000), sphalerite (Song et al., 2001a; Song et al., 2001b), molybdenite (Song et al., 2012; Yang et al., 2015), coal (Liang et al., 2016; Song and Valdivieso, 1998), hematite (Li et al., 2018a; Pascoe and Doherty, 1997; Shibata and Fuerstenau, 2003), apatite (Yang et al., 2018), and scheelite (Chen et al., 2017b).

In the current thesis work, we investigated the effect of salinity on malachite flotation to provide more fundamental theory in the beneficiation of malachite. Floc-flotation of malachite was studied to efficiently recover the malachite fines caused by overgrinding.

Justification

With the depletion of sulfide copper minerals, processing of oxide minerals, especially malachite, has attracted increasing interest. Flotation is the most effective method to process malachite. In the direct flotation of malachite, collectors play a vital role, which can affect the flotation recovery and selectivity greatly. Thus, the flotation behaviors of different collectors were studied.

In the flotation of malachite, a lot of ions dissolve into the solution, which can significantly influence the flotation behavior. Different ions at different condition may have different effect on the flotation. Therefore, flotation in the presence of ions was studied to efficiently recover malachite particles in saline water.

Malachite is a soft mineral, which can be readily overground to fines. It has long been established that fine particles ($<10\ \mu\text{m}$) exhibit low flotation rate and recovery (Trahar and Warren, 1976), while the best flotation rate and recovery occur in the 10-100 μm particle size range for base metal minerals (Sutherland and Wark, 1955). The low flotation rate and recovery have been attributed to the low bubble-particle collision efficiency (Gaudin, 1957; Sutherland, 1948). Fine particles follow the streamlines around the bubbles due to their small inertial force and do not collide with the bubbles using conventional flotation machines. Hydrophobic agglomeration is one of the effective methods to increase the apparent sizes of the fine particles, which can be used before flotation to improve the beneficiation of valuable minerals in fine particle size (Song et al., 2001b; Song et al., 2012). No investigation has conducted concerning floc-flotation of malachite in the literature. Thus, in the present study, floc-flotation of malachite was investigated to efficiently recover the malachite fines.

Hypothesis

In this thesis work, I hypothesize that through studying flotation behavior of different collectors, and the effect of salinity and overgrinding in malachite surface, the malachite can be beneficiated efficiently by altering the reagent scheme and flotation conditions.

General Objective

I attempted to recover malachite efficiently through investigating the flotation behavior of different collectors, and the effects of salinity and overgrinding on malachite flotation.

Goals

- 1) To comparison of adsorption of phenol O-O and N-O chelating collectors at the malachite/water interface in flotation.
- 2) To use combination of alcohols of different chain structures and sodium oleate as collector in malachite flotation.
- 3) To study the effect of grinding media on malachite roughness and flotation behavior.
- 4) To study the effect of salinity on flotation.

- 5) To study the adsorption of octyl hydroxamate on malachite surface.
- 6) To study the effects of the common ions on the adsorption and flotation of malachite.
- 7) To study the effects of calcium ion on the flotation of malachite fines with octyl hydroxamate.
- 8) To use octyl hydroxamate as emulsifier of kerosene and collector in the floc flotation of malachite fines.

Chapter 1. Literature Review

1.1. Malachite flotation

The traditional leaching-SX/EW (solvent extraction and electro winning) technique for treatment of low-grade copper oxide ores also exists evident shortcomings such as long processing cycle, high acid consumption and high extractant cost (Bartos, 2002; Kordosky, 2002). Thus, flotation is widely used in the beneficiation of malachite. However, Oxide copper ores (e.g., malachite) respond poorly to traditional sulfide copper (e.g., thiol) collectors in flotation because of their more hydrophilic oxide surfaces (Miller et al., 2007). In practices, controlled potential sulfidization, prior to the addition of thiol collectors, has been applied to overcome this problem (Castro et al., 1974; Zhou and Chander, 1993), but it is problematic in controlling accuracy, especially for the mixture of sulfide and oxide copper ores, because a slight excess of sulfidizing reagents in the pulp depresses the flotation but an insufficient amount produces poor recoveries (Barbaro et al., 1997). Compared with leaching-SX/EW technique or sulfidation flotation process, the direct flotation recovery of copper oxide minerals might be an attractive and economic approach and has been extensively investigated in the recent decades. Fatty acids, fatty amines, petroleum sulfonates, phosphinic acids and hydroxamic acids have been used as flotation collectors for direct recovery of copper oxide minerals without sulfidation treatment.

Fatty acids dominate non-sulfide flotation because of their low cost and effectiveness, which can be considered to be almost universal collectors because they can be used to float almost all minerals (Miller et al., 2007). Therefore, they are inherently nonselective, and the use of appropriate modifiers alleviates this problem somewhat and allows even difficult mineral separations. Although fatty acids, powerful collectors for malachite flotation, chemisorb at the malachite surface, the intrinsic lack of selectivity has limited their usage, especially in the presence of carbonaceous and dolomitic gangue minerals, and therefore, they are mainly used for the recovery of malachite from siliceous ores (Deng and Chen, 1991).

Primary fatty amines and ether amines constitute the bulk of cationic collector usage in the industry, essentially for silica, silicates, and potash. Amine collectors adsorb at mineral surface through electrostatic interaction. Malachite floats readily in alkaline pulps under laboratory conditions with the addition of amine collector (Bulatovic, 2010), but they also unselectively adsorb onto both malachite and gangue mineral surfaces owing to the fact that most of the gangue minerals in typical malachite ores are also negatively charged above the isoelectric point (IEP) of malachite (i.e., pH 9).

Chelating collectors are considered to be promising collectors for the direct flotation of non-sulfide minerals as they are capable of selectively complexing metal ions under certain solution chemistry conditions. In the flotation of chrysocolla minerals with a new synthetic reagent containing a mixed aliphatic-aromatic structure, the flotation is optimum in the narrow pH range of 5.5 to 6, the disappearance of the S-H peak of this collector due to the saline bond with Cu and appearance of C-N and N-H peaks shifted toward lower frequencies due to a coordinative bond of nitrogen with metal in IR spectra indicate that this collector reacts with copper ion and forms chelates on the mineral surface (Barbaro et al., 1997). In an investigation studying the adsorption of a new synthetic chelating collector, K-MBY, on cerussite, the XPS analysis indicates that Pb links to the thiazole ring probably via a coordination bond to the nitrogen and the nearest sulphur atoms (Cozza et al., 1992).

In literatures, there are investigations focusing on the chelating collectors used in malachite flotation. Li et al. (2015) studied the flotation behavior and adsorption mechanism of α -hydroxyoctyl phosphinic acid to malachite, concluding that this collector exhibited superior collecting performances to direct flotation recovery of malachite and floated out above 80% malachite at pH 5-10. In the adsorption process, Cu(II) species was partly reduced to Cu(I) species during collector chemisorption on the malachite surface, accompanying P(III) oxidation to P(V) species of the collector. Liu et al. (2016) investigated the flotation of malachite using 3-hexyl-4-amino-1,2,4-triazole-5-thione as collector. They found that this collector exhibited a superior flotation performance to malachite in the pH range 7-10 and this collector chemisorb on malachite surfaces by formation of Cu-S and Cu-N bonds with the breakage of S-H bond in the molecule. Oprea et al. (2004) studied the flotation of malachite using 8-hydroxyquinoline and salicylaldehyde as collectors. They found that copper flotation recovery of 90% can be reached and these collectors showed good selectivity in separation malachite from quartz but less selectivity in separation malachite from calcite. In addition, through FTIR analyses, they attribute the flotation of malachite to the formation of Cu(II) oxinate and Cu(II) salicylaldehyde on its surface. Liu et al. (2018) evaluated the flotation performance S-[(2-hydroxyamino)-2-oxoethyl]-N,N-dibutyldithiocarbamate to malachite. They found that this reagent was an excellent collector for malachite flotation and exhibited favorable selectivity for flotation separation of malachite from quartz or calcite under pH 8.5-10.3. Zeta potential and FTIR implied that HABTC might bond with the surface copper atoms of malachite, with releasing the H^+ ions of its hydroxamate group into pulp. ToF-SIMS provided clear evidences that the Cu-hydroxamate and Cu-dithiocarbamate groups were formed on malachite surfaces after HABTC adsorption. XPS revealed that Cu(I)/Cu(II) mixed-valence surface complexes of HABTC anchored on malachite through formation of Cu(I)AS and Cu(II)AO bonds, accompanying with reduction of partial surface Cu(II) to Cu(I).

The use of alkyl, aryl, or alkylaryl hydroxamates in the flotation of minerals that chelate with hydroxamate is also known in the industry. Hydroxamates are powerful collectors in flotation due to their ability to selectively chelate at the surfaces of minerals that contain titanium, yttrium, lanthanum, cerium, niobium, tantalum, tin, iron, manganese, and copper.

In the flotation of cassiterite with benzohydroxamic acid (BHA), separation of cassiterite-quartz mixture was readily achieved, while the separation of cassiterite-calcite mixture could be reached with the addition of sodium hexametaphosphate as depressant; through zeta potential and infrared spectra studies, it was concluded that this collector chemisorbs onto cassiterite surface by forming Sn-BHA compounds rather than electrostatic attraction (Wu and Zhu, 2006). In the flotation of rutile with nonyl hydroxamic acid, chemical adsorption is identified on the surface of rutile, where a chelate of O,O-five-membered rings with Ti^{4+} on the surface of rutile may form; through adsorption measurements, zeta potential test, IR spectrum analyses, and solution chemistry calculations, it was found that the adsorption involves both physical and chemical adsorption, and chemical adsorption plays predominant role (Wang et al., 2016). In the flotation of pyrochlore from calcite with octyl hydroxamic acid, XPS, adsorption density and ToF-SIMS measurements were performed, showing that octyl hydroxamic acid physically adsorbs on calcite surface since a slight shift of the binding energies of the Ca 2p electrons (0.19 eV) on calcite after OHA treatment but the N 1s binding energy spectrum of OHA did not change; octyl hydroxamic acid adsorbed on pyrochlore surface by both physisorption and chemisorption due to the fact that, after treatment of octyl hydroxamic acid on pyrochlore, the binding energies of both Nb 3d and

Ca 2p electrons shifted (0.24 and 0.35 eV, respectively), and the N 1s electron binding energy peak of OHA split from 400.3 eV to 400.7 and 398.5 eV, representing the neutral RNHOH and the ionized RNHO⁻ groups (Ni and Liu, 2012). In the flotation of ilmenite with 2-ethyl-2-hexenoic hydroxamic acid, this collector exhibits superior flotation performance compared to isooctyl hydroxamic acid and octyl hydroxamic acid through both chemisorption and physisorption; this collector was assumed to chelate both Fe and Ti species on ilmenite surfaces by forming five-membered chelates (Xu et al., 2015). In the flotation of wolframite, both octyl hydroxamic anions and acid molecules are chemically adsorbed at the mineral surface, substituting the surface OH⁻ and WO₄²⁻, and complexing with the ferrous/manganous sites to form metal hydroxamate precipitates (Hu et al., 1997). In the flotation of manganese dioxide and cassiterite, the active adsorbing species was reported to be hydroxamic acid molecules, which interact with the metal atom sites on the mineral surface, displacing surface hydroxyls to form the metal hydroxamate (Natarajan and Fuerstenau, 1983; Sreenivas and Padmanabhan, 2002). In the case of the flotation of malachite by octyl hydroxamate, Lenormand et al. (1979) studied the flotation of malachite with octyl hydroxamate, reporting that the hydroxamate flotation of malachite is effective between pH 6 and 10, a region in which HCO₃⁻ and CuOH⁺ ions are the predominant potential determining ions for malachite. They proposed a chemisorption mechanism that a pair of HCO₃⁻ and CuOH⁺ ions on the malachite surface is displaced for each hydroxamate ion adsorbed. Hope et al. (2010 and 2012) found that cupric hydroxamate is formed on the malachite surface after conditioning with alkyl hydroxamate. Marion et al. (2017) stated that the CuOH⁺ ions have a larger effect than HCO₃⁻ ions in the malachite flotation behavior.

1.2. The effects of salinity on flotation

Salinity can either be caused by dissolving of minerals into slurry, recycling of water in flotation plant, or using of sea water in flotation. It introduces ions in the flotation slurry and, as a consequence, negatively or positively affects the flotation behavior.

1.2.1 Negative effects

1.2.1.1 Reduction in particle surface hydrophobicity by metal ions

Metal ions hydrolyze in alkaline pH solutions and precipitate as hydrophilic metal hydroxides, sulfates or carbonates if their concentrations are above their respective solubility limits (Fuerstenau et al., 1985). Formation of metal hydroxides is influenced by aqueous pH (Font et al., 1999). Precipitation of these hydrophilic metal hydroxides on mineral surfaces has been generally described as indiscriminate, resulting in formation of a hydrophilic barrier to collector adsorption on mineral surfaces (Fornasiero and Ralston, 2006; Senior and Trahar, 1991). The reduction in mineral surface hydrophobicity due to the precipitation of hydrophilic metal hydroxides could compromise the efficiency of the particle–bubble attachment sub-process (Koh and Warren, 1980; Schwarz and Grano, 2005). It can also cause lower contents of mineral particles entering the froth, which might compromise the efficiency of the sub-process of formation of stable particle–bubble aggregates (Ali et al., 2000; Ata, 2012; Johansson and Pugh, 1992; Moolman et al., 1996). The presence of dissolved ions in water can also change the stability of particle–bubble aggregates in the froth phase (Farrokhpay and Zanin, 2012).

1.2.1.2 Change in particle surface charge by metal ions

Metal ions in flotation water can alter the surface charge of particles and consequently affect interactions between particles and waste gangue or between particles and collectors. This could affect particle–bubble attachment and also formation of stable particle–bubble aggregates. Investigations have been carried out on the role of calcium ions in modulating the surface properties of molybdenite and in controlling the interaction between molybdenite and the most predominant gangue mineral, namely quartz, in copper porphyries. The results show that the floatability of fine molybdenite particles is significantly reduced when calcium ions and silica coexist in the flotation pulp. This is because the adsorption of calcium ions on molybdenite and quartz reduces the magnitude of negative surface charges and thus causes heterocoagulation of molybdenite and quartz (Raghavan and Hsu, 1984).

1.2.1.3 Inadvertent activation of unwanted minerals by metal ions

Some metal ions can also inadvertently activate unwanted minerals, thus affecting flotation selectivity in varying degrees. For example, metal ions such as lead, silver and iron are present in flotation water as impurities and can inadvertently activate sphalerite surfaces (Chandra and Gerson, 2009; Finkelstein, 1997). The undesirable activation by metal ions, copper (II), iron (II) and calcium (II), causes pyrite to float together with sphalerite in sphalerite flotation circuits, leading to poor selectivity (Boulton et al., 2003; Zhang et al., 1997). Inadvertent activation of sphalerite and pyrite by copper ions in water leads to a low copper grade in copper flotation circuits (Rao and Finch, 1989). Copper (I) cyanide could activate sphalerite in flotation of lead–zinc sulfide ore reducing lead grade (Seke and Pistorius, 2006).

1.2.1.4 Slime coating on mineral surfaces

The formation of a slime coating on valuable mineral surfaces can lead to depression of flotation of valuable minerals. For example, positively charged serpentine gangue minerals, such as chrysotile and lizardite, has been found to severely reduce the flotation of negatively charged (unoxidized) pentlandite by forming a hydrophilic slime coating on pentlandite surfaces (Edwards et al., 1980). The coverage of colloidal iron oxide (hematite) slimes originating from the steel grinding media, iron sulfide minerals and non-sulfide gangue, on galena surfaces can reduce the mineral surface hydrophobicity and therefore have a significant depressing effect on the flotation of galena particles (Bandini et al., 2001). The slime coating of montmorillonite clay on coal is detrimental to coal flotation (Xu et al., 2003).

1.2.1.5 Interactions with flotation reagents

Like metal cations, anions may also have a negative effect on flotation performance by interacting with flotation reagents. For example, anions in treated effluent have been identified as having a negative effect on copper and molybdenum recoveries (Fisher, 1976). Sulfide ions have been found to decompose xanthate collector in the presence of oxygen (Shen et al., 2001). Under solution conditions which favor rapid xanthate decomposition by sulfite, xanthate adsorption onto galena is significantly reduced and galena flotation strongly depressed (Grano et al., 1997). Salts in water are particularly liable to react with fatty acid reagents and form insoluble complexes (Ozkan and Acar, 2004). Calcium ions react with the collector used in apatite flotation, thus reducing its concentration for flotation, leading to a decline in apatite recovery (dos Santos et al., 2010).

1.2.2 Positive effects

1.2.2.1 Compression of electrical double layer

The presence of electrolytes can improve particle-particle interaction or particle–bubble attachment efficiency through compressing the electrical double layer and thus reducing the electrostatic repulsion between particles and bubbles (Kurniawan et al., 2011). Investigation of oil agglomeration of coal in inorganic salt solutions shows that coal recovery increases markedly as salt concentration (NaCl) is raised (Yang et al., 1988). Coal recovery is improved by using saline water due to the enhanced aggregation of coal particles (Ofori et al., 2005; Wang and Peng, 2013). Flotation of methylated quartz is improved with increasing KCl concentration (Laskowski and Kitchener, 1969). The efficiency of the attachment of methylated quartz particles to nitrogen bubbles has been found to increase with the increase in KCl electrolyte concentration (Dai et al., 1999). Flotation improvement in the presence of electrolytes is explained by the compression of the electrical double layer by electrolytes, thus reducing electrical repulsion and subsequently facilitating the particle–bubble attachment process. The reduction in electrostatic repulsion between particles or between particle and bubbles may in turn decrease the adsorption of positively charged hydrophilic slimes such as magnesium silicates and thus increase bubble–particle attachment (Bremmell et al., 2005; Hewitt et al., 1994; Morris et al., 1995).

1.2.2.2 Formation of smaller bubbles

Electrolytes are favorable to the formation of smaller stable bubbles due to the influence of the electrolytes on surface tension and gas solubility (Pugh et al., 1997). Smaller bubbles increase the particle–bubble collision probability (Bournival et al., 2012; Pugh et al., 1997), and also improve particle–bubble attachment efficiencies (Hewitt et al., 1994). Finer gas bubbles in high salt concentrations may result in reduced reagent consumption (Quinn et al., 2007). However, it is noteworthy to mention that along with the benefits discussed above, an increase in ionic strength can cause a negative effect by enhancing frothability and therefore increasing gangue recovery (Manono et al., 2012, 2013).

1.2.2.3 Activation of valuable minerals

Some cations activate certain minerals since the cation species adsorb/react with the mineral surface, leading to higher adsorption of collector. For example, sphalerite is activated by calcium and lead ions when xanthate is used as collector (Dávila-Pulido et al., 2015; Trahar et al., 1997). Li et al. (2016) reported the activation of Pb^{2+} in the flotation of rutile with salicyl hydroxamic acid (SHA). The formation of Ti-O-Pb^+ complex at rutile surface was identified as the reason for the improved adsorption of SHA.

With respect to the effects of ions on the direct flotation of malachite, the literature is limited. Choi et al. (2016) investigated the influence of salt solutions on the flotation behavior of synthetic malachite using a sodium oleate as a collector. They found that the floatability of oleate ions-adsorbed synthetic malachite monotonically increases with an increase in the overall ionic strength (IS) range (1–1000 mM) of the monovalent cation (Na^+), while the floatability sharply increases only up to a level of 30 mM of the divalent cation (Ca^{2+}), followed by decreased floatability with further increases in the IS. For a monovalent salt, Na^+ ions effectively screen a negatively charged bubble surface, reducing the energy barrier for attachment and thus increasing floatability. Through zeta potential, adsorption, and contact angle measurements, they related the

decreased floatability of malachite at Ca^{2+} concentration above 30 mmol/L with the formation of hydration layer by the hydrated Ca^{2+} adsorption onto oleate ions-adsorbed synthetic malachite. Other researches related with effects of ions on malachite flotation usually present in the sulphidisation flotation.

1.3. Flotation of overground mineral particles

In the grinding process, some minerals are easy to be overground so that large quantities of fines are produced. These fine minerals cause serious problems in the flotation process.

1.3.1. Difficulties in overground mineral flotation

Overground particles are a problem of flotation mainly because they have a small mass and high surface area. Small mass leads to: (a) low particle momentum; (b) heterocoagulation; (c) particle entrainment in concentrates (e.g. froth); (d) low probability of collision with a bubble; and (e) difficulty in overcoming the energy barrier between particle and particle and particle and bubble. High surface area directly leads to: (a) a high dissolution rate in water; (b) adsorption of a large quantity of chemicals; (c) rigidity of froth; (d) high pulp viscosity; and (e) undesirable coating of the valuable particles by ultrafine gangue particles.

1.3.2 Approaches for overground mineral flotation

The fundamental reason for the low flotation rate of overground particles is primarily due to their low collision efficiency with conventional flotation bubbles of a given size and velocity (Dai et al., 2000; Fuerstenau, 1980; Trahar and Warren, 1976; Yoon and Luttrell, 1989). Several flotation technologies have been developed, which aim at increasing bubble–particle collision efficiency, either by decreasing bubble size or by increasing apparent particle size.

1.3.2.1 Decreasing bubble size

A decrease in bubble size can be obtained using different methods, which can be divided into mechanical and physiochemical approaches. Mechanical methods include the design of flotation cells, i.e., the shape of the rotor and stator, and the gap size between the rotor and stator, so that the gas bubbles produced at the bottom of the flotation cell can be dispersed into smaller bubble sizes. A microporous material can also be used at the bottom of the cell, through which the gas bubbles are produced. Zhou et al. (1997) have also proposed a method of generating tiny bubbles by hydrodynamic cavitation, which is the process of creation and growth of gas bubbles in a liquid due to the rupture of a liquid–liquid or a liquid–solid interface under the influence of external forces. The bubbles generated on a particle surface by cavitation naturally attach to the particle, eliminating the collision and attachment process, which is often the rate determining step for flotation. Cavitation also improves the flotation efficiency of coarse particles by reducing the detachment probability during the rise of particle–bubble aggregates in the liquid.

Physiochemical methods include dissolved air flotation and electroflotation. Dissolved air flotation is based on Henry's law, where the solubility of air in an aqueous solution is proportional to the partial pressure of air at constant temperature. By subjecting the solution to an over-pressure, air molecules dissolve in the solution. The solution becomes supersaturated when the pressure is released and gas molecules precipitate as small bubbles. Another way to precipitate bubbles is to decrease the pressure by applying a vacuum, a technique called vacuum flotation. The gas bubbles nucleate preferentially on the hydrophobic surfaces of minerals, thus

eliminating the bubble–particle collision step in conventional flotation. Application of electroflotation to fine mineral recovery has become a topic of recent research, due to a combination of uneconomic and inefficient conventional fine mineral flotation techniques accompanied by an increased demand for minerals (Matis and Backhurst, 1984). Electroflotation is based on the use of hydrogen and oxygen bubbles formed by the electrolysis of water. Oxygen is formed at the anode, Eq. (1), and hydrogen is formed at the cathode, Eq. (2). These two gases may be used either separately or together, or in combination with air bubbles in electroflotation.



1.3.2.2 Increasing particle size

Many techniques have been developed which try to increase particle size and mass and decrease surface energy. All of these techniques have the same feature; fine particles are induced to form flocs or aggregates. Depending on the mechanisms of aggregate formation, these techniques can be divided into three classes: selective flocculation, coagulation and hydrophobic aggregation.

In selective flocculation, the flocs are formed due to the bridging ability of long-chain polymer molecules or ions. These polymers first adsorb onto mineral surfaces by electrostatic forces, specific chemical interaction and/or hydrogen bonds followed by bridging other mineral particles and forming loose flocs (Gregory and O'Melia, 1989). It has often been claimed that selective flocculation is a promising technique for fine mineral particles. Several experimental results have showed improved flotation of fine particles by selective flocculation (Attia, 1977; Song et al., 2000). However, as indicated by Rubio et al. (2003), selective flocculation is yet to find general application, for entrapment of gangue is a major issue.

Coagulation of fine particles can be achieved by the addition of electrolyte which decreases the electrostatic repulsion between charged particles. Coagulation is a much-used technique in water purification where no selectivity is required. However, in the minerals processing industry, selectivity is essential. Electrolyte addition often causes heterocoagulation, however it is very hard to obtain selective coagulation only by electrolyte addition. Therefore, this method is rarely used in the minerals processing industry for particle size enlargement.

With hydrophobic aggregation, the fine particles are selectively hydrophobised, similar to conventional froth flotation. In order for the particles to be held together by hydrophobic forces they need to be in very close proximity, achieved by intense agitation (Koh and Warren, 1980; Warren, 1992). Non-polar oil is often added to the solution to increase the strength of the aggregates. Hydrophobic aggregation can be further divided into shear flocculation, emulsion flotation, carrier flotation, oil extended flotation, spherical agglomeration and two liquid extraction. Hydrophobic agglomerates are characterized by compact structure and hydrophobic surfaces, and have similar flotation behavior to normal particles in the same size. There are three key parameters in hydrophobic agglomeration, namely particle hydrophobicity, kinetic energy input and nonpolar oil participation. The more hydrophobic are the particles, the more powerful the hydrophobic agglomeration is, because hydrophobic attraction between particles in aqueous solutions closely correlates with the hydrophobicity of the particles. Kinetic energy input is realized by mechanical agitation (shear field) of fine particles suspensions, which gives the

particles sufficient energy to overcome the potential energy barrier. Nonpolar oil droplets enhance hydrophobic agglomeration through the formation of oil bridges between hydrophobic particles and increasing particle hydrophobicity.

In literatures, no investigation has been reported in the hydrophobic agglomeration and flocculation of malachite fines in aqueous suspensions yet.

Chapter 2. Experimental

2.1 Research line

Research line of the work is presented schematically in Figure 2.1. As it shows, the chapters 1 to 3.3 are the preparation chapters. In chapter 1, the literature concerning the flotation of malachite and effects of salinity and overgrinding in minerals flotation were reviewed. Chapter 2 presents the experimental of the thesis work. In chapter 3.1, the adsorption of phenol O-O and N-O chelating collectors at the malachite/water interface was studied. It provides useful clues for designing novel collectors and selecting the existed reagents as collectors in base metal oxide flotations. In chapter 3.2, the combination use of sodium oleate and alcohols of different structures was investigated. It provides a new reagent scheme in malachite flotation which exhibits superior collecting power and selectivity to sodium oleate. In chapter 3.3, the effect of comminution on malachite flotation was studied. It provides a novel method to increase the flotation recovery of malachite. In chapter 3.4, an example of flotation in salinity water was given. It provides fundamentals in the slime coating of clay minerals on copper mineral surface. In chapter 3.5, the flotation of malachite in the presence of octyl hydroxamate was reexamined. A systematic interaction mechanism between malachite and octyl hydroxamate was proposed in this investigation. In chapter 3.6-3.7, effects of the CO_3^{2-} , H^+ , and Ca^{2+} on the adsorption and flotation of malachite was studied. It gives the guidance for flotation malachite in salt solution. Chapter 3.8 investigated the floc flotation of malachite in the presence of kerosene and octyl hydroxamate, providing a better way in using kerosene in floc flotation.

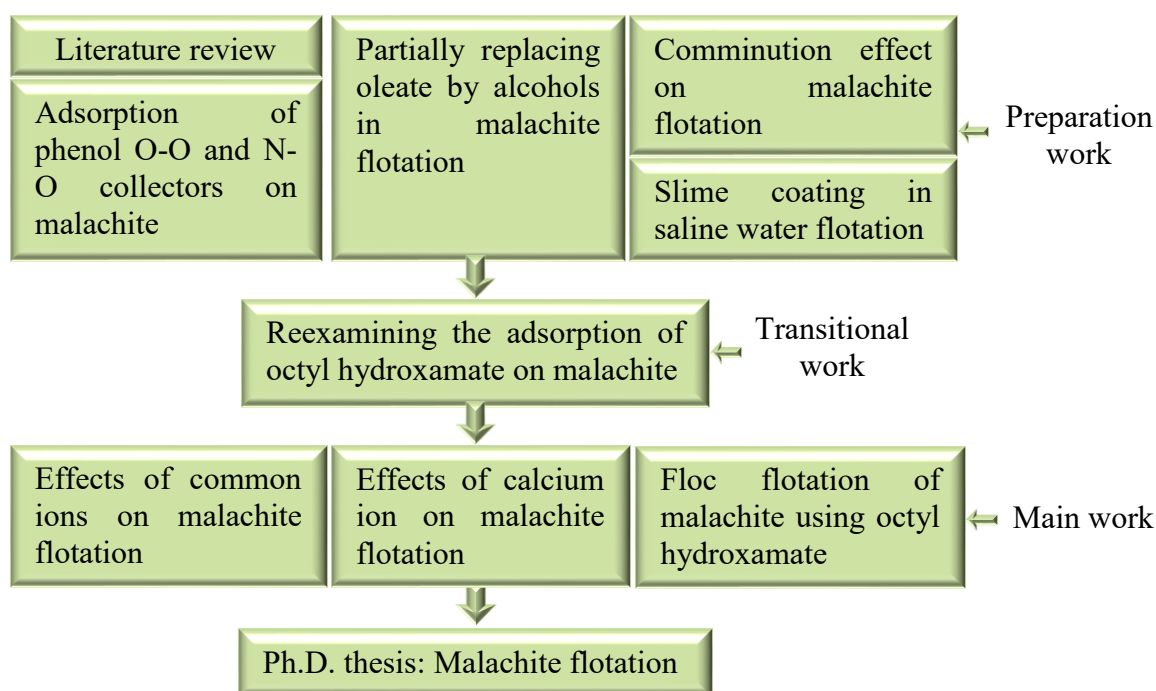


Figure 2.1. Schematic presentation of the research line

2.2 Materials

The natural malachite sample obtained from Lupe mine, Mexico, was crushed, hand-sorted to get lumps for contact angle measurements, and ground to obtain particles of the size fraction $-75+38 \mu\text{m}$ for micro-flotation, and $-25 \mu\text{m}$ for micro-flotation in the presence of CaCl_2 , and

hydrophobic flocculation and micro-flotation, and finer particles, for the solubility, zeta potential, adsorption experiments and FTIR, XPS measurements. X-ray diffraction (XRD, Bruker D8) pattern of the sample in Figure 2.2 showed a high purity malachite ($Cu_2CO_3(OH)_2$), with minor amounts of pseudomalachite ($Cu_5(PO_4)_2(OH)_4$). The setting conditions for the XRD were: Cu $K\alpha$ radiation, 40 keV accelerating voltage, and 0.1s/step (0.01945°/step) scan rate. Quantitative chemical analysis of the mineral sample performed by atomic absorption spectroscopy (AAS), assayed the sample with 54.3 wt% Cu and 0.5 wt% P. Based on the XRD characterization, the P and Cu were assumed to respectively belong to pseudomalachite, and combination of malachite and pseudomalachite; thus, it may be estimated that the sample contains 4.3 wt% of pseudomalachite, 90 wt% of malachite, and 5.7 wt% of other gangue minerals.

High-purity chalcopyrite ($CuFeS_2$) and kaolinite ($Al_2Si_2O_5(OH)_4$) purchased from Da Hong Shan Mine in Yunnan Province, China, were used in the experiments investigating slime coating phenomenon. The lumps of the chalcopyrite were crushed, hand-sorted, and dry-ground with a mechanical agate mortar and pestle. The sample was then dry screened to collect the $-75 + 38 \mu m$ and $-25 \mu m$ fractions, of which the coarser fraction was used in flotation tests and turbidity measurements. The finer fraction was further dry-ground and used in zeta-potential distribution measurements. To minimize oxidation, the chalcopyrite sample was sealed in plastic bottles and stored in a freezer at $-10^\circ C$. The X-ray diffraction (XRD) patterns of the chalcopyrite and kaolinite samples are shown in Figure 2.3-2.4. The chalcopyrite and kaolinite were of high purity, with the chalcopyrite containing a trace amount of quartz. The particle size distribution of the kaolinite sample was determined using a Malvern Mastersizer 2000; the 50% cumulative undersize (D50) and the 85% cumulative undersize (D85) were 5.5 and 11.5 μm , respectively.

To prepare malachite samples for roughness and contact angle measurements, malachite lump samples were polished using grit #2000 abrasive papers followed by diamond paste to get the smoothest surface in the experiments; this was denoted as surface A. The medium rough and roughest surfaces were polished with grit #240 and #80 abrasive papers respectively. The surfaces obtained were denoted as surface B and C. To prepare the samples for BET measurements, malachite lumps were crushed and then dry-ground mixed with quartz ($d_{50}=204.5 \mu m$, $d_{85}=271.6 \mu m$) and montmorillonite ($d_{50}=15.1 \mu m$, $d_{85}=28.3 \mu m$) respectively. After grinding, the samples were sieved to obtain particles of $-75+38 \mu m$. The sample ground with montmorillonite was treated through gravity separation method to remove montmorillonite in the malachite sample for BET measurement. The sample ground with quartz was partially saved to measure the specific area and partially weighted, acid treated at pH 2 to dissolve the malachite particles and weighed again to obtain the percentage of malachite in the sample and get the quartz sample for BET, and then compute the specific surface area of malachite in the sample. As for the samples for micro-flotation, two kinds of samples were prepared. One is malachite ground with quartz and the other one is prepared by the procedure that after removal of montmorillonite, the malachite was mixed with a certain percent of quartz which was equal to that of the malachite ground with quartz.

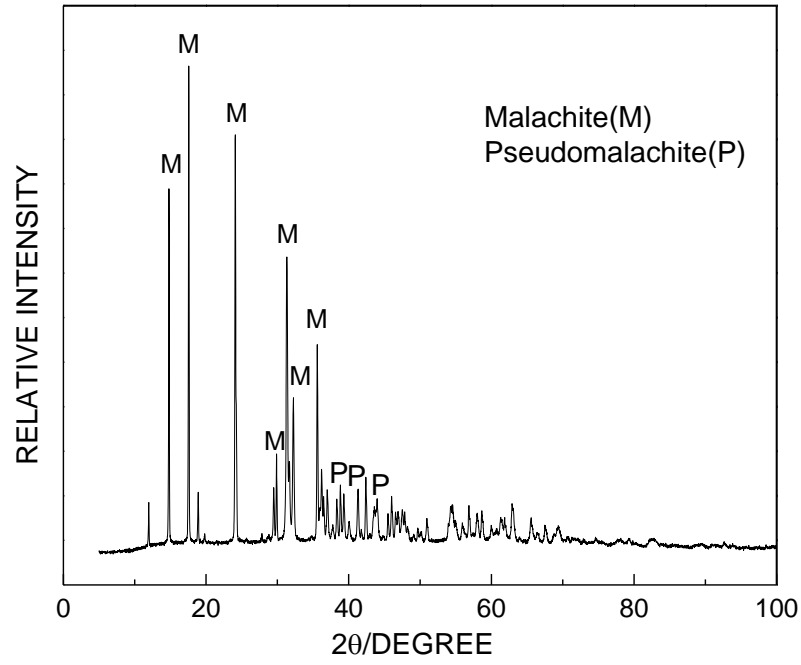


Figure 2.2. XRD pattern of malachite sample

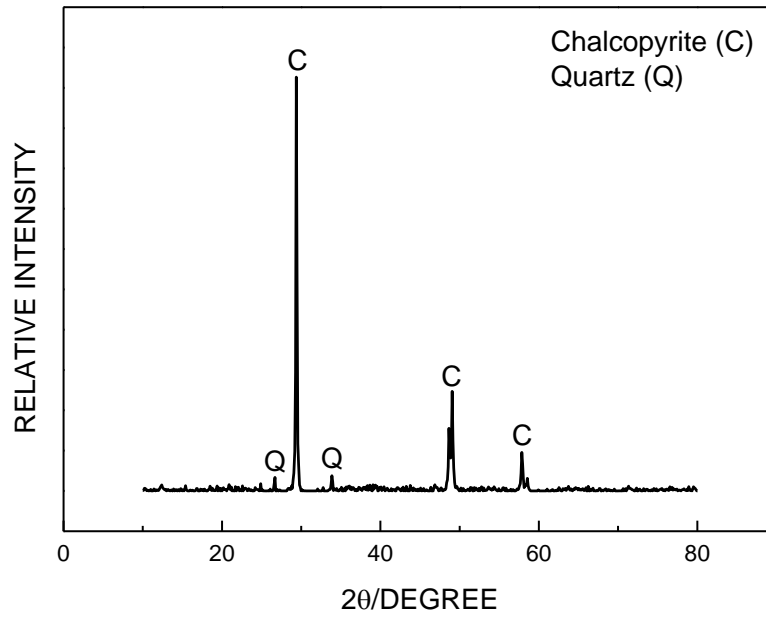


Figure 2.3. XRD pattern of chalcopyrite sample

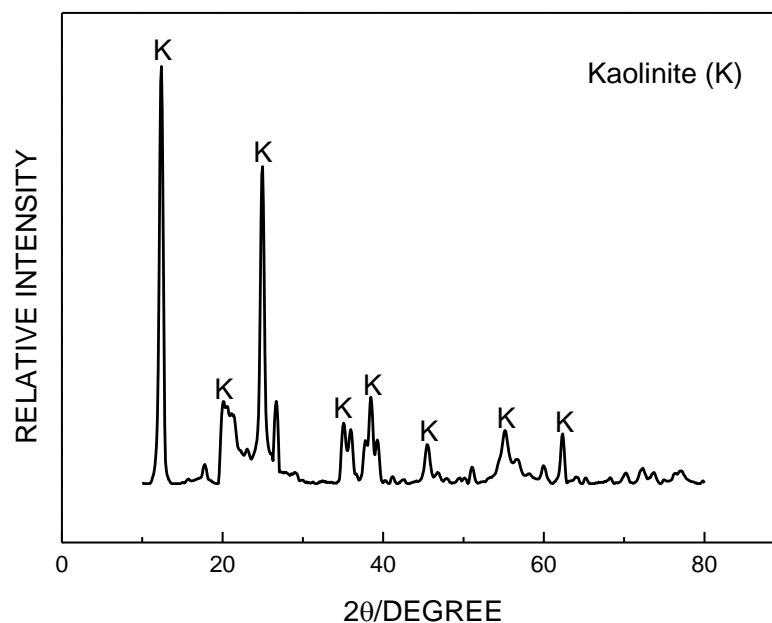


Figure 2.4. XRD pattern of kaolinite sample

2.3 Reagents

Figure 2.5 shows the reagents used in the experiments. Salicylaldehyde of ACS reagent grade was purchased from Energy Chemistry. Salicylhydroxamic acid (ACS reagent grade), reagent-grade potassium ethyl xanthate (KEX), sodium oleate (ACS reagent grade), 1-octanol, 2-ethylhexanol, α -terpineol, and MIBC were purchased from Aladdin Industrial in China. Potassium octyl hydroxamate was synthesized and purified in the laboratory, according to the methods described by Raghavan and Fuerstenau (1975). The kerosene was from the Fisher Scientific without further purification. Sodium carbonate, Calcium chloride and copper chloride used in all experiments were ACS reagent grade. Hydrochloric acid (HCl) and sodium hydroxide (NaOH) of ACS reagent grade were used to regulate the solution pH. Distilled water was used in all the experiments. The seawater was prepared by dissolving 35 g API Aquarium Salt in 1 L deionized water as reported elsewhere (Zhang et al., 2015). The gypsum saturated water was prepared by dissolving 4 g calcium sulfate in 1 L deionized water (Deng et al., 2013). The solution was stirred for one hour, filtered to remove undissolved gypsum, and determined the dissolved gypsum concentration of 2648 ppm (Solubility of gypsum in water is 2400ppm at 25°C) (Gardner and Glueckauf, 1970).

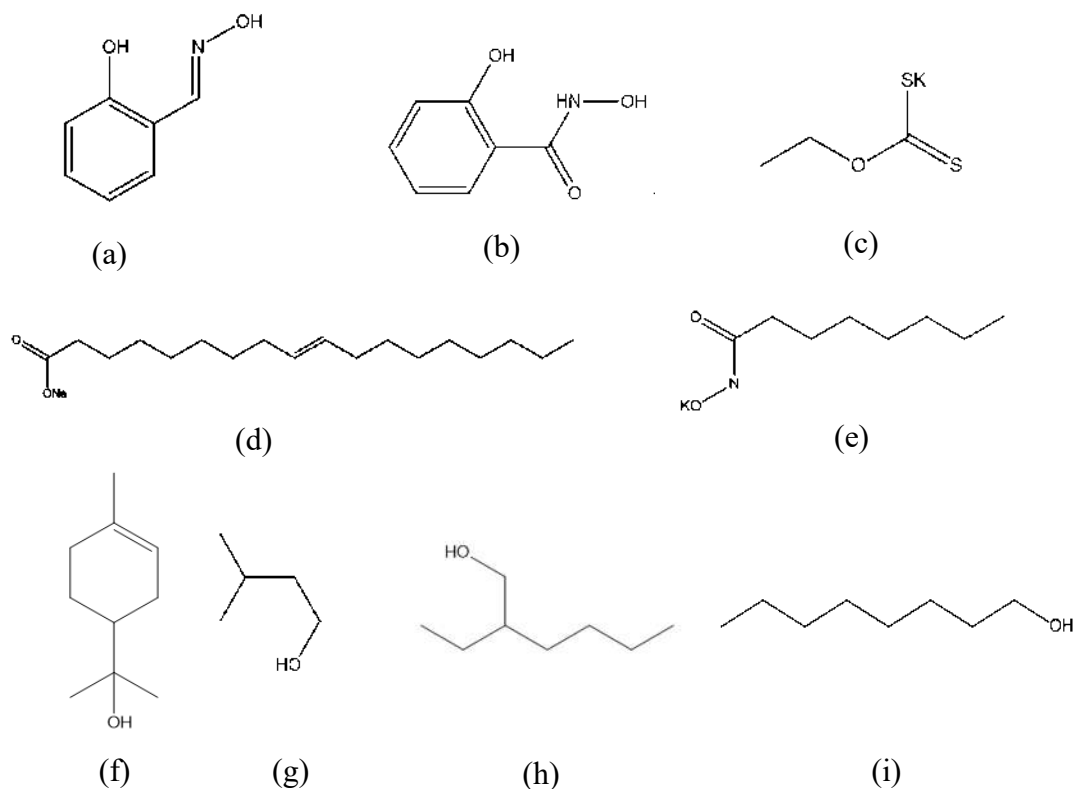


Figure 2.5. Reagents used in the experiments (a) Salicylaldehyde; (b) Salicylhydroxamic acid; (c) potassium ethyl xanthate; (d) Sodium oleate; (e) Octyl hydroxamate; (f) α -terpineol; (g) MIBC; (h) 2-Ethylhexanol; (i) 1-octanol.

2.4 Methods

A 150 mL modified Hallimond tube equipped with a 20 μm frit and a magnetic stirrer was used to test the malachite flotation behavior at different conditions. In each flotation experiment, 3 g or 1 g of malachite sample was conditioned for 2 min in 130 mL distilled water or sodium carbonate solution at the desired concentration; the solution pH was adjusted to the desired value by using HCl or NaOH. Then, a given amount of collectors was added and the slurry was conditioned for 3 min. Next, the slurry was transferred to the Hallimond tube, and the flotation was performed for desired time with nitrogen gas at a flow rate of 20 mL/min. The floated (concentrate) and unfloated (tails) products were separately collected, dried, and weighed, and the recovery was calculated as the mass ratio of floated product/(floated product + unfloated product). In some cases, a given amount of ions were added before the addition of collectors. In the case of studying the slime coating of kaolinite on chalcopyrite, Small-scale flotation tests were conducted by using a 100 mL mechanical flotation cell with 2000 rpm/min agitation speed. In the tests, chalcopyrite of 3 g (3% solid ratio) was mixed with 100 mL of tap water, seawater or gypsum saturated water in the plexiglass cell and the pH was adjusted to a desired value using HCl or NaOH. In flotations with kaolinite, amounts of 90 (0.09% solid ratio), 240 (0.24% solid ratio) and 600 (0.6% solid ratio) mg kaolinite were added into the chalcopyrite slurry. Then, 5×10^{-4} mol/L of KEX and 2×10^{-4} mol/L of MIBC were added and conditioned for 5 min and 1 min, respectively. After flotation of 3 min, the concentrate (floated) and tailing (unfloated) products were separately

collected, dried and weighed, and the floatability of chalcopyrite was calculated based on the dry weights of the products

Slurries of the same reagent conditions as those used in flotation tests of given amounts of chalcopyrite and kaolinite in 100 mL water were prepared for the turbidity measurements in a Turb 555 IR apparatus with the cell of 28×70 mm in dimension. The slurries were first settled in a 100 mL cylinder for 15 min, and then 30 mL upper solution was transferred for the measurements. Turbidity was used to characterize the stability of minerals particles in the slurries, of which the lower was the turbidity; the stronger the coagulation was.

To study the slime coating of kaolinite on chalcopyrite surface, after the flotation experiments, some concentrates or tailings were sampled and observed by a Zeiss Ultra Plus scanning electron microscopy (SEM) for imaging the slime coating of kaolinite on chalcopyrite surface.

A ZetaProbe Analyzer (Colloidal Dynamics, Australia) with electroacoustic technology was used to determine the zeta potential of the malachite particles in aqueous solutions at various pH and reagent conditions. The zeta potential was calculated from the stimulated electro-acoustic sonic amplitude (ESA) values from the malachite particles using the O'Brien equation (O'Brien, 1990; Rao et al., 2009). In a typical measurement, 5 g of malachite sample and a given amount of ions or collectors were conditioned with 250 mL KCl (1×10^{-3} mol/L) solutions in the cell of the ZetaProbe for 10 min. Then, the zeta potential values were measured and reported by the equipment. Alteration in pH was accomplished by the equipment automatically through the addition of 0.1 mol/L KOH and HCl solutions. In the study investigating the slime coating of kaolinite on chalcopyrite, the zeta-potential distributions of chalcopyrite, kaolinite, and their mixtures were measured with a Malvern Zetasizer Nano ZS90 apparatus equipped with a rectangular quartz electrophoresis cell and a 50-mV laser at a scattering angle of 90° . The zeta-potential distributions were determined by dynamic light scattering and computed from mobility measurements through the Smoluchowski equation (Anderson, 1985). In the measurements, 0.05 g of chalcopyrite ($<5 \mu\text{m}$), kaolinite, or their mixture was prepared in 100 mL of a given type of water and the pH value of the resultant suspension was adjusted to the desired level. The solution was transferred to the cell, and the zeta-potential distribution was recorded at room temperature.

Surface topography for polished malachite samples were measured by Nanovea PS 50 3D Non-Contact profiler with Mountains Map Premium Software to report the average surface roughness (R_a) and the root mean squared roughness (R_q). Scans were recorded with an optical pen (1mm scan range along the z-axis and $2.60 \mu\text{m}$ lateral resolutions). Scan step size was of $0.1 \mu\text{m}$ for x axis and $1 \mu\text{m}$ for y axis, respectively. Smaller R_a and R_q values indicate smoother surfaces. Raw data previously recorded during the surface profile measurements were further post-processed by using NANOVEA 3D software.

The Brunauer-Emmett-Teller (BET) surface area measurements were performed using a NOVA touch LX1 surface area and pore size analyser from Quantachrome Instruments (USA), using nitrogen as purge gas. The samples for specific surface area measurements include malachite ground together with quartz, malachite ground together with montmorillonite and purified by gravity separation, and quartz which was the dissolution product (at pH 2) of malachite ground with quartz.

The adsorption of octyl hydroxamate on the malachite surface was measured through a depletion method at ambient temperature. Octyl hydroxamate concentration was determined by means of the ferric hydroxamate method (Zhang et al., 2017), making use of an AquaMate 8000 UV-Vis spectrophotometer (Thermo Scientific), equipped with a cell of 1 cm optical path. Full wave scanning showed that the main absorption peak of octyl hydroxamate occurred at 500 nm, which was used to determine the collector concentration. A series of octyl hydroxamate aqueous solutions of known concentrations were first characterized and recorded in order to correlate their absorbance intensities with their concentrations. For example, absorbance intensity and reagent concentration for distilled water was zero. Then, after the conditioning of the mineral sample with the collector, the solutions were characterized. The concentrations of octyl hydroxamate were obtained by comparing their absorbance intensities with those of solutions of known concentration. In the adsorption tests, 3 g of malachite sample was conditioned by the same conditioning process used in micro-flotation and then the suspension was filtered by means of a membrane filter to get the solutions whose UV absorbance was measured to obtain their collector concentration. The amount of collector absorbed on the mineral surface was calculated by subtracting the residual concentration in the filtered solution from the initial concentration used in the tests.

The adsorption of salicylaldoxime or salicyl hydroxamate on malachite surface was measured through a batch depletion method at 22 °C. An AquaMate 8000 UV-vis spectrophotometer from Thermo Scientific with a cell of 1 cm optical path was used to determine the concentrations of salicylaldoxime and salicyl hydroxamate, which showed the peaks at 303 nm and 295 nm, respectively. A series of salicylaldoxime or salicylhydroxamic acid aqueous solutions with known concentrations were first characterized and recorded for their absorbance intensities that correlate to the concentrations. For example, absorbance intensity and reagents concentrations for clean water were zero. Then, the solutions after adsorption were characterized. The concentrations of salicylaldoxime or salicyl hydroxamate were obtained through comparing their absorbance intensities with previous solution of known concentrations. In adsorption process, a desired amount of malachite was mixed with a given amount of distilled water, and the pH was adjusted to required values. Then the collector was added and conditioned for 5 min. After that, the solid was filtered by membrane and washed. The filtered solutions were measured for their collector concentrations. The amount of collector absorbed on mineral surface was calculated by subtracting the residual concentration in filtered solution from the initial collector concentration.

Contact angle of the malachite sample was measured by a goniometer (DSA-25, Kruss, Germany). The lumps of malachite samples were wet-polished first by hands with 80, 400, 800 and 1200 grit SiC paper, then with 1 μ m alumina powder suspensions. After that, the polished malachite lump was immersed in solutions of different pH or reagent concentrations for 30 min, and then washed with water, in order to obtain a given pH or reagent condition for the surface. In the measurements, air dried malachite lumps were loaded on the goniometer stage and 1.5 μ L distilled water was dropped on them. The advancing and receding contact angles were reported by the DSA-25. When the difference was less than 1% of the receding contact angle, the average value of these two angles was reported as the contact angle. For each condition (e.g., pH 5), at least four measurements were performed and the average contact angle was reported in this work. In order to study the spreading of kerosene on malachite surface, lumps of the prepared malachite sample were immersed in solutions of 2×10^{-4} mol/L octyl hydroxamate for 15 min. Then, the

malachite sample was dried and then immersed in distilled water. After that, a drop of kerosene was introduced with a microsyringe through a U shaped needle underneath the mineral surface. The relaxation of the contact angle was recorded with time. In other cases, the prepared malachite sample was immersed in solutions of 2×10^{-4} mol/L octyl hydroxamate for 15 min. A droplet of kerosene was introduced at the tenth minutes and maintained at the tip of the U shaped needle for 5 min to adsorb the octyl hydroxamate in the solution. After that, the droplet of kerosene was transferred to the malachite surface and the contact angle was recorded.

XPS survey scan and high-resolution spectra were acquired making use of an AXIS 165 X-ray photoelectron spectrometer (Kratos Analytical). Monochromatic Al K α source ($h\nu = 1486.6$ eV) was used at a power of 210 W for all data acquisition. The vacuum pressure inside the analytical chamber was lower than 3×10^{-8} Pa. The analyzed area on the sample surface was $600 \mu\text{m} \times 700 \mu\text{m}$. The resolution of the instrument was 0.55 eV for Ag 3d and 0.70 eV for Au 4f peaks. To prepare the mineral for the XPS analysis, a sample of 2 g malachite was mixed with 100 mL of 1×10^{-3} of octyl hydroxamate or salicylaloxime solution respectively. The suspension was conditioned in a constant temperature shaker bath for 30 min, and the mineral solids were filtered, washed thrice with distilled water and dried in a silica gel desiccator under vacuum at room temperature before XPS analysis. Copper hydroxamate precipitates and copper salicylaloxime were prepared by mixing 1×10^{-3} mol/L hydroxamate solutions with 1×10^{-3} mol/L Cu^{2+} in a volume ratio of 1 to 2.5. The precipitates were filtered, washed thrice with distilled water and dried in a silica gel desiccator under vacuum before XPS analysis. The survey scans were collected in the binding energy range from 1200 eV to 0 eV with analyzer pass energy of 160 eV and a step of 0.4 eV. To collect the high-resolution spectra, the pass-energy was set at 20 eV with a step of 0.1 eV. XPS sampling depth for photoelectrons was 3–10 nm, which was enough to provide information about the mineral surfaces in this work. Advantage version 5.52 software was used to process the XPS data after spectra collection. The Smart-type background subtraction was chosen to optimize the peak height through the high-resolution spectral analysis. The C1s spectrum at 284.8 eV was used to calibrate all the measured spectra as an internal standard for charge compensation.

In order to experimentally measure malachite solubility, 0.25 g of malachite sample was added to 25 mL distilled water or sodium carbonate solution at the desired concentration, contained in a beaker placed on a magnetic stirring plate. Then, the pH was modified to the desired value using HCl or NaOH solution. The dissolution process was considered at equilibrium when the pH remained constant. Next, the suspension was centrifuged and filtered to obtain the solution to determine the concentration of total copper by AAS.

Fourier transform infrared (FTIR) spectra were used to characterize the adsorption of salicylaloxime, salicyl hydroxamate, and ions on the malachite surface. The spectra were recorded at a 4 cm^{-1} resolution in the $4000\text{--}500 \text{ cm}^{-1}$ region in a FTIR-740 infrared spectrometer (Nicolet, USA), making use of KBr disks. To prepare malachite sample after the adsorption of collectors for the measurement, a given amount of collector's solution and fine malachite particles were added to a 250 mL conical flask and the pH was adjusted. After stirring the suspension for 20 h in a constant temperature shaker bath, malachite particles were centrifuged, washed thrice with distilled water, dried in a silica gel desiccator under vacuum at room temperature, and used for infrared detection. Copper salicylaloxime and copper hydroxamate precipitates were prepared by mixing 1×10^{-3} mol/L salicylaloxime or octyl hydroxamate solutions with 1×10^{-3} mol/L copper sulfate in a volume ratio of 1 to 2.5. After filtering, washing

thrice with distilled water and drying in a silica gel desiccator under vacuum, the FTIR spectra of copper salicylaldoxime or copper hydroxamate precipitates were recorded.

Kerosene was added into malachite suspensions in the form of oil emulsion. Two kinds of kerosene emulsion were prepared in the experiments. The first kind of kerosene emulsion was prepared by mixing kerosene with water in the concentration of 1 wt%, followed by ultrasonic treatment for 10 min using an HORIBA ultrasonic processor. To prepare the second kind of kerosene emulsion, 0.05 wt% of octyl hydroxamate was added in the emulsification process so that a layer of octyl hydroxamate formed on oil droplets surface. According to the particle size analysis using a Malvern Mastersizer 2000, the d_{50} of the first and second kind of kerosene emulsion were 2.14 and 0.53 μm , respectively.

The hydrophobic flocculation of malachite fines in aqueous suspensions was performed in a mixing tank of 10 cm inner diameter with four 1 cm width baffles. The mixing head was connected with a Servodyne mixer controller, and the shaft was equipped with a S-shape impeller of 6 cm width and 2 cm height. Suspensions with 1 g malachite sample and 99 ml water were first adjusted for pH using hydrochloric acid or sodium hydroxide solution, followed by the addition of given amount of octyl hydroxamate with conditioning time of 3 min. After that, a desired amount of kerosene emulsion was added, and then the suspensions were strongly conditioned at 900 rev/min for 15 min. Hydrophobic aggregates of malachite fines in aqueous suspensions were achieved after the conditioning.

A Leica DMLP optical microscope equipped with digital camera was used to observe oil droplets in emulsions and hydrophobic aggregates in aqueous suspensions. The samples were prepared by dropping kerosene emulsion or malachite aggregate suspension on a glass plate, followed by putting a thin glass slide on the drop to fix the suspension or emulsion. During the observation, some of kerosene droplets and malachite aggregates were photographed.

Chapter 3. Results and Discussion

3.1. Comparison of adsorption of phenol O-O and N-O chelating collectors at the malachite/water interface in flotation

Figure 3.1.1 presents the effect of salicyl hydroxamate and salicylaldehyde on the zeta potential of malachite as a function of pH. As with most oxide minerals, the malachite has a positive surface charge at low pHs and a negative surface charge at high pHs. It shows the isoelectric point (IEP) of malachite at pH 8.2, which is in good accordance with the IEP (pH 7.9) reported by Lenormand et al. (1979). With the addition of salicyl hydroxamate and salicylaldehyde, zeta potentials of malachite reverse from positive to negative at low pHs and become more negative at high pHs, indicating the chemical adsorption of these chelating reagents on its surface. However, this modification reduces at a pH higher than 10. At pH 11, the zeta potentials of malachite without and with addition of salicyl hydroxamate and salicylaldehyde are close, indicating a weak adsorption. It might be due to the fact that at a pH higher than 10, the predominant hydroxyl species weaken the interaction of chelating reagents on the malachite surface. It is interesting that the salicyl hydroxamate modifies the malachite surface more negatively than the salicylaldehyde does in the pH range of 5–10.

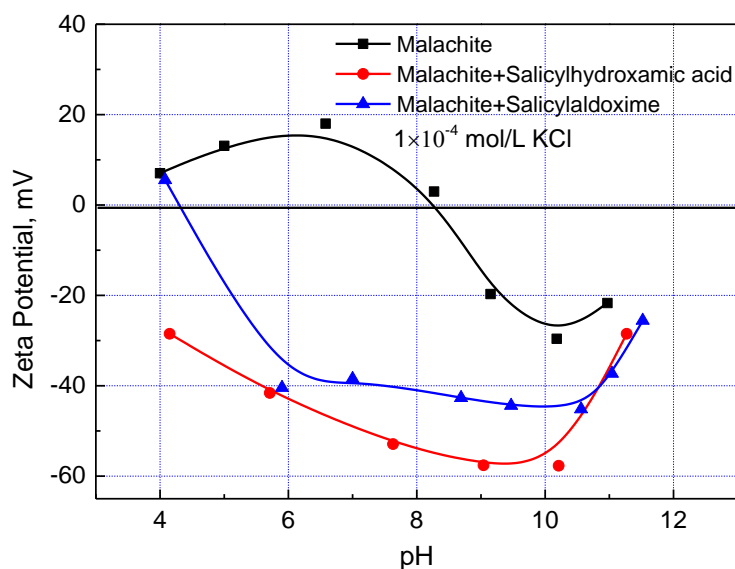


Figure 3.1.1. Effect of salicyl hydroxamate and salicylaldehyde on the zeta potential of malachite as a function of pH.

A batch of salicyl hydroxamate and salicylaldehyde depletion has been studied to explore their chemical adsorption on the malachite surface. At a pH lower than pH 6, cupric ions are highly dissolved from malachite, thus the precipitation of cupric salicyl hydroxamate or salicylaldehyde species are predominant reactions for the depletion of the chelating reagents (Lenormand et al., 1979). Then, at a pH higher than pH 6, chelating reactions (adsorption) on the malachite surface are mainly responsible for the salicyl hydroxamate or salicylaldehyde depletion. Figure 3.1.2 gives their depletion densities in malachite slurry as a function of pH. The depletion of salicyl hydroxamate and salicylaldehyde at pH 3 are as high as 5×10^{-5} mol per gram of malachite minerals, suggesting that both reagents are highly reactive with cupric ions in slurry or malachite

surface. Increasing pH from 3 to 9, the depletion of salicylaldoxime decreases slightly but keeps a high amount, while the depletion of salicyl hydroxamate drops dramatically to the lower magnitude of 5×10^{-6} mol/g. Then, the depletion decreases continually as the pH is increased; and at pH 11, depletions of both salicyl hydroxamate and salicylaldoxime are around zero, which corresponds well with the zeta potential results in Figure 3.1.1. At pH 3 to 9, the higher precipitation and/or adsorption degree of salicylaldoxime on the malachite surface than that of salicyl hydroxamate might be attributed to the different stability constants of these chelating reagents with Cu^{2+} complexes. The stability constants of Cu-salicylaldoxime and Cu-salicylhydroxamate are 12 and 9.05 (O'Brien et al., 2000; Sillen et al., 1964), respectively, indicating that it is easier for salicylaldoxime to react with Cu^{2+} complexes in the form of cupric precipitates or adsorption on the malachite surface.

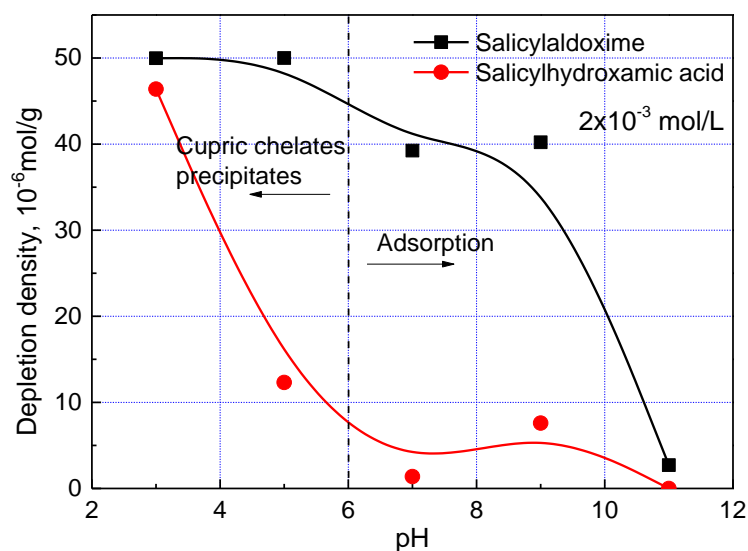


Figure 3.1.2. The depletion of salicyl hydroxamate and salicylaldoxime in malachite slurry as a function of pH.

It is notable from previous discussions that salicyl hydroxamate has a lower adsorption density on the malachite surface (Figure 3.1.2), but modifies the malachite surface to be more negative than salicylaldoxime (Figure 3.1.1). This phenomenon might be due to the distinct chelating reactions of salicylaldoxime and salicyl hydroxamate on the malachite surface because of their different molecular structures. Based on the criteria that chelating reagents must possess at least two donor atoms carrying a long pair of electrons (Fuerstenau et al., 2000), the donor atoms in salicylaldoxime are O ($=\text{N}-\text{OH}$, oxime), N ($-\text{N}=\text{}$, tertiary acyclic) and O ($-\text{OH}$, phenolic), while the donor atoms in salicyl hydroxamate are O, O (both in hydroxamate) and O ($-\text{OH}$, phenolic). As noted, the bond distances between the ligands in the two reagents are different: the bond distances to the carbonyl O in salicyl hydroxamate are around 0.75 \AA longer than those to the tertiary acyclic N in salicylaldoxime, while the third bond distance is of identical 3.89 \AA . Based on the other criteria of the chelating reactions—that they must form a ring structure sterically including the metal atom (Fuerstenau et al., 2000)—salicyl hydroxamate might form the ring structure with only two ligands because of the long bond distances, which leads to one O atom carrying a negative charge on the malachite surface after the adsorption. However, it is possible for salicylaldoxime to form the ring structure with three ligands because of the relatively short

bond distances. Thus, compared with salicylaldoxime, salicyl hydroxamate modifies the malachite surface more negatively by a lower amount of adsorbed molecules. Figure 3.1.3 schematically presents the chelating reactions of salicyl hydroxamate and salicylaldoxime on the malachite surface, in which CuOH^+ and HCO_3^- are defined as the adsorption sites on the malachite surface, as analyzed elsewhere.

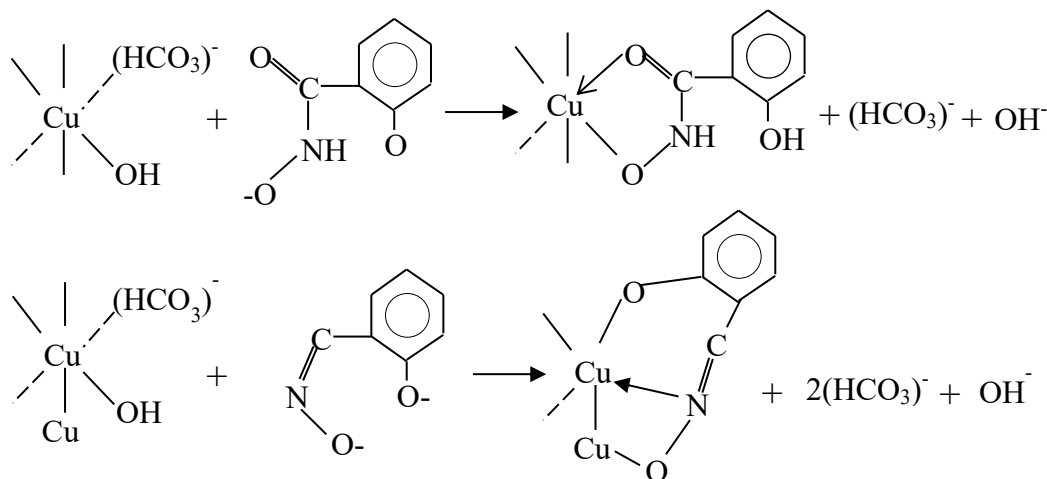
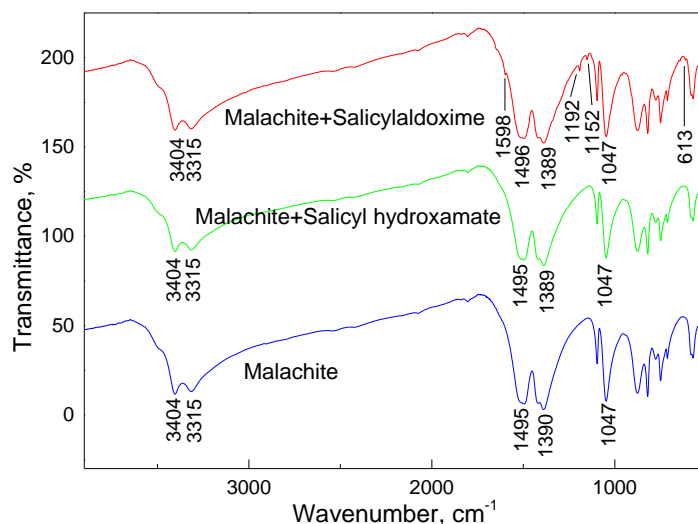
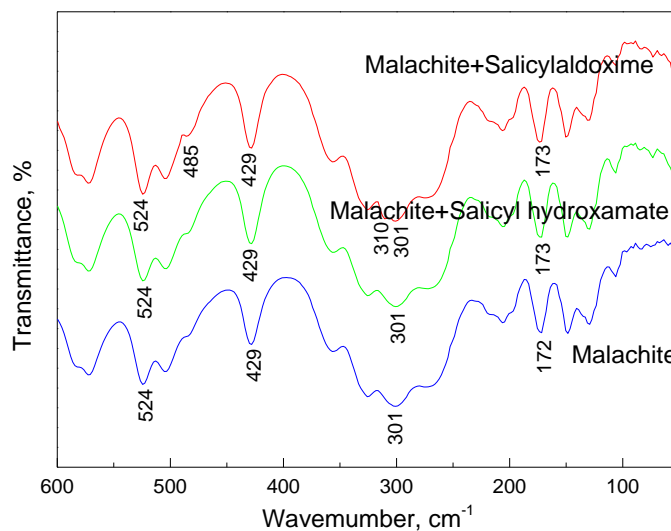


Figure 3.1.3. Schematic illustration of the adsorption of salicyl hydroxamate and salicylaldoxime on the malachite surface.

The proposed adsorption mechanism can be verified from the FTIR spectra of the malachite surface before and after salicylaldoxime or salicyl hydroxamate adsorption. As can be seen in Figure 3.1.4, after salicylaldoxime treatment, the N-Cu and O-Cu stretch vibrations are found at 1193 and 1152 cm^{-1} in the intermediate FTIR spectrum, and 310 and 485 cm^{-1} in the far FTIR spectrum, respectively (Ramesh et al., 1998), representing the chemical adsorption of salicylaldoxime on the malachite surface. In contrast, no new peak appears on the FTIR spectra of malachite after salicyl hydroxamate treatment, indicating that the adsorption density of salicyl hydroxamate on malachite is too low for FTIR to identify, which is in accordance with the adsorption behavior.



(a)



(b)

Figure 3.1.4. Intermediate (a) and far (b) Fourier transform infrared (FTIR) spectra of malachite, malachite with salicylaldoxime and salicyl hydroxamate.

Figure 3.1.5 shows the flotation of malachite as a function of salicylaldoxime and salicyl hydroxamate concentrations at pH 9. By using salicylaldoxime as the collector, the malachite recovery increases to 97% as the salicylaldoxime is increased to 3 mmol/L. Then, the malachite recovery remains constant as the salicylaldoxime concentration is continually increased. In the case of salicyl hydroxamate, the malachite recovery increases slightly to 20% as the collector concentration is increased to 2 mmol/L, and then remains constant. It corresponds well with the adsorption phenomena that (i) both salicylaldoxime and salicyl hydroxamate are chemically

adsorbed on the malachite surface; (ii) the adsorption density of salicylaldehyde is much higher than that of salicyl hydroxamate. Thus, compared with salicyl hydroxamate, salicylaldehyde possesses stronger collecting ability and the flotation of malachite reaches the maximum recovery at a higher collector concentration.

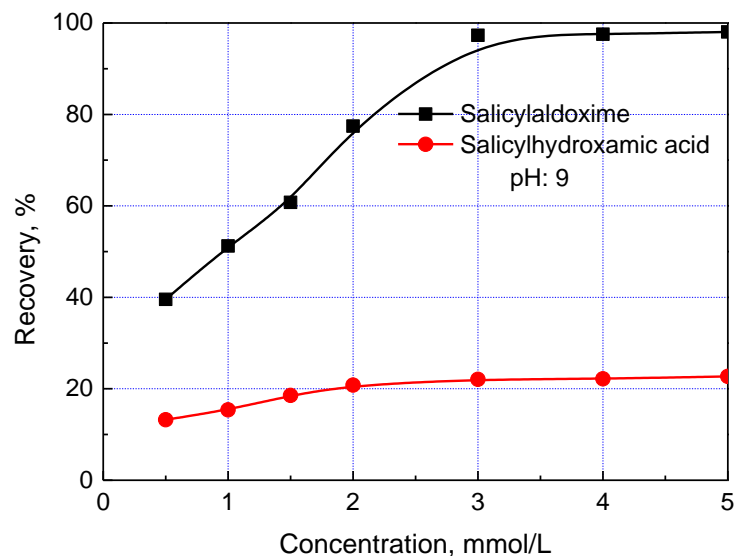


Figure 3.1.5. Flotation of malachite as a function of salicylaldehyde and salicyl hydroxamate concentrations.

The flotation of malachite using salicylaldehyde and salicylhydroxamic collectors as a function of pH is given in Figure 3.1.6. The malachite recovery is less than 20% when using a salicyl hydroxamate collector in the pH range 3–11, in which the maximum recovery of 19% is obtained at pH 9. In contrast, the malachite recovery is around 80% at pH 7–9 with salicylaldehyde as the collector. These results are in good agreement with the precipitation and adsorption of salicylaldehyde and salicyl hydroxamate in aqueous malachite slurries. At a pH lower than 6, the precipitation of cupric salicylaldehyde and salicyl hydroxamate species are predominant reactions of the depletion of collectors, leading to a low adsorption amount and poor flotation performance. At pH 7–9, the recoveries of malachite reach the maximum with both collectors because of the chelating (adsorption) reactions, and because salicylaldehyde possesses a stronger collecting ability than salicyl hydroxamate due to its higher adsorption density. Then, at a pH higher than pH 9 (e.g., pH 11), due to the competition between chelating collectors and hydroxyls on the malachite surface, a low adsorption density takes place, leading to a low malachite recovery. Thus, the proper pH range for malachite flotation with chelating collectors is pH 7–9, which is consistent with malachite flotation by using an octyl hydroxamate collector (Lenormand et al., 1979). In addition, octyl hydroxamate has been reported as an effective collector for oxide (malachite) flotations (Natarajan and Fuerstenau, 1983; Sreenivas and Manohar, 2000), but in our results, salicyl hydroxamate shows a weak collecting ability on malachite. This might be due to the fact that (i) the longer alkyl chain in octyl hydroxamate can render the oxide surfaces hydrophobic more effectively than the benzene ring in salicyl hydroxamate; (ii) the leaving O^- after salicyl hydroxamate adsorption not only modifies the malachite surface more negatively, but also renders it hydrophilic. These results might provide clues for designing a novel collector of oxide flotations in both the carbon chains and the polar heads.

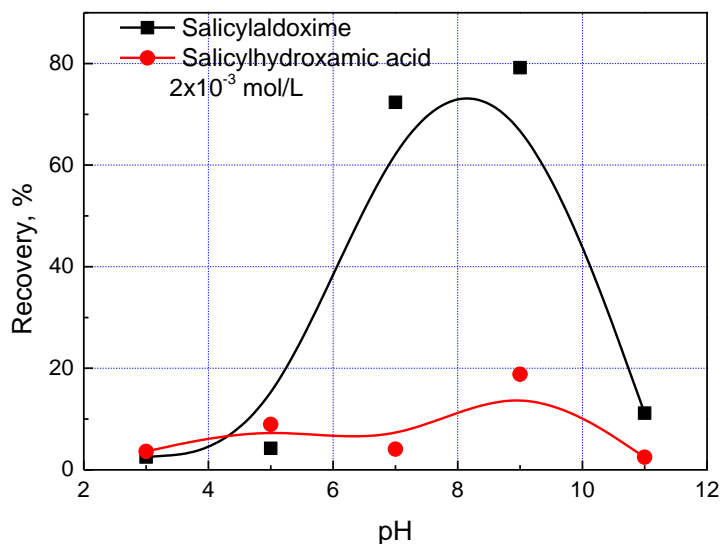


Figure 3.1.6. Effect of pH on the flotation of malachite with salicylaldoxime and salicylhydroxamate collectors.

3.2. Partially replacing sodium oleate by alcohols of different chain structures in malachite flotation

Figure 3.2.1 shows the floatability of malachite with sodium oleate (5×10^{-5} mol/L) as a function of pH. At pH 6–12, the malachite floatability was $\geq 95\%$; particularly at pH 9, the floatability was 99%. It was reported that the complexation of anionic oleate species ($C_{17}H_{33}COO^-$, $(C_{17}H_{33}COO)_2H^-$ or $(C_{17}H_{33}COO)_2^{2-}$) with cupric species (e.g., Cu^{2+} and $CuOH^+$) induced the chemisorption of oleate collectors on the malachite surface (Choi et al., 2016; Woods et al., 1987). At pH > 12, the precipitation of $Cu(OH)_2$ hinders this complexation and adsorption; thus, the floatability decreases sharply; thus, the floatability decreases sharply. Figure 3.2.2 presents the equilibrium diagram of the oleate species as a function of pH in the aqueous solution (Pugh and Stenius, 1985). As can be seen in the figure, at pH < 6, $C_{17}H_{33}COOH(l)$ and $C_{17}H_{33}COOH(aq)$ are mainly formed rather than the anionic oleate species; thus, the malachite floatability is greatly reduced. This result is in good agreement with other studies in terms of the flotation of malachite with an oleate collector at various pH values (Wang and Liu, 2013; Woods et al., 1987).

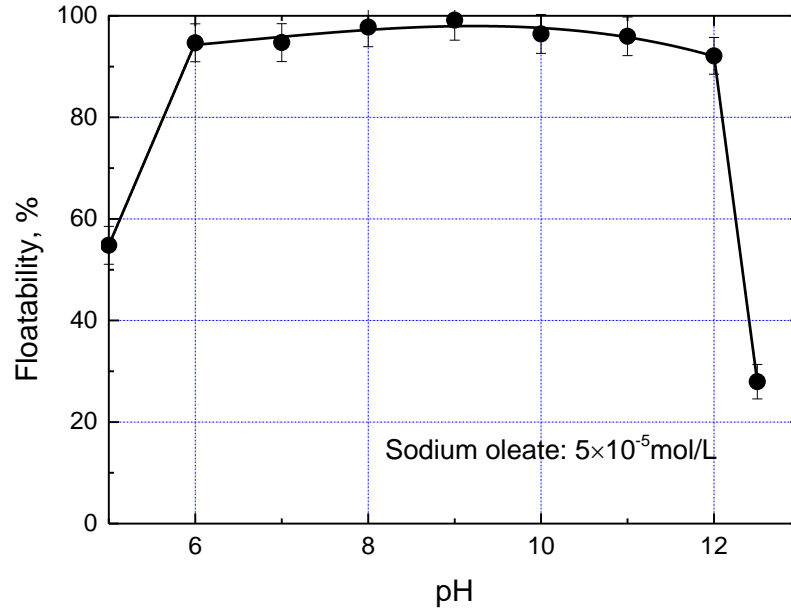


Figure 3.2.1 Malachite flotation with sodium oleate as a function of pH

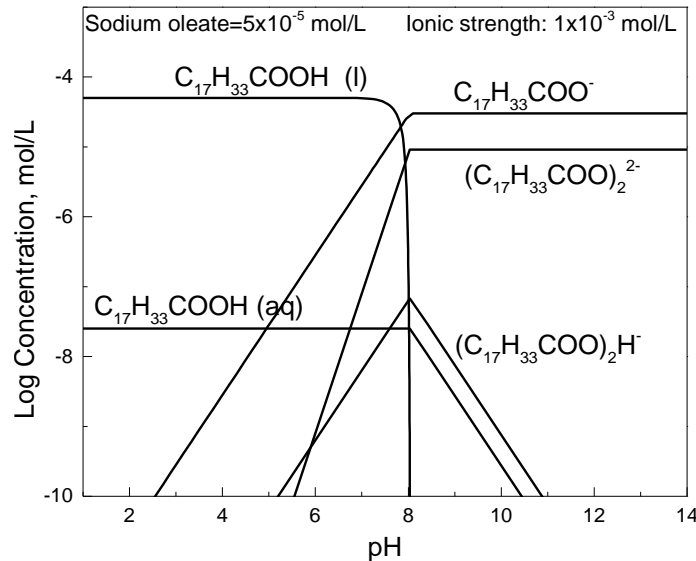


Figure 3.2.2. Equilibrium diagram of oleate species as a function of pH in aqueous solution

Figure 3.2.3 presents the malachite floatability by independently adding sodium oleate and alcohols, with different concentrations. Without reagent, the malachite flotation had high entrainment (14.7%), which is attributed to the fine particle size ($-75+38 \mu\text{m}$) and long flotation time (10 min) in the Hallimond test (Drzymala, 1994). With addition of sodium oleate, the malachite floatability increased steadily up to a concentration of $3 \times 10^{-5} \text{ mol/L}$ and then it kept a plateau at high levels ($>98\%$). At low concentrations of sodium oleate, chemical adsorption of individual ions occurs on the malachite surface, followed by aggregation of the alkyl chains leading to hemi-micelle structures at higher concentrations (Pugh, 1986). Thus, at $3 \times 10^{-5} \text{ mol/L}$, the malachite surface might be formed with a monolayer of the anionic oleate species, leading to

the high floatability of malachite. However, with addition of alcohols, the malachite floatability increased only slightly (<25%) even at a high alcohol concentration (6×10^{-5} mol/L). It suggests that the alcohol molecules cannot adsorb on the malachite surface like the oleate species, but alcohols might improve the flotation hydrodynamic with smaller bubble size and slower rising velocity of bubbles, so that the entrainment increases.

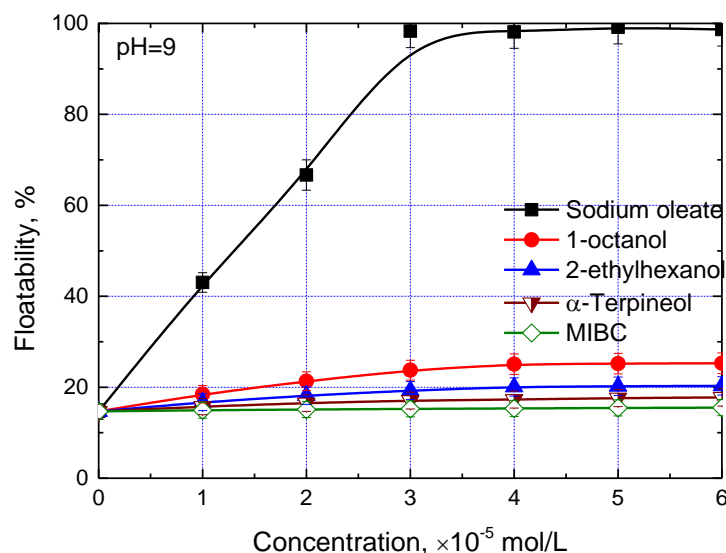


Figure 3.2.3. Malachite flotation at different concentrations of sodium oleate and alcohols

Figure 3.2.4 shows the floatability of malachite with sodium oleate and alcohol mixtures, in which the sodium oleate was maintained at 1×10^{-5} mol/L, while the alcohols were increased from 0 to 4×10^{-5} mol/L. By mixing 1-octanol, 2-ethylhexanol, and α -terpineol with sodium oleate, the malachite floatability increased greatly from 43% to >96% at concentrations up to 3×10^{-5} mol/L and then it kept a plateau. By mixing MIBC with sodium oleate, the malachite floatability increased to 64% at a concentration of 1×10^{-5} mol/L and then it increased slightly; thus, the impact of MIBC was much less than that of the other three alcohols. These results indicate that the addition of alcohols to the sodium oleate collector induced a significant malachite flotation, but alcohols of short hydrocarbon chain (e.g., MIBC) might limit this effect.

The mixture may provide a better selectivity for the sodium oleate based collector. Figure 3.2.5 shows the micro-flotation of mixed minerals (malachite:calcite=1:1) with sodium oleate alone, and the mixture of 2-ethylhexanol-oleate, where the solid lines represent the floatability of malachite and calcite using sodium oleate alone, while the dash-dotted lines are those using mixtures of 1×10^{-5} mol/L oleate and variable concentrations of 2-ethylhexanol. Whether using sodium oleate alone or 2-ethylhexanol-oleate, the floatability of malachite increased significantly at concentrations up to 3×10^{-5} mol/L, and then it kept virtually constant. However, the floatability of calcite using sodium oleate alone was around 17% higher than that using 2-ethylhexanol-oleate, when the concentrations were higher than 3×10^{-5} mol/L. Therefore, the mixture of 2-ethylhexanol-oleate induced a higher selectivity for the mixed minerals of malachite and calcite in micro-flotation. It has been reported that a low selectivity of malachite from calcium and magnesium gangue minerals (e.g., calcite, magnesite, and feldspar) was obtained

using a sodium oleate collector, and this is believed to be because the complexation between the anionic oleate species and the hydrolysed Ca^{2+} or Mg^{2+} species also takes place on the gangue minerals surface (Miller et al., 2007). However, it should be noted that the solubility product constants (K_{sp}) of copper oleate, calcium oleate, and magnesium oleate are 10–19.4, 10–15.4, and 10–13.8 (Fuerstenau and Han, 2003), respectively, indicating that the oleate is slightly preferred for adsorption on the malachite surface. In many malachite-flotation practices, this selectivity is usually sacrificed in order to obtain a high copper recovery by using high dosages of sodium oleate. The partial replacement of sodium oleate by alcohols in the form of a collector mixture may result in a tendency for the formation of copper oleate, resulting in a better selectivity of the sodium oleate based collectors. Nevertheless, as reported by Liu and Peng (1999), because 1-octanol, α -terpineol, and 2-ethylhexanol are sparingly soluble in water, the prerequisites for the large-scale application of the collector mixture are: (1) an effective emulsification and (2) that the added emulsifier has no impact on the flotation.

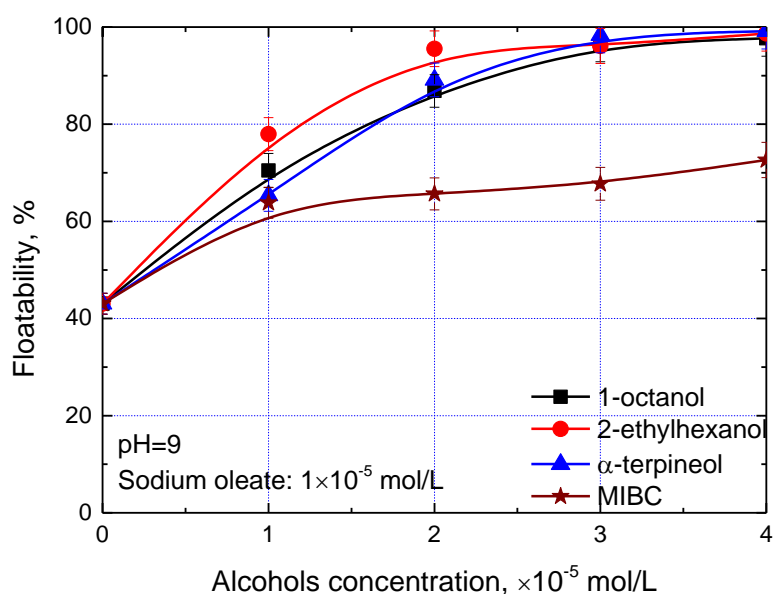


Figure 3.2.4. Malachite flotation with sodium oleate and alcohol mixture

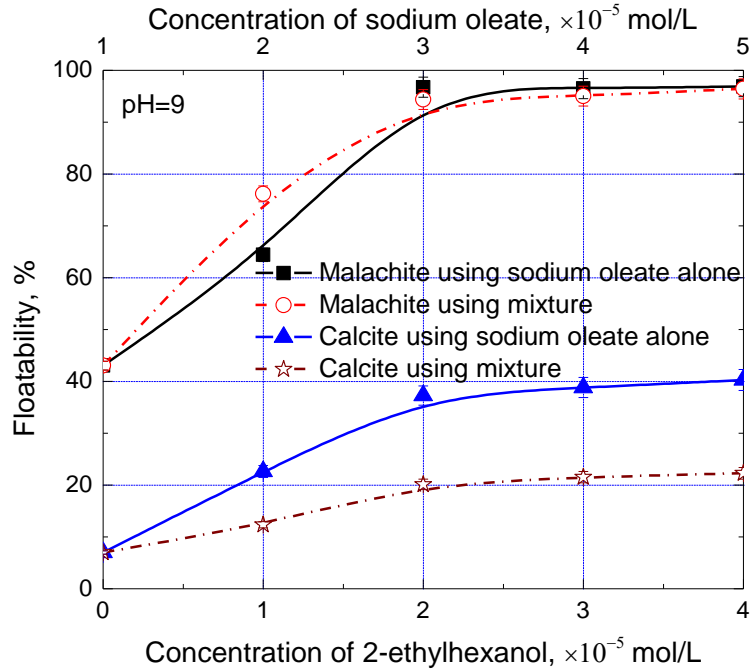


Figure 3.2.5. Micro-flotation of mixed minerals (malachite:calcite=1:1) with sodium oleate alone and 2-ethylhexanol-oleate.

Contact angle and zeta potential measurements were performed to study the adsorption of sodium oleate and alcohols on the malachite surface. Figure 3.2.6 presents contact angle images and the results of malachite lumps treated with sodium oleate of different concentrations at pH 9. The contact angle of pure malachite was 37.9° . After the treatment with sodium oleate, the adsorbed anionic oleate species made the malachite hydrophobic, with their hydrophobic tail orientating into water. As the sodium oleate concentration increased from 0 to 1×10^{-5} , 2×10^{-5} , and 3×10^{-5} mol/L, the contact angle increased significantly, from 37.9° to 45° , 62.4° , and 70° , respectively. Then, it increased slightly, to 72.8° and 77.4° , as the sodium oleate concentration increased continually, to 4×10^{-5} and 5×10^{-5} mol/L. Thus, the sodium oleate concentration of 3×10^{-5} mol/L is the inflection point of concentration that renders the malachite surface highly hydrophobic, which is in good agreement with the malachite flotation results as a function of sodium oleate concentration (Figure 3.2.3).

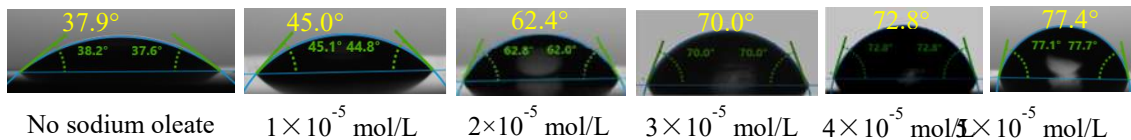


Figure 3.2.6. Contact angle images and results of malachite treated with sodium oleate of different concentrations at pH 9

Figure 3.2.7 shows the contact angle results of malachite lumps treated with sodium oleate alone and with a mixture of sodium oleate and alcohols. With the addition of the mixture (1×10^{-5} mol/L sodium oleate and alcohols), the contact angle increased in a concave-type trend as the alcohols concentrations increased. It increased steadily at low alcohols concentrations (1×10^{-5} mol/L and 2×10^{-5} mol/L), and increased greatly at high alcohols concentrations (3×10^{-5} mol/L and 4×10^{-5}

mol/L). However, the malachite floatability (Figure 3.2.4) with the same mixture and the contact angle with various concentrations of sodium oleate (Figure 3.2.6) behaved in a convex-type increase, in which high increases of floatability and contact angle were observed at low reagents concentrations. This inconsistency might suggest the different adsorption forces between sodium oleate and alcohols on the malachite surface. In the measurements of contact angle, the malachite surfaces treated with reagents were washed before drying for the measurements. With sodium oleate alone, the wash could not induce desorption because it is chemically adsorbed on the malachite surface. Thus, malachite floatability and contact angle behaved with the same trend. However, with the sodium oleate and alcohol mixtures, alcohols might be co-adsorbed with sodium oleate, and thus, the wash could induce the fall of some alcohol parts. It makes the contact angle of malachite behave in a concave-type trend when treated with a 1×10^{-5} mol/L sodium oleate and alcohol mixture, in which, for rendering the malachite surface hydrophobic, a high concentration of alcohols was required to offset the fall of alcohol. Besides, compared with 1-octanol, α -terpineol, and 2-ethylhexanol, the contact angle of the malachite treated with sodium oleate and MIBC was smaller, but the difference was much smaller than that of malachite flotation with the sodium oleate and alcohol mixture (Figure 3.2.4). It is in good agreement with other reports that the contact angle of a mineral is not linearly correlated to flotation behaviour (Chau et al., 2009).

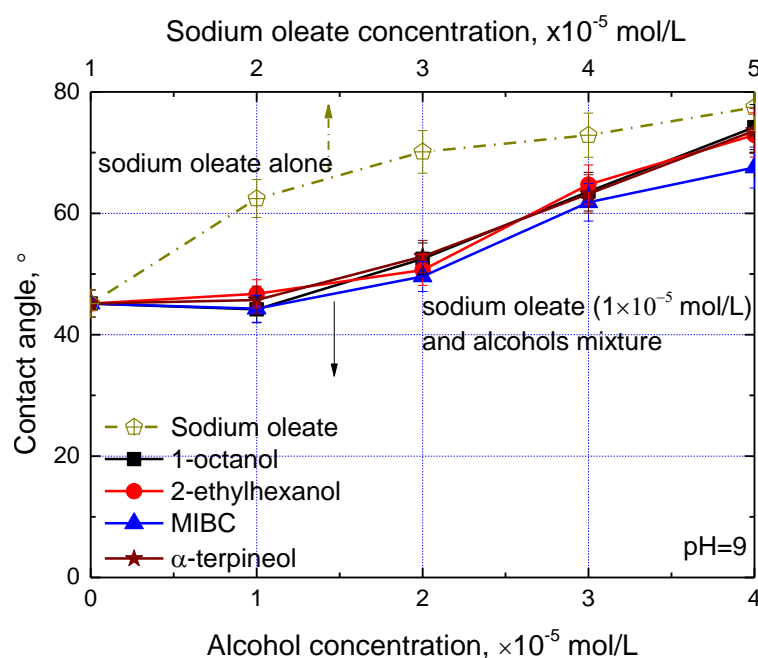
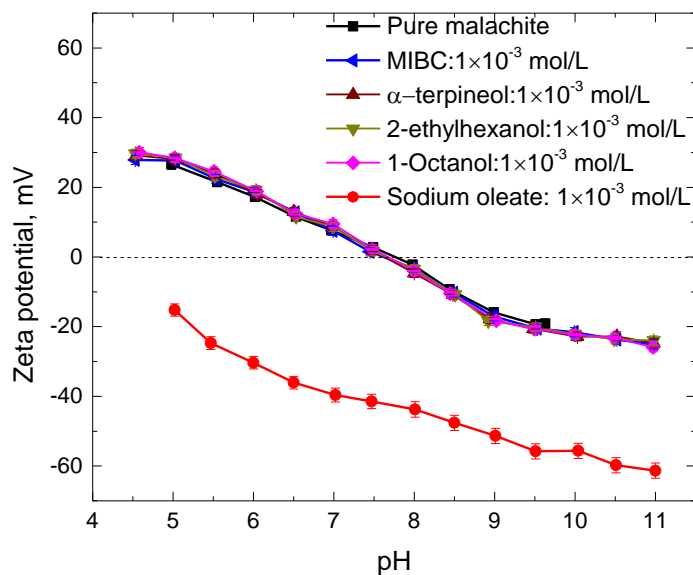


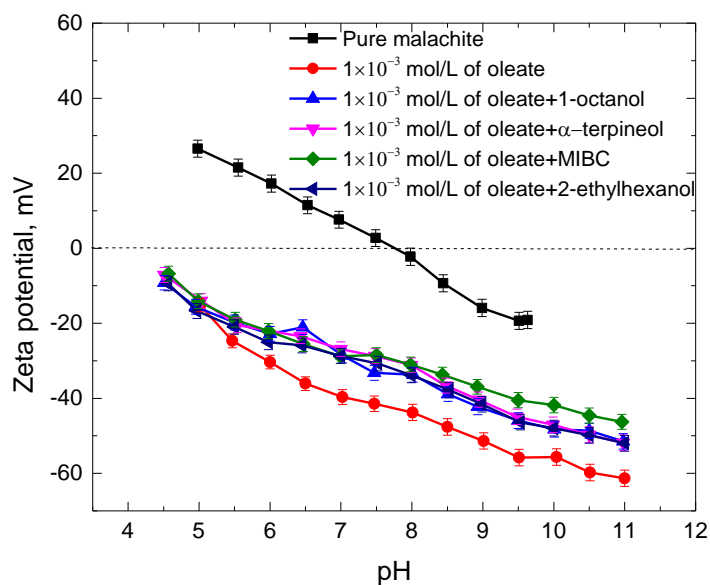
Figure 3.2.7. Contact angle results of malachite treated with sole sodium oleate and mixture of sodium oleate and alcohols

Figure 3.2.8 presents the zeta potentials of malachite in the presence of various concentrations of sodium oleate (a), alcohols (a), and their mixtures (b). The zeta potential of pure malachite decreased with increasing pH, and it found a value of isoelectric point (IEP) at pH 7.8, which is in good agreement with the reported IEP of malachite at pH 8.3 in other study (Li et al., 2015). In the presence of alcohols, namely 1-octanol, 2-ethylhexanol, α -terpineol, and MIBC, the zeta potential of malachite kept the same value (Figure 3.2.8(a)), suggesting that alcohols were not

chemically adsorbed on the malachite surface. In contrast, in the presence of 1×10^{-3} mol/L sodium oleate, the zeta potentials of malachite decreased significantly and the IEP decreased to lower pH value. As analysed by Quast (2016) with the equilibrium diagram of oleate species at various pH (Figure 3.2.2), the mechanism for decreasing the zeta potential of malachite by oleate is different in acidic conditions from that in alkaline solutions. In alkaline solutions, the adsorption of anionic oleate species ($C_{17}H_{33}COO^-$, $(C_{17}H_{33}COO)_2H^-$, and $(C_{17}H_{33}COO)_2^{2-}$) on the malachite surface renders it more negative. In acidic solutions, the decrease of zeta potentials is attributed to the coagulation/precipitation of the colloidal oleate species ($C_{17}H_{33}COOH(l)$ and $C_{17}H_{33}COOH(aq)$), which have isoelectric points around 2–3, on the malachite surface. Notably in Figure 3.2.8(b), in the presence of mixtures of sodium oleate (1×10^{-3} mol/L) and alcohol, the zeta potentials became more negative than that of malachite but were higher than that of the sole sodium oleate (1×10^{-3} mol/L). It suggests the competition/replacement of alcohols to sodium oleate on the malachite surface when the mixture was applied. A similar phenomenon of competition/replacement has been observed and reported in other studies. For example, Rybinski and Schwuger (1986) investigated the single and binary adsorption of anionic alkyl sulfosuccinate and non-ionic nonylphenol pentaglycol ether on scheelite and calcite minerals, and reported that the addition of non-ionic surfactant reduced the adsorption of alkyl sulfosuccinate on both minerals. Lu et al. (1999) found that the presence of polyethylene oxide (PEO) decreased the adsorption of oleate species on apatite, while the contact angle increased.



(a)



(b)

Figure 3.2.8. Zeta potentials of malachite in the presence of (a) sodium oleate, alcohols, and (b) their mixture

In flotation tests, it is shown that the addition of alcohols to the sodium oleate greatly increases the malachite floatability (Figure 3.2.4). In contact angle measurements, co-adsorption of alcohols with sodium oleate on the malachite surface was confirmed. However, a weaker adsorption force of alcohols than that of sodium oleate was hypothesized because of the concave and convex increase of the contact angle with the mixture and the sole sodium oleate, respectively (Figure 3.2.7). In the zeta potential measurements, the competition/replacement of alcohols to sodium oleate on the malachite surface was observed by comparing the zeta potentials of malachite with the mixture and the sole sodium oleate (Figure 3.2.8). Therefore, the co-adsorption of alcohols with sodium oleate on the malachite surface, through hydrophobic interactions between the hydrocarbon chains of sodium oleate and alcohols, is hypothesized and schematically presented in Figure 3.2.9. Furthermore, compared with 1-octanol, 2-ethylhexanol, and α -terpineol, MIBC has a shorter hydrocarbon chain, and thus, there is a weaker hydrocarbon chain interaction between MIBC and sodium oleate. This makes the co-adsorption of MIBC more difficult to render the malachite surface hydrophobic.

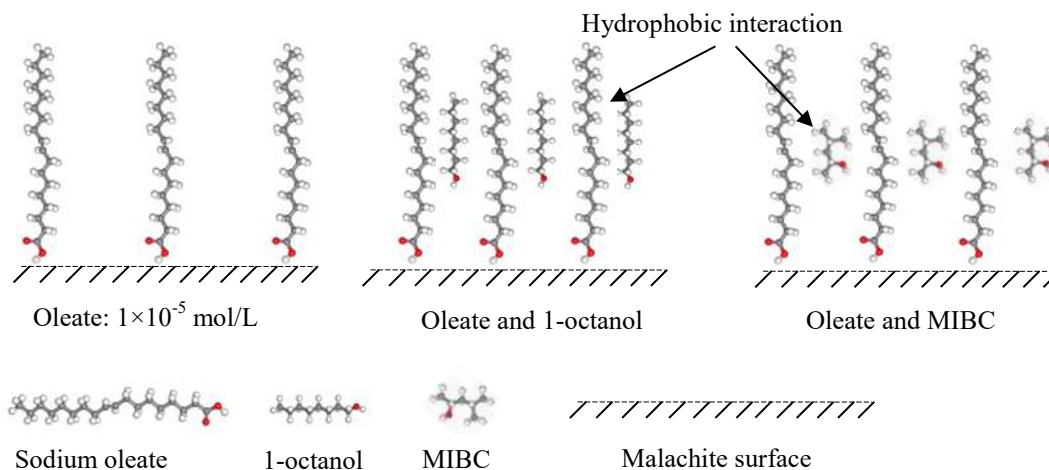


Figure 3.2.9. Schematic presentation of the co-adsorption of sodium oleate and alcohols on malachite surface

3.3 Comminution effect on surface roughness and flotation behavior of malachite surface

Figures 3.3.1–3 show the profiles height and section analyses of the surface A, B, and C measured using 3D non-contact profilometer. From the profile height image, it is easy to observe that, the roughness of surfaces changed from low to high levels in the order of surface A, surface B, and surface C. From the section analysis, R_a and R_q were obtained and the results are shown in Table 3.3.1. R_a value varies from $0.327 \mu\text{m}$ to $3.620 \mu\text{m}$ and R_q value varies from $0.351 \mu\text{m}$ to $4.449 \mu\text{m}$ from surface A to surface C. Section analysis clearly shows that, there were significant differences in the surface roughness among the surfaces. The differences in R_a and R_q values were sufficient to significantly alter the wetting behavior of different malachite surfaces. Comparing the section analysis image, peaks and valleys from surface A and surface B were the same in shape but different in magnitude. There were wide peaks and valleys containing small peaks and small valleys on surface C, hence, in surface C, they were different from surface A and surface B not only in magnitude but also in shape of peaks and valleys.

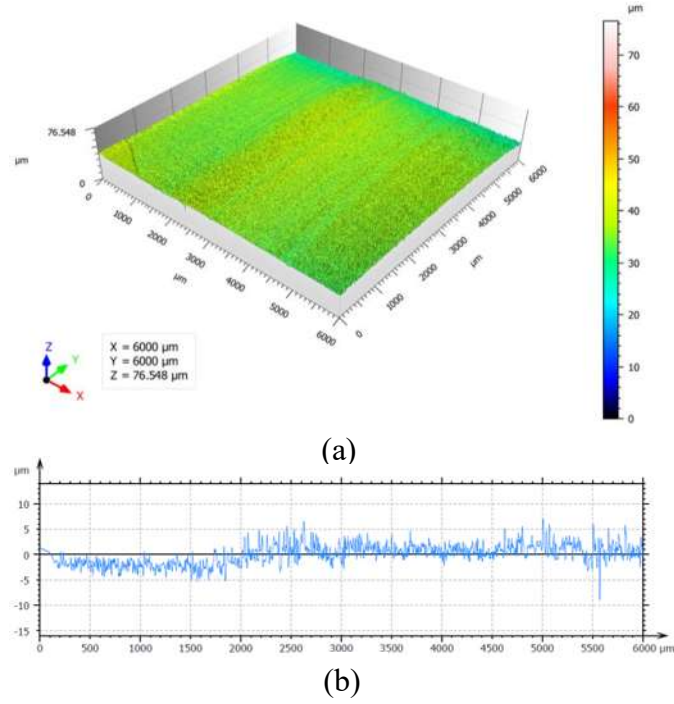


Figure 3.3.1. Profile of malachite surface A: (a) profile height; (b) section analysis.

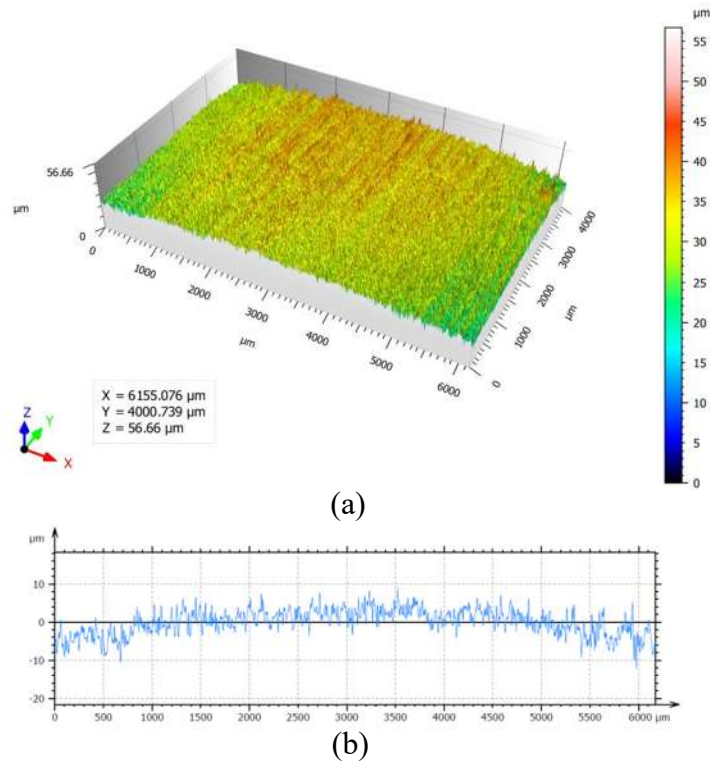


Figure. 3.3.2. Profile of malachite surface B: (a) profile height; (b) section analysis.

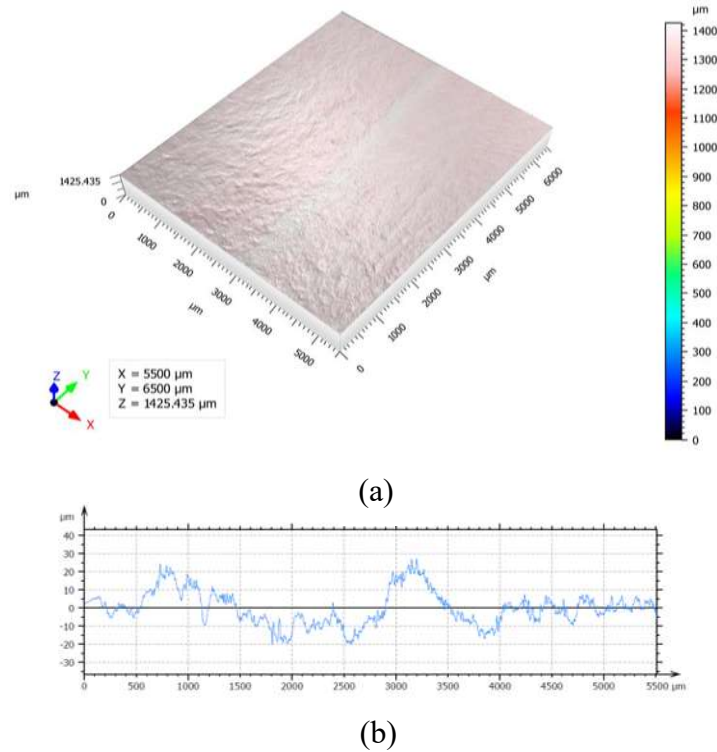


Figure 3.3.3. Profile of malachite surface C: (a) profile height; (b) section analysis.

Table 3.3.1. Roughness parameters of surfaces

Surface	R_a (μm)	R_q (μm)
Surface A	0.327	0.351
Surface B	1.569	1.951
Surface C	3.620	4.449

It is well known that malachite is a hydrophilic mineral, and therefore, the contact angle on malachite surface should be small. Figure 3.3.4 shows the contact angle of malachite surface without sodium oleate treatment. The contact angle value of surface A was 28.3° . For surface B and surface C, as soon as the water droplets contact the surface, they spread into the water film, through which the contact angles were too low to be measured. Müller et al. (2001) also reported that measurements of contact angles below 15° exhibit large error bars. The contact angle results of surface A, B, and C can be explained by the Wenzel model shown in Figure 3.3.5. It is a classical model used to explain the influence of surface roughness on contact angle. Wenzel model considers that surface roughness leads to the increase of liquid-solid contact area. In this case, roughed surface has an actual surface area r times of the ideal surface (perfectly smooth), thus the energy gained in forming the solid-liquid interface will be $r(\gamma_{sg} - \gamma_{sl})$, and the energy required to form liquid-gas interface is the same with an ideal surface. Based on the above, Wenzel put forward Wenzel model in 1936 (Wenzel, 1936).

$$\cos\theta_0 = r \frac{(\gamma_{sg} - \gamma_{sl})}{\gamma_{lg}} = r \cos\theta \text{ (Wenzel equation)}$$

where θ_0 is the contact angle on rough surface, θ is the contact angle on smooth surface, and r is the ratio between the actual surface areas of a rough surface to the projected area.

Since surface A is the smoothest surface among surface A, B, and C, and the surface is hydrophilic, the contact angle value was 28.3° . While the roughness of surface B and C is much greater than that of surface A, so the values of $\cos\theta$ were higher and the contact angle were smaller, and it is reasonable that the contact angle values cannot be measured.



Figure 3.3.4. Contact angle of surface A



Figure 3.3.5. Wetting state on smooth surface (a) and rough surface (b) with hydrophilic materials (Wenzel model).

It is well established that sodium oleate is a powerful collector for malachite (Choi et al., 2016). When it adsorbs on malachite surface, it can change the hydrophilic malachite surface to hydrophobic. As shown in Figure 3.3.6, after sodium oleate treatment, the contact angle from surface A, B, and C changed to 113.3° , 122.0° , and 132.8° respectively. The contact angle values increased with the increase of surface roughness. The difference of contact angle on these surfaces can be explained by both the Cassie model and Wenzel model, which are presented in Figure 3.3.7. For “Wenzel state” liquid droplet, it penetrates the “valleys” of the surface, so the ratio between the actual surface areas of a rough surface to the projected area is more than 1. In addition, the malachite surface now is hydrophobic, and therefore, the hydrophobicity is increased due to the increment of surface roughness. Cassie and Baxter extended the rough surface to heterogeneous surfaces. The energy gained to form the solid-liquid interface will be $r_1(\gamma_{S_1G} - \gamma_{S_1L}) + r_2(\gamma_{S_2G} - \gamma_{S_2L})$ and the energy required to form the liquid-gas interface will stay the same. Therefore, the contact angle can be computed by the Cassie equation (Cassie and Baxter, 1944).

$$\cos\theta_0 = x_1 \cos\theta_1 + x_2 \cos\theta_2 \text{ (Cassie equation)}$$

where θ_1 and θ_2 are the contact angles on different types of surface, and x_1 and x_2 are the fractional areas of different types of surface. The surface can be an air surface caused by trapping

or heterogeneities because of different chemical composition. For “Cassie state” liquid droplet, as shown in Figure 3.3.7 c, it sits on top of the surface structure without penetrating the “valleys”, so the air is enclosed and composite surface forms. The advantage of Cassie model over the Wenzel model is that it describes real systems more accurately (Miller et al., 1996). Surface A is the smoothest among surfaces, so the fractional areas of the air surface is the smallest and the wetting state is more similar to that presented in Figure 3.3.7 a. There are greater air surface percentages with the increase of surface roughness, so the contact angles increased with the increment of surface roughness and the contact angle increased in order of surface A, then B, and then C. Another reasonable explanation to the increment of contact angle is that the surface roughness increases the sites for sodium oleate adsorption on the malachite surface, so larger amount of sodium oleate was adsorbed on the surface at the same projected area, resulting in a larger contact angle of malachite surface. In this system, the increment of contact angle may be attributed to the both reasons explained above.

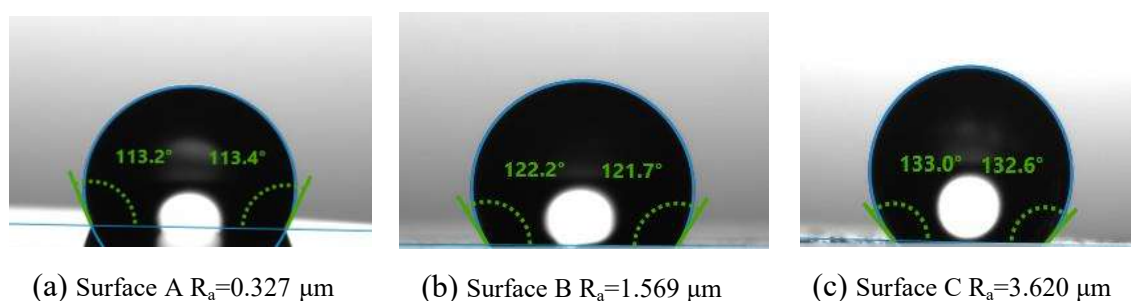


Figure 3.3.6. Contact angle of malachite surface A, B, and C after treatment of 5×10^{-5} mol/L sodium oleate at pH 9.

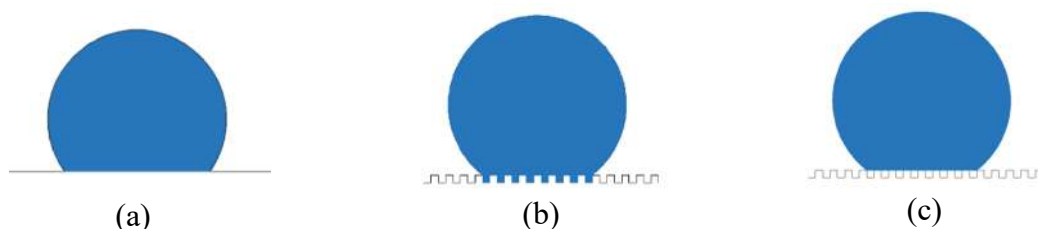


Figure 3.3.7. Wetting state on (a) smooth surface, (b) rough surface (Wenzel model) and (c) rough surface (Cassie model).

Table 3.3.2 presents the specific surface area of malachite samples ground with quartz and montmorillonite measured through the BET method. The specific surface area of malachite ground mixed with quartz is larger than the one with montmorillonite and the values were 1.13 and $0.75 \text{ m}^2/\text{g}$ respectively. The difference between the specific surface areas might be related with the hardness of gangue minerals, which are act as grinding media in this paper. Quartz, which is of greater hardness, can make more scratches on the malachite surface, so the specific surface area of malachite ground with quartz is larger. It is reported that surface roughness can be computed using the following equation (Rahimi et al., 2012):

$$\lambda = \frac{\rho D A_{BET}}{6}$$

where A_{BET} is the BET specific surface area (m^2/g), ρ is the grain density (g/cm^3), D is the average grain diameter (μm), λ is the surface roughness (dimensionless). In this paper, the grain density for malachite is the same and the average grain diameter is almost the same ($-75+38 \mu\text{m}$). Therefore, the difference of A_{BET} from the two samples indicates that malachite ground with quartz have greater roughness than that of ground with montmorillonite.

Table 3.3.2. Specific surface area of malachite

Sample	Malachite (quartz)	Malachite (Montmorillonite)
Specific surface area (m^2/g)	1.13	0.75

Recoveries of malachite ground with quartz and montmorillonite in presence of 2×10^{-5} mol/L sodium oleate are plotted in Figure 3.3.8. The malachite recovery altered slightly at pH range 7-10. While the recoveries of malachite ground with quartz were around 12% higher than the one of ground with montmorillonite. In addition, contact angle measurements showed that surface roughness can affect the contact angle values. Therefore, it is reasonable to conclude that higher roughness of malachite surface leads to larger contact angle after sodium oleate adsorption, as a consequence, the malachite recovery is greater.

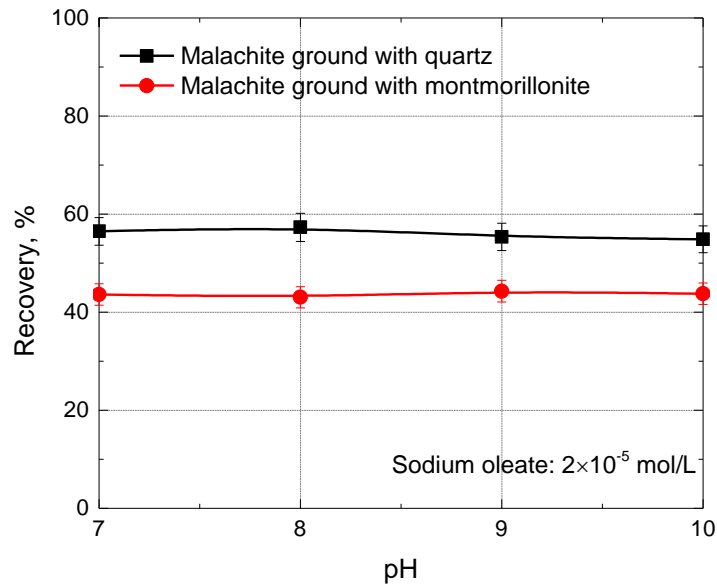


Figure 3.3.8. Recovery of malachite ground with quartz and montmorillonite in the presence of 2×10^{-5} mol/L sodium oleate.

3.4. An example of salinity in flotation: Slime coating of kaolinite on chalcopyrite

Figure 3.4.1 shows the flotation of chalcopyrite in tap water without kaolinite and with 0.09 wt%, 0.24 wt%, and 0.60 wt% of kaolinite. Without kaolinite, high chalcopyrite floatability ($>72\%$)

was obtained in the pH value range from 4 to 11 because of chemisorption of ethyl xanthate onto chalcopyrite (CuEX) (Fuerstenau et al., 2007). A slight decrease of floatability was observed in alkaline solutions with pH values from 8 to 11, in good agreement with the results of Liu and Zhang (2000), who reported that chalcopyrite floatability decreases when the solution pH value is increased to the very alkaline region. In the presence of 0.09 wt% kaolinite, the floatability showed similar behavior as that without kaolinite in pH value range from 4 to 11; however, the floatability was 2% lower. This result suggests that a small amount of kaolinite slightly affects chalcopyrite flotation. In the presence of a medium amount of kaolinite (0.24 wt%), chalcopyrite flotation was moderately affected in pH value range from 4 to 6. However, it was greatly affected in the alkaline pH value range, where the floatability decreased by approximately 10%. In the presence of a large amount of kaolinite (0.60 wt%), chalcopyrite flotation behavior was similar to that with a medium amount of kaolinite, but the floatability was 2% lower.

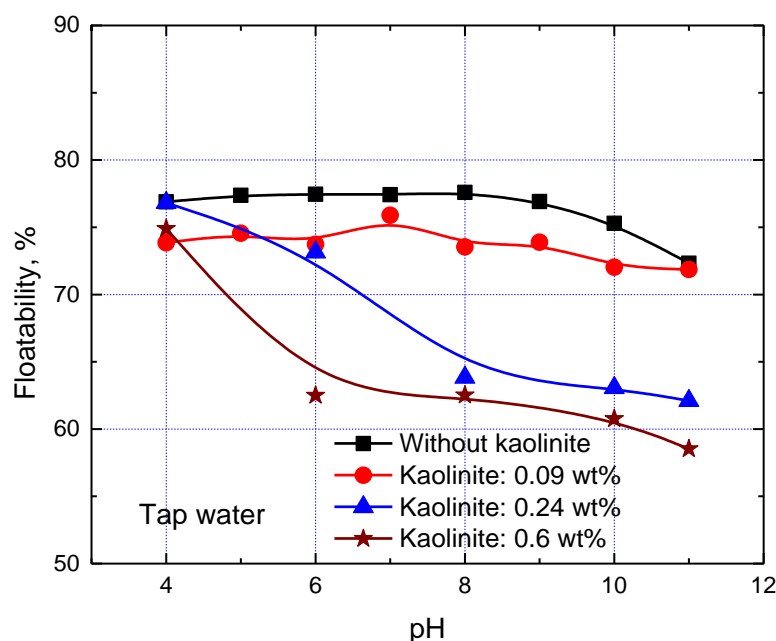


Figure 3.4.1. Flotation of chalcopyrite in tap water with and without kaolinite.

However, at a pH value of 6, the floatability decreased greatly compared with that in the absence of kaolinite. On the basis of these results, the following conclusions can be obtained: (1) the impact of kaolinite on chalcopyrite flotation is higher at alkaline pH levels than at acidic pH levels; (2) a small amount of kaolinite affects chalcopyrite flotation slightly, but this effect increases sharply when the kaolinite amount is increased to a medium level and is maintained in the presence of a large amount of kaolinite; (3) the floatability decreases greatly at a pH value of 6 when a large amount of kaolinite is present. The low floatability of chalcopyrite might be attributable to slime coating or heterocoagulation of kaolinite on chalcopyrite particles, which can be measured on the basis of the turbidity of the slurry. Figure 3.4.2 presents the turbidity of chalcopyrite and kaolinite slurries in tap water at various pH levels. At pH 5, the turbidity was

high, indicating dispersion or low coagulation of the slurry. The turbidity then decreased with increasing pH value, suggesting stronger coagulation at higher pH levels. In the range of $7 \leq \text{pH} \leq 9$, a plateau of turbidity was observed. After this plateau, the turbidity decreased sharply at pH values of 10 and 11, suggesting high coagulation in highly alkaline solutions. Compared with the stability of suspensions with only kaolinite particles, which exhibit coagulation at pH 2.5 and stable dispersions at $5 \leq \text{pH} \leq 10.5$ (Rao et al., 2011), these results indicate heterocoagulation or slime coating is the main factor affecting the stability of chalcopyrite and kaolinite slurries. The stability correlated well with the effect of kaolinite on chalcopyrite flotation, where slime coating was high at high pH levels, resulting in low floatability (Figure 3.4.1).

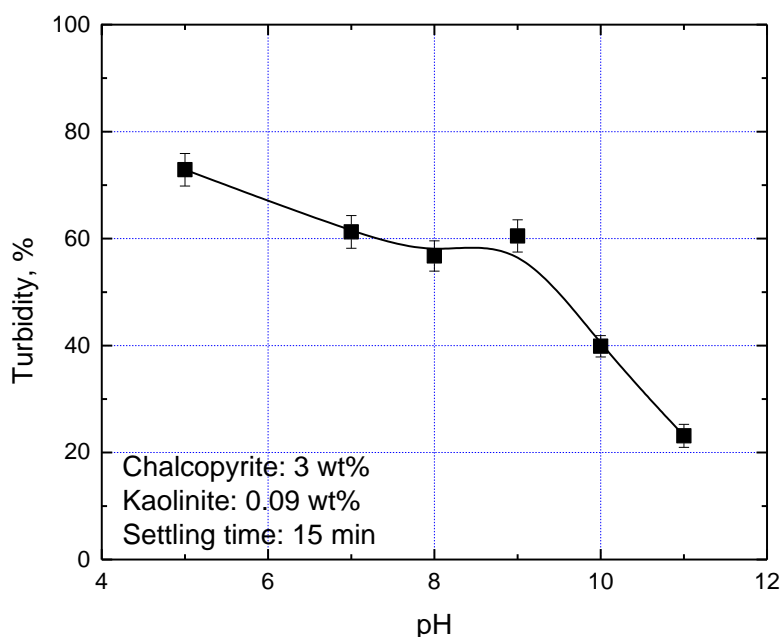


Figure 3.4.2. Turbidity of suspension of chalcopyrite and kaolinite particles in tap water solutions as a function of pH.

The electrokinetic properties of particles have become an important method in studying the stability of suspensions. Figure 3.4.3 presents the zeta-potential distributions of kaolinite, chalcopyrite, and their mixture at various pH levels. The peak zeta potentials of kaolinite were -13.5 , -13.6 , -16.7 , and -19.2 mV at pH 5, 7, 9, and 11, respectively, which is in accordance with a report that the zeta potential of kaolinite is negative and decreases with increasing pH value (Rao et al., 2011). The peak zeta potentials of chalcopyrite were -14.7 , -17.4 , -12.8 , and -6.2 mV at pH 5, 7, 9, and 11, suggesting that the chalcopyrite zeta potential is negative and possesses two high points: one at a pH value less than 5 and one at a pH value greater than 9, consistent with previously reported results (Das and Natarajan, 1997). The zeta-potential distributions of the kaolinite and chalcopyrite mixtures were similar to those of chalcopyrite at

pH 5 and 7, indicating a low slime coating of kaolinite on chalcopyrite at acidic pH levels. However, they resembled the zeta-potential distributions of kaolinite at alkaline pH levels, indicating high slime coating (Chen et al., 2017a). For alkaline pH levels, for example, at pH 11, the interaction of the electrical double layers of chalcopyrite and kaolinite is repulsive; however, coagulation occurred because the absolute zeta potential value of chalcopyrite was too low to produce a strong energy barrier between the particles.

According to the Derjaguin–Landau–Verwey–Overbeek (DLVO) theory (Derjaguin and Landau, 1993), the stability of colloidal dispersions is due to the existence of a potential energy barrier between the particles, which arises from interactions of the electrical double layers and the van der Waals energy. The total potential energy of interaction between the particles (V_T) can be expressed as:

$$V_T = V_R + V_A \quad (1)$$

where V_R and V_A are the electrostatic energy and van der Waals energy between the particles, respectively. The potential energy of the electrical double layer interaction between a plate and a sphere particle can be expressed as (Hiemenz and Rajagopalan, 1997)

$$V_R = \pi \varepsilon_r \varepsilon_0 a \left[(\psi_1^2 + \psi_2^2) \ln \left(\frac{\exp(2\kappa h) + 1}{\exp(2\kappa h) - 1} \right) + 2\psi_1 \psi_2 \ln \left(\frac{\exp(\kappa h) + 1}{\exp(\kappa h) - 1} \right) \right] \quad (2)$$

where ε_0 is the permittivity in vacuum, ε_r is the permittivity of the solvent, a is the particle radius, ψ_1 and ψ_2 are the surface potentials of the sphere and the plate, respectively, and h is the shortest distance between the sphere and the plate. Parameter κ is the Debye reciprocal length and is given by

$$\kappa = \left(\frac{8\pi e^2 CZ^2}{\varepsilon_a k_B T} \right)^{\frac{1}{2}} \quad (3)$$

where e is the charge of the electron (1.602×10^{-19} C), C is the cubic molar concentration of the ion (mol/m^3), Z is the valence of the ion, T is the absolute temperature (K), ε_a is the permittivity of the particle, and k_B is the Boltzmann constant (1.38×10^{-23} J/K)

The van der Waals energy interaction between a plate and a spherical particle is expressed by (Hiemenz and Rajagopalan, 1997)

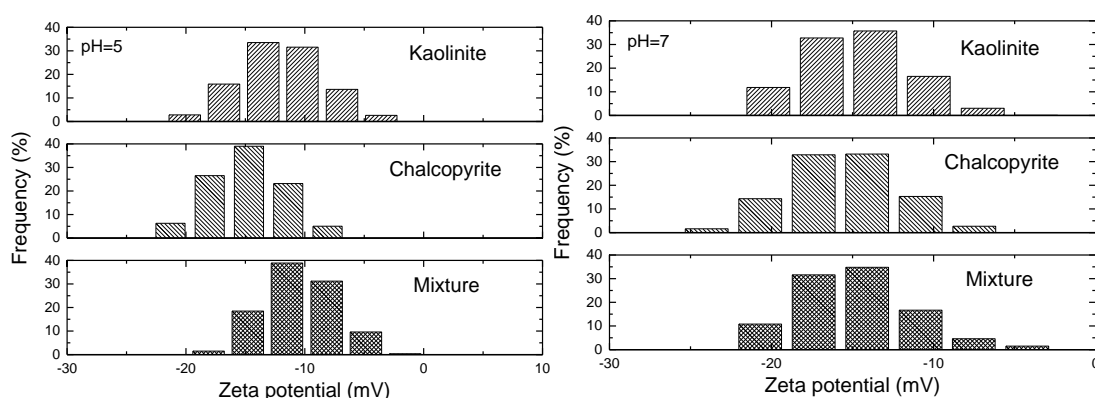
$$V_A = -\frac{A_{123}}{6} \left[\frac{2a(h+a)}{h(h+2a)} + \ln \frac{h}{h+2a} \right] \quad (4)$$

where A_{123} is the Hamaker constant of a plate and a spherical particle in medium 3. And

$$A_{132} \approx (\sqrt{A_{11}} - \sqrt{A_{33}})(\sqrt{A_{22}} - \sqrt{A_{33}}) \quad (5)$$

where A_{11} , A_{22} , and A_{33} are the Hamaker constants of particles 1 and 2 and medium 3 in vacuum, respectively. On the basis of DLVO theory, we calculated the total potential energy of interaction between kaolinite and chalcopyrite particles in aqueous solutions as a function of distance between the particles. The energy barrier was $12k_B T$ at pH 11, which is less than the $15k_B T$ required to inhibit the coagulation of the particles (Chen et al., 2017a; Rao et al., 2011).

Electrical double layers of particles are compressed by salinity in aqueous solutions (Hiemenz and Rajagopalan, 1997; Rao et al., 2017; Rao et al., 2011). Therefore, the slime coating of kaolinite on the chalcopyrite surface and the flotation of chalcopyrite might exhibit different behaviors in saline water solutions. Figure 3.4.4 shows the flotation of chalcopyrite in seawater without kaolinite and with 0.09 wt%, 0.24 wt%, and 0.6 wt% of kaolinite. In the water without kaolinite, the chalcopyrite floatability maintained approximately 80%, indicating that salinity had little effect on the chalcopyrite floatability. Similar as in tap water, the floatability decreased slightly at pH levels greater than 8. In the presence of 0.09 wt% kaolinite, the tendency of floatability at various pH levels resembled that in the absence of kaolinite, whereas the floatability decreased approximately 7%. This decrease was much greater than that of chalcopyrite flotation in tap water (2%) and suggests that a greater slime coating deteriorates chalcopyrite floatability in seawater flotation in the presence of 0.09 wt% kaolinite. This behavior might be a consequence of the salinity compressing the electrical double layers of the particles. At 0.24 wt% of kaolinite, the floatability decreased sharply in the pH value range from 4 to 6 and maintained a plateau of low floatability (about 61%) in the pH value range from 6 to 11. At 0.60 wt% kaolinite, the chalcopyrite floatability exhibited the same tendency as that at 0.24 wt% kaolinite but decreased 3%. These results and the flotation results in tap water (Figure 3.4.1) indicate that 0.24 wt% kaolinite might result in a “saturated” slime coating of kaolinite on the chalcopyrite particles.



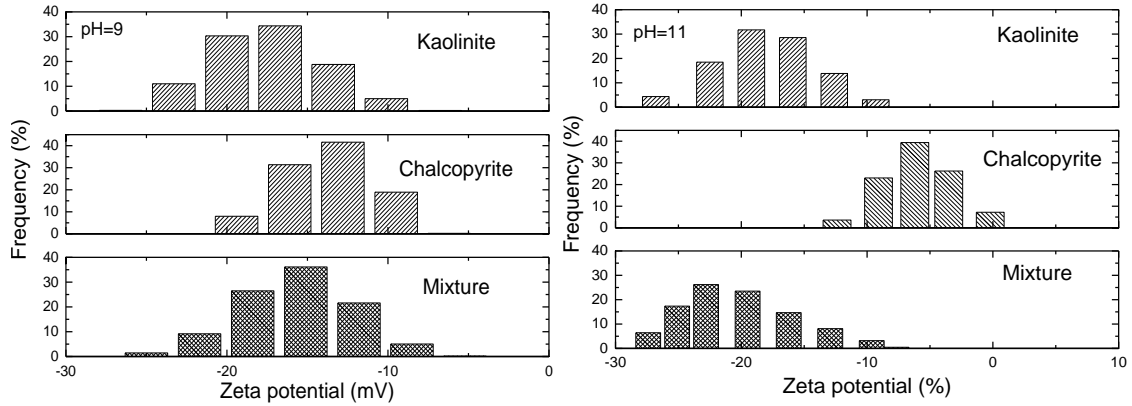


Figure 3.4.3. Zeta potential distribution of kaolinite, chalcopyrite and their mixture as a function of pH.

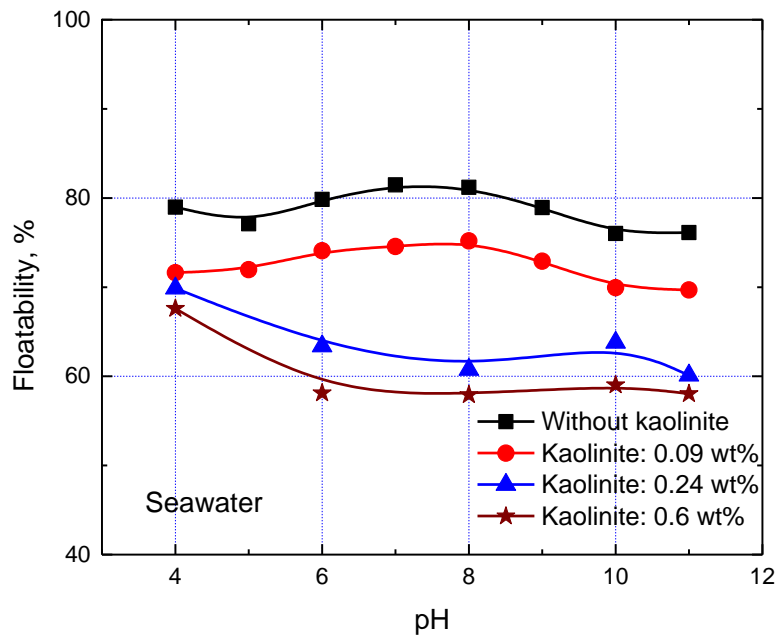


Figure 3.4.4. Flotation of chalcopyrite in seawater without and with kaolinite.

Figure 3.4.5 shows the turbidity of chalcopyrite and kaolinite slurries in seawater at various pH levels. The turbidity at pH 5 was high, indicating dispersion of the suspension. The turbidity then decreased with increasing pH value, which suggests coagulation or formation of a slime coating at higher pH levels. Compared with the plateau of turbidity at $7 \leq \text{pH} \leq 9$ in tap water (Figure 3.4.2), the turbidity decreased continually in seawater. This observation confirms that salinity

compresses the electrical double layers and lowers the energy barriers to induce coagulation of kaolinite and chalcopyrite particles at lower pH levels.

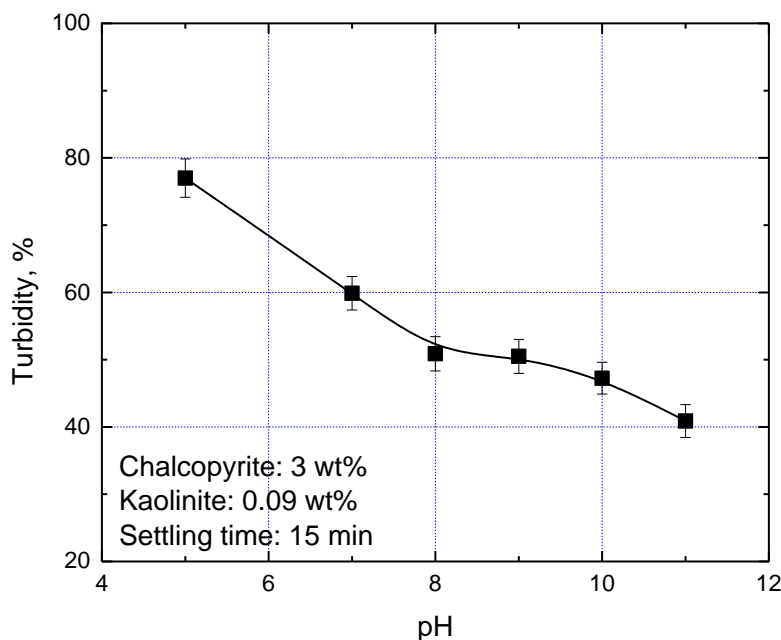


Figure 3.4.5. Turbidity of suspension of chalcopyrite and kaolinite particles in seawater solutions as a function of pH.

In sulfide mineral flotation practice, the process water with recycled water is usually saturated or supersaturated with gypsum (Deng et al., 2013). The salinity of this water differs from that of seawater, which might lead to a distinguishable effect on the slime coating of kaolinite on chalcopyrite. Figure 3.4.6 shows the flotation of chalcopyrite in gypsum-saturated water without kaolinite and with 0.09 wt%, 0.24 wt%, and 0.60 wt% of kaolinite. In the absence of kaolinite, the chalcopyrite floatability was high at $4 \leq \text{pH} \leq 10$ and then decreased at pH 11. In the presence of 0.09 wt% kaolinite, the chalcopyrite floatability decreased approximately 2% from pH 4 to pH 11 compared with that in the absence of kaolinite. In the presence of 0.24 wt% of kaolinite, a slight decrease of floatability was noted at pH 4; the floatability then decreased sharply as the pH value was increased to 8. It thereafter maintained a plateau at $8 \leq \text{pH} \leq 11$. In the presence of 0.60 wt% kaolinite, the chalcopyrite floatability decreased sharply at $4 \leq \text{pH} \leq 6$, but slightly at $8 \leq \text{pH} \leq 11$ compared with that in the case of 0.24 wt% kaolinite, which might be attributable to calcium ions (Ca^{2+}) and hydrolyzed calcium ions ($\text{Ca}(\text{OH})^+$) adsorbing specifically onto kaolinite and inducing extensive slime coating of kaolinite on chalcopyrite. The adsorption of $\text{Ca}(\text{OH})^+$ and Ca^{2+} can reverse the zeta potential of kaolinite, resulting in attractive interaction between electrical double layers of chalcopyrite and kaolinite. The adsorption models of $\text{Ca}(\text{OH})^+$ and Ca^{2+} ions on the surface of kaolinite are shown as follows (Rao et al., 2011; Rao et al., 2012):

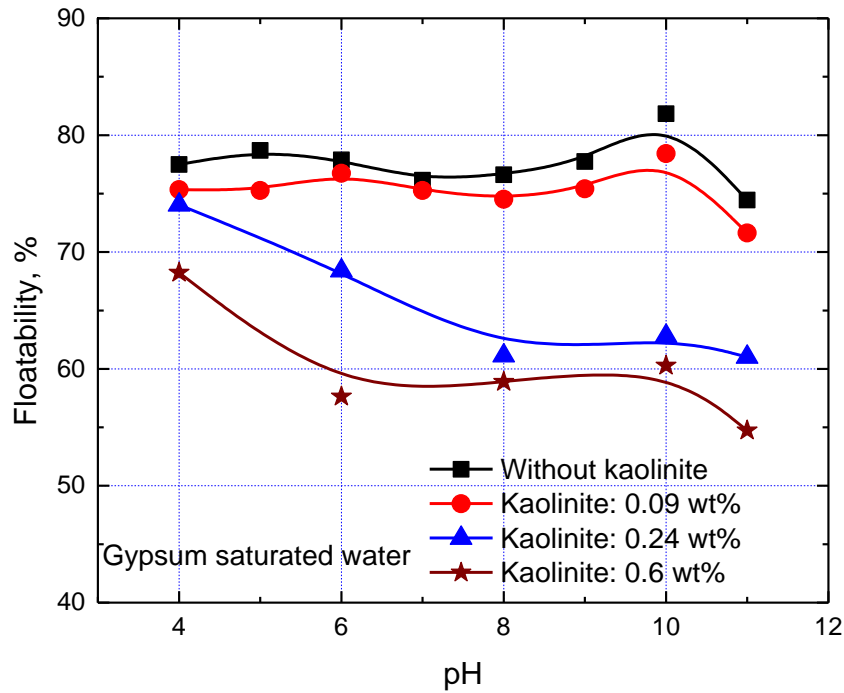
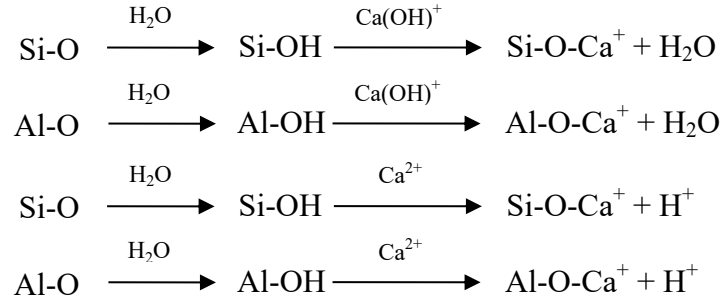


Figure 3.4.6. Flotation of chalcopyrite in gypsum saturated water with and without kaolinite.

Figure 3.4.7 shows the turbidity of chalcopyrite and kaolinite suspensions in gypsum-saturated water at various pH levels. The turbidity decreased with increasing pH value, indicating that coagulation occurred with increasing pH value. The same as with the suspensions in tap water, a plateau of turbidity at $7 \leq \text{pH} \leq 9$ was observed. Notably, the turbidity in gypsum-saturated water with pH 5 was much lower than that in pH 5 tap water or seawater. This result corresponds well with the flotation results (0.60 wt% kaolinite) and verifies the specific adsorption of Ca^{2+} and hydrolyzed Ca^{2+} onto the kaolinite surface, resulting in the negative surface charge decreasing or reversing, thus inducing coagulation (Rao et al., 2011).

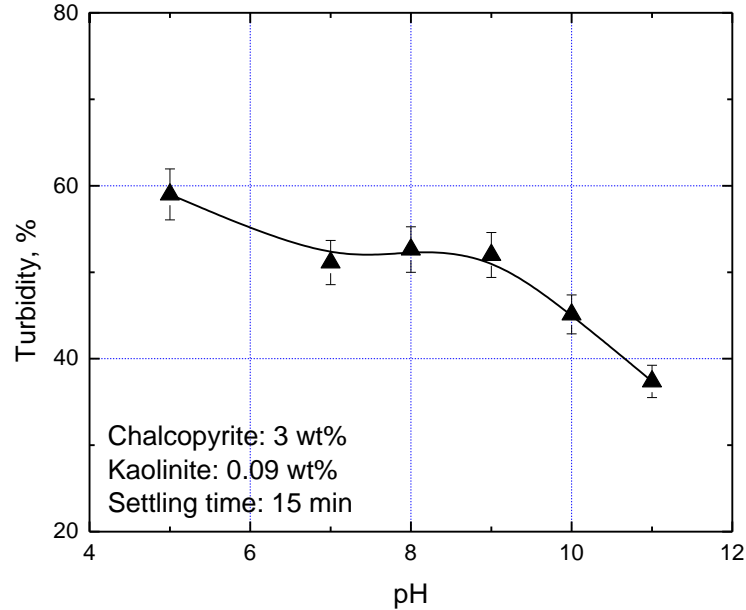
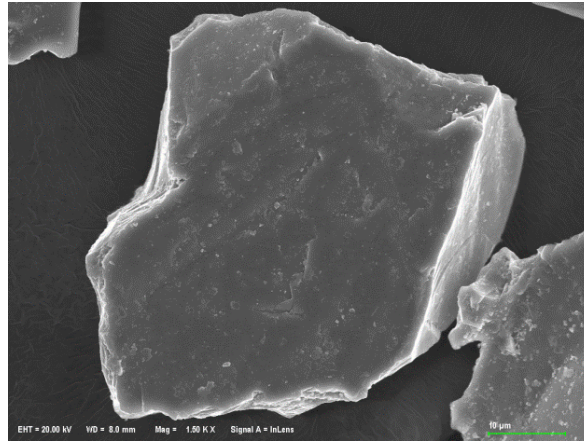
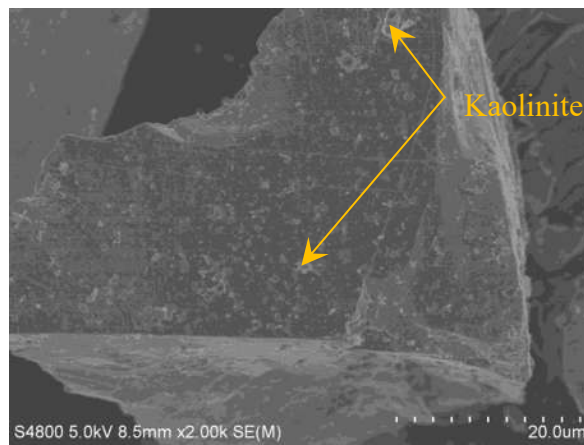


Figure 3.4.7. Turbidity of suspension of chalcopyrite and kaolinite particles in gypsum saturated solutions as a function of pH.

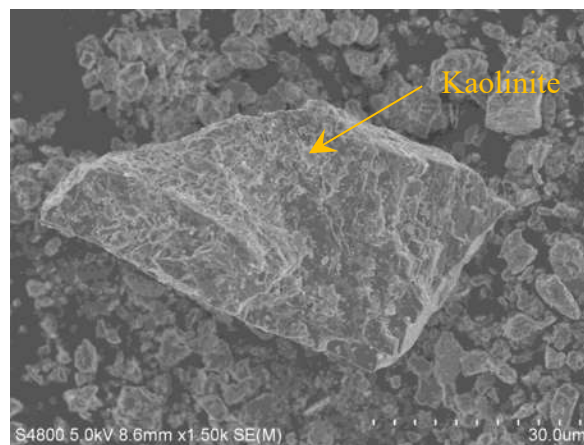
Notably, the relationship between the slime coating (kaolinite on chalcopyrite) and the floatability of chalcopyrite is nonlinear because a sufficient coating is required to depress the flotation. As noted in the discussion of the flotation results in tap water, seawater, and gypsum-saturated water, the increase of the kaolinite content from 0.09 wt% to 0.24 wt% induced a substantial decrease of chalcopyrite floatability in the pH value range of slime coating ($6 \leq \text{pH} \leq 11$). This decrease might be explained by the different degrees of coating of kaolinite on chalcopyrite particles. At 0.09 wt% kaolinite, although a slime coating is formed under some specific conditions, the coating of kaolinite is insufficient to prevent flotation of the chalcopyrite particles. Figure 3.4.8 shows scanning electron microscopy (SEM) images of a chalcopyrite particle, concentrate, and tailing corresponding to chalcopyrite flotation in tap water with 0.24 wt% of kaolinite. A slime coating is observed on the concentrated chalcopyrite particles, and extensive slime coating is required to depress flotation.



(a)



(b)



(c)

Figure 3.4.8. SEM images of a chalcopyrite particle (a), concentrate (b), and tailing (c) in chalcopyrite flotation in tap water with 0.24 wt% of kaolinite.

3.5 Reexamining the adsorption of octyl hydroxamate on malachite surface: forms of molecules and anions

Figure 3.5.1 presents the depletion amount of octyl hydroxamate as a function of pH at an equilibrium concentration of 4×10^{-4} mol/L, showing that the depletion amount first decreased with the increase of pH, reaching a minimum at around pH 7.5, to increase from pH 7.5 to 9, reaching the maximum at about 9. The depletion amount decreased again with further increases of pH. It is worth pointing out that the depletion amount includes both the hydroxamate adsorbed onto the malachite surface and that precipitated as copper hydroxamate in bulk solution. As shown in the species distribution diagram of octyl hydroxamate in Figure 3.5.2, octyl hydroxamate molecules and anions predominate at pH below and above 9, respectively, reaching the equal concentration at pH 9 (i.e., $pK_a=9$). Using the database available in Medusa thermodynamic software (Puigdomenech, 2004), the malachite solubility diagram of Figure 3.5.3 was prepared, which shows the logarithmic concentration distribution of copper and carbonate species as a function of pH. As shown in this figure, Cu^{2+} is the predominant species at pH below 6, which is capable of precipitating hydroxamate, depleting the collector available for malachite flotation. Thus, from pH 4.5 to 6, most of octyl hydroxamate added was in the molecular form and was consumed by the dissolved copper ions in the bulk solution (Lenormand et al., 1979), and this phenomenon was more evident at pH 4.5 since all the octyl hydroxamate added to the solution was consumed. With increasing pH from 6 to 7.5, both adsorption of octyl hydroxamate molecule and bulk precipitation of copper hydroxamate may account for the depletion of octyl hydroxamate, while adsorption plays an increasingly dominant role with the decrease of Cu^{2+} concentration in the bulk solution. At pH above 7.5, the removal of hydroxamate increased due to higher adsorption of the molecule on the malachite surface, while the maximum adsorption occurred in the vicinity of pH 9, most probably result from the coadsorption of both molecules and anions. The change of octyl hydroxamate depletion from pH 9 to 7 and 9 to 11 is not significant and does not reflect the substantial change in the concentration of the molecular and ionic forms of the collector in the two pH ranges. This behavior probably indicates that both the octyl hydroxamate molecule and anion are capable of adsorbing on the malachite surface. Finally, at pH above 11, the removal of octyl hydroxamate decreased sharply due to the electrostatic repulsion that occurs between the octyl hydroxamate anions and the highly negatively charged malachite surface.

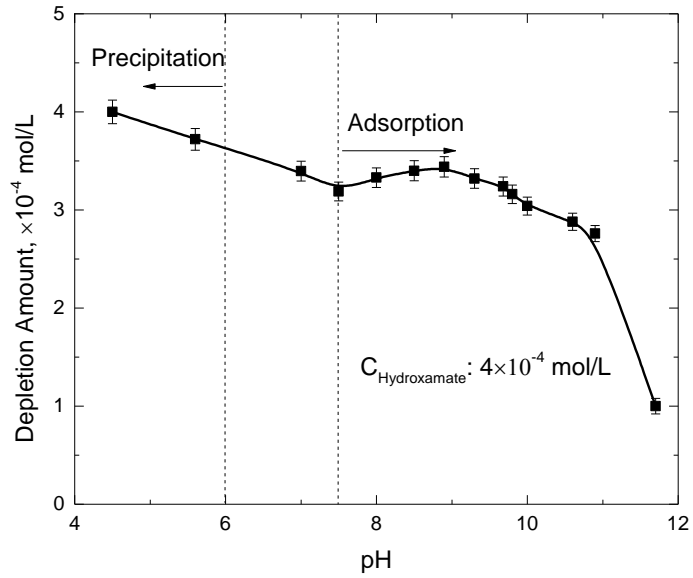


Figure 3.5.1. Depletion amount of K-octyl hydroxamate as a function of pH at concentration of 4×10^{-4} mol/L.

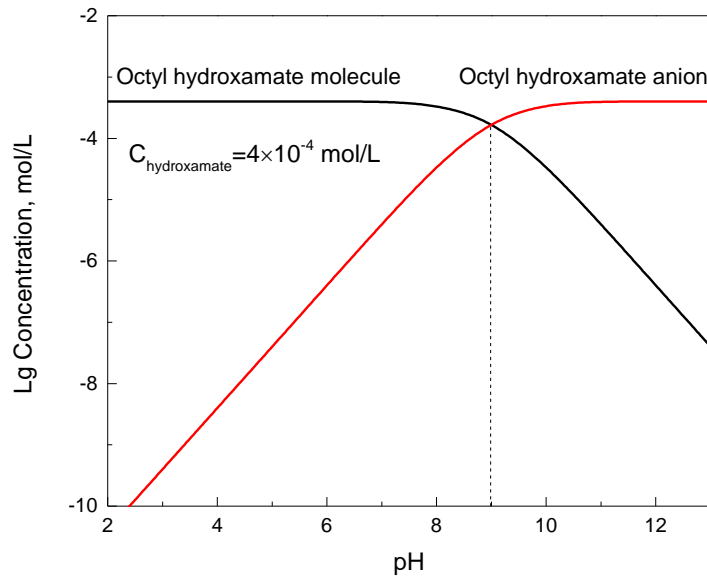


Figure 3.5.2. Logarithmic diagram of potassium-octyl hydroxamate hydrolysis components.

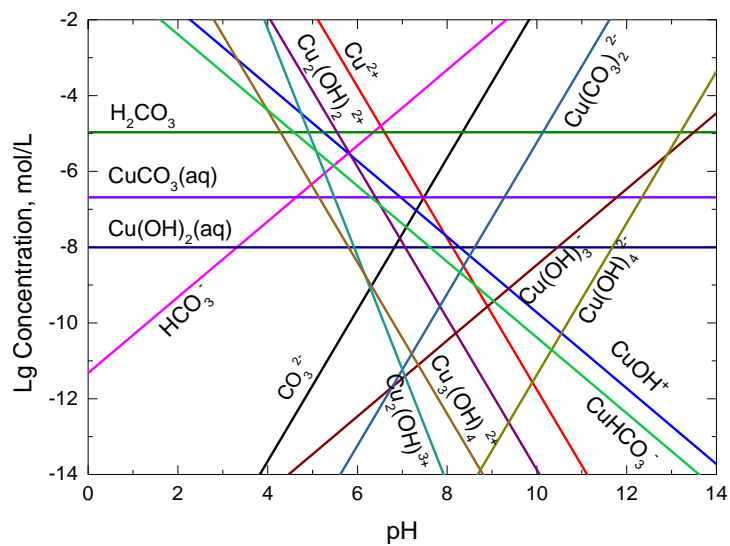


Figure 3.5.3. Solubility diagram of malachite (saturated solution) showing the logarithmic concentration distribution of copper and carbonate species as a function of pH, in equilibrium with the atmosphere (activity of $\text{CO}_2(\text{g})$ equal to $1 \times 10^{-3.5}$ atm).

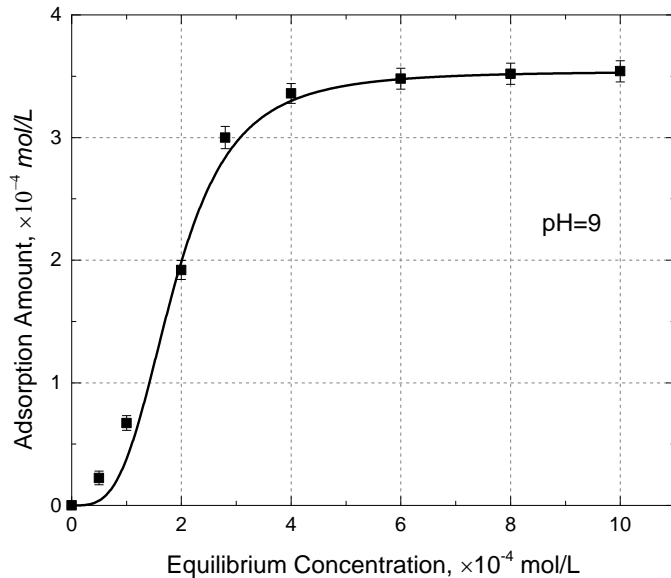


Figure 3.5.4. Adsorption isotherm of K-octyl hydroxamate on malachite at pH 9 (ambient temperature).

Figure 3.5.4 exhibits the adsorption isotherm of octyl hydroxamate on malachite at pH 9, showing that with the increase of the equilibrium concentration of octyl hydroxamate, the

adsorption amount increased steadily, reaching a plateau at the initial concentration about 4×10^{-4} mol/L octyl hydroxamate. The isotherm belongs to the Langmuir isotherm behavior, suggesting that octyl hydroxamate chemically adsorbs onto the malachite surface.

The effect of potassium octyl hydroxamate on the zeta potential of malachite was measured as a function of pH, and the results are plotted in Figure 3.5.5. The zeta potential of pure malachite decreased as pH was increased, showing the occurrence of the isoelectric point at pH 8.4, which is in good agreement with that reported at pH 8.7 by Liu et al. (2016). The shift of IEP and the adsorption of octyl hydroxamate anion at the negatively charged malachite surface at pH above 8.4, indicate that octyl hydroxamate adsorbs at the malachite surface by chemical adsorption. Take the zeta potential of hydroxamate treated malachite and copper hydroxamate into consideration, octyl hydroxamate did not cover all the particle surfaces. With the increase of hydroxamate concentration, the zeta potential of the malachite surface was progressively becoming similar to that of copper hydroxamate precipitates, inferring the formation of copper hydroxamate chelates at the malachite surface (Ananthapadmanabhan and Somasundaran, 1985). At pH above 9, the anion form of octyl hydroxamate predominates, so it is reasonable to attribute the decrease of zeta potential to the adsorption of octyl hydroxamate anions at the malachite surface. It is interesting to note that at pH below 9, where the octyl hydroxamate molecule is the predominant species, zeta potential values of malachite were still reduced in the presence of octyl hydroxamate. There are two possible reasons for the behavior observed at pH 7.5-9. First, acidic nature of N-H group in octyl hydroxamate molecule reduces the zeta potential of the mineral surface (Raghavan and Fuerstenau, 1975). Secondly, the surface chelate formed through the specific interaction of the octyl hydroxamate species with the malachite surface, resulting in a highly negative charge of precipitated copper hydroxamate. At pH below 7.5, where precipitation of copper hydroxamate plays an increasingly important role with decreasing pH for the depletion of octyl hydroxamate in the bulk solution, the zeta potential measured may be the result of the weighted average of the zeta potentials of the malachite bearing adsorbed octyl hydroxamate and the copper octyl hydroxamate precipitate.

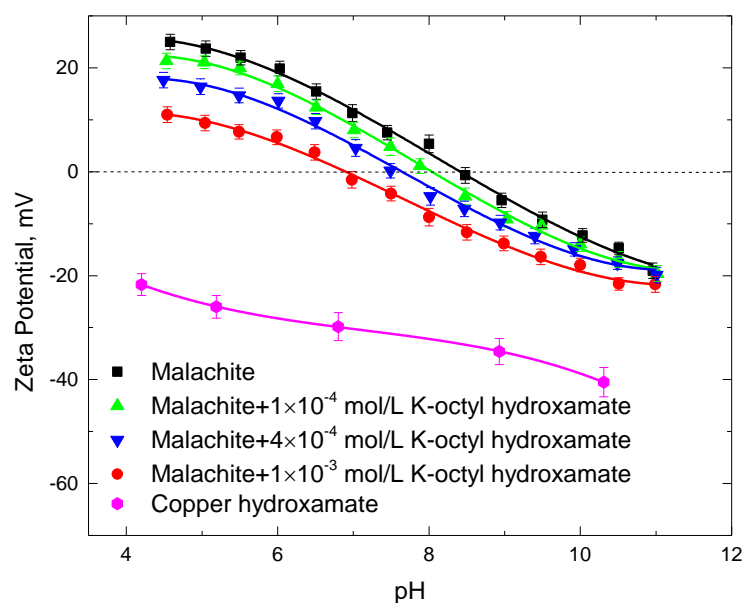


Figure 3.5.5. Zeta potential of malachite as function of pH in the presence and absence of octyl hydroxamate. The zeta potential of copper hydroxamate precipitates is also shown.

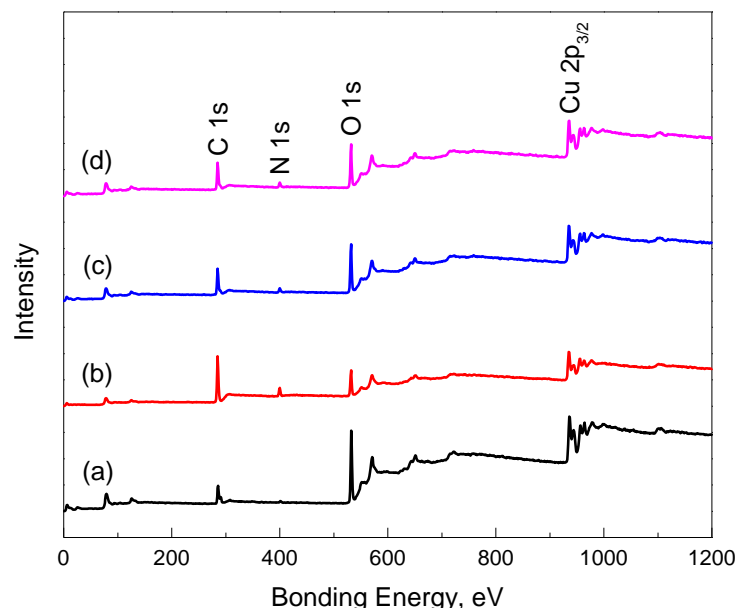


Figure 3.5.6. The XPS survey spectra of malachite (a), synthesized copper hydroxamate precipitates (b), and malachite conditioned with octyl hydroxamate at pH 7 (c) and 9 (d).

Figure 3.5.6 shows the XPS survey spectra of malachite, copper hydroxamate precipitates, and malachite treated with octyl hydroxamate at pH 7 and 9, over a binding energy range of 0 to 1200 eV. The appearance of N 1s peaks after contacting malachite with octyl hydroxamate at pH 7 and 9 indicates that both octyl hydroxamate anion and molecule adsorb onto the malachite surface. The atomic concentrations of elements N 1s, O 1s, and Cu 2p_{3/2} determined by XPS are summarized in Table 3.5.1, along with their atomic concentration ratio with respect to Cu. Since additional carbon was added for XPS measurements, the concentrations of C 1s are not listed. In the copper hydroxamate precipitate, the atomic concentration ratio of N and O with respect to Cu was 1.09 and 2.14, respectively. So C₈H₁₆NO₂Cu may correspond to the condensed formula of the precipitate, suggesting that one octyl hydroxamate molecule or anion reacts with one copper ion (the hypothetical number of C and H atoms were added). After conditioning malachite with octyl hydroxamate at pH 7 and 9, N/Cu and O/Cu ratio shifted to intermediate values of that in malachite and copper hydroxamate, which may suggest the formation of a layer of copper hydroxamate on the malachite surface.

Table 3.5.1. Atomic concentration of N, O, and Cu in malachite, copper hydroxamate precipitate, and malachite conditioned with octyl hydroxamate at pH 7 and 9.

Species	Atomic concentration (%)			Atomic concentration ratio with respect to Cu (%)		
	N	O	Cu	N	O	Cu
Malachite	0.44	45.26	14.80	0.03	3.06	1
Copper octyl hydroxamate	7.37	14.39	6.74	1.09	2.14	1
Malachite + octyl hydroxamate (pH=7)	5.04	34.35	11.34	0.44	3.03	1
Malachite + octyl hydroxamate (pH=9)	5.13	32.06	11.16	0.46	2.87	1

Figure 3.5.7 presents the high-resolution XPS $\text{Cu } 2p_{3/2}$ spectra of malachite, copper hydroxamate, and malachite after conditioning with octyl hydroxamate at pH 7 and 9. In these spectra, the peaks occurring at around 935.73 and 935.04 eV were respectively assigned to copper of the malachite surface lattice and to copper of the copper hydroxamate precipitate. After malachite conditioning with octyl hydroxamate at pH 9, the $\text{Cu } 2p_{3/2}$ XPS bands of the malachite surface were divided into two components: one at around 934.96 eV owing to the complexing of octyl hydroxamate with the copper of malachite surface, and the second at around 935.62 eV, belonging to the copper of the malachite surface. This indicates that hydroxamate chelates are formed on the malachite surface after conditioning with octyl hydroxamate at pH 9. After malachite conditioning with octyl hydroxamate at pH 7, the $\text{Cu } 2p_{3/2}$ XPS bands of malachite surface showed the same components (934.97 eV) as those occurring at pH 9, indicating the formation of the same copper hydroxamate chelates on the malachite surface.

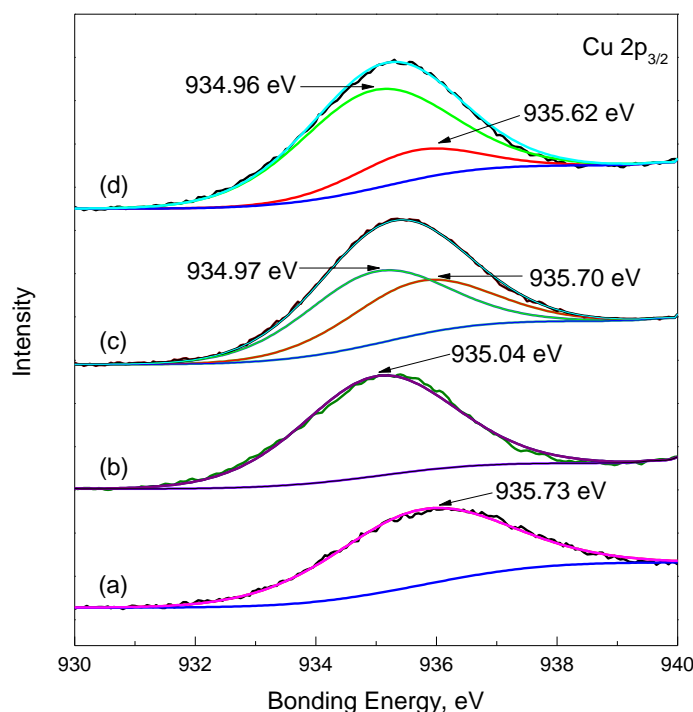


Figure 3.5.7. High-resolution XPS $\text{Cu } 2p_{3/2}$ spectra of malachite (a), synthesized copper hydroxamate precipitates (b), malachite after conditioning with octyl hydroxamate at pH 7 (c), and 9 (d).

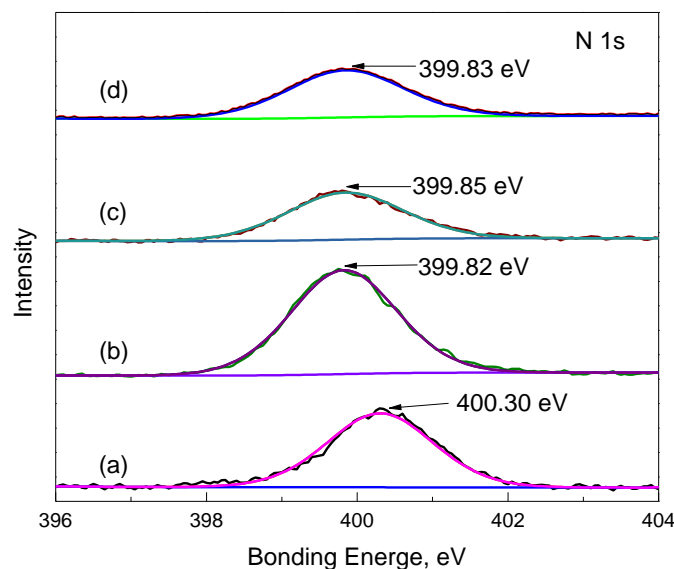


Figure 3.5.8. High-resolution XPS N 1s spectra of potassium octyl hydroxamate (a), synthesized copper hydroxamate precipitates (b), and malachite after conditioning with octyl hydroxamate at pH 7 (c) and 9 (d).

The presence of hydroxamate on the malachite surface can be best shown by comparing the N 1s signals from the XPS spectra since the other two elements, oxygen and carbon, in octyl hydroxamate are easily overlapped by signals from the substrate and/or contaminants. Figure 3.5.8 presents the high-resolution XPS N 1s spectra of potassium octyl hydroxamate, synthesized copper hydroxamate precipitates, and malachite after conditioning with octyl hydroxamate at pH 7 and 9. The peaks occurring at 400.30 and 399.82 eV correspond to the N atom in potassium octyl hydroxamate and synthesized copper hydroxamate precipitates, respectively, which are in good agreement with that reported at 400.30 eV for octyl hydroxamate by Ni and Ni and Liu (2012), and at 400.00 eV for copper hydroxamate precipitates by Hope et al. (2011). The peak belonging to N in potassium octyl hydroxamate shifts from 400.3 eV to 399.85 and 399.83 eV, respectively, after conditioning with malachite at pH 7 and 9, suggesting that octyl hydroxamate chemically adsorbs at the malachite surface. After conditioning malachite with octyl hydroxamate at pH 7 and 9, the N 1s spectra showed similar peaks to those of copper hydroxamate precipitates, indicating the formation of this compound on the malachite surface. No peaks occurred at 400.30 eV after conditioning malachite with octyl hydroxamate, inferring the absence of physically adsorbed octyl hydroxamate at pH 7 and 9.

The XPS spectra in Figure 3.5.6 and data in Table 3.5.1 suggest that octyl hydroxamate adsorbs on the malachite surface at both pH 7 and 9, while the Cu 2p_{3/2} spectra of Figure 3.5.7 suggest that the copper atoms on the malachite surface participate in the adsorption process, and the same copper octyl hydroxamate chelate is formed on the malachite surface at pH 7 and 9. In turn, the N 1s spectra in Figure 3.5.8 indicate that no physically adsorbed octyl hydroxamate is observed at pH 7 and 9. It has been suggested that, for semi-soluble minerals, interactions between mineral and hydroxamate occur mainly through surface reactions and bulk precipitation (Marion et al., 2017). It has also been reported that the most probable mechanism for hydroxamates adsorption onto minerals is that cations from the mineral surface hydrolyze in solution, forming complexes

that chemisorb at the interface, providing sites for collector adsorption (Assis et al., 1996). Thus, the aqueous speciation of malachite plays a crucial role in collector adsorption. As shown in Figure 3.5.3, Cu^{2+} is the predominant species at pH below 6, which is capable of precipitating hydroxamate, depleting the collector available for malachite flotation. While $\text{Cu}(\text{OH})^+$ and $\text{Cu}(\text{CO}_3)_2^{2-}$ are the main hydrolysate species in the solution at pH 6-9 and 9-11, respectively. In addition, it has been reported that after reacting with copper, octyl hydroxamate changes from the keto Z conformation to enol configuration (Hope et al., 2011). According to the above discussion, the interaction mechanisms suggested in this work are shown in Figure 3.5.9. At pH below 6, octyl hydroxamate is mainly consumed by dissolved copper ions in the bulk solution. In the pH range 6-9, the predominant interaction is that octyl hydroxamate molecules chemically react with the $\text{Cu}(\text{OH})^+$ site at the malachite surface. While there is still a certain amount of octyl hydroxamate molecules are consumed by dissolved copper ions in pH range 6-7.5. At pH above 9, the interaction involves octyl hydroxamate anions, which react chemically with the $\text{Cu}(\text{CO}_3)_2^{2-}$ site at the malachite surface, rendering the surface hydrophobic. At pH 9, where the maximum adsorption occurs, octyl hydroxamate molecules and anions co-adsorb at the malachite surface. Moreover, the formation of the same copper hydroxamate chelates on the malachite surface at pH above 6 substantiates the proposed interaction mechanism. The release of H^+ into solution at pH 9 during adsorption, as shown in Figure 3.5.9, has been confirmed in the adsorption experiment by continuously monitoring the pH. The slowly dropped pH during the adsorption process supports the proposed interaction mechanism.

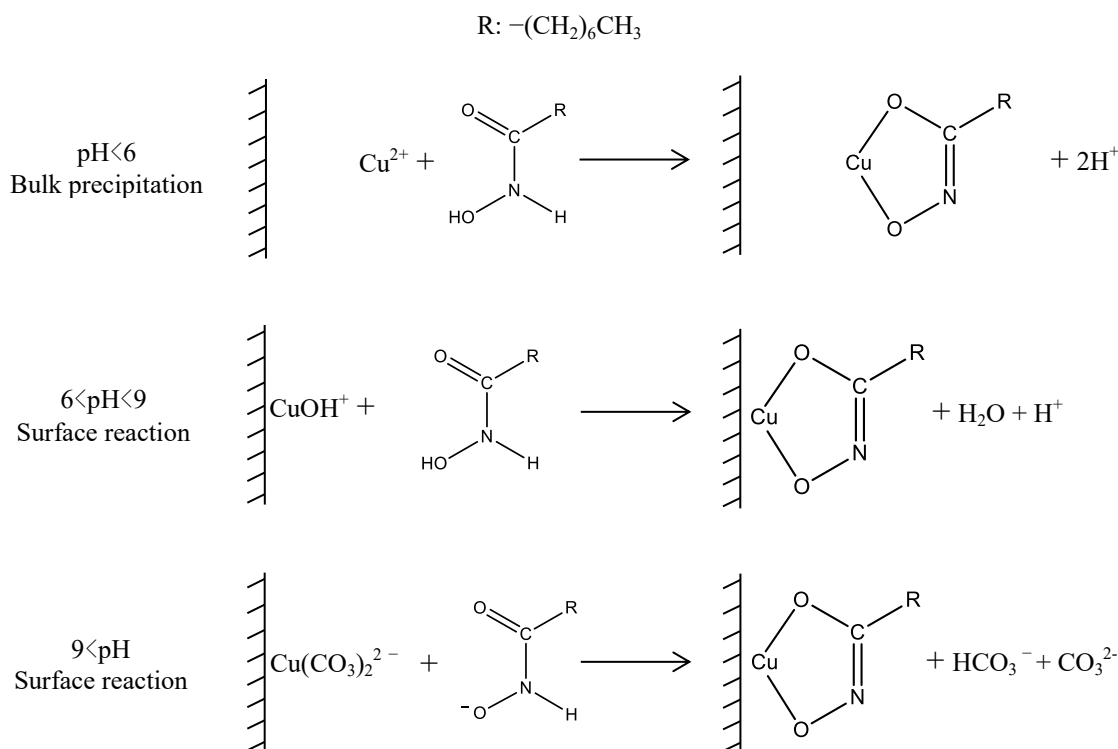


Figure 3.5.9. Proposed interaction model of K-octyl hydroxamate with malachite.

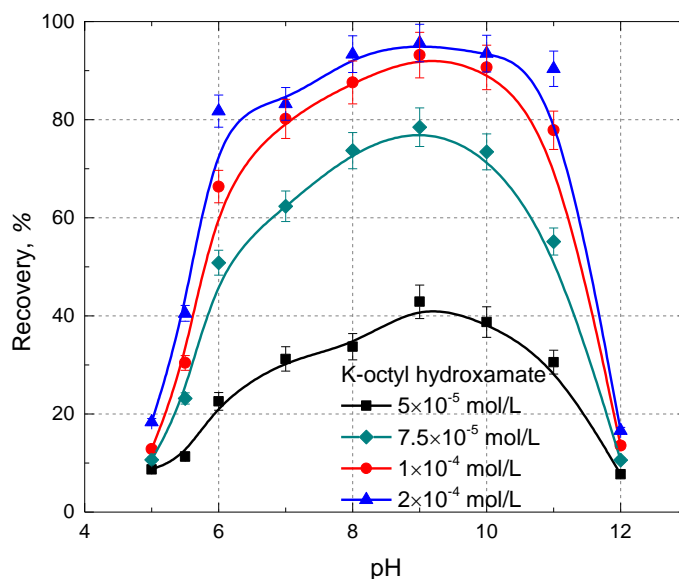


Figure 3.5.10. Flotation recovery of malachite as a function of pH at different concentration of K-octyl hydroxamate.

Figure 3.5.10 presents the flotation recovery of malachite ($-75 + 38 \mu\text{m}$) as a function of pH at different concentration of K-octyl hydroxamate. At 5×10^{-5} mol/L octyl hydroxamate, the recovery of malachite was relatively low (below about 43%), sharply increased when the concentration of octyl hydroxamate was increased to 1×10^{-4} mol/L due to the increasing adsorption of octyl hydroxamate, and increased gradually from 1×10^{-4} to 2×10^{-4} mol/L because limited sites on the malachite surface remained available for octyl hydroxamate adsorption. In terms of the flotation pH, the recovery of malachite increased from pH 5 to 9, reaching its maximum at pH 9, and decreased upon further increase of the pH. It is also observed in Figure 3.5.10 that the decrease in recovery of malachite was relatively small as the pH was lowered from 9 to 6, and raised from 9 to 11. This behavior suggests that both octyl hydroxamate molecules and anions are effective species for the flotation of malachite, which is in line with the adsorption results and the proposed adsorption mechanism in Figure 3.5.9. The sharp decrease of malachite recovery observed at pH below 6, is attributed to the precipitation of hydroxamate molecules by the dissolved copper ions that predominate at pH below 6. Furthermore, the decrease of malachite recovery observed at pH above 11, is attributed to the electrostatic repulsion of the octyl hydroxamate anions by the highly negatively charged malachite surface. The maximum recovery occurs at around pH 9, similar to the case of hematite and manganese, which is the pKa of octyl hydroxamate. The optimum flotation appears to take place where the concentration of neutral molecules and anions are about equal, indicating that coadsorption may be responsible for the pronounced chemisorption, which is in agreement with the adsorption results presented and discussed in current work.

3.6 Effects of the common ions on the adsorption and flotation of malachite with salicylaldehyde

Regarding malachite solubility in an aqueous solution open to the atmosphere (e.g., $P_{CO_2}=10^{-3.5}$ atm), the following reactions are reported by Medusa thermodynamic software at 25 °C (Puigdomenech, 2004):

Reaction	log K
$2Cu^{2+} + CO_3^{2-} + 2H_2O \leftrightarrow Cu_2CO_3(OH)_2(c) + 2H^+$	5.179
$Cu^{2+} + 2H_2O \leftrightarrow 2H^+ + Cu(OH)_2(aq)$	-16.24
$Cu^{2+} + 3H_2O \leftrightarrow 3H^+ + Cu(OH)_3^-$	-26.7
$Cu^{2+} + 4H_2O \leftrightarrow 4H^+ + Cu(OH)_4^{2-}$	-39.6
$2Cu^{2+} + 2H_2O \leftrightarrow 2H^+ + Cu_2(OH)_2^{2+}$	-10.35
$2Cu^{2+} + H_2O \leftrightarrow H^+ + Cu_2(OH)^{3+}$	-6.7
$3Cu^{2+} + 4H_2O \leftrightarrow 4H^+ + Cu_3(OH)_4^{2+}$	-21.2
$Cu^{2+} + H_2O \leftrightarrow H^+ + Cu(OH)^+$	-7.96
$Cu^{2+} + 2CO_3^{2-} \leftrightarrow Cu(CO_3)_2^{2-}$	9.83
$Cu^{2+} + CO_3^{2-} \leftrightarrow Cu(CO_3)(aq)$	6
$Cu^{2+} + H^+ + CO_3^{2-} \leftrightarrow CuHCO_3^+$	13.029
$2H^+ + CO_3^{2-} \leftrightarrow CO_2(g) + H_2O$	18.149
$2H^+ + CO_3^{2-} \leftrightarrow H_2CO_3$	16.681
$H^+ + CO_3^{2-} \leftrightarrow HCO_3^-$	10.329

where K is the equilibrium constant. The solubility (S) of malachite in a solution open to the atmosphere can be expressed in terms of the total dissolved copper species, as per the following equation:

$$2S = [Cu^{2+}] + [Cu(CO_3)_2^{2-}] + [CuCO_3(aq)] + [CuHCO_3^-] + [Cu(OH)_2(aq)] + [Cu(OH)_3^-] + [Cu(OH)_4^{2-}] + 2[Cu_2(OH)_2^{2+}] + 2[Cu_2OH^{3+}] + 3[Cu_3(OH)_4^{2+}] + [CuOH^+]$$

The solubility of malachite is calculated as a function of pH using equations above and the results are plotted in Figure 3.6.1. It shows that malachite solubility decreases as pH increases up to about 8.4; above this value, which marks the minimum, solubility increases with further increase of pH.

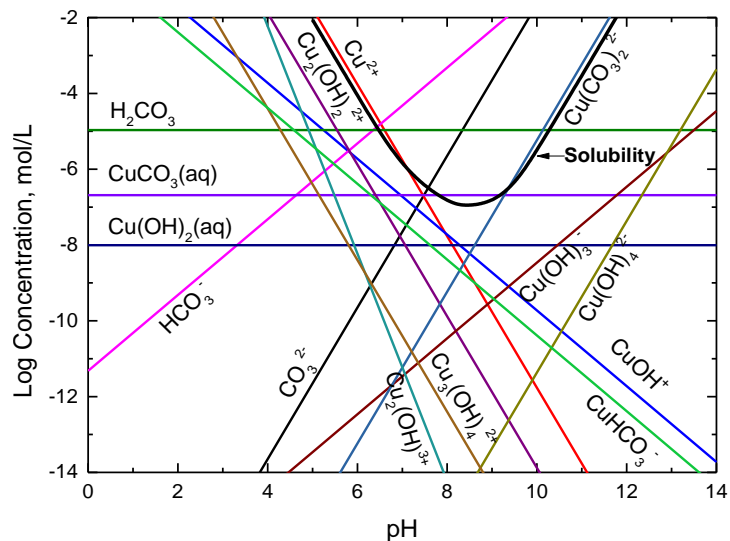


Figure 3.6.1. Solubility of malachite and logarithmic concentration distribution of copper and carbonate species as a function of pH, in equilibrium with the atmosphere (activity of CO_2 (g) equal to $1 \times 10^{-3.5}$ atm)

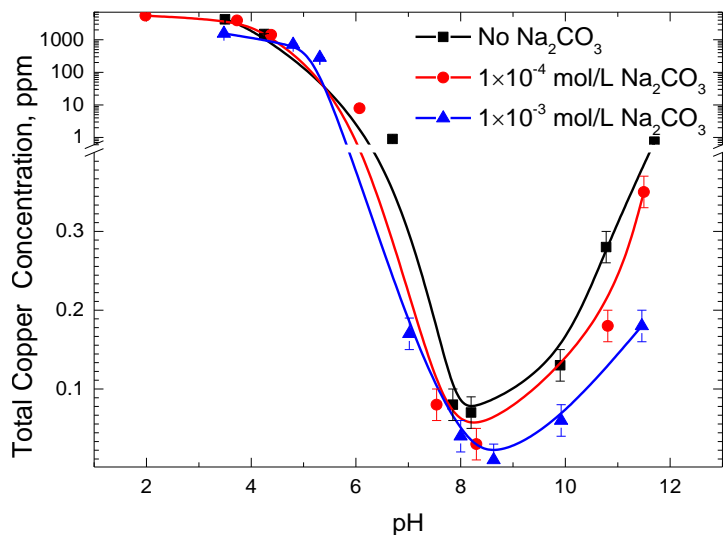


Figure 3.6.2. Solubility of malachite as a function of pH in aqueous solutions containing 0, 1×10^{-4} mol/L, and 1×10^{-3} mol/L Na_2CO_3

Figure 3.6.2 presents the solubility of malachite as a function of pH in the absence and presence of different concentrations of Na_2CO_3 . It shows that regardless of the Na_2CO_3 concentration, the solubility of malachite decreased sharply with the increase of pH from 3 to 8.2 and reached the minimum at about pH 8.2. Above this pH value, the solubility increased with further increase of pH. The minimum solubility occurred at about pH 8.2, which is slightly different from the thermodynamic prediction, which showed that the minimum solubility occurred at pH 8.4. The probable reason for the discrepancy observed may be the lack of equilibrium between the CO_2 in the atmosphere and in the solution, mainly caused by the relatively short time of the experiment to measure the solubility. Malachite may dissolve in acid media of pH below 6, given rise to substantially high copper concentrations. Furthermore, malachite solubility appears to decrease with the increase of sodium carbonate concentration, which may suggest that both CO_3^{2-} and OH^- ions have a significant influence on its solubility.

Figure 3.6.3 gives the micro-flotation recovery of malachite ($-75 + 38 \mu\text{m}$) as a function of pH, when this was conditioned in the presence and absence of sodium carbonate. Malachite recovery increased with the increase of pH reaching a maximum at about pH 8. At pH above 8, recovery decreased with further increase of pH. The recovery of malachite conditioned in the presence of $1 \times 10^{-2} \text{ mol/L Na}_2\text{CO}_3$, was higher compared to that of malachite conditioned in the absence of Na_2CO_3 . For example, at pH 7, malachite recovery was around 97% in the presence of $1 \times 10^{-2} \text{ mol/L Na}_2\text{CO}_3$, while in the absence of Na_2CO_3 recovery was about 64%. The maximum recovery was achieved at pH 8, which corresponds to the pH at which the minimum solubility of malachite was observed. Comparing the flotation and solubility measurements, it is observed that recovery and solubility show opposite behavior, that is, recovery increases as solubility decreases. According to the above, it can be concluded that OH^- and CO_3^{2-} impact the solubility of malachite, thus affecting its flotation. With regard to the stability of the surfactant in the pH range tested, it is worth mentioning that the UV spectrum of salicylaldoxime remains practically invariant in the pH range from 5 to 9, while showing some variation at pH 10 and 11, suggesting the conversion of the collector to different species. These species might be of less surface active strength, resulting in the decrease of malachite recovery.

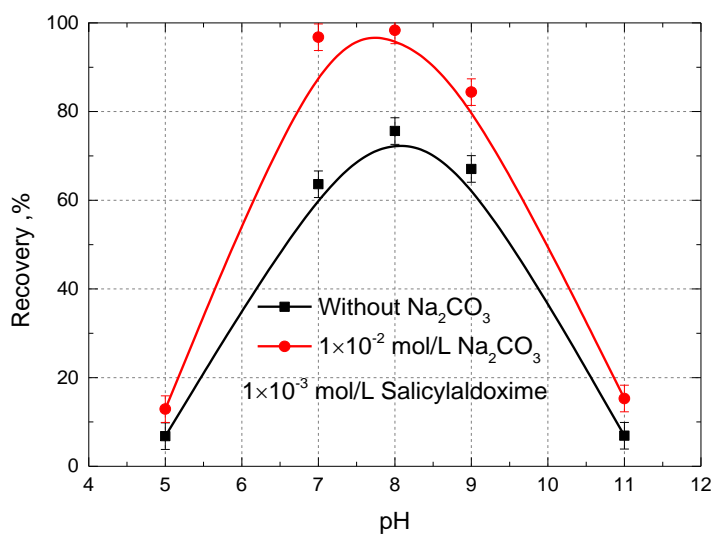


Figure 3.6.3. Flotation recovery of malachite with salicylaldoxime as a function of pH; malachite was previously conditioned in the presence and absence of sodium carbonate

Figure 3.6.4 shows the effect of Na_2CO_3 conditioning concentration on malachite recovery when floated with 1×10^{-3} mol/L salicylaldoxime at pH 8. It is observed that when Na_2CO_3 concentration used in the conditioning was increased, the recovery of malachite increased linearly from about 73% (absence of Na_2CO_3) to around 98% (1×10^{-3} mol/L Na_2CO_3). As mentioned above, the addition of Na_2CO_3 decreases malachite solubility (Figure 3.6.2) and therefore increases its floatability.

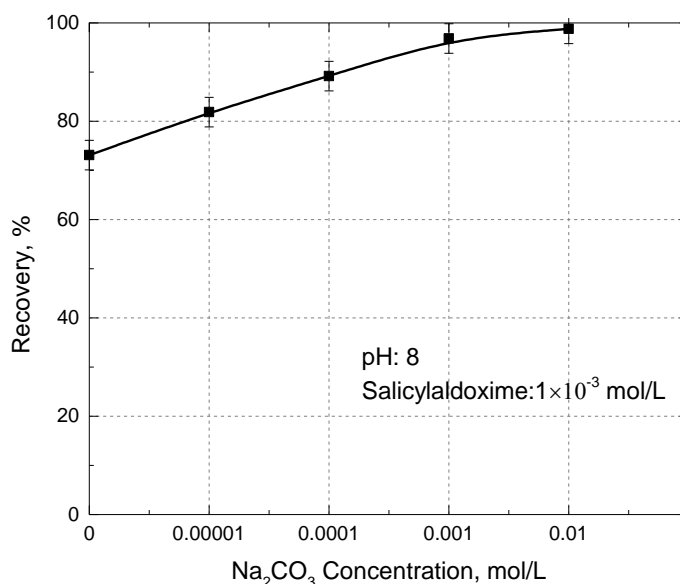


Figure 3.6.4. Recovery of malachite conditioned under different Na_2CO_3 concentrations with 1×10^{-3} mol/L salicylaldoxime at pH 8

It has been reported that salicylaldoxime is chemically adsorbed on the malachite surface through the formation of salicylaldoxime copper (Li et al., 2017b). Therefore, at low solubility of malachite (e.g., pH 8), a high amount of stable adsorption sites of copper atoms are accessible for this adsorption, leading to the high floatability and recovery of malachite. At high solubility of malachite (e.g., pH 5), many copper atoms on its surface are unstable because of the dissolution, and the dissolved cupric ions (Cu^{2+}) consume the salicylaldoxime ions around the particle surface, resulting in low adsorption of salicylaldoxime on malachite surface, and hence the low recovery of malachite. However, further effort is required to understand the chemical interaction between salicylaldoxime species and copper atoms on malachite surface, in order to support this hypothesis.

The effect of salicylaldoxime on the zeta potential of malachite was measured as a function of pH, and the results obtained are presented in Figure 3.6.5. The zeta potential of pure malachite decreased as the pH is increased, showing the occurrence of the isoelectric point value (IEP) at pH 8.2, which is in good agreement with that reported at pH 8.7 by Liu et al. (2016). The zeta potential of copper salicylaldoxime is negative during the measured pH range from pH 4.5 to pH 10. When the malachite was conditioned with salicylaldoxime, its zeta potential changed to more negative values, and the IEP shifted from pH 8.2 to pH 7.6, pH 7.0 and pH 5.4 at salicylaldoxime concentrations of 1×10^{-4} , 1×10^{-3} and 1×10^{-2} mol/L, respectively. This behavior may suggest that

salicylaldehyde adsorbed onto malachite surface by chemical adsorption; alternatively, formation of highly negatively charged compound (copper-salicylaldehyde) may occurred at the surface. It is worth to note that malachite solubility substantially increased at pH below 6 and that under those conditions, a certain amount of copper-salicylaldehyde may be formed; thus, the zeta potential measured at pH below 6, may be the result of the weighted average values of zeta potentials of the malachite adsorbed with salicylaldehyde and the copper-salicylaldehyde.

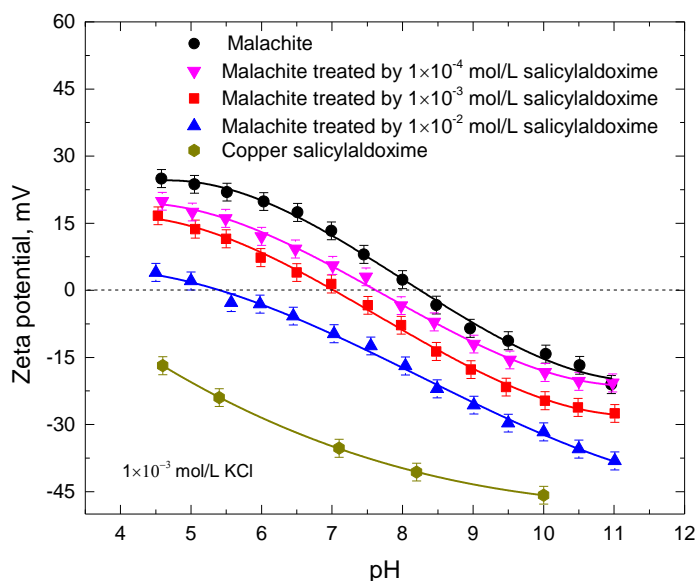


Figure 3.6.5. Zeta potential of malachite and malachite conditioned with different concentration of salicylaldehyde. The zeta potential of synthesized copper salicylaldehyde is also shown

Figure 3.6.6 presents the Fourier transform infrared spectra of malachite, salicylaldehyde, copper-salicylaldehyde precipitated at pH 8, and malachite conditioned with salicylaldehyde at pH 8. The FTIR spectrum of malachite obtained in this work is similar to that reported in the literature (Cecile et al., 1981). In Figure 3.6.6a, the absorption bands at 3380 and 1500 cm^{-1} are characteristic of the hydroxyl and carbonate groups in malachite, respectively. Figure 3.6.6b shows that the O-H stretching vibration of salicylaldehyde, C=N stretching vibration of oxime group, phenyl ring, O-H bending vibration (in plane), aromatic C-O stretching vibration, OH deformation vibration (out of plane), and N-O stretching vibration are found at 3380 , 1621 , 1576 , 1290 , 1254 , 989 , and 896 cm^{-1} , respectively (Ramesh et al., 1998). In turn, Figures 3.6.6c and 3.5.6d show that C=N stretching vibration of oxime group appears at 1650 cm^{-1} and phenyl ring vibration of copper salicylaldehyde is found at 1547 cm^{-1} (Ramesh et al., 1998); this suggests that when malachite was conditioned with salicylaldehyde (Figure 3.6.6d), the formation of a copper-salicylaldehyde chelate took place on its surface. The peak belonging to C=N stretching vibration of oxime group shifts from 1621 to 1650 cm^{-1} and peak belonging to phenyl ring vibration shifts from 1576 to 1547 cm^{-1} after adsorption of salicylaldehyde at malachite surface, which allows to infer that salicylaldehyde may adsorb onto malachite by a chemisorption mechanism. It is in agreement with the zeta potential results in Figure 3.6.5. In addition, the strong N-O stretching frequency appearing at 1190 cm^{-1} after adsorption of salicylaldehyde at malachite surface indicates that the formed copper salicylaldehyde chelate is bis-

salicylaloximato copper (II). In this compound, two salicylaldoxime molecules are complexed with one copper.

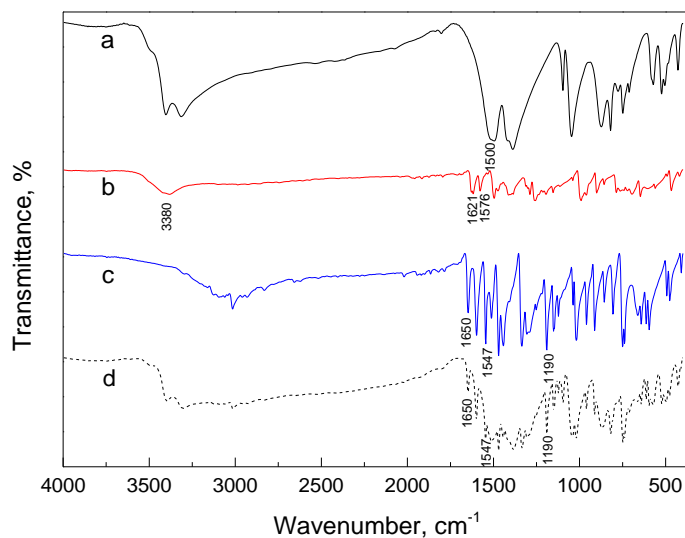


Figure 3.6.6. Infrared spectra of malachite (a), salicylaldoxime (b), synthesized copper salicylaldoxime (c), and malachite conditioned with salicylaldoxime at pH 8 (d)

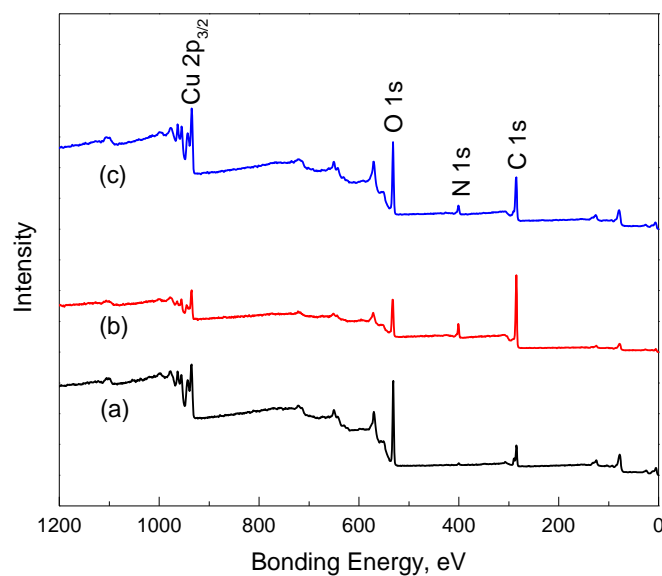


Figure 3.6.7. The XPS survey spectra of malachite (a), copper-salicylaldoxime precipitates (b), and malachite conditioned with salicylaldoxime (c)

Zeta potential and FTIR measurements showed that salicylaldoxime chemically adsorbs at the malachite surface. In an attempt to obtain more details about this chemical adsorption, XPS measurements were performed. Figure 3.6.7 shows the XPS survey spectra of malachite, copper-salicylaldoxime precipitates, and malachite treated with salicylaldoxime over a binding energy range of 0 to 1200 eV. The atomic concentration of elements C 1s, N 1s, O 1s, and Cu 2p_{3/2} determined by XPS is summarized in Table 3.6.1, along with their atomic concentration ratio with respect to Cu. The table shows that in the case of the copper-salicylaldoxime precipitate, the atomic concentration ratio of C, N and O with respect to Cu was 16.58, 1.96, and 3.99, respectively. Taking into consideration the carbon added for the XPS measurement, the condensed formula of the precipitate may be expressed as C₁₄H₁₂N₂O₄Cu, suggesting that two salicylaldoxime molecules react with one copper ion (the hypothetical number of H atoms were added to the formula). In turn, after malachite conditioning with salicylaldoxime, the concentration of N and C increased, while the concentration of O and Cu decreased. This behavior suggests that salicylaldoxime was adsorbed onto malachite surface.

Table 3.6.1. Atomic concentration of C, N, O, and Cu in malachite, copper salicylaldoxime precipitate, and malachite conditioned with salicylaldoxime at pH 8.

Species	Atomic concentration (%)				Atomic concentration ratio with respect to Cu (%)			
	C	N	O	Cu	C	N	O	Cu
Malachite	37.82	2.13	45.26	14.80	2.56	0.14	3.06	1.00
Copper salicylaldoxime	70.46	8.34	16.94	4.25	16.58	1.96	3.99	1.00
Malachite + salicylaldoxime	54.57	6.69	27.75	10.98	4.97	0.61	2.53	1.00

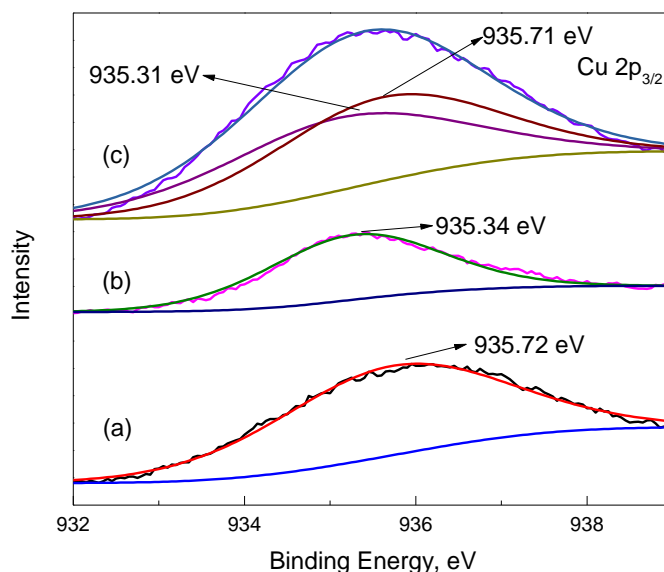


Figure 3.6.8. High-resolution XPS Cu 2p_{3/2} spectra of malachite (a), synthesized copper salicylaldoxime (b), and malachite after conditioning with salicylaldoxime (c)

Figure 3.6.8 presents the high-resolution XPS Cu 2p_{3/2} spectra of malachite, copper salicylaldoxime, and malachite after conditioning with salicylaldoxime. In these spectra, the

peaks occurring at around 935.72 and 935.34 eV were respectively assigned to copper onto malachite surface and to copper of copper salicylaldoxime precipitate. After malachite conditioning with salicylaldoxime, the Cu 2p_{3/2} XPS bands of malachite surface were divided into two components: one at round 935.31 eV owing to the complexing of salicylaldoxime with the copper of malachite surface, and the second at around 935.71 eV, belonging to the copper of the malachite surface. These results suggest that copper at the malachite surface reacted with salicylaldoxime in the adsorption process.

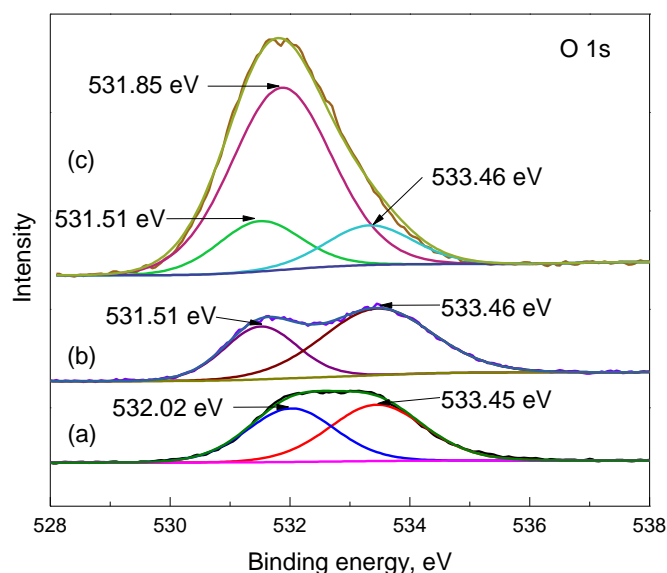


Figure 3.6.9. High-resolution XPS O 1s spectra of salicylaldoxime (a), copper salicylaldoxime (b), and malachite conditioned with salicylaldoxime (c)

Figure 3.6.9 illustrates the high-resolution XPS O 1s spectra of salicylaldoxime, copper salicylaldoxime, and malachite conditioned with salicylaldoxime. The two peaks at around 532.02 and 533.45 eV belong to the two different O atoms in the salicylaldoxime molecule. Because of conjugation effect, the electron density of O in N-OH is lower than that in C-OH, thus the peaks at 532.02 and 533.45 eV assign to O in C-OH and N-OH respectively. Once copper salicylaldoxime has precipitated as result of the reaction of salicylaldoxime with copper ions in the solution, the peak at 532.02 eV shifted to 531.51 eV and the peak at 533.45 eV remained practically in the same binding energy, indicating that only hydroxyl group on the benzene ring participates in the complexing reaction. After conditioning of malachite with salicylaldoxime, peaks belonging to copper salicylaldoxime appeared, suggesting the presence of copper salicylaldoxime onto the malachite surface. The peak at 531.85 eV in Figure 3.6.9(c), additional to those of salicylaldoxime (Figure 3.6.9(a)) and copper salicylaldoxime (Figure 3.6.9(b)), is caused by the O atoms of malachite (Feng et al., 2017). These results suggest that only hydroxyl group on the benzene ring participated in the adsorption reaction of salicylaldoxime on the malachite.

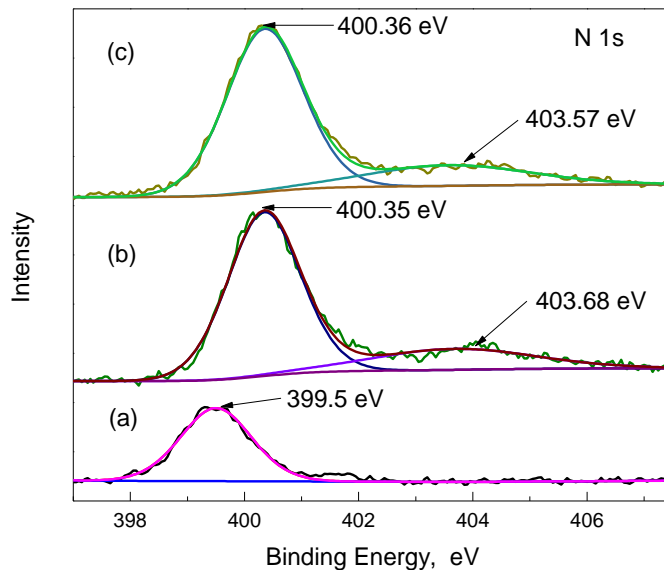


Figure 3.6.10. High-resolution XPS N 1s spectra of salicylaldoxime (a), synthesized copper salicylaldoxime (b), and malachite after conditioning with salicylaldoxime (c).

Figure 3.6.10 presents the high-resolution XPS N 1s spectra of salicylaldoxime, synthesized copper salicylaldoxime, and malachite after conditioning with salicylaldoxime at pH 8. The peak occurring at 399.5 eV corresponds to the N atom in the salicylaldoxime molecule. The N 1s peak for copper salicylaldoxime could not be fitted with a single symmetrical component and appeared at around 400.35 and 403.68 eV in the spectra. The high intensity component at a bonding energy of around 400.35 eV belongs to the copper salicylaldoxime, while the low intensity component may be due to the decomposition of the copper salicylaldoxime caused by the X-ray irradiation (Hope et al., 2010). The peak belonging to N in the salicylaldoxime molecule shifts from 399.5 to 400.35 eV after reacting with copper ions. In addition, hydroxyl group connected to N did not participate in the complex reaction. It suggests that the N atom participates in the complexing reaction. After conditioning malachite with salicylaldoxime, the N 1s spectra showed similar peaks to those of copper salicylaldoxime, indicating that N participated in the adsorption reaction of salicylaldoxime on the malachite.

From the above XPS results, it infers that two salicylaldoxime molecules react with one copper ion on the malachite surface by N atom and the O atom combined with benzene ring, which is presented in Figure 3.6.11. The adsorption mechanism is in good agreement with the flotation results. Under conditions of lower solubility, a high amount of stable adsorption sites of copper atoms are accessible for this adsorption, leading to the high floatability and recovery of malachite.

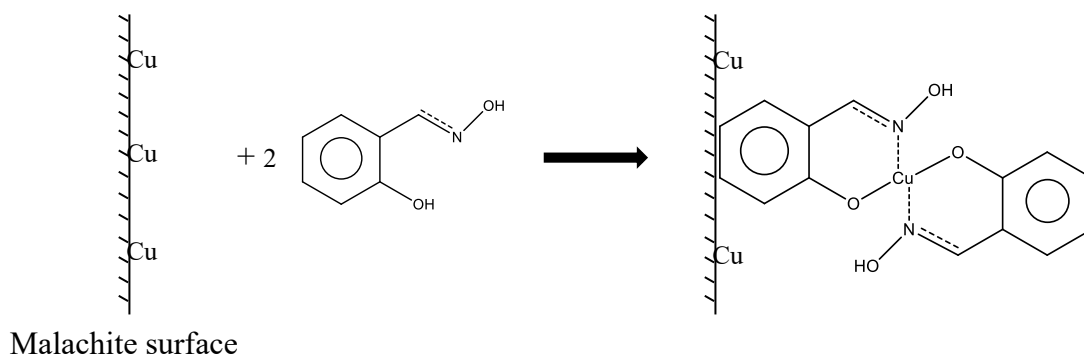


Figure 3.6.11. A schematic presentation of interaction between salicylaldehyde and malachite.

3.7. The effect of calcium ions in the flotation of malachite with octyl hydroxamate

The flotation tests of malachite ($-25 \mu\text{m}$) as a function of CaCl_2 concentration in the presence of $8 \times 10^{-4} \text{ mol/L}$ octyl hydroxamate at pH 9 were conducted, and the results are shown in Figure 3.7.1. The flotation recovery sharply increased from 52.0% to 69.9% with the addition of $1 \times 10^{-4} \text{ mol/L}$ CaCl_2 . Further addition of CaCl_2 up to $1 \times 10^{-2} \text{ mol/L}$ gradually improved the recovery of malachite up to 87.7%. This indicates that the addition of CaCl_2 at such a concentration is beneficial to malachite flotation, which is similar to the flotation of malachite with sodium oleate in the presence of Ca^{2+} reported by Choi (2016). It needs to be noted that Ca^{2+} was added after the adsorption of sodium oleate in Choi's study, whereas Ca^{2+} was added before the adsorption of octyl hydroxamate in the current research. In addition, octyl hydroxamate and sodium oleate adsorb onto malachite surface by similar mechanism, namely, chemical adsorption (Lenormand et al., 1979; Li, Z., et al., 2018). It may suggest that the addition order of Ca^{2+} and collectors plays a negligible role on malachite flotation.

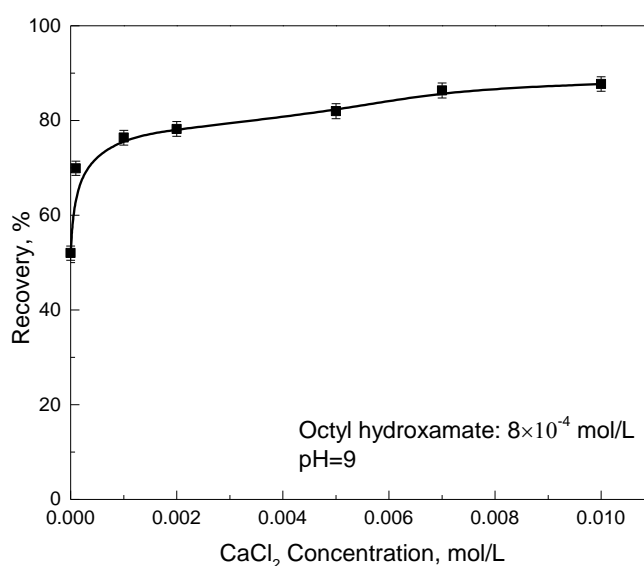


Figure 3.7.1. Flotation recovery of malachite at different CaCl_2 concentrations at pH 9.

The flotation tests of malachite as a function of pH in the presence and absence of 1×10^{-2} mol/L CaCl_2 were performed, and the results are presented in Figure 3.7.2. In the absence of CaCl_2 , the flotation recovery of malachite increased drastically from pH 5 to 6, and then increased steadily until a maximum recovery of 50% reached at pH 9. It is also observed that the flotation recovery dropped down to a low value with further increasing of pH to 13. The poor flotation performance in mildly acidic medium can be attributed to the precipitation of octyl hydroxamate by dissolved copper ions in bulk solution (Lenormand et al., 1979). The increased flotation recovery in near neutral and mildly alkaline medium indicates the adsorption of octyl hydroxamate onto malachite surface. The maximum flotation recovery achieved at around pH 9, similar to the flotation of hematite (Raghavan and Fuerstenau, 1975) and manganese dioxide (Natarajan and Fuerstenau, 1983), which is the pKa of octyl hydroxamate, indicating co-adsorption of octyl hydroxamate anion and molecule (Natarajan and Fuerstenau, 1983). The deteriorated flotation recovery in alkaline medium could be attributed to the electrostatic repulsion between octyl hydroxamate anion and negatively charged malachite surface.

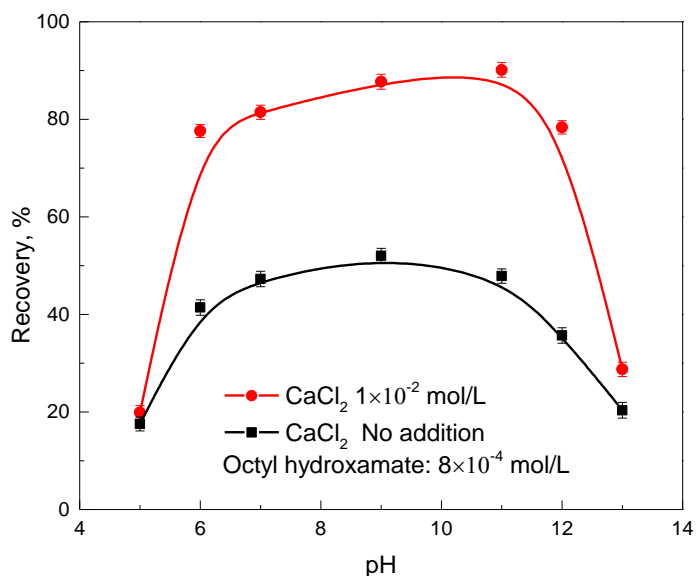


Figure 3.7.2. Flotation recovery of malachite as a function of pH in the presence and absence of 1×10^{-2} mol/L CaCl_2 .

In the presence of 1×10^{-2} mol/L CaCl_2 , the flotation recovery of malachite as a function of pH almost followed the same trend as that in the absence of CaCl_2 except that the maximum flotation recovery altered to pH 11. It is noted that the flotation recovery was much higher than that in the absence of CaCl_2 over a wide pH range. This is in line with that reported by Chio et al. (2016) in the flotation of malachite with the addition of Ca^{2+} using sodium oleate as collector at pH 9.5. This difference in flotation behavior might be caused by the interaction of calcium-bearing species with malachite.

To understand the interaction of calcium-bearing species with malachite surface, zeta potential of malachite as a function of pH in the absence and presence of different concentration of CaCl_2

were measured, and the results are given in Figure 3.7.3. The zeta potential of pure malachite decreased as pH was increased, with the occurrence of the isoelectric point (IEP) at pH 8.2. This is in agreement with the IEP at pH 7.8 reported in other study (Li, Z., et al., 2018). With the addition of CaCl_2 , zeta potential of malachite moved to more positive values, accompanied by the shift of IEP to higher values. This indicates that calcium-bearing species are capable of specifically adsorbing onto the malachite surface. Generally, the positive shift of zeta potential as a result of CaCl_2 addition was much more pronounced in alkaline region, inferring that a larger amount of calcium-bearing species adsorbed onto the malachite surface. Also, more calcium-bearing species adsorb onto malachite surface with the increase of CaCl_2 concentration. With CaCl_2 concentration at 1×10^{-2} mol/L, malachite particles were positively charged over the whole pH range investigated with the disappearance of IEP. It is also interesting to note that the zeta potential became more positive in alkaline region above pH 11 at this CaCl_2 concentration.

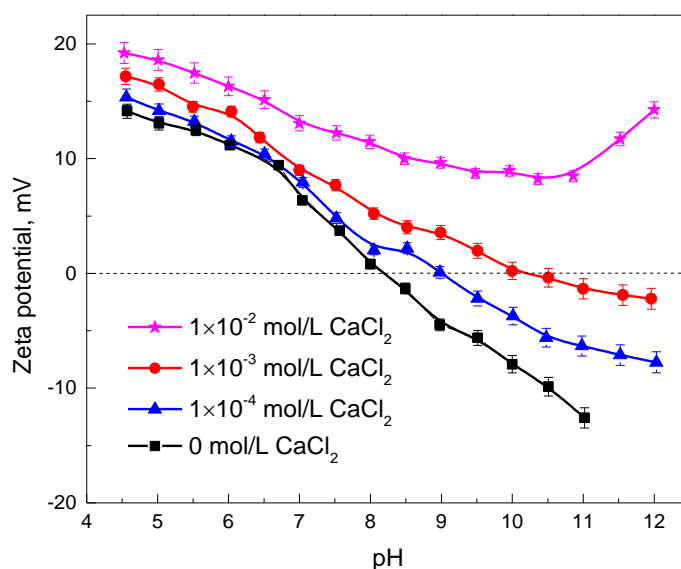


Figure 3.7.3. Zeta potential of malachite at different CaCl_2 concentrations.

The calcium speciation of CaCl_2 solution was simulated using the database available in Medusa thermodynamic software (Puigdomènech, 2010). The concentration of each calcium species as a function of pH at a total calcium concentration of 1×10^{-2} mol/L were plotted in Figure 3.7.4. At pH below and above 12.6, Ca^{2+} and $\text{Ca}(\text{OH})_2$ are the predominant species, respectively. The concentration of $\text{Ca}(\text{OH})^+$ increases as the pH is increased, reaching a maximum in the vicinity of pH 12.6, followed by a decrease with further increasing pH. It is seen from Figure 3.7.3 that the shift of zeta potential as a result of CaCl_2 addition differs significantly in acidic and in alkaline region. Given that Ca^{2+} is the overwhelmingly dominant species over the whole pH range investigated in zeta potential measurements, this species is not responsible for the shift of zeta potential. Obviously, precipitate of $\text{Ca}(\text{OH})_2$ is not formed at pH below 12.6. Thus, this species is not related with the shift of zeta potential. In addition, the adsorption of calcium onto malachite occurred more readily in the alkaline environment, corresponding well with the pH region where

more Ca(OH)^+ occurred. In view of the foregoing, it is reasonable to attribute the shift of zeta potential to the adsorption of Ca(OH)^+ onto malachite surface.

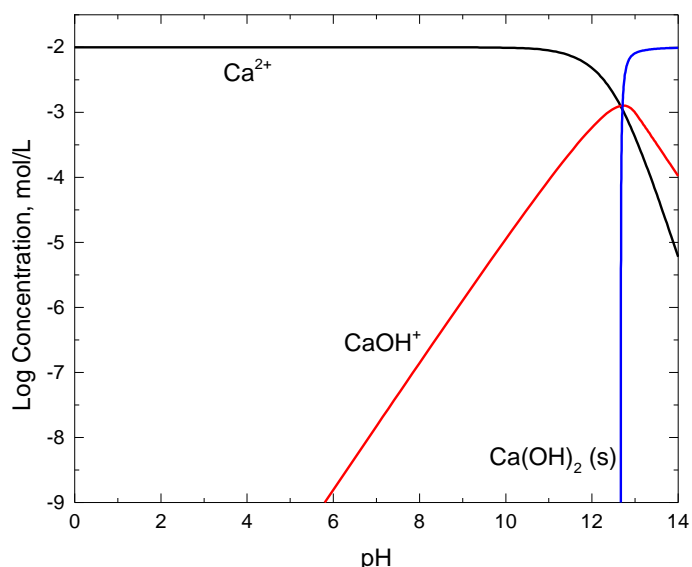


Figure 3.7.4. Calculations of the concentration of each calcium species as a function of pH at a total calcium concentration of 1×10^{-2} mol/L.

The adsorption of collector onto minerals and their hydrophobicity is an essential influencing factor of the flotation behavior. Zeta potential, adsorption amount and contact angle measurements were taken to investigate the malachite surface in hydroxamate containing solution. The zeta potential of malachite in the presence of potassium octyl hydroxamate and a combination of CaCl_2 and octyl hydroxamate were measured as a function of pH, and the results are plotted in Figure 3.7.5. With the addition of octyl hydroxamate alone, the zeta potential of malachite shifted to more negative values with the IEP decreasing from pH 8.2 to 7.4 and the octyl hydroxamate anions adsorbed onto the negatively charged malachite surface above IEP, suggesting the chemisorption of octyl hydroxamate (Fuerstenau, 2005). With the addition of 1×10^{-2} mol/L Ca^{2+} , followed by 8×10^{-4} mol/L octyl hydroxamate, the zeta potential of malachite shifted to more negative values compared to that treated merely by 1×10^{-2} mol/L Ca^{2+} . It indicates that octyl hydroxamate still can adsorb onto the malachite surface after the adsorption of Ca(OH)^+ . In addition, a large amount of hydrophilic Ca(OH)^+ adsorbed onto malachite surface at pH 11, while the recovery of malachite reached the maximum at this pH. It may suggest that the covering of octyl hydroxamate onto Ca(OH)^+ .

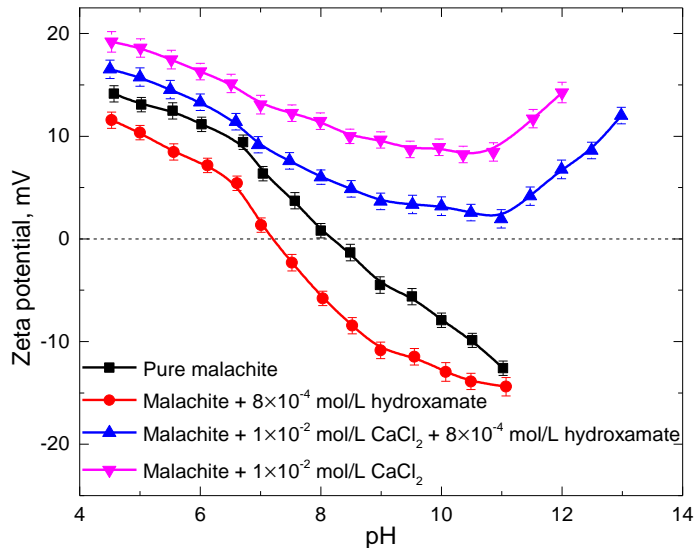


Figure 3.7.5. Zeta potential of malachite in the presence of CaCl_2 or/and hydroxamate.

The adsorption amount of octyl hydroxamate on malachite surface was measured at pH 9 with the same conditioning process as utilized in micro-flotation, and the results are plotted in Figure 3.7.6. In the absence of CaCl_2 , almost all octyl hydroxamate added to the suspension were adsorbed by malachite particles. With the increase of CaCl_2 addition, the adsorption amount of octyl hydroxamate maintained virtually constant.

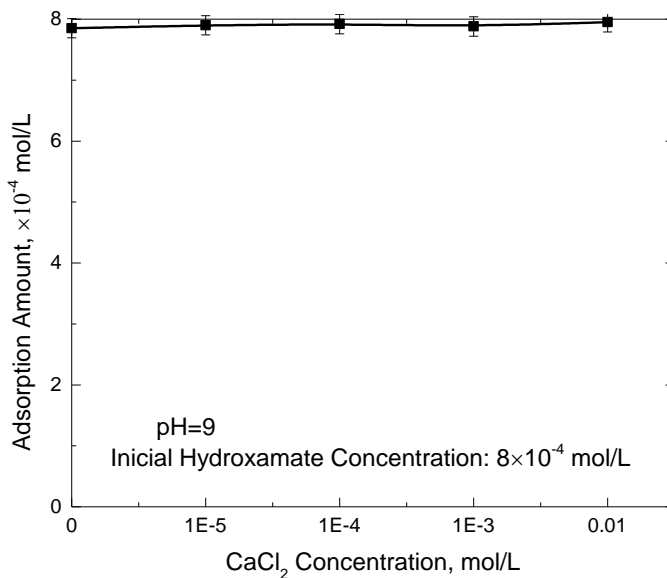


Figure 3.7.6. Adsorption of octyl hydroxamate in the presence of different concentration of CaCl_2 .

Contact angle of malachite with and without the addition of 1×10^{-2} mol/L CaCl_2 was measured in the presence of 8×10^{-4} mol/L hydroxamate at pH 9, and the obtained images are analyzed in Figure 3.7.7. Similar contact angles were obtained in the absence and presence of 1×10^{-2} mol/L CaCl_2 , demonstrating the identical hydrophobicity of malachite surface under these two conditions. Cations may function as activators in some cases and promote the adsorption of collector, leading to increased hydrophobicity, and therefore, enhanced flotation performance. However, the present study revealed the adsorption of collector and the hydrophobicity of malachite were not influenced by the addition of CaCl_2 at an optimized flotation pH 9. Therefore, calcium must affect the malachite flotation in other way in this pH region.

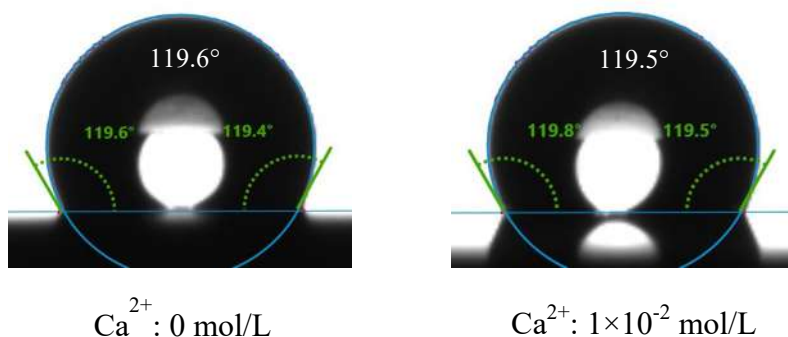


Figure 3.7.7. Contact angle of malachite in the presence and absence of 1×10^{-2} mol/L CaCl_2 with the addition of 8×10^{-4} mol/L octyl hydroxamate at pH 9.

After the adsorption of octyl hydroxamate, the zeta potential of malachite is positive and negative in the presence and absence of CaCl_2 , respectively. Given that the zeta potential of bubbles is negative above pH 2.5 and it decreased with the increase of pH (Okada et al., 1990), the electrostatic forces between bubbles and malachite particles are always attractive in the presence of CaCl_2 and repulsive at pH above 7.4 in the absence of CaCl_2 . At pH below 7.4, although the electrostatic forces between bubbles and malachite particles are attractive in the absence of CaCl_2 , the zeta potential values are smaller and the attraction is much weaker compared to that of in the presence of CaCl_2 . Thus, the malachite particles more readily attached to bubbles in the presence of CaCl_2 because the lowered energy barrier, which is one reason for the enhanced malachite recovery in the presence of CaCl_2 over a wide pH range. This is in line with Chio's study (Chio et al., 2016).

In the conditioning process of micro-flotation experiments, it was found that the malachite suspensions settled faster in the presence of CaCl_2 , which may provide another mechanism for the enhanced flotation recovery. The images of malachite suspension after 15 s settling in the presence of different reagents at pH 9 were present in Figure 3.7.8. It clearly shows that the malachite particles with the addition of 8×10^{-4} mol/L octyl hydroxamate settled faster compared to that without the addition of octyl hydroxamate, and this effect was more evident with the addition of 1×10^{-2} mol/L CaCl_2 . It may provide another mechanism for the enhanced flotation recovery.

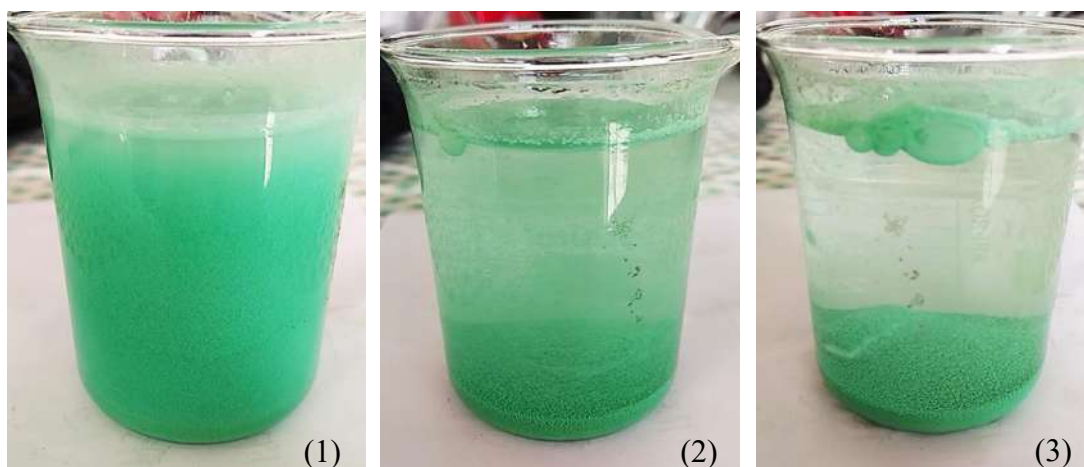


Figure 3.7.8. Images of malachite suspension after 15 s settling with the addition of different reagents at pH 9, (a) no reagent addition, (b) 8×10^{-4} mol/L octyl hydroxamate, (c) 1×10^{-2} mol/L CaCl_2 and 8×10^{-4} mol/L octyl hydroxamate.

Particle size distributions of malachite treated with different reagents at pH 9 were measured and the results are present in Figure 3.7.9. With the addition of octyl hydroxamate, malachite particle size increased, and the increase was more evident with a combination of Ca^{2+} and octyl hydroxamate. It indicates that the addition of octyl hydroxamate induces the formation of flocs, and the presence of Ca^{2+} promotes this effect. The hydrophobic force induced by the adsorption of octyl hydroxamate between malachite surfaces may cause the aggregation in malachite suspensions. In the flotation of fine hematite, the aggregation of these mineral particles in the presence of sodium oleate or hydroxamic acids has also been reported (Li, H., et al., 2018).

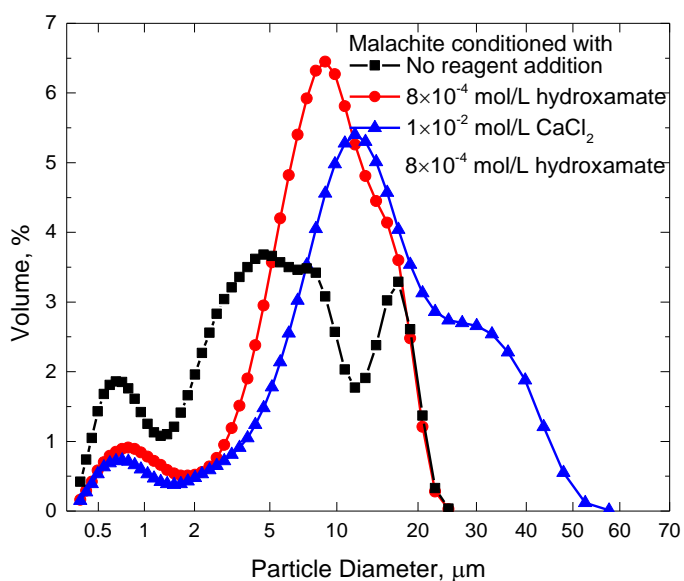


Figure 3.7.9. Malachite particle size distribution with the addition of different reagents at pH 9.

It is well documented that electrolytes compress electrical double layers and therefore reduce their electrical double layer repulsive forces (Rattanakawin and Hogg, 2001; Wang and Peng, 2013), which may enhance the aggregation in mineral suspensions. In the current research, the zeta potential of malachite in the presence of 8×10^{-4} mol/L hydroxamate alone is -10.86 mV at pH 9. By the addition of CaCl_2 before the addition of hydroxamate, the zeta potential of malachite was 3.66 mV at pH 9. It is obvious that the addition of CaCl_2 lowered the electrical double layer repulsive forces between malachite particles, and therefore, enhancing their aggregation. It is well accepted in mineral flotation of base metals that high recoveries can be obtained within particle size range 10 to 70 μm , while the recoveries decrease for various reasons when the particle size out of this range (Jameson et al., 2007). In the current study, most of the malachite particles were below 10 μm without addition of reagents. After the addition of CaCl_2 and octyl hydroxamate, malachite particle size increased and the maximum didn't exceed 70 μm . With larger particle size, the particle momentum is higher, making it easier to overcome the energy barrier between particle and bubble, resulting in higher probability of collision between particle and bubble, as a consequence, enhanced flotation recovery (Sivamohan, 1990; Miettinen et al., 2010; Song et al., 2012). At pH 11, the absolute value of zeta potential with a combination of CaCl_2 and hydroxamate is lower than that of pH 9, which may leads to higher aggregation of malachite particles, and therefore, increased malachite recovery compared to pH 9. It needs to be noted that with the reduction of zeta potential at pH 11 compared to pH 9, the electrostatic force between malachite particle and bubbles may kept constant since the zeta potential of bubbles decreased to more negative values. At pH above 11, the absolute values of zeta potential became bigger in both Ca-free and Ca-bearing suspensions, raising the difficulty level for particle-particle aggregation and therefore possible interpretation for lower flotation recovery.

In view of the foregoing, the mechanisms of calcium effect on malachite flotation using octyl hydroxamate as collector were illustrated in Figure 3.7.10. The presence of Ca-bearing species in the malachite suspension has negligible effect on the adsorption amount of octyl hydroxamate at pH 9, and therefore the hydrophobicity, whereas it reduced the electrical double layer repulsive forces between malachite particles, leading to higher aggregation degree of these particles, and subsequently, the enhanced flotation performance. In addition, the electrostatic force between bubbles and particles changed from repulsion to attraction in the presence of 1×10^{-2} mol/L CaCl_2 , which is another reason for the improved flotation recovery at pH 9.

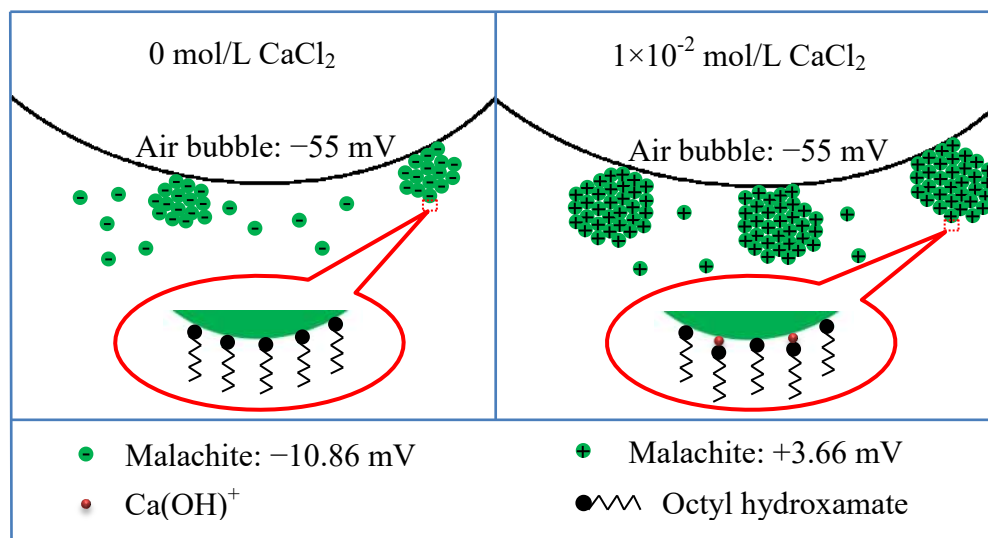


Figure 3.7.10. The schematic diagrams of the influence of calcium on malachite fines flotation with the addition of octyl hydroxamate at pH 9.

In alkaline region (pH above 11), the flotation recovery was generally deteriorated for either bear malachite or Ca-contaminated malachite. These could be interpreted in addition to particle-bubble collision and particle-particle aggregation. Without the addition of 1×10^{-2} mol/L CaCl_2 , the zeta potential difference at pH 11 between the presence and absence of octyl hydroxamate is small owing to its lower adsorption, which is accord with the micro-flotation results that the flotation recovery at this pH is low. With regard to zeta potential difference with the addition of 1×10^{-2} mol/L CaCl_2 between the presence and absence of octyl hydroxamate, it kept virtually constant at pH above 9, which may suggest that the adsorption of octyl hydroxamate at this pH range is constant. At this pH region, more Ca(OH)^+ adsorbed onto malachite surface and octyl hydroxamate added was not sufficient to cover all hydrophilic Ca(OH)^+ sites on malachite surface. Thus, the hydrophobicity of malachite surface decreased, leading to declined flotation recovery. At high concentration of Ca^{2+} , the decrease in hydrophobicity of monazite due to the adsorption of large amount of CaOH^+ was also reported by Zhang et al. (2017). At pH 13, where substantial Ca(OH)_2 forms, the flotation recovery decreased sharply, owing to the covering of substantial hydrophilic Ca(OH)^+ and Ca(OH)_2 precipitate at malachite surface.

3.8 Using octyl hydroxamate as emulsifier of kerosene and collector in the floc flotation of malachite fines

Figure 3.8.1 presents the flotation recovery of malachite ($-25 \mu\text{m}$) with the addition of two kinds of kerosene emulsions as a function of octyl hydroxamate concentration. The flotation recovery increased as the octyl hydroxamate concentration was increased, exhibiting flotation recovery around 15% in the absence of octyl hydroxamate. With the addition of octyl hydroxamate, malachite recovery raised drastically, inferring that prehydrophobicization of malachite surface is essential when kerosene is adopted in the floc flotation. With the utilization of octyl hydroxamate

in the emulsification process, higher flotation recovery of malachite was achieved, indicating that it is beneficial to add octyl hydroxamate in the emulsification process. It needs to be noted that, at the concentration of 2×10^{-4} mol/L octyl hydroxamate, the addition of 0.05 wt% octyl hydroxamate emulsified kerosene introduced 6.4% more octyl hydroxamate, which is negligible to this system.

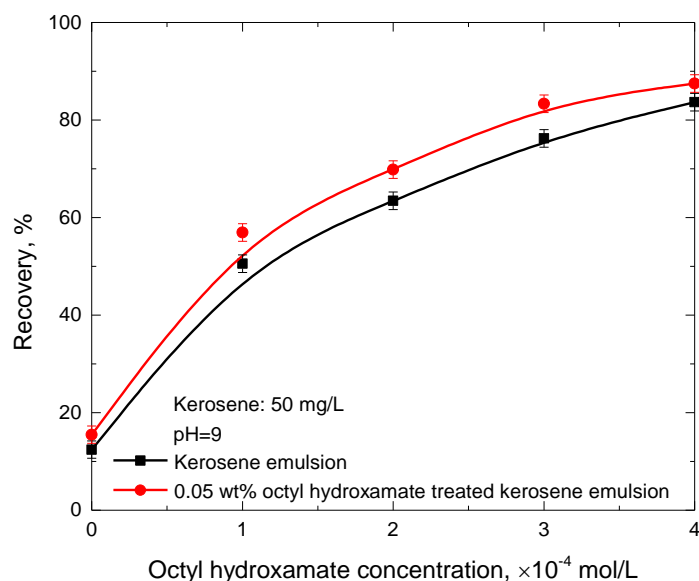


Figure 3.8.1. Flotation recovery of malachite with the addition of two kinds of kerosene emulsions as a function of octyl hydroxamate concentration.

Figure 3.8.2 gives the flotation recovery of malachite with the addition of two kinds of kerosene emulsions at pH 9. The flotation recovery increased steadily with the increase of kerosene dosage, indicating that kerosene has a remarkable influence on the malachite flotation. In the conditioning process, octyl hydroxamate was first adsorbed onto malachite surface to make the mineral surface pre-hydrophobic, so that the kerosene droplets were capable of interacting with its surface. The coating of kerosene can substantially enhance flocculation through the formation of oil bridges between hydrophobic particles and increasing particle hydrophobicity (Song et al., 2012). With the utilization of octyl hydroxamate in the emulsification process, higher flotation recovery of malachite was achieved. This phenomenon is more evident in the presence of greater dosage of kerosene with recovery increase around 12.5% at 80 mg/L kerosene. It suggests that the addition of 0.05 wt% octyl hydroxamate in the emulsification process promotes the floc flotation.

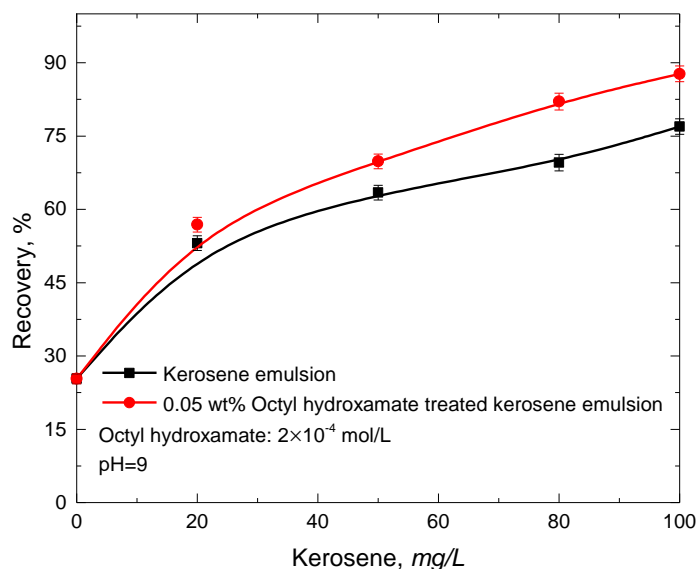


Figure 3.8.2. Flotation recovery of malachite with the addition of two kinds of kerosene emulsions as a function of kerosene dosage.

Two kinds of kerosene emulsions were prepared to enhance the flocculation process by using ultrasonic processor in the presence and absence of 0.05 wt% octyl hydroxamate. In order to understand the roles of oil droplets size distribution in the flocculation process, the optical microscopy images of the two kinds of kerosene emulsions were photographed and shown in Figure 3.8.3. The kerosene emulsion produced by ultrasonic processor in the presence of 0.05 wt% octyl hydroxamate was smaller than that in the absence of 0.05 wt% octyl hydroxamate. In addition, the droplets were much uniform in size. Therefore, in the same dosage of kerosene, the kerosene emulsion prepared in the presence of 0.05 wt% octyl hydroxamate had much more kerosene surfaces to contact malachite particles and then to enhance the hydrophobic flocculation, and therefore, the flotation performance.

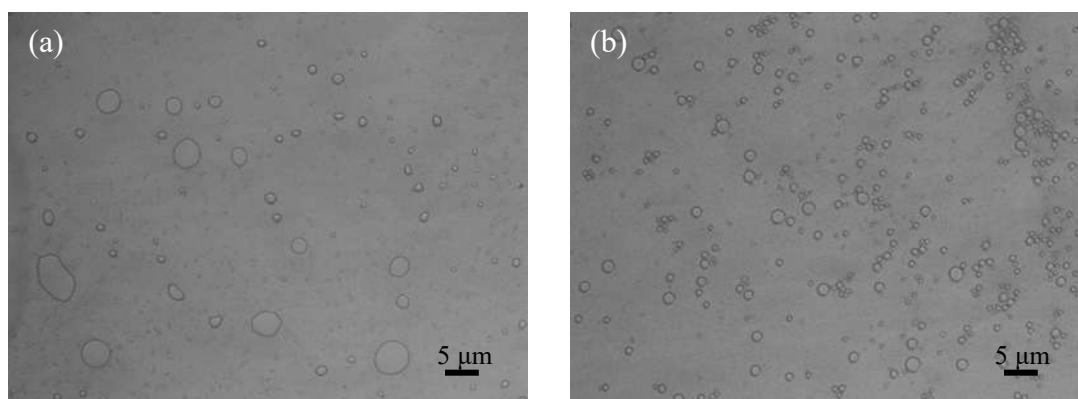


Figure 3.8.3. Optical microscopy images of the kerosene emulsions prepared by ultrasonic processor (a) without the addition of octyl hydroxamate (b) with the addition of 0.05 wt% octyl hydroxamate.

Figure 3.8.4 presents the spreading of kerosene droplets at malachite surface measured with the captive bubble method, showing that the spreading of kerosene droplets was a relatively slow process, which continued for 900 s. The kerosene droplets spread fast within 120s, followed by a gradually spreading in the subsequent 780 s. The 5 μL kerosene droplet showed a greater contact angle at the same spreading time compared to 1.5 μL kerosene droplets, indicating bigger kerosene droplet more readily spread on the malachite surface. In addition, 1.5 μL kerosene droplet treated with octyl hydroxamate exhibited greater contact angle compared to 1.5 μL kerosene droplet without the treatment of octyl hydroxamate, suggesting that kerosene droplet treated by octyl hydroxamate interacts more strongly with malachite surface, resulting in higher contact angle on the malachite surface, which increases the hydrophobicity of malachite surface, and therefore, flotation recovery.

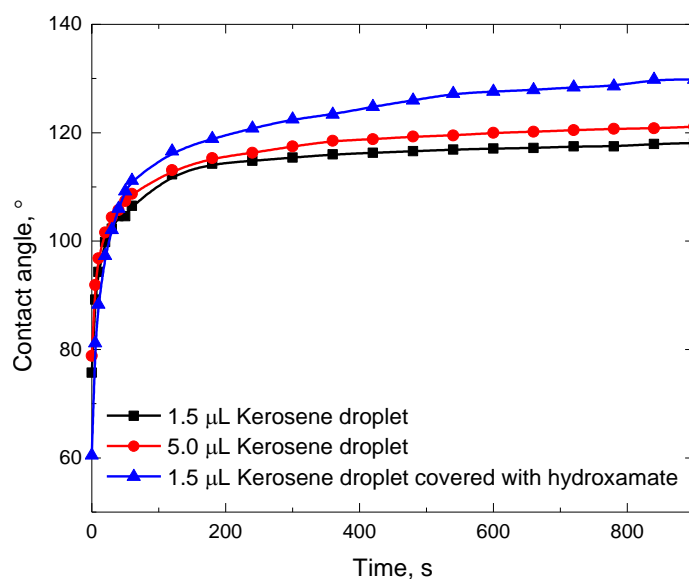


Figure 3.8.4. Spreading of kerosene droplets on malachite surface measured with the captive bubble method.

Figure 3.8.5 gives the optical microscope images of malachite aggregates with the addition of two kinds of kerosene emulsions at the dosage of 50 mg/L with the addition of 2×10^{-4} mol/L octyl hydroxamate to make malachite surface pre-hydrophobic. The aggregates in the presence of octyl hydroxamate treated kerosene emulsion were larger than those in the presence of kerosene emulsion without the treatment of octyl hydroxamate, which is in accord with the results in Figure 3.8.3 and Figure 3.8.4. With the addition of 0.05 wt% octyl hydroxamate treated kerosene in the aggregation process, more oil surfaces contacted malachite particles and the oil droplets spread more readily on the malachite surface, leading to higher coverage of kerosene on malachite surface, and as a consequence, greater hydrophobicity and aggregation.

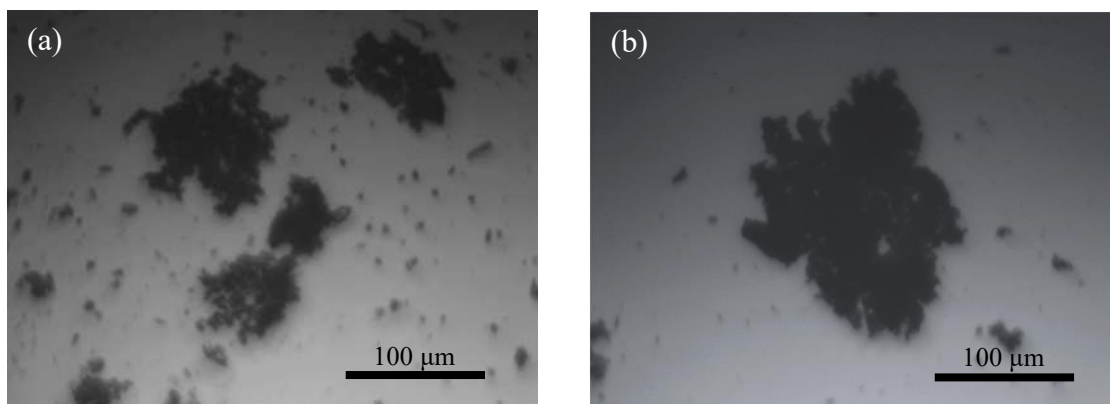


Figure 3.8.5. Optical microscopy images of the malachite aggregates (a) with the addition of kerosene emulsion; (b) with addition of 0.05 wt% octyl hydroxamate treated kerosene emulsion.

Figure 3.8.6 presents the zeta potentials of malachite particles in the absence or presence of 2×10^{-4} mol/L octyl hydroxamate as a function of pH. The zeta potentials of malachite decreased steadily with increasing solution pH, exhibiting its isoelectric point (IEP) at around 8.1, which was in good agreement with that reported at pH 7.8 in another study (Li et al., 2018b). In the presence of octyl hydroxamate, the IEP of malachite particles shifted to the proximity of 7.7, implying the chemisorption of octyl hydroxamate on malachite surface since both malachite and collector were charged negatively at $\text{pH} > \text{IEP}$.

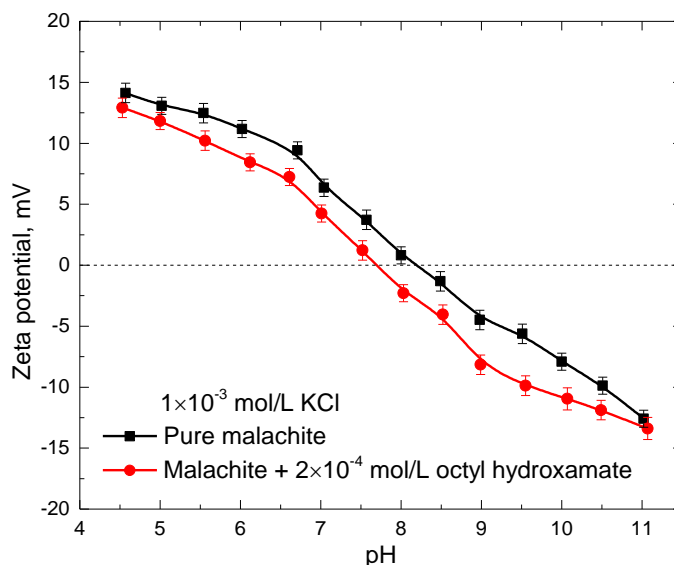


Figure 3.8.6. Zeta potential of malachite in the presence and absence of 2×10^{-4} mol/L octyl hydroxamate.

Figure 3.8.7 gives the zeta potential of kerosene and octyl hydroxamate treated kerosene emulsion, showing that the zeta potentials of kerosene decreased steadily with increasing the

solution pH. With the addition of octyl hydroxamate, the zeta potential of kerosene moved to more positively values, which may be caused by the binding of the neutral octyl hydroxamate molecules to kerosene since octyl hydroxamate molecules and anions co-exist throughout the pH range (Li et al., 2018a).

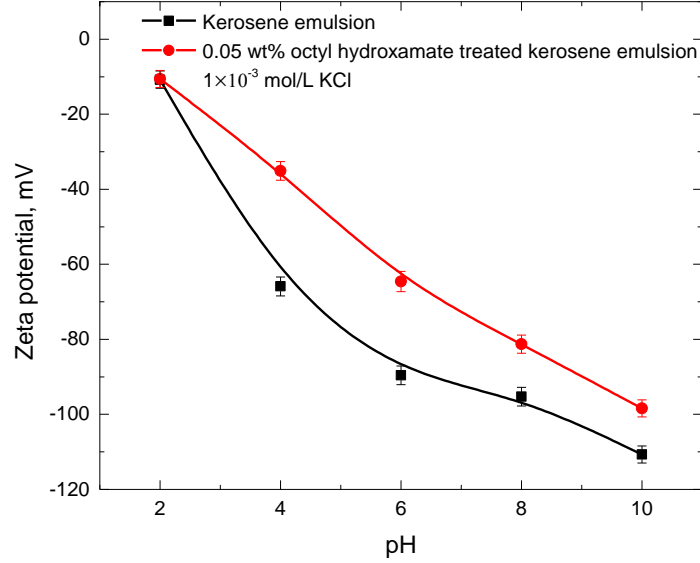


Figure 3.8.7. Zeta potential of kerosene emulsion and 0.05 wt% octyl hydroxamate treated kerosene emulsion.

In an attempt to investigate the energetics of the studied malachite-collector-kerosene system, the EDLVO theory calculation was performed. In the EDLVO theory, the total interaction energy comprises van der Waals interaction (V_W), electrical (Coulombic) interactions under constant potential (V_E), and hydrophobic or hydration interaction (V_H) (Chrysikopoulos and Syngouna, 2012; Piñeres and Barraza, 2011). The total interaction energy can be calculated by the following equation:

$$V_{TED} = V_W + V_E + V_H \quad (1)$$

where V_{TED} is the total interaction energy, V_W is the Van der Waals interaction, V_E is the electrostatic interaction, and V_H is the hydrophobic interaction.

The values of the above interaction energies are calculated based on the following expressions:

$$V_W = -\frac{AR_1R_2}{6H(R_1+R_2)} \quad (2)$$

where R_1 and R_2 are the equivalent spherical radius of malachite particles and oil droplets. The Hamaker constant A is obtained through the Lifshitz approach (Lifshitz, 1992). For malachite particle₁ and oil droplet₂ interacting in aqueous solution₃, A_{132} is given as

$$A_{132} = \frac{3}{4} k_B T \left(\frac{\varepsilon_1 - \varepsilon_3}{\varepsilon_1 + \varepsilon_3} \right) \left(\frac{\varepsilon_2 - \varepsilon_3}{\varepsilon_2 + \varepsilon_3} \right) + \frac{3h_p v_e}{8\sqrt{2}} \frac{(n_1^2 - n_3^2)(n_2^2 - n_3^2)}{\sqrt{(n_1^2 + n_3^2)}\sqrt{(n_2^2 + n_3^2)}\left\{\sqrt{(n_1^2 + n_3^2)} + \sqrt{(n_2^2 + n_3^2)}\right\}} \quad (3)$$

where k_B denotes the Boltzmann constant (1.381×10^{-23} J/K), T is the absolute temperature, ε denotes the static dielectric permittivity, n is the refractive index in the visible range, h_p is the Planck's constant (6.626×10^{-34} m² kg/s), v_e is the main electronic absorption frequency (approximately 3×10^{15} s⁻¹).

The electrostatic double layer energy between malachite particles and oil droplets using the Derjaguin approximation is expressed as (Hogg et al., 1966):

$$V_E = \pi \varepsilon_0 \varepsilon_r \frac{R_1 R_2}{R_1 + R_2} (\psi_1^2 + \psi_2^2) \left\{ \frac{2\psi_1 \psi_2}{\psi_1^2 + \psi_2^2} \ln \left[\frac{1 + \exp(-\kappa H)}{1 - \exp(-\kappa H)} \right] + \ln[1 - \exp(-2\kappa H)] \right\} \quad (4)$$

where ε_0 is the permittivity of vacuum (8.854×10^{-12} C²/J/m), ε_r denotes the dielectric constant of the aqueous medium (78.54 at 25 °C), ψ_1 and ψ_2 are the surface potentials or the stern layer potentials of the particles and droplets, which can be approximated by zeta potentials. κ^{-1} is the Debye length (9.6 nm in 1×10^{-3} mol/L KCl), and can be calculated using Eq. (5).

$$\kappa = \left(\frac{\sum_i C_{i,0} e^2 Z_i^2}{\varepsilon_0 \varepsilon_r k_B T} \right)^{\frac{1}{2}} \quad (5)$$

where $C_{i,0}$ denotes the ion strength in the medium, e is electronic charge (1.602×10^{-19} C), and Z_i denotes the ion valence.

The empirical hydrophobic interaction energy equation between asymmetric spheres can be described as (Li et al., 2018a):

$$V_H = -\frac{K_{132} R_1 R_2}{6H(R_1 + R_2)} \quad (6)$$

The hydrophobic parameter of malachite particle₁ and oil droplets₂ in aqueous medium₃, K_{132} , can be obtained with geometric mean combing rule and expressed as follows (Yoon et al., 1997)

$$K_{132} \approx \sqrt{K_{131} K_{232}} \quad (7)$$

Where K_{131} is the hydrophobic parameter of two malachite₁/aqueous solution₃ interfaces; Similarly, K_{232} is the hydrophobic parameter of two kerosene₂/aqueous solution₃ interfaces. Mao (1998) showed that the K_{232} of oil droplets is approximately 6×10^{-18} J without surfactant, which decreased slightly when the concentration of surfactant was lower than 10^{-4} mol/L. Therefore, the value of K_{232} was simplified as 6×10^{-18} J as an approximation in this work. The K_{131} was obtained by adopting empirical expression Eq. (8) from Yoon and Luttrell (1992).

$$\log K_{131} = -3.194 \times \cos \theta_w - 18.229 \quad (8)$$

where θ_w denotes the water contact angle of malachite mineral. In this study, the contact angle of malachite mineral with the addition of 2×10^{-4} mol/L octyl hydroxamate at pH 9 was measured by captive bubble method and the value was 34.5°.

The interaction energies between malachite particles and kerosene droplets/octyl hydroxamate treated kerosene droplets are shown in Figure 3.8.8 and 3.8.9, respectively. The energies of van der Waals, electrical double layer and hydrophobic interaction were calculated based on Eqs. (1-8). The EDLVO interaction energy estimation could be used to predict the adhesion of kerosene droplets onto the hydrophobic malachite particles. The total interaction energies in the two cases are negative, indicating the attractive interaction force between these particles, thus, the emulsified kerosene droplets and kerosene droplets emulsified with octyl hydroxamate can collide and adhere onto malachite particle surface, making the surface more hydrophobic, forming large hydrophobic aggregates, resulting in improved flotation recovery. However, the interaction strength between emulsified kerosene droplets and malachite particles is greater than that between 0.05 wt% octyl hydroxamate emulsified kerosene droplets and malachite surface. Combined with the micro-flotation results, it infers that the interaction strength calculated by EDLVO theory doesn't play a significant role in this system, which is accord with that reported by Lin et al. (2018).

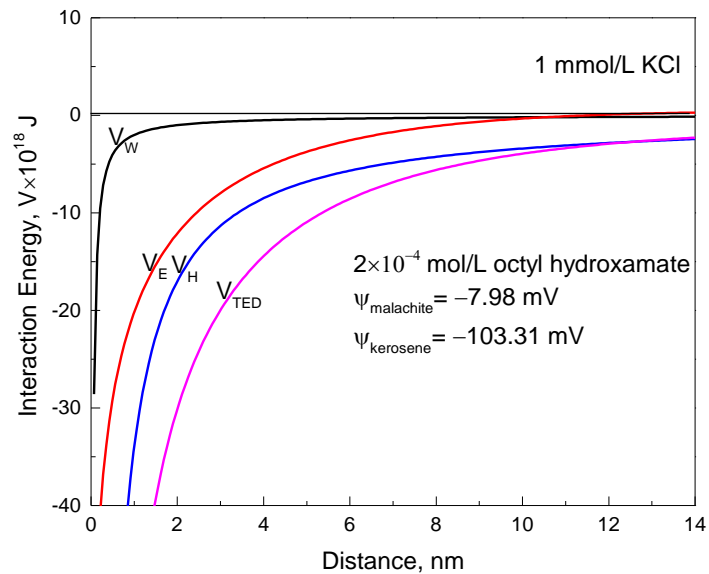


Figure 3.8.8. The interaction energy between malachite particles and emulsified kerosene droplets as a function of separation distance, malachite radius: $2.10 \mu\text{m}$ and kerosene radius: $1.07 \mu\text{m}$.

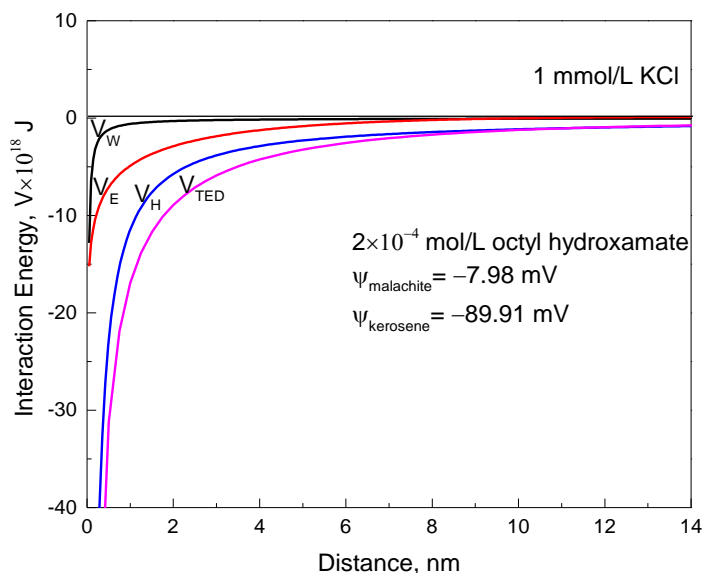


Figure 3.8.9. The interaction energy between malachite particles and 0.05 wt% octyl hydroxamate treated kerosene droplets as a function of separation distance, malachite radius: 2.10 μm and kerosene radius: 0.27 μm .

The EDLVO theory delineated the adherence of kerosene droplets and octyl hydroxamate treated kerosene droplets onto hydrophobic malachite surface. In terms of the spreading phenomenon, the schematic representation of enhancement of kerosene spreading on malachite surface by using octyl hydroxamate as an emulsifier was present in Figure 3.8.10. With the addition of octyl hydroxamate on the kerosene emulsification process, octyl hydroxamate adsorbed on the kerosene droplets surface with the polar group orienting to the water side and hydrophobic tail orienting to the kerosene side. After kerosene droplets adhering to malachite surface, at the three-phase contact line, the octyl hydroxamate on kerosene chemically adsorbs onto the malachite surface and co-adsorbs with the pre-adsorbed octyl hydroxamate, which may provide an additional force to enhance the spreading of kerosene.

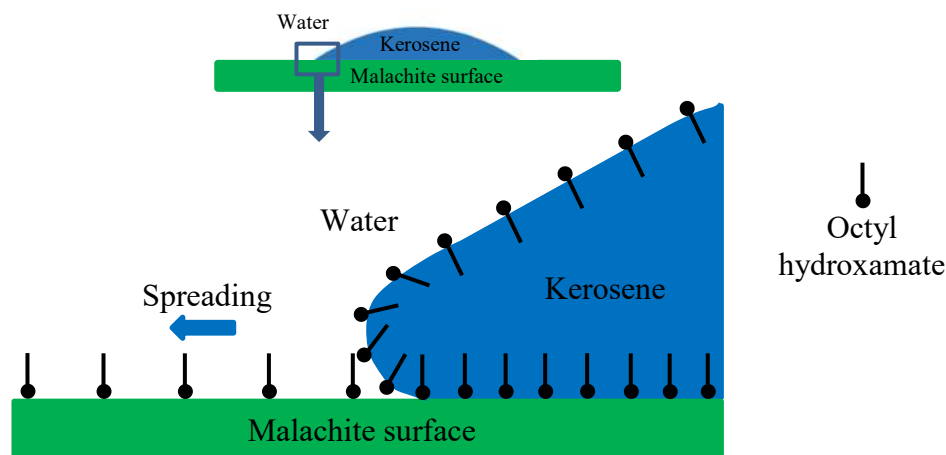


Figure 3.8.10. Schematic representation of enhancement of kerosene spreading on malachite surface by using octyl hydroxamate as an emulsifier.

Chapter 4. Conclusions

Conclusions

- 1) Salicylaldoxime and salicyl hydroxamate are of molecular structures that resemble each other, but with different bond distances in the ligand atoms, resulting in their unusual adsorption behavior and collecting ability, which might provide useful clues for designing novel collectors in base metal oxide flotations.
- 2) The combination use of alcohols and sodium oleate increase the collecting power and selectivity of sodium oleate. The length of hydrocarbon chain, not the straight or branched chain of alcohols, plays a significant role.
- 3) The grinding media influences the minerals surface roughness, thus affecting the wettability of their surface and, consequently, the flotation performance.
- 4) The content of kaolinite and the zeta potential plays a significant role in slime coating of kaolinite on chalcopyrite. With the increase of kaolinite content, the floatability decreased. The decreasing in electric repulsion force caused by the compress of electric double layer due to salinity, and the electric attraction between kaolinite and chalcopyrite caused by calcium increase the slime coating of kaolinite on chalcopyrite.
- 5) At pH below 6, the formation of copper hydroxamate precipitate controls the flotation behavior. While the interaction between octyl hydroxamate molecules and chemisorbed $\text{Cu}(\text{OH})^+$, and the interaction between octyl hydroxamate anions and chemisorbed $\text{Cu}(\text{CO}_3)_2^{2-}$ govern the flotation behavior in the pH range 6-9 and 9-11 respectively.
- 6) The solubility of malachite plays a role in the flotation of malachite with salicylaldoxime. Modifying pH and adding sodium carbonate changes the flotation behavior by altering the solubility, and therefore, the flotation performance.
- 7) CaCl_2 adsorbed onto malachite surface in the form of $\text{Ca}(\text{OH})^+$. The lowered energy barrier between malachite particles and bubbles, and the aggregation of malachite particles account for the increased the floatability of malachite in the presence of 0-0.01 mol/L CaCl_2 .
- 8) The addition of octyl hydroxamate in the emulsification process of kerosene produces kerosene droplets with smaller and uniform size, and superior spreading ability, resulting in enhanced aggregation, and therefore, floatability of malachite.

Recommendations for future work

In the thesis work, all investigations were based on the minerals of high purity to study the fundamental mechanism. In the future work, we recommend using these fundamental in larger scale flotation to beneficiate malachite ore.

Reference

- Ahmadi, R., Khodadadi, D.A., Abdollahy, M., Fan, M., 2014. Nano-microbubble flotation of fine and ultrafine chalcopyrite particles. *International Journal of Mining Science and Technology*. 24, 559-566.
- Ananthapadmanabhan, K., Somasundaran, P., 1985. Surface precipitation of inorganics and surfactants and its role in adsorption and flotation. *Colloids and Surfaces*. 13, 151-167.
- Anderson, J.L., 1985. Effect of nonuniform zeta potential on particle movement in electric fields. *Journal of colloid and interface science*. 105, 45-54.
- Assis, S., Montenegro, L., Peres, A., 1996. Utilisation of hydroxamates in minerals froth flotation. *Minerals engineering*. 9, 103-114.
- Ata, S., 2012. Phenomena in the froth phase of flotation—A review. *International Journal of Mineral Processing*. 102, 1-12.
- Attia, Y., 1977. Synthesis of PAMG chelating polymers for the selective flocculation of copper minerals. *International Journal of Mineral Processing*. 4, 191-208.
- Bandini, P., Prestidge, C.A., Ralston, J., 2001. Colloidal iron oxide slime coatings and galena particle flotation. *Minerals Engineering*. 14, 487-497.
- Barbaro, M., Urbina, R.H., Cozza, C., Fuerstenau, D., Marabini, A., 1997. Flotation of oxidized minerals of copper using a new synthetic chelating reagent as collector. *International journal of mineral processing*. 50, 275-287.
- Bartos, P., 2002. SX-EW copper and the technology cycle. *Resources policy*. 28, 85-94.
- Boulton, A., Fornasiero, D., Ralston, J., 2003. Characterisation of sphalerite and pyrite flotation samples by XPS and ToF-SIMS. *International journal of mineral processing*. 70, 205-219.
- Bournival, G., Pugh, R., Ata, S., 2012. Examination of NaCl and MIBC as bubble coalescence inhibitor in relation to froth flotation. *Minerals Engineering*. 25, 47-53.
- Bremmell, K.E., Fornasiero, D., Ralston, J., 2005. Pentlandite–lizardite interactions and implications for their separation by flotation. *Colloids and Surfaces A: Physicochemical and engineering aspects*. 252, 207-212.
- Bulatovic, S.M., 2010. *Handbook of Flotation Reagents Volume 2, Chemistry, Theory and Practice, Flotation of Gold, PGM and Oxide Minerals*. Elsevier.
- Cassie, A., Baxter, S., 1944. Wettability of porous surfaces. *Transactions of the Faraday society*. 40, 546-551.

- Castro, S., Goldfarb, J., Laskowski, J., 1974. Sulphidizing reactions in the flotation of oxidized copper minerals, I. Chemical factors in the sulphidization of copper oxide. *International journal of mineral processing*. 1, 141-149.
- Cecile, J., Cruz, M., Barbery, G., Fripiat, J., 1981. Infrared spectral study of species formed on malachite surface by adsorption from aqueous salicylaldehyde solution. *Journal of Colloid and Interface Science*. 80, 589-597.
- Chandra, A., Gerson, A., 2009. A review of the fundamental studies of the copper activation mechanisms for selective flotation of the sulfide minerals, sphalerite and pyrite. *Advances in colloid and interface science*. 145, 97-110.
- Chau, T., Bruckard, W., Koh, P., Nguyen, A., 2009. A review of factors that affect contact angle and implications for flotation practice. *Advances in colloid and interface science*. 150, 106-115.
- Chen, T., Zhao, Y., Song, S., 2017a. Electrophoretic mobility study for heterocoagulation of montmorillonite with fluorite in aqueous solutions. *Powder Technology*. 309, 61-67.
- Chen, W., Feng, Q., Zhang, G., Li, L., Jin, S., 2017b. Effect of energy input on flocculation process and flotation performance of fine scheelite using sodium oleate. *Minerals Engineering*. 112, 27-35.
- Choi, J., Choi, S.Q., Park, K., Han, Y., Kim, H., 2016. Flotation behaviour of malachite in mono- and di-valent salt solutions using sodium oleate as a collector. *International Journal of Mineral Processing*. 146, 38-45.
- Chrysikopoulos, C.V., Syngouna, V.I., 2012. Attachment of bacteriophages MS2 and Φ X174 onto kaolinite and montmorillonite: Extended-DLVO interactions. *Colloids and Surfaces B: Biointerfaces*. 92, 74-83.
- Cozza, C., Di Castro, V., Polzonetti, G., Marabini, A., 1992. An X-ray photoelectron spectroscopy (XPS) study of the interaction of mercapto-benzo-thiazole with cerussite. *International journal of mineral processing*. 34, 23-32.
- Dávila-Pulido, G., Uribe-Salas, A., Álvarez-Silva, M., López-Saucedo, F., 2015. The role of calcium in xanthate adsorption onto sphalerite. *Minerals Engineering*. 71, 113-119.
- Dai, Z., Fornasiero, D., Ralston, J., 1999. Particle–bubble attachment in mineral flotation. *Journal of colloid and interface science*. 217, 70-76.
- Dai, Z., Fornasiero, D., Ralston, J., 2000. Particle–bubble collision models—a review. *Advances in Colloid and Interface Science*. 85, 231-256.
- Das, K.K., Natarajan, K., 1997. The effect of constituent metal ions on the electrokinetics of chalcopyrite. *Journal of colloid and interface science*. 196, 1-11.

- Deng, M., Liu, Q., Xu, Z., 2013. Impact of gypsum supersaturated solution on surface properties of silica and sphalerite minerals. *Minerals Engineering*. 46, 6-15.
- Deng, T., Chen, J., 1991. Treatment of oxidized copper ores with emphasis on refractory ores. *Mineral Processing and Extractive Metallurgy Review*. 7, 175-207.
- Derjaguin, B.V., Landau, L., 1993. Theory of the stability of strongly charged lyophobic sols and of the adhesion of strongly charged-particles in solutions of electrolytes. *Progress in Surface Science*. 43, 30-59.
- dos Santos, M.A., Santana, R.C., Capponi, F., Ataíde, C.H., Barrozo, M.A., 2010. Effect of ionic species on the performance of apatite flotation. *Separation and Purification Technology*. 76, 15-20.
- Drzymala, J., 1994. Characterization of materials by Hallimond tube flotation. Part 1: maximum size of entrained particles. *International journal of mineral processing*. 42, 139-152.
- Edwards, C., Kipkie, W., Agar, G., 1980. The effect of slime coatings of the serpentine minerals, chrysotile and lizardite, on pentlandite flotation. *International Journal of Mineral Processing*. 7, 33-42.
- Farrokhpay, S., Zanin, M., 2012. An investigation into the effect of water quality on froth stability. *Advanced Powder Technology*. 23, 493-497.
- Feng, Q., Zhao, W., Wen, S., Cao, Q., 2017. Copper sulfide species formed on malachite surfaces in relation to flotation. *Journal of industrial and engineering chemistry*. 48, 125-132.
- Finkelstein, N., 1997. The activation of sulphide minerals for flotation: a review. *International Journal of Mineral Processing* 52. 81-120.
- Fisher, W.W., 1976. Utilization of Municipal Waste Water for Froth Flotation of Copper and Molybdenum Sulfides. Arizona Bureau of Mines, Mineral Technology Branch Circular 17, 1976. 17 p, 13 fig, 11 tab, 7 ref. \$ 0. 75. OWRT A-046-ARIZ (2). 14-34-0001-6003.
- Font, R., Garcia, P., Rodriguez, M., 1999. Sedimentation test of metal hydroxides: hydrodynamics and influence of pH. *Colloids and Surfaces A: Physicochemical and Engineering Aspects*. 157, 73-84.
- Fornasiero, D., Ralston, J., 2006. Effect of surface oxide/hydroxide products on the collectorless flotation of copper-activated sphalerite. *International Journal of Mineral Processing*. 78, 231-237.
- Fuerstenau, D., 1980. Fine particle flotation in *Fine Particles Processing*, (ed.) P. Somasundaran, SME/AIME, N. York, 669.
- Fuerstenau, D., 2005. Zeta potentials in the flotation of oxide and silicate minerals. *Advances in colloid and interface science*. 114, 9-26.

- Fuerstenau, D., Herrera-Urbina, R., McGlashan, D., 2000. Studies on the applicability of chelating agents as universal collectors for copper minerals. *International Journal of Mineral Processing*. 58, 15-33.
- Fuerstenau, M.C., Lopez-Valdivieso, A., Fuerstenau, D.W., 1988. Role of hydrolyzed cations in the natural hydrophobicity of talc. *International Journal of Mineral Processing*. 23(3-4), 161-170.
- Fuerstenau, M.C., Chander, S., Woods, R., 2007. Sulfide mineral flotation. Froth flotation a century of Innovation. Society for Mining, Metallurgy, and Exploration, Inc.(SME), Littleton, Colorado, 425-464.
- Fuerstenau, M.C., Han, K.N., 2003. Principles of mineral processing. SME.
- Fuerstenau, M.C., Miller, J.D., Kuhn, M.C., 1985. Chemistry of flotation. Soc of Mining Engineers of AIME.
- Gardner, A., Glueckauf, E., 1970. Thermodynamic data of the calcium sulphate solution process between 0 and 200 C. *Transactions of the Faraday Society*. 66, 1081-1086.
- Gaudin, A.M., 1957. Flotation. McGraw-Hill. pp. 16-93.
- Grano, S.R., Prestidge, C.A., Ralston, J., 1997. Solution interaction of ethyl xanthate and sulphite and its effect on galena flotation and xanthate adsorption. *International Journal of Mineral Processing*. 52, 161-186.
- Gregory, J., O'Melia, C.R., 1989. Fundamentals of flocculation. *Critical Reviews in Environmental Science and Technology*. 19, 185-230.
- Hewitt, D., Fornasiero, D., Ralston, J., 1994. Bubble particle attachment efficiency. *Minerals Engineering*. 7, 657-665.
- Hiemenz, P.C., Rajagopalan, R., 1997. Principles of Colloid and Surface Chemistry, revised and expanded. CRC press.
- Hogg, R., Healy, T.W., Fuerstenau, D., 1966. Mutual coagulation of colloidal dispersions. *Transactions of the Faraday Society*. 62, 1638-1651.
- Hope, G., Numprasanthai, A., Buckley, A., Parker, G., Sheldon, G., 2012. Bench-scale flotation of chrysocolla with n-octanohydroxamate. *Minerals Engineering*. 36, 12-20.
- Hope, G., Woods, R., Parker, G., Buckley, A., McLean, J., 2010. A vibrational spectroscopy and XPS investigation of the interaction of hydroxamate reagents on copper oxide minerals. *Minerals Engineering*. 23, 952-959.

- Hope, G.A., Woods, R., Parker, G.K., Buckley, A.N., McLean, J., 2011. Spectroscopic characterisation of copper acetohydroxamate and copper n-octanohydroxamate. *Inorganica Chimica Acta*. 365, 65-70.
- Hu, Y., Wang, D., Xu, Z., 1997. A study of interactions and flotation of wolframite with octyl hydroxamate. *Minerals engineering*. 10, 623-633.
- Jameson, G.J., Nguyen, A.V., Ata, S., 2007. The flotation of fine and coarse particles. *Froth Flotation: A Century of Innovation*, 339-372.
- Johansson, G., Pugh, R., 1992. The influence of particle size and hydrophobicity on the stability of mineralized froths. *International Journal of Mineral Processing*. 34, 1-21.
- Koh, P., Warren, L., 1980. A pilot plant test of the shear-flocculation of ultrafine scheelite, Chemeca 80: Process Industries in the 80's; 8th Australian Chemical Engineering Conference. Institution of Chemical Engineers, Institution of Engineers, Australia and the Royal Australian Chemical Institute, pp. 90.
- Kordosky, G., 2002. Copper recovery using leach/solvent extraction/electrowinning technology: Forty years of innovation, 2.2 million tonnes of copper annually. *Journal of the Southern African Institute of Mining and Metallurgy*. 102, 445-450.
- Kurniawan, A., Ozdemir, O., Nguyen, A., Ofori, P., Firth, B., 2011. Flotation of coal particles in MgCl₂, NaCl, and NaClO₃ solutions in the absence and presence of Dowfroth 250. *International Journal of Mineral Processing*. 98, 137-144.
- Laskowski, J., Kitchener, J., 1969. The hydrophilic—hydrophobic transition on silica. *Journal of Colloid and Interface Science*. 29, 670-679.
- Lee, J., Nagaraj, D., Coe, J., 1998. Practical aspects of oxide copper recovery with alkyl hydroxamates. *Minerals Engineering*. 11, 929-939.
- Lenormand, J., Salman, T., Yoon, R., 1979. Hydroxamate flotation of malachite. *Canadian Metallurgical Quarterly*. 18, 125-129.
- Li, D., Yin, W., Liu, Q., Cao, S., Sun, Q., Zhao, C., Yao, J., 2017a. Interactions between fine and coarse hematite particles in aqueous suspension and their implications for flotation. *Minerals Engineering*. 114, 74-81.
- Li, F., Zhong, H., Xu, H., Jia, H., Liu, G., 2015. Flotation behavior and adsorption mechanism of α -hydroxyoctyl phosphinic acid to malachite. *Minerals Engineering*. 71, 188-193.
- Li, H., Liu, M., Liu, Q., 2018a. The effect of non-polar oil on fine hematite flocculation and flotation using sodium oleate or hydroxamic acids as a collector. *Minerals Engineering*. 119, 105-115.

- Li, H., Mu, S., Weng, X., Zhao, Y., Song, S., 2016. Rutile flotation with Pb^{2+} ions as activator: Adsorption of Pb^{2+} at rutile/water interface. *Colloids and Surfaces A: Physicochemical and Engineering Aspects*. 506, 431-437.
- Li, Z., Rao, F., García, R.E., Li, H., Song, S., 2018b. Partial replacement of sodium oleate using alcohols with different chain structures in malachite flotation. *Minerals Engineering*. 127, 185-190.
- Li, Z., Rao, F., Song, S., 2017b. Comparison of adsorption of phenol OO and NO chelating collectors at the malachite/water interface in flotation. *Minerals*. 7, 20.
- Liang, L., Tan, J., Li, Z., Peng, Y., Xie, G., 2016. Coal flotation improvement through hydrophobic flocculation induced by polyethylene oxide. *International Journal of Coal Preparation and Utilization*. 36, 139-150.
- Lifshitz, E.M., Hamermesh, M., 1992. The theory of molecular attractive forces between solids. In *Perspectives in Theoretical Physics*. (pp. 329-349). Pergamon.
- Lin, Q., Gu, G., Wang, H., Liu, Y., Fu, J., Wang, C., 2018. Flotation mechanisms of molybdenite fines by neutral oils. *International Journal of Minerals, Metallurgy, and Materials*. 25, 1-10.
- Liu, G., Huang, Y., Qu, X., Xiao, J., Yang, X., Xu, Z., 2016. Understanding the hydrophobic mechanism of 3-hexyl-4-amino-1, 2, 4-triazole-5-thione to malachite by ToF-SIMS, XPS, FTIR, contact angle, zeta potential and micro-flotation. *Colloids and Surfaces A: Physicochemical and Engineering Aspects*. 503, 34-42.
- Liu, Q., Peng, Y., 1999. The development of a composite collector for the flotation of rutile. *Minerals Engineering*. 12, 1419-1430.
- Liu, Q., Zhang, Y., 2000. Effect of calcium ions and citric acid on the flotation separation of chalcopyrite from galena using dextrin. *Minerals Engineering*. 13, 1405-1416.
- Liu, S., Zhong, H., Liu, G., Xu, Z., 2018. Cu (I)/Cu (II) mixed-valence surface complexes of S-[(2-hydroxyamino)-2-oxoethyl]-N, N-dibutyldithiocarbamate: Hydrophobic mechanism to malachite flotation. *Journal of colloid and interface science*. 512, 701-712.
- Müller, B., Riedel, M., Michel, R., De Paul, S.M., Hofer, R., Heger, D., Grützmacher, D., 2001. Impact of nanometer-scale roughness on contact-angle hysteresis and globulin adsorption. *Journal of Vacuum Science & Technology B: Microelectronics and Nanometer Structures Processing, Measurement, and Phenomena*. 19, 1715-1720.
- Manono, M., Corin, K., Wiese, J., 2012. An investigation into the effect of various ions and their ionic strength on the flotation performance of a platinum bearing ore from the Merensky reef. *Minerals Engineering*. 36, 231-236.

- Manono, M., Corin, K., Wiese, J., 2013. The effect of ionic strength of plant water on foam stability: A 2-phase flotation study. *Minerals Engineering*. 40, 42-47.
- Mao, L., 1998. Application of Extended DLVO Theory: Modeling of Flotation and Hydrophobicity of Dodecane. Virginia Tech.
- Marion, C., Jordens, A., Li, R., Rudolph, M., Waters, K.E., 2017. An evaluation of hydroxamate collectors for malachite flotation. *Separation and Purification Technology*. 183, 258-269.
- Matis, K., Backhurst, J., 1984. Laboratory studies of electrolytic flotation as a separation technique. J. Gregory, Ellis Horwood, London, 29.
- Miettinen, T., Ralston, J., Fornasiero, D., 2010. The limits of fine particle flotation. *Minerals Engineering*. 23, 420-437.
- Miller, J., Khalek, N.A., Basilio, C., Shall, H., Fa, K., Forssberg, K., Fuerstenau, M., Mathur, S., Nalaskowski, J., Rao, K., 2007. Flotation chemistry and technology of nonsulfide minerals. *Froth Flotation: A Century of Innovation*; Fuerstenau, MC, Jameson, G., Yoon, RH, Eds, 465-553.
- Miller, J., Veeramasuneni, S., Drelich, J., Yalamanchili, M., Yamauchi, G., 1996. Effect of roughness as determined by atomic force microscopy on the wetting properties of PTFE thin films. *Polymer Engineering & Science*. 36, 1849-1855.
- Moolman, D., Eksteen, J., Aldrich, C., Van Deventer, J., 1996. The significance of flotation froth appearance for machine vision control. *International Journal of Mineral Processing*. 48, 135-158.
- Morris, G., Fornasiero, D., Ralston, J., 1995. The surface properties of depressants at the talc-water interface. In: XIX International Mineral Processing Congress. Society for Mining, Metallurgy, and Exploration, Inc., Littleton, Colorado (USA), pp. 43-47.
- Nagaraj, D., Ravishankar, S., 2007. Flotation reagents—A critical overview from an industry perspective. *Froth flotation: A century of innovation*, 375-424.
- Natarajan, R., Fuerstenau, D., 1983. Adsorption and flotation behavior of manganese dioxide in the presence of octyl hydroxamate. *International Journal of Mineral Processing*. 11, 139-153.
- Ni, X., Liu, Q., 2012. The adsorption and configuration of octyl hydroxamic acid on pyrochlore and calcite. *Colloids and Surfaces A: Physicochemical and Engineering Aspects*. 411, 80-86.
- O'Brien, E.C., Farkas, E., Gil, M.J., Fitzgerald, D., Castineras, A., Nolan, K.B., 2000. Metal complexes of salicylhydroxamic acid (H₂Sha), anthranilic hydroxamic acid and benzohydroxamic acid. Crystal and molecular structure of [Cu(phen)₂(Cl)]Cl·H₂Sha, a model for a peroxidase-inhibitor complex. *Journal of inorganic biochemistry*. 79, 47-51.
- Ofori, P., Firth, B., Franks, G., Nguyen, A., Jameson, G., 2005. Impact of saline water on coal flotation. ACARP Project C13051 final report.

- Okada, K., Akagi, Y., Kogure, M., Yoshioka, N., 1990. Effect on surface charges of bubbles and fine particles on air flotation process. *The Canadian Journal of Chemical Engineering*. 68, 393-399.
- Oprea, G., Mihali, C., Danciu, V., Podariu, M., 2004. The study of 8-hydroxyquinoline and salicylaldoxime action at the malachite flotation. *Journal of Mining and Metallurgy A: Mining*. 40, 49-63.
- Ozkan, S., Acar, A., 2004. Investigation of impact of water type on borate ore flotation. *Water research*. 38, 1773-1778.
- Pascoe, R., Doherty, E., 1997. Shear flocculation and flotation of hematite using sodium oleate. *International journal of mineral processing*. 51, 269-282.
- Petrov, T., Protopopov, E., Shuyskiy, A., 2013. Decorative grown malachite. *Nature and technology. Russian journal of earth sciences*. 13.
- Piñeres, J., Barraza, J., 2011. Energy barrier of aggregates coal particle–bubble through the extended DLVO theory. *International Journal of Mineral Processing*. 100, 14-20.
- Pugh, R., 1986. The role of the solution chemistry of dodecylamine and oleic acid collectors in the flotation of fluorite. *Colloids and surfaces*. 18, 19-41.
- Pugh, R., Stenius, P., 1985. Solution chemistry studies and flotation behaviour of apatite, calcite and fluorite minerals with sodium oleate collector. *International Journal of Mineral Processing*. 15, 193-218.
- Pugh, R., Weissenborn, P., Paulson, O., 1997. Flotation in inorganic electrolytes; the relationship between recover of hydrophobic particles, surface tension, bubble coalescence and gas solubility. *International Journal of Mineral Processing*. 51, 125-138.
- Puigdomenech, I., 2004. Make equilibrium diagrams using sophisticated algorithms (MEDUSA). *Inorganic Chemistry*.
- Quast, K., 2016. Literature review on the interaction of oleate with non-sulphide minerals using zeta potential. *Minerals Engineering*. 94, 10-20.
- Quinn, J., Kracht, W., Gomez, C., Gagnon, C., Finch, J., 2007. Comparing the effect of salts and frother (MIBC) on gas dispersion and froth properties. *Minerals Engineering*. 20, 1296-1302.
- Raghavan, S., Fuerstenau, D., 1975. The adsorption of aqueous octylhydroxamate on ferric oxide. *Journal of Colloid and Interface Science*. 50, 319-330.
- Raghavan, S., Hsu, L.L., 1984. Factors affecting the flotation recovery of molybdenite from porphyry copper ores. *International Journal of Mineral Processing*. 12, 145-162.

- Rahimi, M., Dehghani, F., Rezai, B., Aslani, M.R., 2012. Influence of the roughness and shape of quartz particles on their flotation kinetics. *International Journal of Minerals, Metallurgy, and Materials*. 19, 284-289.
- Ramesh, V., Umasundari, P., Das, K.K., 1998. Study of bonding characteristics of some new metal complexes of salicylaldehyde (SALO) and its derivatives by far infrared and UV spectroscopy. *Spectrochimica Acta Part A: Molecular and Biomolecular Spectroscopy*. 54, 285-297.
- Rao, F., Lázaro, I., Ibarra, L., 2017. Solution chemistry of sulphide mineral flotation in recycled water and sea water: a review. *Mineral Processing and Extractive Metallurgy*. 126, 139-145.
- Rao, F., Ramirez-Acosta, F.J., Sanchez-Leija, R.J., Song, S., Lopez-Valdivieso, A., 2011. Stability of kaolinite dispersions in the presence of sodium and aluminum ions. *Applied clay science*. 51, 38-42.
- Rao, F., Song, S., Lopez-Valdivieso, A., 2009. Electrokinetic studies of minerals in aqueous solutions through electroacoustic measurement. *Surface Review and Letters*. 16(1), 65-71.
- Rao, F., Song, S., Lopez-Valdivieso, A., 2012. Specific adsorption of chromium species on kaolinite surface. *Mineral Processing and Extractive Metallurgy Review*. 33, 180-189.
- Rao, S., Finch, J., 1989. A review of water re-use in flotation. *Minerals Engineering*. 2, 65-85.
- Rattanakawin, C., Hogg, R., 2001. Aggregate size distributions in flocculation. *Colloids and Surfaces A: Physicochemical and engineering aspects*. 177, 87-98.
- Rubio, J., Capponi, F., Matiolo, E., Nunes, D., Guerrero, C., Berkowitz, G., 2003. Advances in flotation of mineral fines, *Proceedings XXII International Mineral Processing Congress, Cape-Town, África do Sul*, pp. 1002-1014.
- Schwarz, S., Grano, S., 2005. Effect of particle hydrophobicity on particle and water transport across a flotation froth. *Colloids and Surfaces A: Physicochemical and Engineering Aspects*. 256, 157-164.
- Seke, M.D., Pistorius, P.C., 2006. Effect of cuprous cyanide, dry and wet milling on the selective flotation of galena and sphalerite. *Minerals Engineering*. 19, 1-11.
- Senior, G., Trahar, W., 1991. The influence of metal hydroxides and collector on the flotation of chalcopyrite. *International journal of mineral processing* 33, 321-341.
- Shen, W.Z., Fornasiero, D., Ralston, J., 2001. Flotation of sphalerite and pyrite in the presence of sodium sulfite. *International Journal of Mineral Processing*. 63, 17-28.
- Shibata, J., Fuerstenau, D., 2003. Flocculation and flotation characteristics of fine hematite with sodium oleate. *International Journal of Mineral Processing*. 72, 25-32.

Sillen, L.G., Martell, A.E., Bjerrum, J., 1964. Stability constants of metal-ion complexes. Chemical Society.

Sivamohan, R., 1990. The problem of recovering very fine particles in mineral processing—a review. *International Journal of Mineral Processing*. 28, 247-288.

Song, S., Lopez-Valdivieso, A., Reyes-Bahena, J., Lara-Valenzuela, C., 2001a. Flocculation of galena and sphalerite fines. *Minerals Engineering*. 14, 87-98.

Song, S., Lopez-Valdivieso, A., Reyes-Bahena, J.L., Bermejo-Perez, H.I., 2001b. Hydrophobic flocculation of sphalerite fines in aqueous suspensions induced by ethyl and amyl xanthates. *Colloids and Surfaces A: Physicochemical and Engineering Aspects*. 181, 159-169.

Song, S., Lopez-Valdivieso, A., Reyes-Bahena, J.L., Bermejo-Perez, H.I., Trass, O., 2000. Hydrophobic flocculation of galena fines in aqueous suspensions. *Journal of Colloid and Interface Science*. 227, 272-281.

Song, S., Valdivieso, A.L., 1998. Hydrophobic flocculation flotation for beneficiating fine coal and minerals. *Separation science and technology*. 33, 1195-1212.

Song, S., Zhang, X., Yang, B., Lopez-Mendoza, A., 2012. Flotation of molybdenite fines as hydrophobic agglomerates. *Separation and Purification Technology*. 98, 451-455.

Sreenivas, T., Manohar, C., 2000. Adsorption of octyl hydroxamic acid/salt on cassiterite. *Mineral Processing and Extractive Metallurgy Review*. 20, 503-519.

Sreenivas, T., Padmanabhan, N., 2002. Surface chemistry and flotation of cassiterite with alkyl hydroxamates. *Colloids and Surfaces A: Physicochemical and Engineering Aspects*. 205, 47-59.

Sutherland, K., 1948. Physical chemistry of flotation. XI. Kinetics of the flotation process. *The Journal of Physical Chemistry*. 52, 394-425.

Sutherland, K.L., Wark, I.W., 1955. Principles of flotation. Australasian Institute of Mining and Metallurgy.

Trahar, W., Senior, G., Heyes, G., Creed, M., 1997. The activation of sphalerite by lead—a flotation perspective. *International Journal of Mineral Processing*. 49, 121-148.

Trahar, W., Warren, L., 1976. The flotability of very fine particles—a review. *International Journal of Mineral Processing*. 3, 103-131.

Von Rybinski, W., Schwuger, M., 1986. Adsorption of surfactant mixtures in froth flotation. *Langmuir*. 2, 639-643.

Wang, B., Peng, Y., 2013. The behaviour of mineral matter in fine coal flotation using saline water. *Fuel*. 109, 309-315.

- Wang, J., Cheng, H.W., Zhao, H.B., Qin, W.Q., Qiu, G.Z., 2016. Flotation behavior and mechanism of rutile with nonyl hydroxamic acid. *Rare Metals*. 35, 419-424.
- Wang, K., Liu, Q., 2013. Adsorption of phosphorylated chitosan on mineral surfaces. *Colloids and Surfaces A: Physicochemical and Engineering Aspects*. 436, 656-663.
- Warren, L., 1992. Shear flocculation, *Colloid chemistry in mineral processing*. Elsevier Amsterdam, pp. 309-329.
- Wenzel, R.N., 1936. Resistance of solid surfaces to wetting by water. *Industrial & Engineering Chemistry*. 28, 988-994.
- Woods, R., Somasundaran, P., Moudgil, B., 1987. Reagents in Mineral Technology. Somasundaran P, Moudgil BM.(Eds.), 39-78.
- Wu, X., Zhu, J., 2006. Selective flotation of cassiterite with benzohydroxamic acid. *Minerals engineering*. 19, 1410-1417.
- Xing, Y., Gui, X., Cao, Y., 2016. Effect of calcium ion on coal flotation in the presence of kaolinite clay. *Energy & Fuels*. 30, 1517-1523.
- Xu, H., Zhong, H., Tang, Q., Wang, S., Zhao, G., Liu, G., 2015. A novel collector 2-ethyl-2-hexenoic hydroxamic acid: Flotation performance and adsorption mechanism to ilmenite. *Applied Surface Science*. 353, 882-889.
- Xu, Z., Liu, J., Choung, J., Zhou, Z., 2003. Electrokinetic study of clay interactions with coal in flotation. *International Journal of Mineral Processing*. 68, 183-196.
- Yang, B., Huang, P., Song, S., Luo, H., Zhang, Y., 2018. Hydrophobic agglomeration of apatite fines induced by sodium oleate in aqueous solutions. *Results in Physics*. 9, 970-977.
- Yang, B., Song, S., Lopez-Valdivieso, A., 2015. Kinetics of hydrophobic agglomeration of molybdenite fines in aqueous suspensions. *Physicochemical Problems of Mineral Processing*. 51, 181-189.
- Yang, G., Markuszewski, R., Wheelock, T., 1988. Oil agglomeration of coal in inorganic salt solutions. *Coal Preparation*. 5, 133-146.
- Yoon, R.H., Flinn, D.H., Rabinovich, Y.I., 1997. Hydrophobic interactions between dissimilar surfaces. *Journal of colloid and interface science*. 185, 363-370.
- Yoon, R., Luttrell, G., 1989. The effect of bubble size on fine particle flotation. *Mineral Processing and Extractive Metallurgy Review*. 5, 101-122.
- Yoon, R., Luttrell, G., 1992. Development of the selective hydrophobic coagulation process. Virginia Center for Coal and Minerals Processing, Blacksburg, VA (United States).

Zhang, M., Peng, Y., Xu, N., 2015. The effect of sea water on copper and gold flotation in the presence of bentonite. *Minerals Engineering*. 77, 93-98.

Zhang, Q., Xu, Z., Bozkurt, V., Finch, J., 1997. Pyrite flotation in the presence of metal ions and sphalerite. *International Journal of Mineral Processing*. 52, 187-201.

Zhang, W., Honaker, R., Groppo, J., 2017. Flotation of monazite in the presence of calcite part I: Calcium ion effects on the adsorption of hydroxamic acid. *Minerals Engineering*. 100, 40-48.

Zhou, R., Chander, S., 1993. Kinetics of sulfidization of malachite in hydrosulfide and tetrasulfide solutions. *International journal of mineral processing*. 37, 257-272.

Zhou, Z., Xu, Z., Finch, J., Hu, H., Rao, S., 1997. Role of hydrodynamic cavitation in fine particle flotation. *International Journal of Mineral Processing*. 51, 139-149.

APPENDIX

List of Articles Published and Submitted During the P.h.D Study

1. Articles published in international journals during the P.h.D study

- 1) **Li, Z.**, Rao, F., Song, S., 2017. Comparison of adsorption of phenol O-O and N-O chelating collectors at the malachite/water interface in flotation. *Minerals*, 7(2), 20.
- 2) **Li, Z.**, Rao, F., Song, S., Li, Y., Liu, W., 2018. Slime coating of kaolinite on chalcopyrite in saline water flotation. *International Journal of Minerals, Metallurgy, and Materials*, 25(5), 481-488.
- 3) **Li, Z.**, Rao, F., García, R.E., Li, H., Song, S., 2018. Partial replacement of sodium oleate using alcohols with different chain structures in malachite flotation. *Minerals Engineering*, 127, 185-190.
- 4) **Li, Z.**, Rao, F., Corona-Arroyo, M., Bedolla-Jacuinde, Arnoldo., Song, S., 2019. Comminution effect on surface roughness and flotation behavior in of malachite particles. *Minerals Engineering*, 132, 1-7.

2. Articles submitted to international journals during the P.h.D study

- 1) **Li, Z.**, Rao, F., Song, S., Uribe-Salas, A., López-Valdivieso, A., Reexamining the adsorption of octyl hydroxamate on malachite surface: forms of molecules and anions. *Mineral Processing and Extractive Metallurgy Review*. 2018. 9.
- 2) **Li, Z.**, Rao, F., Song, S., Uribe-Salas, A., López-Valdivieso, A., Effects of the common ions on the adsorption and flotation of malachite with salicylaldoxime. *Colloids and Surfaces A: Physicochemical and Engineering Aspects*. 2018. 11.
- 3) **Li, Z.**, Rao, F., Guo, B., Song, S., López-Valdivieso, A., The improvement of malachite flotation by Ca^{2+} ions with octyl hydroxamate collector. *Minerals Engineering*. 2018. 12
- 4) **Li, Z.**, Rao, F., Guo, B., Song, S., López-Valdivieso, A., Using octyl hydroxamate as emulsifier of kerosene and collector in the floc flotation of malachite fines. *Minerals Engineering*. 2018. 12.

Article

Comparison of Adsorption of Phenol O-O and N-O Chelating Collectors at the Malachite/Water Interface in Flotation

Zhili Li ^{1,2}, Feng Rao ^{2,*} and Shaoxian Song ^{1,*}

¹ School of Resources and Environmental Engineering, Wuhan University of Technology, Luoshi Road 122, Wuhan 430070, China; lizhilijg@gmail.com

² Instituto de Investigación en Metalurgia y Materiales, Universidad Michoacana de San Nicolás de Hidalgo, Ed. "U", Ciudad Universitaria, Morelia, Michoacán 58030, México

* Correspondence: fengrao@umich.mx (F.R.); sxx851215@whut.edu.cn (S.S.);
Tel.: +52-443-322-3500 (F.R.); +86-027-8764-9431 (S.S.)

Academic Editor: William Skinner

Received: 20 December 2016; Accepted: 30 January 2017; Published: 14 February 2017

Abstract: To separate one base metal mineral from another by flotation, it is indispensable to identify chemical reagents that specifically interact with the surface metal sites of one mineral or a group of minerals. This work studies the interactions of chelating collectors which offer the best potential for collecting abilities and mineral specificity with a typical refractory oxide mineral (malachite). Zeta potential, adsorption and Fourier transform infrared (FTIR) measurements are applied to differentiate the interactions of salicylaldoxime and salicyl hydroxamate on the malachite surface. Salicylaldoxime and salicyl hydroxamate are of molecular structures that resemble each other, but with different bond distances in the ligand atoms which result in their unusual adsorption behavior and collecting ability. Thus, the flotation of malachite behaves differently with the two chelating collectors. This study might provide useful clues for designing novel collectors in base metal oxide flotations.

Keywords: malachite; flotation; chelating collector; adsorption

1. Introduction

With the depletion of easy-to-process sulfide copper ores, refractory copper oxides have been increasingly studied to process all over the world. Leaching-solvent extraction-electrowinning (L-SX-EW) and froth flotation are the two methods to beneficiate these ores, of which froth flotation is more economic. Particularly for mixed copper sulfide and oxide ores (e.g., Minto Mine in Yukon, Canada) that are not amenable to L-SX-EW, the development of complementary chemical agents to float the oxides becomes the primary option [1]. However, oxide copper ores (e.g., malachite) respond poorly to traditional sulfide copper (e.g., thiol) collectors in flotation because of their more hydrophilic oxide surfaces [2]. In practices, controlled potential sulfidization, prior to the addition of thiol collectors, has been applied to overcome this problem [3,4], but it is problematic in controlling accuracy, especially for the mixture of sulfide and oxide copper ores, because a slight excess of sulfidizing agents in the pulp depresses the flotation but an insufficient amount produces poor recoveries [5]. Therefore, chelating reagents with superior collecting abilities and strong metal and mineral specificity to float copper oxides independently have been extensively explored. Chelating collector molecules contain a reactive functional group with ligand atoms such as S, N and O in positions capable of bonding the same metal atom through two or more different ligand atoms to form a heterocyclic ring in which the metal atom is one of the members. They are classified into S-S, S-N, N-N, N-O and O-O types based on their bidentate ligands [6]. Although the study of chelating collectors dates back to 1940s and one type

of S-S chelating collector, namely xanthate, has found great success in sulfide flotation [7], in oxide flotations, most of the chelating reagents have only been synthesized and tested for their collecting power in laboratory without commercial applications.

Hydroxamate, which is an O-O type chelating reagent, is the most intensively studied reagent in the development of novel collectors in oxide flotation. In the early stage, potassium octyl hydroxamate was found to chemically adsorb on the malachite surface, so as to be an effective collector for malachite flotation between pH 6 and 10 [8]. While complete flotation of chrysocolla was obtained with potassium octyl hydroxamate as the collector at pH 6 at room temperature, and the flotation response was enhanced with increased temperature when low additions of hydroxamate were involved [9]. Furthermore, hydroxamate was used for the removal of colored titaniferous impurities from kaolin clay in flotation industries [10]. In recent years, advanced surface characterization techniques have been employed to study the interaction of hydroxamate on oxide minerals. For example, X-ray photoelectron spectroscopy (XPS) investigation of the copper oxide minerals cuprite and malachite, and the gangue mineral quartz, showed formation of a copper hydroxamate-like species on cuprite and malachite but no hydroxamate derived species was found on the quartz. Raman spectroscopy confirmed the existence of a copper *n*-octanohydroxamate layer on the surface of treated malachite [11]. Density functional theory (DFT) computation indicated that the dianion of cyclohexyl hydroxamic acid (CHA) or benzoylhydroxamic acid (BHA) exhibited stronger chemical reactivity than their anions and neutral molecules, and that the replacement of the phenyl group by the cyclohexyl group in the BHA molecule significantly impacted the electron donating ability of hydroxamate collectors [12]. Through studying the surface chemistry features of bastnaesite with respect to octyl hydroxamate adsorption, sum-frequency vibrational spectroscopy (SFVS) spectra indicate that a well-ordered monolayer was formed at a hydroxamate concentration of about 1×10^{-4} mol/L [13]. Meanwhile, some studies reported the chelating behavior of salicylaldoxime on oxide minerals, which is an O-N type chelating reagent. For example, salicylaldoxime was utilized for copper flotation from the synthetic mixtures malachite–quartz, of which a good copper recovery (92%) and a great copper percent (46%) demonstrated a good selectivity of the reagent [14]. Jain et al. [15] performed DFT computations to study the interactions of salicylaldoxime (SALO) and its derivatives possessing appropriate alkyl group substitution in the main chain (CM-SALO) or side chain (CS-SALO) with copper, zinc and lead divalent ions. They found that the relative order of selectivity, as per the computed interaction energies, was $\text{Cu} > \text{Zn} > \text{Pb}$. In addition, the derivatives of hydroxamate and salicylaldoxime have been synthesized and applied in oxide flotations. Xu et al. [16] prepared 2-ethyl-2-hexenoic hydroxamic acid (EHHA) for the adsorption and flotation of ilmenite. They found that EHHA exhibited superior flotation performance compared to isooctyl hydroxamic acid (IOHA) and octyl hydroxamic acid (OHA), and floated out 84.03% ilmenite at pH 8.0 with 250 mg/L dosage. Liu et al. [17] reported the adsorption of 3-hexyl-4-amino-1,2,4-triazole-5-thione (HATT) on the malachite surface via its anionic amino-triazole-thione group, thus inducing the malachite surface to be hydrophobic in flotation.

However, these studies were carried out on a case to case basis and the adsorption mechanism of the various chelating ligands is still elusive. Considering the important roles that chelating reagents play in developing oxide collectors, we attempt to first compare the adsorption of phenol O-O and N-O chelating collectors at the malachite/water interface and the corresponding flotation behavior of malachite. It aimed to find out the difference of chelating reactions on the malachite surface when their polar heads are different, so as to offer information for the design of novel collectors, and to provide a solid understanding of the commercial application of chelating collectors in the near future.

2. Experimental

2.1. Materials

The malachite sample obtained from Lupe mine, Mexico, was crushed, hand-sorted and dry-ground in a mechanical agate mortar and pestle. Then, the sample was dry screened to collect

+ 38 μm and -25 μm fractions, of which the coarser fraction was used in flotation tests. The finer fraction was further dry-ground and utilized in adsorption experiments, zeta potential and Fourier transform infrared (FTIR) measurements, of which 50% of the cumulative under size is 8 μm , as measured by a SAIL-D-1100 laser diffraction analyzer (Shimadzu, Tokyo, Japan). The malachite sample showed one X-ray diffraction (XRD) pattern (Figure 1) of high purity in malachite ($\text{Cu}_2(\text{CO}_3)(\text{OH})_2$) with minor amounts of pseudomalachite ($\text{Cu}_2(\text{BO}_3)(\text{OH})_2$). The sample assayed 64.27% Cu and 0.46% P, indicating 90.01% malachite and 4.29% pseudomalachite. Salicylaldehyde and salicylhydroxamic acid (ACS reagent grade) purchased from Energy Chemistry and Aladdin Industrial in China (ACS reagent grade) purchased from Energy Chemistry and Aladdin Industrial in China (ACS reagent grade) were used as chelating collectors for malachite. Their molecular structures were modeled by Materials Studio (MS) 8.0 and presented in Figure 2. The distances between bonds were calculated through their mid points using MS software. Hydrochloric acid (HCl) and sodium hydroxide (NaOH) of ACS reagent grade purchased from Sigma-Aldrich (St. Louis, MO, USA) were used to adjust pH. Methyl isobutyl carbonyl (MIBC) obtained from Aladdin Industrial, Shanghai, China was utilized as frother in the flotation tests. The water used in all experiments was distilled water.

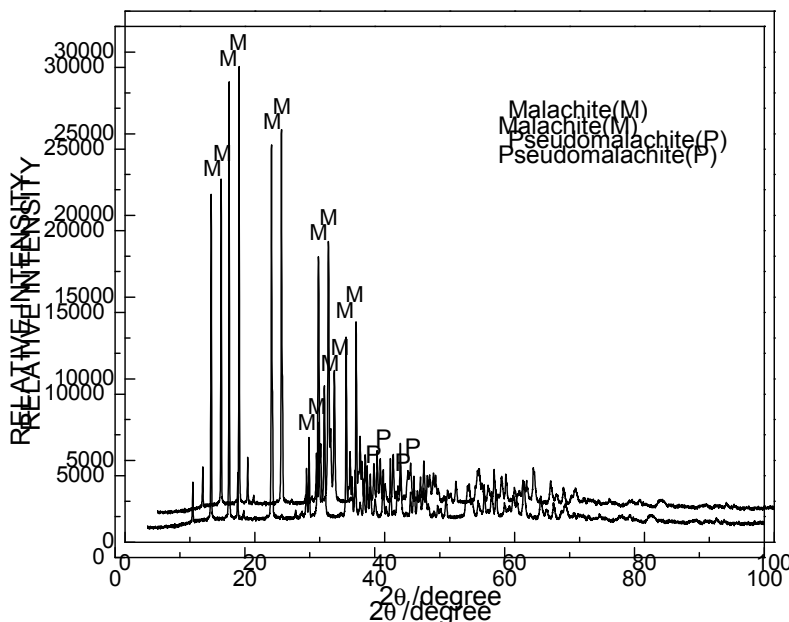
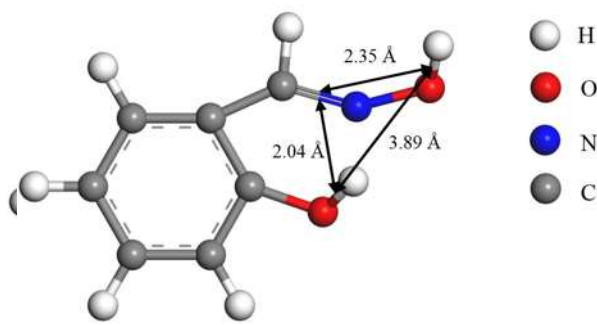


Figure 1. XRD pattern of the malachite sample.



(a)

Figure 2. Cont.

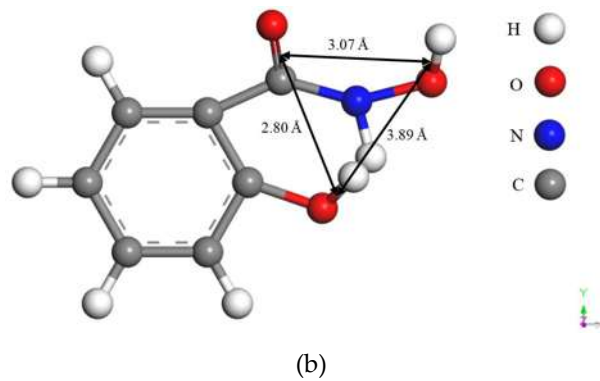


Figure 2. Molecular structures of the (a) salicylaldehyde and (b) salicylhydroxamic acid.

2.2. Methods
 2.2. Methods

The small-scale flotation tests were conducted by using a mechanical flotation machine with a plexiglass 100 mL cell of 2000 rpm/min agitation speed. In each flotation, 3 g malachite ($-75 + 38 \mu\text{m}$) was mixed with 80 mL of water and the pH was adjusted to a desired value. This is followed by the addition of salicylaldehyde or salicylhydroxamic acid and MIBC sequentially with the conditioning time of 3 and 1 min, respectively. Then, the flotation was conducted for 5 min. The concentrate (float) and tailing (unfloat) products were separately collected, dried, and weighed, and the recovery was calculated based on the dry weights of the products. The flotation at each pH was repeated at least three times to obtain the average recovery.

Zeta potential measurements were conducted with a ZETA SIZER NANO ZS90 apparatus (Malvern Instruments, Malvern, UK). The zeta potential was determined by dynamic light scattering and computed after an angle of 90° through the Smoluchowski equation [18]. Instead of the pH was adjusted by NaOH or HCl solutions. If needed, a given dosage of salicylaldehyde and salicylhydroxamic acid was added into the suspension and conditioned for 5 min. Then, the suspension was transferred into the cell and the average zeta potentials of the suspended particles were recorded.

The adsorption of salicylaldehyde or salicylhydroxamate on the malachite surface was measured from Thermo Scientific (Waltham, MA, USA) with a cell of 1 cm optical path was used to determine through a batch depletion method at 22 °C. An AquaMate 8000 UV-vis spectrophotometer from Thermo Scientific (Waltham, MA, USA) with a cell of 1 cm optical path was used to determine the concentrations of salicylaldehyde or salicylhydroxamate, which showed peaks at 303 and 295 nm, respectively. A series of salicylaldehyde or salicylhydroxamic acid aqueous solutions with known concentrations were first characterized and recorded for their absorbance intensities that correlate to the concentrations. For example, the absorbance intensity and reagents' concentrations concentrations were first characterized and recorded for their absorbance intensities that correlate for clean water were zero. Then, the solutions after adsorption were characterized. The concentrations of salicylaldehyde or salicylhydroxamate were obtained through comparing their absorbance intensities with a previous solution of known concentrations. In the adsorption process, 1 g malachite was mixed with 100 mL water, and the pH was adjusted to the required values. Then, the collector was added and conditioned for 5 min. After that, the solid was filtered by membrane and washed with 100 mL water, and the pH was adjusted to the required values. Then, the collector was added and conditioned for 5 min. After that, the solid was filtered by membrane and washed. The filtered solutions were measured for their collector concentrations. The amount of collector adsorbed on the mineral surface was calculated by subtracting the residual concentration in the filtered solution from the collector concentrations. The amount of collector adsorbed on the mineral surface was calculated by subtracting the residual concentration in the filtered solution from the collector concentrations. The amount of collector adsorbed on the mineral surface was calculated by subtracting the residual concentration in the filtered solution from the collector concentrations.

The FTIR spectra were measured from the mineral (FTIR) spectra obtained from Malvern (6700) spectrophotometer from Thermo Scientific. Salicylaldehyde and salicylhydroxamic acid were dissolved in distilled water and distilled water and distilled water and distilled water were mixed in with distilled water and distilled water. The dried samples were mixed with potassium bromide (KBr) for the FTIR measurements. Then, the malachite particles were centrifuged, washed twice

with distilled water and dried at room temperature. The dried samples were molded with potassium bromide (KBr) for the FTIR measurements.

3. Results and Discussion

Minerals 2017, 7, 20

5 of 10

Figure 3 presents the effect of salicyl hydroxamate and salicylaldoxime on the zeta potential of malachite as a function of pH. As with most oxide minerals, the malachite has a positive surface charge at low pHs and a negative surface charge at high pHs. It shows the point of zero charge (PZC) of malachite at pH 8.2, which is in good accordance with the PZC (pH 7.9) reported by Lenormand et al. [8]. With the addition of salicyl hydroxamate and salicylaldoxime, zeta potentials of malachite reverse from positive to negative at low pHs and become more negative at high pHs, indicating the chemical adsorption of these chelating reagents on the surface. However, this modification reduces a pH higher than 10. At pH 11, the zeta potentials of malachite without and with addition of salicyl hydroxamate and salicylaldoxime are close, indicating a weak adsorption. It might be due to the fact that at a pH higher than 10, the predominant hydroxyl species weaken the interaction of chelating reagents on the malachite surface. It is interesting that the salicyl hydroxamate modifies the malachite surface more negatively than the salicylaldoxime does in the pH range of 5–10.

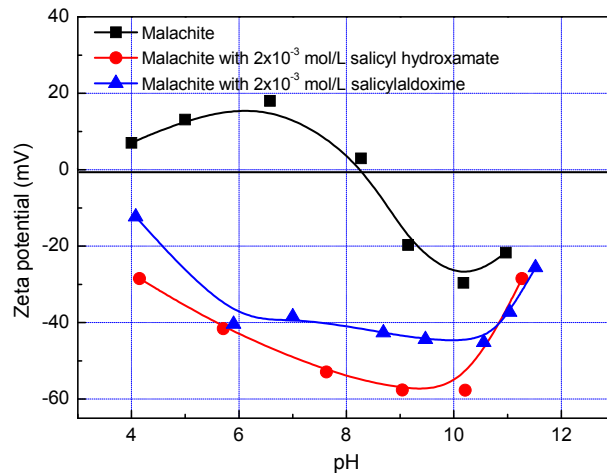


Figure 3. Effect of salicyl hydroxamate and salicylaldoxime on the zeta potential of malachite as a function of pH.

A batch of salicyl hydroxamate and salicylaldoxime depletion has been studied to explore their chemical adsorption on the malachite surface. At a pH lower than pH 6, cupric ions are highly dissolved from malachite, thus the precipitation of cupric salicyl hydroxamate or salicylaldoxime species are predominant reactions for the depletion of the chelating reagents [8]. Then, at a pH higher than pH 6, the chelating reactions (adsorption) on the malachite surface are mainly responsible for the depletion of salicyl hydroxamate or salicylaldoxime. Figure 4 shows their depletion densities in malachite slurry as a function of pH. The depletion of salicyl hydroxamate and salicylaldoxime at pH 3 are as high as 5×10^{-5} mol per gram of malachite minerals, suggesting that both reagents are highly reactive with cupric ions in slurry or malachite surface. Increasing pH from 3 to 9, the depletion of salicylaldoxime decreases slightly but keeps a high amount, while the depletion of salicyl hydroxamate drops dramatically to the lower magnitude of 5×10^{-6} mol/g. Then, the depletion of salicylaldoxime decreases slightly but keeps a high amount, while the depletion of salicyl hydroxamate drops dramatically to the lower magnitude of 5×10^{-6} mol/g. The malachite depletion of salicylaldoxime might be attributed to the different stability constants of these chelating reagents with Cu^{2+} complexes. The stability constants of Cu-salicylaldoxime and Cu-salicyl hydroxamate are 12 and 9.05 [19,20], respectively, indicating that it is easier for salicylaldoxime to react with Cu^{2+} complexes in the form of cupric precipitates or adsorption on the malachite surface. At pH 3 to 9, the higher precipitation and/or adsorption degree of salicylaldoxime on the malachite surface than that of salicyl hydroxamate might be attributed to the different stability constants of these chelating reagents with Cu^{2+} complexes. The stability constants of Cu-salicylaldoxime and Cu-salicyl

The proposed adsorption mechanism can be verified from the FTIR spectra of the malachite surface before and after salicylaldehyde or salicyl hydroxamate adsorption. As can be seen in Figure 6, after salicylaldehyde treatment, the N-Cu and O-Cu stretch vibrations are found at 1193 and 1152 cm^{-1} in the intermediate FTIR spectrum, and 310 and 485 cm^{-1} in the far FTIR spectrum, respectively [21], representing the chemical adsorption of salicylaldehyde on the malachite surface. In contrast, no new peak appears on the FTIR spectra of malachite after salicyl hydroxamate treatment, indicating that the adsorption density of salicyl hydroxamate on malachite is too low for FTIR to identify, which is in accordance with the adsorption behavior.

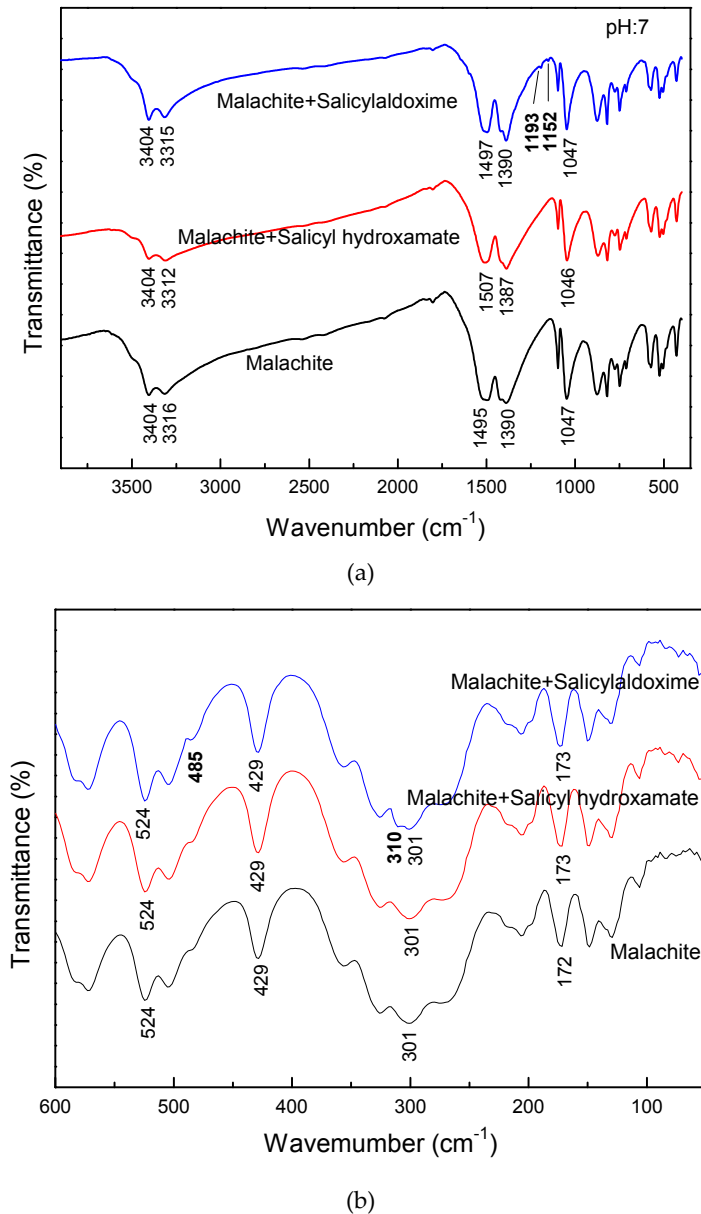


Figure 6. Intermediate (a) and far (b) Fourier transform infrared (FTIR) spectra of malachite, malachite with salicylaldehyde and salicyl hydroxamate.

Figure 7 shows the flotation of malachite as a function of salicylaldehyde and salicyl hydroxamate concentrations at pH 9. By using salicylaldehyde as the collector, the malachite recovery increases to 97% as the salicylaldehyde is increased to 3 mmol/L. Then, the malachite recovery increases to 97% as the salicylaldehyde is increased to 3 mmol/L. Then, the malachite recovery remains constant as the salicylaldehyde concentration is continually increased. In the case of salicyl hydroxamate

remains constant as the salicyldoxime concentration is continually increased. In the case of salicyl hydroxamate collector, the malachite recovery increases slightly to 20% as the collector concentration is increased to 2 mmol/L, and then remains constant. It corresponds well with the adsorption phenomena that (i) both salicyldoxime and salicyl hydroxamate are chemically adsorbed on the malachite surface; (ii) the adsorption density of salicyldoxime is much higher than that of salicyl hydroxamate. Thus, compared with salicyl hydroxamate, salicyldoxime possesses stronger collecting ability and the flotation of malachite reaches the maximum recovery at a higher collector concentration.

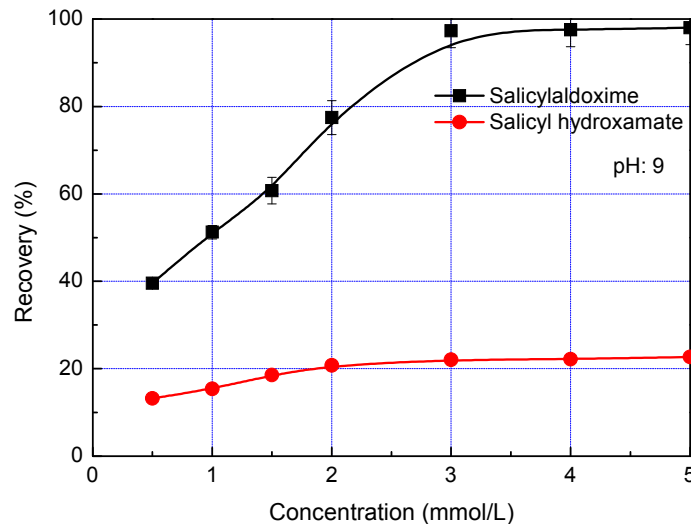


Figure 7. Flotation of malachite as a function of salicyldoxime and salicyl hydroxamate concentrations.

The flotation of malachite using salicyldoxime and salicyl hydroxamic collectors as a function of pH is given in Figure 8. The malachite recovery is less than 20% when using salicyl hydroxamate collector in the pH range 3–11, in which the maximum recovery of 19% is obtained at pH 9. In contrast, the malachite recovery is around 80% at pH 7–9 with salicyldoxime as the collector. These results are in good agreement with the precipitation and adsorption of salicyldoxime and salicyl hydroxamate in aqueous malachite slurries. At a pH lower than 6, the precipitation of copper salicyladsorption amphoteric and poor flotation performance of copper collector is observed, leading to a low recovery. At a pH higher than pH 9 (e.g., pH 11) due to the competition between chelating collectors and hydroxyls on the malachite surface, a low adsorption density takes place, leading to a low malachite recovery. Thus, the proper pH range for malachite flotation with chelating collectors is pH 7–9, which is consistent with malachite flotation by using an oxyl hydroxamate collector [8].

In addition, oxyl hydroxamate has been reported as an effective collector for oxide (malachite) flotation [22,23], but in our results, salicyl hydroxamate shows a weak collecting ability on malachite. This might be due to the fact that (i) the longer alkyl chain in oxyl hydroxamate can render the oxide surface hydrophobic more effectively than the benzene ring in salicyl hydroxamate; (ii) the leaving group after salicyl hydroxamate adsorption might modify the malachite surface more negatively, but also renders it hydrophilic. These results might provide clues for designing a novel collector of oxide flotations in both the carbon chains and the polar heads.

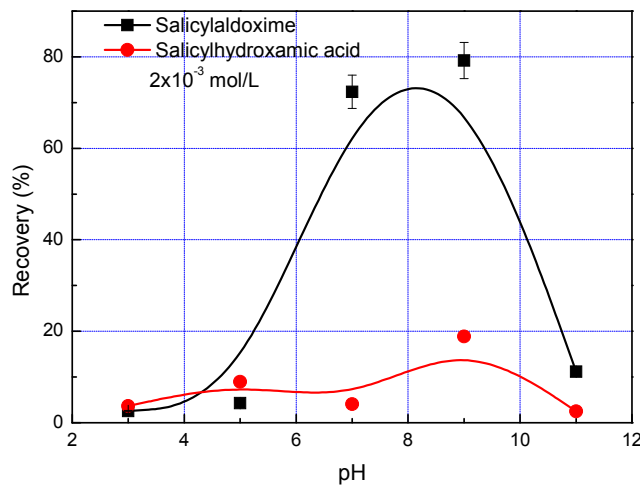


Figure 8. Effect of pH on the flotation of malachite with salicylaldoxime and salicyl hydroxamate collectors.

4. Conclusions

1. Salicylaldoxime and salicyl hydroxamate resemble phenol chelating reagents, but salicylaldoxime induces a much higher adsorption density on the malachite surface than salicylhydroxamate at a pH less than pH 9 because it has a higher stability constant with cupric ions. Thus, in malachite flotation at pH 7–9, the recovery rates are around 80% and 20% when using salicylaldoxime and salicyl hydroxamate as collectors respectively.
2. The large bond distances of ligands in salicyl hydroxamate make its chelating reaction on the malachite surface form a ring structure by two donor atoms with one extra donor oxygen (O⁻) carrying a negative charge. However, in the case of salicylaldoxime, the interactions of N- and O- ligands are detected by FTIR measurements. Therefore, compared with salicylaldoxime, salicyl hydroxamate modifies the malachite surface more negatively by a lower adsorption amount.
3. Salicyl hydroxamate possesses many similarities with two strong malachite collectors, namely salicylaldoxime and octyl hydroxamate, but its collecting ability is very low. This might provide useful clues for the future design of novel collectors in oxide flotations.

Acknowledgments: The financial supports for this work from the Natural Science Foundation of Hubei Province of China under the grant No. 2016CFA013, the Wuhan Science and Technology Bureau of China under the project No. 2016070204020156 and the Consejo Nacional de Ciencia y Tecnología (CONACyT) of Mexico under the grant No. 270986 are gratefully acknowledged.

Zhili Li would like to thank the CONACyT for offering him the scholarship No. 717627 during his PhD studying.

Author Contributions: Feng Rao and Shaoxian Song conceived and designed the experiments; Zhili Li performed the experiments; Feng Rao and Shaoxian Song analyzed the data; Shaoxian Song contributed reagents/materials/analysis tools; Feng Rao wrote the paper.

Conflicts of Interest: The authors declare no conflict of interest.

Conflicts of Interest: The authors declare no conflict of interest.

References

References

1. Lee, K.; Archibald, D.; Mclean, J.; Reuter, M.A. Flotation of mixed copper oxide and sulphide minerals with malachite and chalcocite. *Int. J. Miner. Metall. Process.* **2009**, *22*, 695–700. [\[CrossRef\]](#)
1. Lee, K.; Archibald, D.; Mclean, J.; Reuter, M.A. Flotation of mixed copper oxide and sulphide minerals with malachite and chalcocite. *Int. J. Miner. Metall. Process.* **2009**, *22*, 695–700. [\[CrossRef\]](#)
2. xamirah, J.; Hylton-Kamat, C.N.; Bastian, M. *Miner. Eng.* **2009**, *22*, 223–230. [\[CrossRef\]](#)
2. Miller, N.; Abdel-Khalik, K.H.; Basilio, R.; Al-Shalabi, H.; Al-Faraj, S.; Fueshida, A.; Math, S.; Nalaskowski, J.; Rao, F.; et al. Flotation Chemistry and Technology of Iron-Sulfide Minerals. In *Coth Flotation 2007*; Proceedings of the 11th International Conference on Flotation, Denver, CO, USA, 2007; pp. 165–171.
3. U.S.A. *Gold*; p. 165–171.
3. Castro, G.; Jordan, J.; Laskowski, J. Sulphidizing reactions in the flotation of oxidized copper minerals. I. Chemical factors in the sulphidization of copper oxide. *Int. J. Miner. Process.* **1974**, *1*, 141–149. [\[CrossRef\]](#)

4. Zhou, R.; Chander, S. Kinetics of sulfidization of malachite in hydrosulfide and tetrasulfide solutions. *Int. J. Miner. Process.* **1993**, *37*, 257–272. [[CrossRef](#)]
5. Barbaro, M.; Urbina, R.H.; Cozza, C.; Fuerstenau, D.W.; Marabini, A. Flotation of oxidized minerals of copper using a new synthetic chelating reagent as collector. *Int. J. Miner. Process.* **1997**, *50*, 275–287. [[CrossRef](#)]
6. Fuerstenau, D.W.; Herrera-Urbina, R.; Mcglashan, D.W. Studies on the applicability of chelating agents as universal collectors for copper minerals. *Int. J. Miner. Process.* **2000**, *58*, 15–33. [[CrossRef](#)]
7. Gutzeit, G. Chelate-forming organic compounds as flotation reagents. *Trans. Am. Inst. Min. Eng.* **1946**, *169*, 272–286.
8. Lenormand, J.; Salman, T.; Yoon, R.H. Hydroxamate flotation of malachite. *Can. Metall. Q.* **1979**, *18*, 125–129. [[CrossRef](#)]
9. Peterson, H.D.; Fuerstenau, M.C.; Rickard, R.S.; Miller, J.D. Chrysocolla flotation by the formation of insoluble surface chelates. *Trans. Am. Inst. Min. Eng.* **1965**, *232*, 388–392.
10. Yoon, R.H.; Hilderbrand, T.M. Purification of Kaolin Clay by Froth Flotation Using Hydroxamate Collectors. U.S. Patent 4629556 A, 16 December 1986.
11. Hope, G.A.; Woods, R.; Parker, G.K.; Buckley, A.N.; Mclean, J. A vibrational spectroscopy and XPS investigation of the interaction of hydroxamate reagents on copper oxide minerals. *Miner. Eng.* **2010**, *23*, 952–959. [[CrossRef](#)]
12. Zhao, G.; Zhong, H.; Qiu, X.; Wang, S.; Gao, Y.; Dai, Z.; Huang, J.; Liu, G. The DFT study of cyclohexyl hydroxamic acid as a collector in scheelite flotation. *Miner. Eng.* **2013**, *49*, 54–60. [[CrossRef](#)]
13. Zhang, X.; Du, H.; Wang, X.; Miller, J.D. Surface chemistry aspects of bastnaesite flotation with octyl hydroxamate. *Int. J. Miner. Process.* **2014**, *133*, 29–38. [[CrossRef](#)]
14. Oprea, G.; Mihali, C.; Danciu, V.; Podariu, M. The study of 8-hydroxyquinoline and salicylaldoxime action at the malachite flotation. *J. Min. Metall. A Min.* **2004**, *40*, 49–63.
15. Jain, V.; Rai, B. Density functional theory computations for design of salicylaldoxime derivatives as selective reagents in solvent extraction of copper. *Trans. Indian Inst. Met.* **2016**, *69*, 135–141. [[CrossRef](#)]
16. Xu, H.; Zhong, H.; Tang, Q.; Wang, S.; Zhao, G.; Liu, G. A novel collector 2-ethyl-2-hexenoic hydroxamic acid: Flotation performance and adsorption mechanism to ilmenite. *Appl. Surf. Sci.* **2015**, *353*, 882–889. [[CrossRef](#)]
17. Liu, G.; Huang, Y.; Qu, X.; Xiao, J.; Yang, X.; Xu, Z. Understanding the hydrophobic mechanism of 3-hexyl-4-amino-1,2,4-triazole-5-thione to malachite by ToF-SIMS, XPS, FTIR, contact angle, zeta potential and micro-flotation. *Colloids Surf. A Physicochem. Eng. Asp.* **2016**, *503*, 34–42. [[CrossRef](#)]
18. Hiemenz, P.; Rajagopalan, R. *Principle of Colloid and Surface Chemistry*, 3rd ed.; Marcel Dekker: New York, NY, USA, 1997; pp. 499–533.
19. Sillen, L.G.; Martell, A.E.; Bjerrum, J. *Stability Constants of Metal-Ion Complexes*; Chemical Society: London, UK, 1971; pp. 153–161.
20. O'Brien, E.C.; Farkas, E.; Gil, M.J.; Fitzgerald, D.; Castineras, A.; Nolan, K.B. Metal complexes of salicylhydroxamic acid (H₂Sha), anthranilic hydroxamic acid and benzohydroxamic acid. Crystal and molecular structure of [Cu(phen)₂(Cl)]Cl·H₂Sha, a model for a peroxidase-inhibitor complex. *J. Inorg. Biochem.* **2000**, *79*, 47–51. [[CrossRef](#)]
21. Ramesh, V.; Umasundari, P.; Das, K.K. Study of bonding characteristics of some new metal complexes of salicylaldoxime (SALO) and its derivatives by far infrared and UV spectroscopy. *Spectrochim. Acta Part A Mol. Biomol. Spectrosc.* **1998**, *54*, 285–297. [[CrossRef](#)]
22. Natarajan, R.; Fuerstenau, D.W. Adsorption and flotation behavior of manganese dioxide in the presence of octyl hydroxamate. *Int. J. Miner. Process.* **1983**, *11*, 139–153. [[CrossRef](#)]
23. Sreenivas, T.; Manohar, C. Adsorption of Octyl Hydroxamic acid/salt on cassiterite. *Min. Proc. Extr. Metall. Rev.* **2000**, *20*, 503–519. [[CrossRef](#)]





Partial replacement of sodium oleate using alcohols with different chain structures in malachite flotation

Zhili Li^{a,b}, Feng Rao^{a,b,*}, Ramiro Escudero García^b, Hongqiang Li^c, Shaoxian Song^{d,**}

^a School of Zijin Mining, Fuzhou University, Fuzhou 350108, China

^b CONACYT Instituto de Investigación en Metalurgia y Materiales, Universidad Michoacana de San Nicolás de Hidalgo, Morelia 58030, Mexico

^c School of Resources and Civil Engineering, Wuhan Institute of Technology, Wuhan 430205, China

^d School of Resources and Environmental Engineering, Wuhan University of Technology, Wuhan 430070, China

ARTICLE INFO

Keywords:

Malachite flotation
Sodium oleate
Alcohols
Co-adsorption

ABSTRACT

The sodium oleate collector used in malachite flotation usually exhibits low selectivity. By partially replacing sodium oleate with alcohols, this study presents a method for increasing the selectivity of sodium oleate-based collectors in malachite flotation. By combining 3×10^{-5} mol/L alcohols, such as 1-octanol, 2-ethylhexanol, and α -terpineol, with 1×10^{-5} mol/L sodium oleate, malachite floatability values higher than 98% are achieved. Contact angle and zeta potential measurements reveal that the co-adsorption of alcohols with sodium oleate may be resulted from the hydrophobic interactions between their hydrocarbon chains. The co-adsorption of methyl isobutyl carbinol, along with its shorter hydrocarbon chain, makes it more difficult to render the malachite surface highly hydrophobic. However, the co-adsorption of straight-chain and branched-chain alcohols with sodium oleate shows the ability consistently to induce high malachite floatability.

1. Introduction

Malachite, which usually results from the weathering of copper ores, is a typical carbonate copper mineral that is employed in the mineral processing industry. The flotation of malachite has attracted much attention (Li et al., 2015, 2017; Yang et al., 2017; Liu et al., 2018), particularly with the depletion of easy-to-process sulfide copper ores. It has been found that malachite responds poorly to sulfhydryl collectors (Gaudin, 1957). Consequently, sulfide activators are used for the sulfidisation of malachite before flotation with sulfhydryl collectors (Feng et al., 2017). However, it is not easily controlled in industries as its effectiveness is highly dependent on dosage, and the use of high dosages often leads to poor flotation performance (Herrera-Urbina et al., 1999; Park et al., 2016; Li et al., 2017). Therefore, oxhydryl collectors such as carboxylates (Bulatovic, 2010; Choi et al., 2016), hydroxamates (Lee et al., 1998, 2009; Bulatovic, 2010; Marion et al., 2017) and phosphinic acids (Li et al., 2015) have been studied for the flotation of malachite, but their industrial applications are limited because of several shortcomings. Carboxylates such as fatty acids have affinities to most types of cations, and they therefore have inherently low selectivity in mineral flotation (Nagaraj and Ravishankar, 2007). Furthermore, some commonly dissolved species in the slurry of

malachite flotation have detrimental effects on its flotation with carboxylates collectors. For example, in the flotation of synthetic malachite using sodium oleate as a collector, Choi et al. (2016) reported that the malachite floatability decreased sharply at elevated Ca^{2+} concentrations because of the presence of the hydration layer of adsorbed Ca^{2+} in the oleate-malachite interface. Hydroxamates have been reported as promising chelating collectors for oxide minerals, and a few commercial applications of hydroxamate were achieved with Russian hydroxamate of IM50 and similar compounds produced in China (Bulatovic, 2010). However, the large-scale usage of hydroxamates is limited owing to their practical guidelines, efficacy, and cost in plants (Lee et al., 1998; Phetla and Muzenda, 2010).

There have been studies to develop a collector mixture that can be manufactured economically for oxide flotations. Alcohols combined with collectors have been reported to co-adsorb on the mineral surface through the interaction of the hydrocarbon chain (Liu and Peng, 1999; Filippov et al., 2010). For example, neutral dodecyl alcohol was mixed with dodecyl amine in quartz flotation. It was reported that the contact angle of quartz with a mixture of dodecyl amine and dodecyl alcohol was 10° higher than that with dodecyl amine alone, indicating the co-adsorption of dodecyl alcohol and dodecyl amine (Smith, 1963). Similarly, the mixture of dodecyl amine and hexanol has been found to

* Corresponding author at: School of Zijin Mining, Fuzhou University, Fuzhou 350108, China.

** Corresponding author.

E-mail addresses: fengrao@umich.mx (F. Rao), shaoxian@uaslp.mx (S. Song).

improve the floatability of KCl significantly (Monte and Oliveira, 2004). El-Shall et al. (2000) studied the mixture of polyglycol alcohol (15–30 ppm) and fatty acid in the column flotation of Florida phosphate, and it produced concentrates that have good recovery (99%) and high grade (29–31% P_2O_5). Sis and Chander (2003) reported that fatty acids mixed with non-ionic surfactants have a number of synergistic advantages over the use of a single surfactant in phosphate flotations.

The usage of mixtures of alcohols and collectors in oxide flotations may have the following advantages. First, the mixture of collectors and alcohols is more economical compared to the single oxhydryl collector with a high molecular weight (e.g., fatty acid and sodium oleate). The unit price of the alcohols is usually lower than that of the collectors (Nagaraj and Ravishankar, 2007); for example, in 2016, sodium oleate and 2-ethylhexanol were equal to around 0.7 and 0.17 dollars/mol in China. In addition, as reported by Liu and Peng (1999) in the flotation of rutile with the mixture of styryl phosphonic acid and octanol, the use of only 0.1–1% of emulsifier in the mixture was required for the emulsification. Secondly, the replacement of the oxhydryl collector (e.g., sodium oleate) with alcohol reduces its dosage, which may increase its sensitivity and selectivity.

In the present work, the flotation of malachite was studied with a fatty acid type collector (sodium oleate) partially replaced by four types of alcohols, namely 1-octanol, 2-ethylhexanol, α -terpineol, and methyl isobutyl carbinol (MIBC). These alcohols are different with respect to the length and branching of their chain structures. The work was aimed at illustrating the effect of the chain structure of alcohols on the replacement of the sodium oleate collector in malachite flotation.

2. Experimental

2.1. Materials

A natural malachite sample was obtained from the Lupe mine, Puebla, Mexico. The sample was crushed, hand-sorted and dry-ground to obtain different fractions for different applications, namely, lumps for contact angle measurements, particles of $-75 + 38 \mu\text{m}$ for micro-flotation tests, and fine particles for zeta potential measurements. The size distribution of the fine particles fraction was measured using a Shimadzu SALD-1100 laser diffraction analyser (Japan) with d_{50} and d_{85} values of 3.4 and 8.7 μm , respectively. A Bruker D8 (USA) X-ray diffraction (XRD) meter was used to obtain the XRD pattern of the malachite sample, which was operated with Cu K α radiation, a 40-keV accelerating voltage, and a 0.1 s/step (0.01945°/step) scan rate for the 2θ range of 5–100°. The XRD pattern showed high purity malachite ($\text{Cu}_2\text{CO}_3(\text{OH})_2$) with very small amounts of pseudomalachite ($\text{Cu}_5(\text{PO}_4)_2(\text{OH})_4$). A chemical analysis using atomic absorption spectroscopy (AAS) measurements assayed the sample of 54% Cu and 0.46% P. Based on the XRD characterisation, the P and Cu were assumed to be from pseudomalachite and combination of malachite and pseudomalachite, respectively; thus, it could be determined that 4.3% of pseudomalachite, 90% of malachite, and 5.7% of other impurity minerals were in the sample. The XRD pattern showed high-purity calcite was used in mixed mineral flotation. Sodium oleate (ACS reagent grade) purchased from Aladdin Industrial, China, was used as the malachite collector in the micro-flotation. Alcohols of 1-octanol, 2-ethylhexanol, α -terpineol, and MIBC obtained from Aladdin Industrial were used to partially replace the sodium oleate. The molecular structures of the alcohols are given in Fig. 1, where the MIBC has short branched hydrocarbon chain, while the 1-octanol has straight hydrocarbon chain. Hydrochloric acid (HCl) and sodium hydroxide (NaOH) with reagent grade ACS were used to modify the pH of the solution. Distilled water was used in all the experiments.

2.2. Methods

A 150 mL Hallimond tube equipped with a 20 μm frit and a

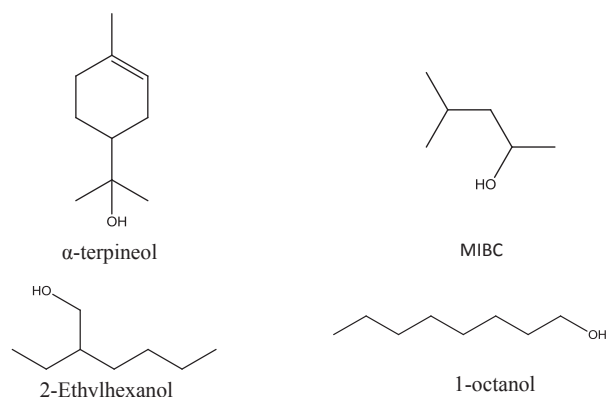


Fig. 1. Molecular structure of the alcohols used in micro-flotation.

magnetic stirrer was used to test the malachite floatability with different reagent mixtures. In each flotation, 3 g of the malachite sample ($-75 + 38 \mu\text{m}$) or mixed mineral (malachite : calcite = 1:1) was conditioned for 2 min in 130 mL of distilled water, and the solution was adjusted to the desired pH by using HCl or NaOH. Then, a given amount of reagents was added and conditioned for 3 min. After that, the conditioned slurry was transferred to the Hallimond tube, and the flotation was performed for 10 min with nitrogen gas at a flow rate of 20 mL/min. The floated (concentrate) and unfloated (tailing) products were separately collected, dried and weighed, and the recovery was calculated based on the percentage of floated product/(mass of floated product + unfloated product). In the micro-flotation tests, the variables used were the pH of the slurry, concentration of sodium oleate and alcohols from 0 to 6×10^{-5} mol/L, and a mixture of sodium oleate and alcohols.

The contact angle of the malachite sample was measured by a goniometer (DSA-25, Kruss, Germany) The DSA-25 goniometer was equipped with a CM4210 optics module with a zoom lens, and was operated using the sessile drop method in the software ADVANCE. In the measurements, lumps of the prepared mineral samples were loaded on the goniometer stage and 1.5 μL of distilled water was dropped on them. The advancing and receding contact angles were then reported. When the difference was less than 1% of the receding contact angle, the average value of these two angles was reported as the contact angle. For each condition (e.g., sodium oleate concentration: 1×10^{-5} mol/L), at least four measurements were performed and the average contact angle was reported in this work. The lumps of the malachite samples were first wet-polished with 80, 400, 800, and 1200 grit SiC paper, and then with 1 μm of alumina powder suspensions. After that, in order to obtain a given pH or reagent condition for the surface, the polished malachite lump was immersed in solutions with different pH values and reagent concentrations for 30 min, and then washed with water.

A ZetaProbe Analyzer (Colloidal Dynamics, Australia) with electroacoustic technology was used to determine the zeta potential of the malachite particles in aqueous solutions for various pH values and reagent concentrations. The zeta potential was calculated from the stimulated electro-acoustic sonic amplitude (ESA) values from the malachite particles using the O'Brien equation (O'Brien, 1990; Rao et al., 2009). In a typical measurement, 5 g of malachite sample and a given amount of sodium oleate and/or alcohol were conditioned with 250 mL KCl (1×10^{-3} mol/L) solutions in the cell of the ZetaProbe for 10 min. Then, the zeta potential values were reported by the equipment. In some cases, changes in the pH were accomplished automatically by the equipment through the addition of 0.1 mol/L KOH and HCl solutions.

3. Results and discussion

Fig. 2 shows the floatability of malachite with sodium oleate (5×10^{-5} mol/L) as a function of the pH. For pH values of 6–12, the

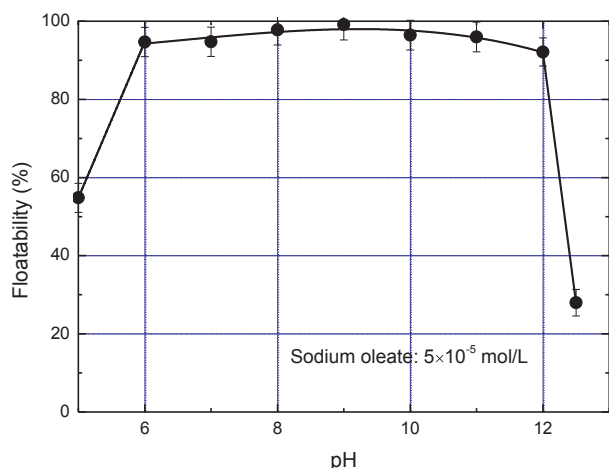


Fig. 2. Malachite flotation with sodium oleate as a function of pH.

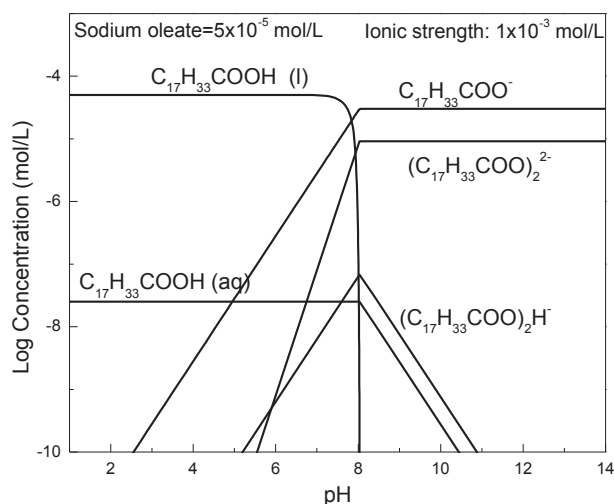


Fig. 3. Equilibrium diagram of oleate species as a function of pH in aqueous solution (Pugh and Stenius, 1985).

malachite floatability was $\geq 95\%$; in particular, at pH 9, the floatability was 99%. It was reported that the complexation of anionic oleate species ($C_{17}H_{33}COO^-$, $(C_{17}H_{33}COO)_2H^-$ or $(C_{17}H_{33}COO)_2^{2-}$) with cupric species (e.g., Cu^{2+} and $CuOH^+$) induced the chemisorption of oleate collectors on the malachite surface (Somasundaran, 1987; Choi et al., 2016). At $pH > 12$, the precipitation of $Cu(OH)_2$ hinders this complexation and adsorption; thus, the floatability decreases sharply. Fig. 3 shows the equilibrium diagram of the oleate species as a function of pH in the aqueous solution. As can be seen in the figure, at $pH < 6$, $C_{17}H_{33}COOH(l)$ and $C_{17}H_{33}COOH(aq)$ are mainly formed rather than the anionic oleate species; thus, the malachite floatability is greatly reduced. This result is in good agreement with other studies in terms of the flotation of malachite with an oleate collector at various pH values (Somasundaran, 1987; Wang and Liu, 2013).

Fig. 4 shows the malachite floatability by independently adding sodium oleate and alcohols, with different concentrations. Without the reagent, the malachite flotation had a high entrainment (15%), which is attributed to the fine particle size ($-75 + 38 \mu m$) and long flotation time (10 min) in the Hallimond test (Drzymala, 1994). Upon the addition of sodium oleate, the malachite floatability increased steadily up to a concentration of $3 \times 10^{-5} \text{ mol/L}$ and then it remained constant at high levels ($> 98\%$). At low concentrations of sodium oleate, the chemical adsorption of individual ions occurs on the malachite surface, followed by the aggregation of the alkyl chains leading to hemi-micelle structures at higher concentrations (Pugh, 1986). Thus, at 3×10^{-5}

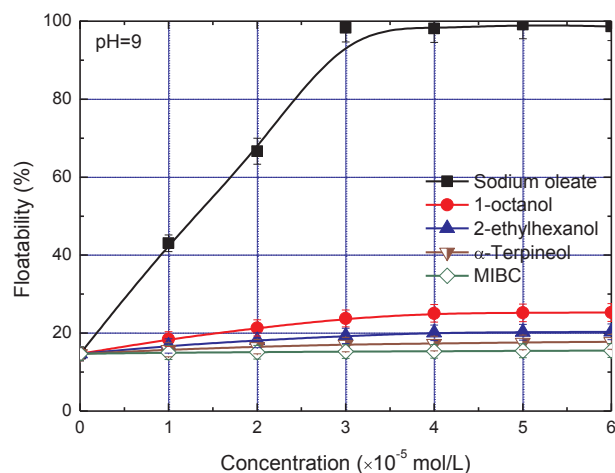


Fig. 4. Malachite flotation at different concentrations of sodium oleate and alcohols.

mol/L, the malachite surface may be formed with a monolayer of the anionic oleate species, leading to the high floatability of malachite. However, with the addition of alcohols, the malachite floatability increased only slightly ($< 25\%$), even at a high concentration of alcohols ($6 \times 10^{-5} \text{ mol/L}$). This indicates that the alcohols result in greater frothing and therefore potentially more entrainment. They also allow for the creation of smaller bubbles and therefore a larger available surface area for mineral attachment. However, compared with sodium oleate, alcohol molecules cannot adsorb on the malachite surface to induce high floatability.

Fig. 5 shows the floatability of malachite with sodium oleate and alcohol mixtures, where the sodium oleate was maintained at $1 \times 10^{-5} \text{ mol/L}$, while the alcohols were increased from 0 to $4 \times 10^{-5} \text{ mol/L}$. By mixing 1-octanol, 2-ethylhexanol, and α -terpineol with sodium oleate, the malachite floatability increased significantly from 43% to $> 96\%$ at concentrations up to $3 \times 10^{-5} \text{ mol/L}$, after which it remained virtually constant. By mixing MIBC with sodium oleate, the malachite floatability increased to 64% at a concentration of $1 \times 10^{-5} \text{ mol/L}$, and then it increased slightly; thus, the impact of MIBC was much less than that of the other three alcohols. These results indicate that the addition of alcohols to the sodium oleate collector induced a significant malachite flotation, but alcohols with short hydrocarbon chains (e.g., MIBC) may limit this effect. Interestingly, a high malachite floatability ($> 95\%$) can be achieved with either $3 \times 10^{-5} \text{ mol/L}$ sodium oleate (Fig. 4) alone or a mixture of sodium oleate ($1 \times 10^{-5} \text{ mol/L}$) and alcohols ($2 \times 10^{-5} \text{ mol/L}$) (Fig. 5). As discussed previously, a mixture

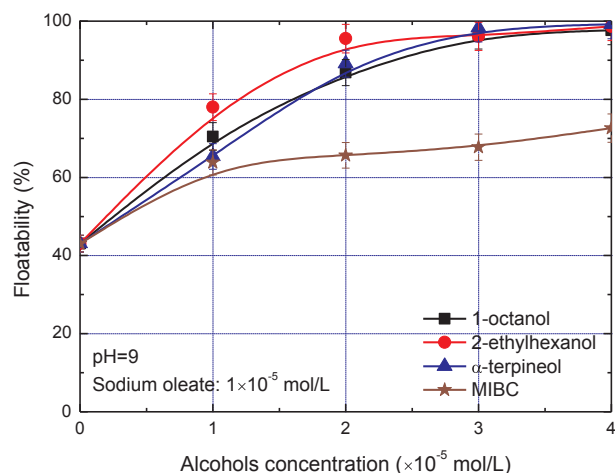


Fig. 5. Malachite flotation with sodium oleate and alcohol mixture.

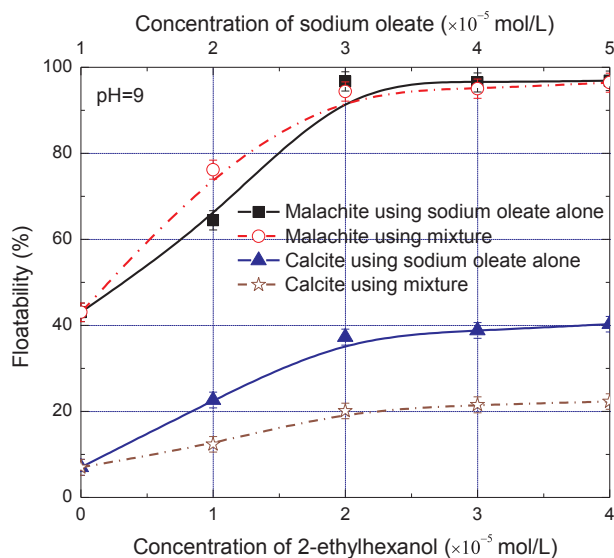


Fig. 6. Micro-flotation of mixed minerals (malachite:calcite = 1:1) with sodium oleate alone and 2-ethylhexanol-oleate.

of sodium oleate and alcohols is a more cost-effective collector than sodium oleate alone in malachite flotation.

The mixture may provide a better selectivity for the sodium oleate-based collector. Fig. 6 shows the micro-flotation of mixed minerals (malachite:calcite = 1:1) with sodium oleate alone, and the mixture of 2-ethylhexanol-oleate, where the solid lines represent the floatability of malachite and calcite using sodium oleate alone, while the dash-dotted lines are those using mixtures of 1×10^{-5} mol/L oleate and variable concentrations of 2-ethylhexanol. Whether using sodium oleate alone or 2-ethylhexanol-oleate, the floatability of malachite increased significantly at concentrations up to 3×10^{-5} mol/L, and then it kept virtually constant. However, the floatability of calcite using sodium oleate alone was around 17% higher than that using 2-ethylhexanol-oleate, when the concentrations were higher than 3×10^{-5} mol/L. Therefore, the mixture of 2-ethylhexanol-oleate induced a higher selectivity for the mixed minerals of malachite and calcite in micro-flotation. It has been reported that a low selectivity of malachite from calcium and magnesium gangue minerals (e.g., calcite, magnesite, and feldspar) was obtained using a sodium oleate collector, and this is believed to be because the complexation between the anionic oleate species and the hydrolysed Ca^{2+} or Mg^{2+} species also takes place on the gangue minerals surface (Miller et al., 2007). However, it should be noted that the solubility product constants (K_{sp}) of copper oleate, calcium oleate, and magnesium oleate are $10^{-19.4}$, $10^{-15.4}$, and $10^{-13.8}$ (Fuerstenau and Han, 2003), respectively, indicating that the oleate is slightly preferred for adsorption on the malachite surface. In many malachite-flotation practices, this selectivity is usually sacrificed in order to obtain a high copper recovery by using high dosages of sodium oleate. The partial replacement of sodium oleate by alcohols in the form of a collector mixture may result in a tendency for the formation of copper oleate, resulting in a better selectivity of the sodium oleate-based collectors. Nevertheless, as reported by Liu and Peng (1999), because 1-octanol, α -terpineol, and 2-ethylhexanol are sparingly soluble in water, the prerequisites for the large-scale application of the collector mixture are: (1) an effective emulsification and (2) that the added emulsifier has no impact on the flotation.

Contact angle and zeta potential measurements were performed to study the adsorption of sodium oleate and alcohols on the malachite surface. Fig. 7 presents contact angle images and the results of malachite lumps treated with sodium oleate having different concentrations at pH 9. The contact angle of pure malachite was 38° . After the treatment with sodium oleate, the adsorbed anionic oleate species made the

malachite hydrophobic, with their hydrophobic tail orientating into water. As the sodium oleate concentration increased from 0 to 1×10^{-5} , 2×10^{-5} , and 3×10^{-5} mol/L, the contact angle increased significantly from 38° to 45° , 62° , and 70° , respectively. Then, it increased slightly to 73° and 77° as the sodium oleate concentration increased continually to 4×10^{-5} and 5×10^{-5} mol/L, respectively. Thus, the sodium oleate concentration of 3×10^{-5} mol/L is the inflection point of the concentration which renders the malachite surface highly hydrophobic, and is in good agreement with the malachite flotation results as a function of the sodium oleate concentration (Fig. 4).

Fig. 8 shows the contact angle results of malachite lumps treated with sodium oleate alone and with a mixture of sodium oleate and alcohols. With the addition of the mixture (1×10^{-5} mol/L sodium oleate and alcohols), the contact angle increased in a concave-type trend as the concentrations of alcohols increased. It increased steadily at low concentrations of alcohols (1×10^{-5} mol/L and 2×10^{-5} mol/L), and increased sharply at high concentrations of alcohols (3×10^{-5} mol/L and 4×10^{-5} mol/L). However, the malachite floatability (Fig. 5) with the same mixture and the contact angle with various concentrations of sodium oleate (Fig. 7) exhibited a convex-type increase, where high increases of the floatability and contact angle were observed at low reagent concentrations. This inconsistency may indicate the different adsorption forces between sodium oleate and alcohols on the malachite surface. In the contact angle measurements, the malachite surfaces treated with reagents were washed before drying for the measurements. With sodium oleate alone, the wash could not induce desorption because it is chemically adsorbed on the malachite surface. Thus, malachite floatability and contact angle exhibited the same trend. However, with the sodium oleate and alcohol mixtures, alcohols may be co-adsorbed with sodium oleate, and the wash could therefore induce the desorption of some alcohol parts. This makes the contact angle of malachite exhibit a concave-type trend when treated with a 1×10^{-5} mol/L sodium oleate and alcohol mixture, where to render the malachite surface hydrophobic, a high concentration of alcohols was required to offset the desorption of alcohol. Besides, compared with 1-octanol, α -terpineol, and 2-ethylhexanol, the contact angle of the malachite treated with sodium oleate and MIBC was smaller, but the difference was much smaller than that of malachite flotation with the sodium oleate and alcohol mixture (Fig. 5). This result is in good agreement with other studies, in which the contact angle of the mineral is not linearly correlated with the flotation behaviour (Chau et al., 2009).

Fig. 9 shows the zeta potentials of malachite in the presence of various concentrations of sodium oleate (a), alcohols (a), and their mixtures (b). The zeta potential of pure malachite decreased with increasing pH, and it gave an isoelectric point (IEP) value at pH 7.8, which is in good agreement with the reported IEP of malachite at pH 8.3 in another study (Li et al., 2015). In the presence of alcohols, namely 1-octanol, 2-ethylhexanol, α -terpineol, and MIBC, the zeta potential of malachite kept the same value (Fig. 9(a)), indicating that alcohols were not chemically adsorbed on the malachite surface. In contrast, in the presence of 1×10^{-3} mol/L sodium oleate, the zeta potentials of malachite decreased significantly and the IEP decreased to $\text{pH} < 5$. As reported by Quast (2016), with the equilibrium diagram of oleate species at various pH values (Fig. 3), the mechanism for decreasing the zeta potential of malachite by oleate is different in acidic conditions when compared with the case in alkaline solutions. In alkaline solutions, the adsorption of anionic oleate species ($\text{C}_{17}\text{H}_{33}\text{COO}^-$, $(\text{C}_{17}\text{H}_{33}\text{COO})_2\text{H}^-$, and $(\text{C}_{17}\text{H}_{33}\text{COO})_2^{2-}$) on the malachite surface renders it more negative. In acidic solutions, the decrease of zeta potentials is attributed to the coagulation/precipitation of the colloidal oleate species ($\text{C}_{17}\text{H}_{33}\text{COOH}$ (l) and $\text{C}_{17}\text{H}_{33}\text{COOH}$ (aq)), which have IEPs around 2–3, on the malachite surface. Notably, in Fig. 9(b), in the presence of mixtures of sodium oleate (1×10^{-3} mol/L) and alcohol, the zeta potentials became more negative than that of malachite, but were higher than that of the sole sodium oleate (1×10^{-3} mol/L). This

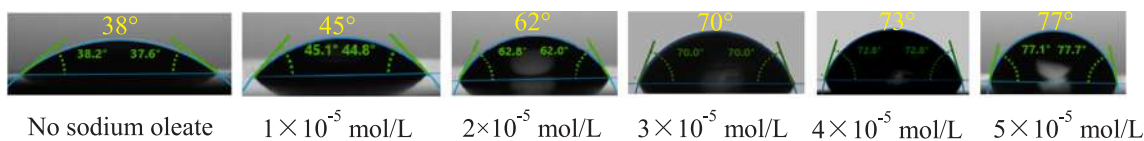


Fig. 7. Contact angle images and results of malachite treated with sodium oleate of different concentrations at pH 9.

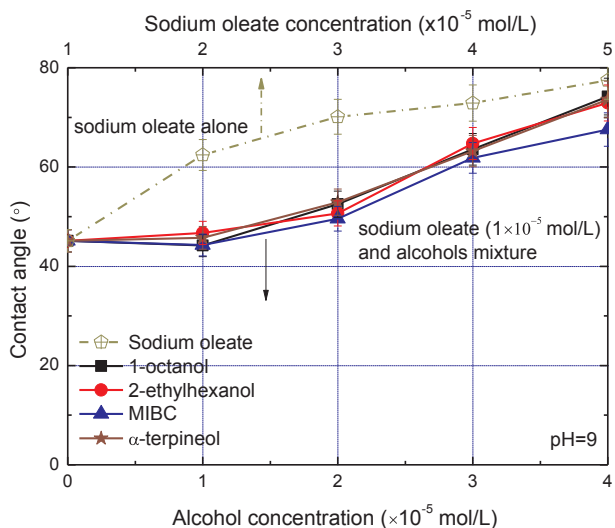


Fig. 8. Contact angle results of malachite treated with sole sodium oleate and a mixture of sodium oleate and alcohols.

indicates the competition/replacement of alcohols to sodium oleate on the malachite surface when the mixture was applied. A similar phenomenon involving competition/replacement has been observed and reported in other studies. For example, Rybinski and Schwuger (1986) investigated the single and binary adsorption of anionic alkyl sulfosuccinate and non-ionic nonylphenol pentaglycol ether on scheelite and calcite minerals, and they reported that the addition of non-ionic surfactant reduced the adsorption of alkyl sulfosuccinate on both minerals. Lu et al. (1999) reported that the presence of polyethylene oxide (PEO) decreased the adsorption of oleate species on apatite, while the contact angle increased.

For the flotation tests, Fig. 5 showed that the addition of alcohols to the sodium oleate significantly increased the malachite floatability. In contact angle measurements, the co-adsorption of alcohols with sodium oleate on the malachite surface was confirmed. However, a weaker adsorption force of alcohols relative to that of sodium oleate was hypothesised because of the concave and convex increase of the contact angle with the mixture and the sole sodium oleate, respectively (Fig. 7). In the zeta potential measurements, the competition/replacement of alcohols with sodium oleate on the malachite surface was observed by comparing the zeta potentials of malachite with the mixture and the sole sodium oleate (Fig. 9). Therefore, the co-adsorption of alcohols with sodium oleate on the malachite surface, by way of hydrophobic interactions between the hydrocarbon chains of sodium oleate and alcohols, is hypothesised and schematically presented in Fig. 10. Furthermore, compared with 1-octanol, 2-ethylhexanol, and α -terpineol, MIBC has a shorter hydrocarbon chain, and there is therefore a weaker hydrocarbon chain interaction between MIBC and sodium oleate. This makes it more difficult for the co-adsorption of MIBC to render the malachite surface hydrophobic.

4. Conclusion

This work studies the partial replacement of sodium oleate using alcohols with different chain structures in malachite flotation. The results are as follows:

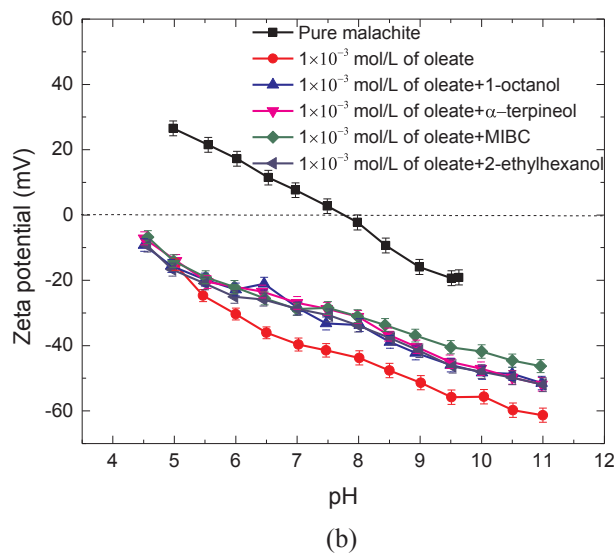
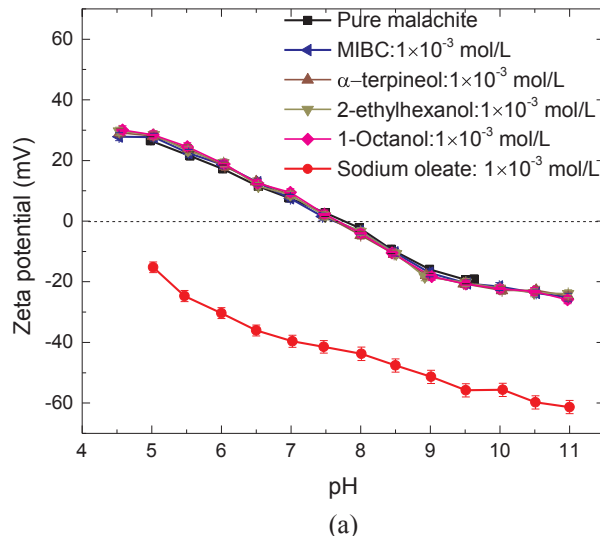


Fig. 9. Zeta potentials of malachite in the presence of various concentrations of sodium oleate, alcohols, and their mixture.

1. The malachite floatability was found to be higher than 95% using sodium oleate collectors at pH 6–12, while alcohols could not render the malachite surface hydrophobic; meanwhile, its floatability reached approximately 15% owing to the entrainment caused by the fine particle size and long flotation time. However, the malachite floatability exceeded 98% when using 1×10^{-5} mol/L of sodium oleate and 3×10^{-5} mol/L of alcohols such as 1-octanol, 2-ethylhexanol, and α -terpineol, indicating the co-adsorption of alcohols with sodium oleate on the malachite surface. This may reduce the cost and increase the selectivity of sodium oleate-based collectors.
2. Zeta potential and contact angle measurements indicate that the co-adsorption of alcohols with oleate species on the malachite surface takes place owing to the hydrophobic interaction between their hydrocarbon chains. Of the 1-octanol, 2-ethylhexanol, α -terpineol, and MIBC, MIBC has a shorter chain, which makes it more difficult

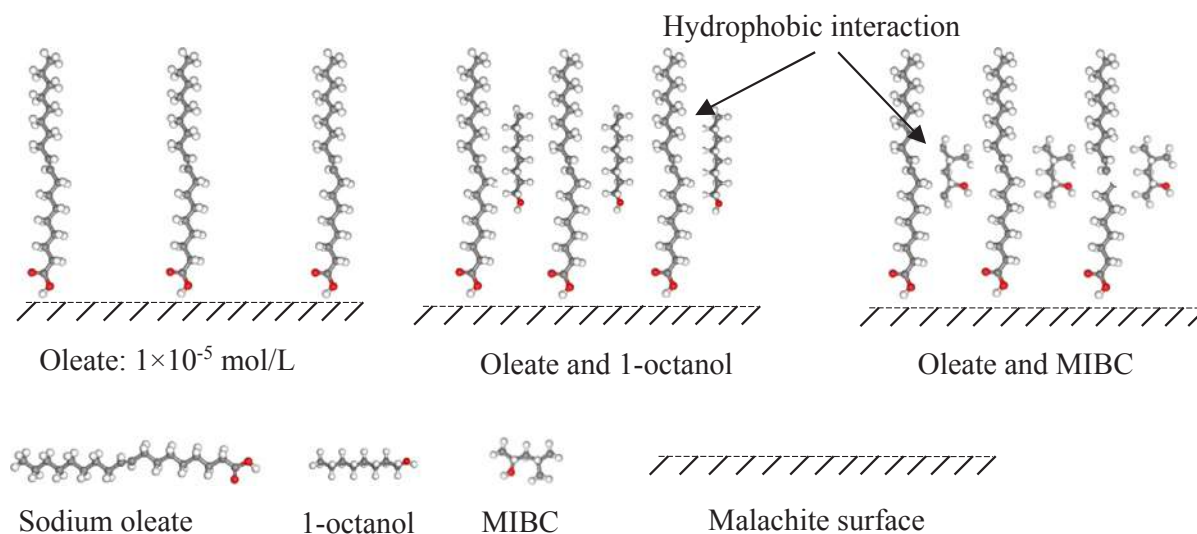


Fig. 10. Schematic presentation of the co-adsorption of sodium oleate and alcohols on malachite surface.

to increase the floatability of malachite.

- Of the three alcohols 1-octanol, 2-ethylhexanol and α -terpineol, the latter two have branched chains. However, they have a similar capability as that of 1-octanol with respect to rendering the malachite surface hydrophobic and increasing its floatability.

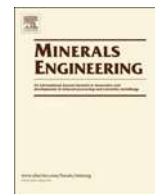
Acknowledgement

This study was financially supported by the Consejo Nacional de Ciencia y Tecnología (CONACYT) of Mexico under Grant No. 270186, the Natural Science Foundation of Hubei Province of China under Grant No. 2016CFA013, and the Wuhan Science and Technology Bureau of China under Project No. 2016070204020156, for which the authors are grateful. Z. Li would like to thank the CONACYT for offering him the scholarship No. 717627 during his PhD studies.

References

- Bulatovic, S.M., 2010. Handbook of flotation reagents, first ed. Elsevier, pp. 14–15.
- Choi, J., Choi, S.Q., Park, K., Han, Y., Kim, H., 2016. Flotation behaviour of malachite in mono- and di-valent salt solutions using sodium oleate as a collector. *Inter. J. Miner. Process.* 146, 38–45.
- Chau, T.T., Bruckard, W.J., Koh, P.T.L., Nguyen, A.V., 2009. A review of factors that affect contact angle and implications for flotation practice. *Adv. Colloid. Interface. Sci.* 150, 106–115.
- Drzymala, J., 1994. Characterization of materials by Hallimond tube flotation. Part 1: maximum size of entrained particles. *Inter. J. Miner. Process.* 42 (3–4), 139–152.
- El-Shall, H., Abdel-Khalek, N.A., Svoronos, S., 2000. Collector-frother interaction in column flotation of Florida phosphate. *Inter. J. Miner. Process.* 58 (1), 187–199.
- Feng, Q., Zhao, W., Wen, S., Cao, Q., 2017. Copper sulfide species formed on malachite surfaces in relation to flotation. *J. Ind. Eng. Chem.* 48, 125–132.
- Filippov, L.O., Filippova, I.V., Severov, V.V., 2010. The use of collectors mixture in the reverse cationic flotation of magnetite ore: the role of Fe-bearing silicates. *Miner. Eng.* 23 (2), 91–98.
- Fuerstenau, M.C., Han, K.N. (Eds.), 2003. Principles of Mineral Processing. SME, pp. 255–257.
- Gaudin, A.M., 1957. Flotation, second ed. McGraw-Hill, New York, pp. 16–83.
- Herrera-Urbina, R., Sotillo, F.J., Fuerstenau, D.W., 1999. Effect of sodium sulfide additions on the pulp potential and amyl xanthate flotation of cerussite and galena. *Inter. J. Miner. Process.* 55 (3), 157–170.
- Lee, J.S., Nagaraj, D.R., Coe, J.E., 1998. Practical aspects of oxide copper recovery with alkyl hydroxamates. *Miner. Eng.* 11 (10), 929–939.
- Lee, K., Archibald, D., McLean, J., Reuter, M.A., 2009. Flotation of mixed copper oxide and sulphide minerals with xanthate and hydroxamate collectors. *Miner. Eng.* 22 (4), 395–401.
- Li, F., Zhong, H., Xu, H., Jia, H., Liu, G., 2015. Flotation behavior and adsorption mechanism of α -hydroxyoctyl phosphinic acid to malachite. *Miner. Eng.* 71, 188–193.

- Li, Z., Rao, F., Song, S., 2017. Comparison of adsorption of phenol O-O and N-O chelating collectors at the malachite/water interface in flotation. *Minerals* 7 (2), 20.
- Liu, Q., Peng, Y., 1999. The development of a composite collector for the flotation of rutile. *Miner. Eng.* 12 (12), 1419–1430.
- Liu, S., Zhong, H., Liu, G., Xu, Z., 2018. Cu (I)/Cu (II) mixed-valence surface complexes of S-[(2-hydroxyamino)-2-oxoethyl]-N, N-dibutylthiocarbamate: hydrophobic mechanism to malachite flotation. *J. Colloid. Interf. Sci.* 512, 701–712.
- Lu, Y., Liu, N., Wang, X., Miller, J.D., 1999. In: Beneficiation of Phosphates: Advances in Research and Practice, pp. 3–19.
- Marion, C., Jordens, A., Li, R., Rudolph, M., Waters, K.E., 2017. An evaluation of hydroxamate collectors for malachite flotation. *Sep. Purif. Technol.* 183, 258–269.
- Miller, J.D., Khalek, N.A., Basilio, C., Shall, H.E., Fa, K., Forssberg, K.S.E., 2007. Flotation chemistry and technology of nonsulfide minerals. In: Fuerstenau, M.C., Jameson, G. J., Yoon, R.H. (Eds.), Froth Flotation: A Century of Innovation. SME Inc., Littleton, Colorado, USA, pp. 465–553.
- Monte, M.B.M., Oliveira, J.F., 2004. Flotation of sylvite with dodecylamine and the effect of added long chain alcohols. *Miner. Eng.* 17 (3), 425–430.
- Nagaraj, D.R., Ravishankar, S.A., 2007. Flotation reagents—a critical overview from an industry perspective. In: Fuerstenau, M.C., Jameson, G.J., Yoon, R.H. (Eds.), Froth Flotation: A Century of Innovation. Society for Mining, Metallurgy, and Exploration, Littleton, Colorado, pp. 375–424.
- O'Brien, R.W., 1990. The electroacoustic equations for a colloidal suspension. *J. Fluid. Mech.* 212, 81–93.
- Park, K., Park, S., Choi, J., Kim, G., Tong, M., Kim, H., 2016. Influence of excess sulfide ions on the malachite-bubble interaction in the presence of thiol-collector. *Sep. Purif. Technol.* 168, 1–7.
- Phetla, T.P., Muzenda, E., 2010. A multistage sulphidisation flotation procedure for a low grade malachite copper ore. *World. Acad. Sci. Eng. Technol.* 70, 256–261.
- Pugh, R., Stenius, P., 1985. Solution chemistry studies and flotation behaviour of apatite, calcite and fluorite minerals with sodium oleate collector. *Inter. J. Miner. Process.* 15 (3), 193–218.
- Pugh, R.J., 1986. The role of the solution chemistry of dodecylamine and oleic acid collectors in the flotation of fluorite. *Colloids Surf.* 18 (1), 19–41.
- Quast, K., 2016. Literature review on the interaction of oleate with non-sulphide minerals using zeta potential. *Miner. Eng.* 94, 10–20.
- Rao, F., Song, S., Lopez-Valdivieso, A., 2009. Electrokinetic studies of minerals in aqueous solutions through electroacoustic measurement. *Surf. Rev. Lett.* 16 (1), 65–71.
- Sis, H., Chander, S., 2003. Reagents used in the flotation of phosphate ores: a critical review. *Miner. Eng.* 16 (7), 577–585.
- Smith, R.W., 1963. Co-adsorption of dodecylamine ion and molecule on quartz. *Trans. AIME.* 226, 427–433.
- Somasundaran, P., 1987. Reagents in Mineral Technology, vol. 27. CRC Press, pp. 203–210.
- Rybinski, W., Schwuger, M.J., 1986. Adsorption of surfactant mixtures in froth flotation. *Langmuir* 2 (5), 639–643.
- Wang, K., Liu, Q., 2013. Adsorption of phosphorylated chitosan on mineral surfaces. *Colloid. Surf. A* 436, 656–663.
- Yang, X., Liu, S., Liu, G., Zhong, H., 2017. A DFT study on the structure–reactivity relationship of aliphatic oxime derivatives as copper chelating agents and malachite flotation collectors. *J. Ind. Eng. Chem.* 46, 404–415.



Short communication

Comminution effect on surface roughness and flotation behavior of malachite particles

 Zhili Li^{a,b}, Feng Rao^{a,b,*}, Mario A. Corona-Arroyo^c, Arnoldo Bedolla-Jacuinde^b, Shaoxian Song^{d,**}
^a School of Zijin Mining, Fuzhou University, Fuzhou 350108, China

^b CONACYT Instituto de Investigación en Metalurgia y Materiales, Universidad Michoacana de San Nicolás de Hidalgo, Morelia 58030, Mexico

^c División de Ingenierías, Departamento de Minas, Metalurgia y Geología, Universidad de Guanajuato, Guanajuato 36020, Mexico

^d School of Resources and Environmental Engineering, Wuhan University of Technology, Wuhan 430070, China


ARTICLE INFO

Keywords:

Surface roughness

Contact angle

Comminution

Flotation separation

ABSTRACT

In this research, malachite particles with different roughness values were produced by grinding malachite sample together with quartz (mohs hardness: 7) and montmorillonite (mohs hardness: 1–2), respectively. Micro-flotation results showed that higher recovery was achieved by using malachite particles of higher surface roughness as feed. The contact angle measurements demonstrated that the contact angle of natural malachite surface decreased with the increase of its surface roughness, while the contact angle of malachite conditioned with 5×10^{-5} mol/L sodium oleate increased with the increase of its surface roughness. It might be concluded that grinding media can influence minerals surface roughness, thus affecting the wettability of their surface and, consequently, the flotation performance.

1. Introduction

Flotation is a physico-chemical separation process that makes use of differences between surface properties of valuable minerals and unwanted gangue minerals (Napier-Munn and Wills, 2006). In addition to particle size and shape, the floatability of a mineral is mainly related to the hydrophobicity and wettability of the mineral surface (Chen et al., 2018). It is well established that the contact angle, which mirrors the wettability of materials, is determined by both chemical composition and geometrical micro or nanostructure of the surface (Johnson and Dettre, 1964; Dupuis and Yeomans, 2005; Chen et al., 1999). Although the effect of reagents on mineral's contact angle has been extensively studied, in flotation process, only few researchers have studied the influence of mineral surface roughness on contact angle and flotation performance, and their conclusions are contradictory. In an investigation to find the relationship between surface roughness and wettability of minerals, calcite, barite, talc and quartz were ground in ball, rod and autogenous mills to produce samples for roughness and wettability tests. The results indicated that particles having rougher surfaces lead to higher wettability (Ulusoy and Yekeler, 2005). In another study, autogenously ground barite showed lower roughness and acuteness compared to ball milling ground barite and the flotation tests using A-

845 (Cytec) succinamate surfactant as collector revealed that particles with smooth surfaces gave better floatability (Hicyilmaz et al., 2005). In turn, Hassas et al. (2016) studied the effect of roughness on flotation characteristics of glass beads. They concluded that surface roughness improved the flotation recovery, contact angle, and bubble attachment with hexadecyl trimethyl ammonium bromide as collector. Ahmed (2010) found that dry grinding produced relatively rough particle surfaces with a high concentration of microstructural defects compared to wet grinding and the dry ground samples exhibited more stable, higher loaded froths, and faster flotation kinetics. In the literature concerning flotation, methods used to change the mineral surface roughness include change the grinding method, for example, wet grinding and dry grinding (Ahmed, 2010) and grinding mill, for example, ball, rod and autogenous grinding (Yekeler et al., 2004). However, no studies have been published about the effect of mineral comminution media on the roughness of mineral surface and flotation behavior.

In this work, malachite particles with different roughness values were produced by grinding malachite sample with quartz and montmorillonite (different mineral media), in order to study the wettability and floatability of malachite sample of different roughness. It was found that interactions of particles in comminution process can affect the

* Corresponding author at: CONACYT Instituto de Investigación en Metalurgia y Materiales, Universidad Michoacana de San Nicolás de Hidalgo, Morelia 58030, Mexico.

** Corresponding author.

E-mail addresses: fengrao@umich.mx (F. Rao), shaoxian@uaslp.mx (S. Song).

<https://doi.org/10.1016/j.mineng.2018.11.056>

Received 22 June 2018; Received in revised form 24 September 2018; Accepted 30 November 2018

0892-6875/© 2018 Elsevier Ltd. All rights reserved.

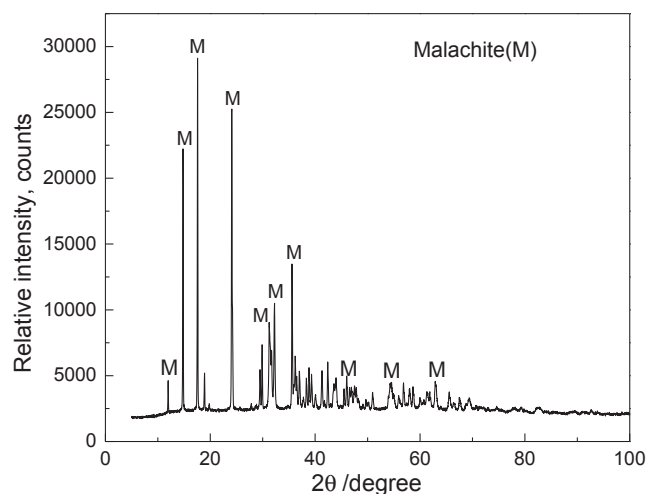


Fig. 1. XRD pattern of the malachite sample.

roughness of mineral surface, and thus, changing the wettability of natural and reagent treated mineral surface and, consequently, altering the floatability of mineral.

2. Experimental

2.1. Materials

Natural malachite samples were obtained from “Lupe” mine in Puebla, Mexico. The samples were hand-sorted to obtain lumps for roughness and contact angle measurements; some lumps were crushed then dried-ground mixed with quartz and montmorillonite to obtain malachite particles for BET (Brunauer-Emmett-Teller) characterization and flotation tests. In addition, some lumps were crushed and dried-ground to obtain fine particles to perform X-ray diffraction (XRD) and chemical analysis. Chemical analysis and X-ray diffraction pattern (Fig. 1) indicated that the malachite was of high purity. To prepare malachite samples for roughness and contact angle measurements, malachite lump samples were polished using grit #2000 abrasive papers followed by diamond paste to get the smoothest surface in the experiments; this was denoted as surface A. The medium rough and roughest surfaces were polished with grit #240 and #80 abrasive papers respectively. The surfaces obtained were denoted as surface B and C. To prepare the samples for BET measurements, malachite lumps were crushed and then dry-ground mixed with quartz ($d_{50} = 204.5 \mu\text{m}$, $d_{85} = 271.6 \mu\text{m}$) and montmorillonite ($d_{50} = 15.1 \mu\text{m}$, $d_{85} = 28.3 \mu\text{m}$) respectively. After grinding, the samples were sieved to obtain particles of $-75 + 38 \mu\text{m}$. The sample ground with montmorillonite was treated through gravity separation method to remove montmorillonite in the malachite sample for BET measurement. The sample ground with quartz was partially saved to measure the specific area and partially weighted, acid treated at pH 2 to dissolve the malachite particles and weighed again to obtain the percentage of malachite in the sample and get the quartz sample for BET, and then compute the specific surface area of malachite in the sample. As for the samples for micro-flotation, two kinds of samples were prepared. One is malachite ground with quartz and the other one is prepared by the procedure that after removal of montmorillonite, the malachite was mixed with a certain percent of quartz which was equal to that of the malachite ground with quartz. Sodium oleate (ACS reagent grade) purchased from Aladdin Industrial, from China, was used as collector. Hydrochloric acid (HCl) and sodium hydroxide (NaOH) of ACS reagent grade were used to modify the pH. Distilled water was used in all experiments.

2.2. Methods

Surface topography for polished malachite samples were measured by Nanovea PS 50 3D Non-Contact profiler with Mountains Map Premium Software to report the average surface roughness (Ra) and the root mean squared roughness (Rq). Scans were recorded with an optical pen (1 mm scan range along the z-axis and $2.60 \mu\text{m}$ lateral resolutions). Scan step size was of $0.1 \mu\text{m}$ for x axis and $1 \mu\text{m}$ for y axis, respectively. Smaller Ra and Rq values indicate smoother surfaces. Raw data previously recorded during the surface profile measurements were further post-processed by using NANOVEA 3D software.

The contact angle of malachite samples was measured with a goniometer (DSA-25, Kruss, Germany). The DSA-25 goniometer was equipped with a CM4210 optics module with zoom lens and was operated using the sessile drop method in the ADVANCE software. For measurements of polished natural malachite samples, air dried malachite lumps were loaded on the goniometer stage and $1.5 \mu\text{L}$ distilled water was dropped on them. The advancing and receding contact angles were reported. When the difference between the two contact angles (advancing and receding) was less than 1%, the average value of these two angles was reported as the contact angle. For each roughness condition (e.g., $R_a = 0.327 \mu\text{m}$), at least four measurements were performed, and the average contact angle was reported in this work. For measurements of collector treated malachite samples, the lumps were immersed in solutions of $5 \times 10^{-5} \text{ mol/L}$ sodium oleate at pH 9 for about 30 min, and then washed with distilled water. After that, their contact angles were measured through the same procedure of natural malachite samples.

The Brunauer-Emmett-Teller (BET) surface area measurements were performed using a NOVA touch LX1 surface area and pore size analyzer from Quantachrome Instruments (USA), using nitrogen as purge gas. The samples for specific surface area measurements include malachite ground together with quartz, malachite ground together with montmorillonite and purified by gravity separation, and quartz which was the dissolution product (at pH 2) of malachite ground with quartz.

A 150 mL Hallimond tube equipped with a $20 \mu\text{m}$ frit and a magnetic stirrer was used to test the effect of sample roughness on malachite flotation. In each flotation, 3 g of sample ($-75 + 38 \mu\text{m}$) were conditioned for 2 min in 130 mL distilled water, and the solution was adjusted to a desired pH by using HCl or NaOH. Then, a given amount of sodium oleate was added and conditioned for about 3 min. After that, the conditioned slurry was transferred to the Hallimond tube, and the flotation was performed for about 5 min with nitrogen gas at a flow rate of 30 mL/min. The floated (concentrate) and unfloated (tailing) products were separately collected, dried, weighed, dissolved in acid solution (pH = 2), weighed again, and the recovery was computed based on the mass ratio of the floated malachite.

3. Results and discussion

Figs. 2–4 show the profiles height and section analyses of the surface A, B, and C measured using 3D non-contact profilometer. From the profile height image, it is easy to observe that, the roughness of surfaces changed from low to high levels in the order of surface A, surface B, and surface C. From the section analysis, Ra and Rq were obtained and the results are shown in Table 1. Ra value varies from $0.327 \mu\text{m}$ to $3.620 \mu\text{m}$ and Rq value varies from $0.351 \mu\text{m}$ to $4.449 \mu\text{m}$ from surface A to surface C. Section analysis clearly shows that, there were significant differences in the surface roughness among the surfaces. The differences in Ra and Rq values were sufficient to significantly alter the wetting behavior of different malachite surfaces. Comparing the section analysis image, peaks and valleys from surface A and surface B were the same in shape but different in magnitude. There were wide peaks and valleys containing small peaks and small valleys on surface C, hence, in surface C, they were different from surface A and surface B not only in magnitude but also in shape of peaks and valleys.

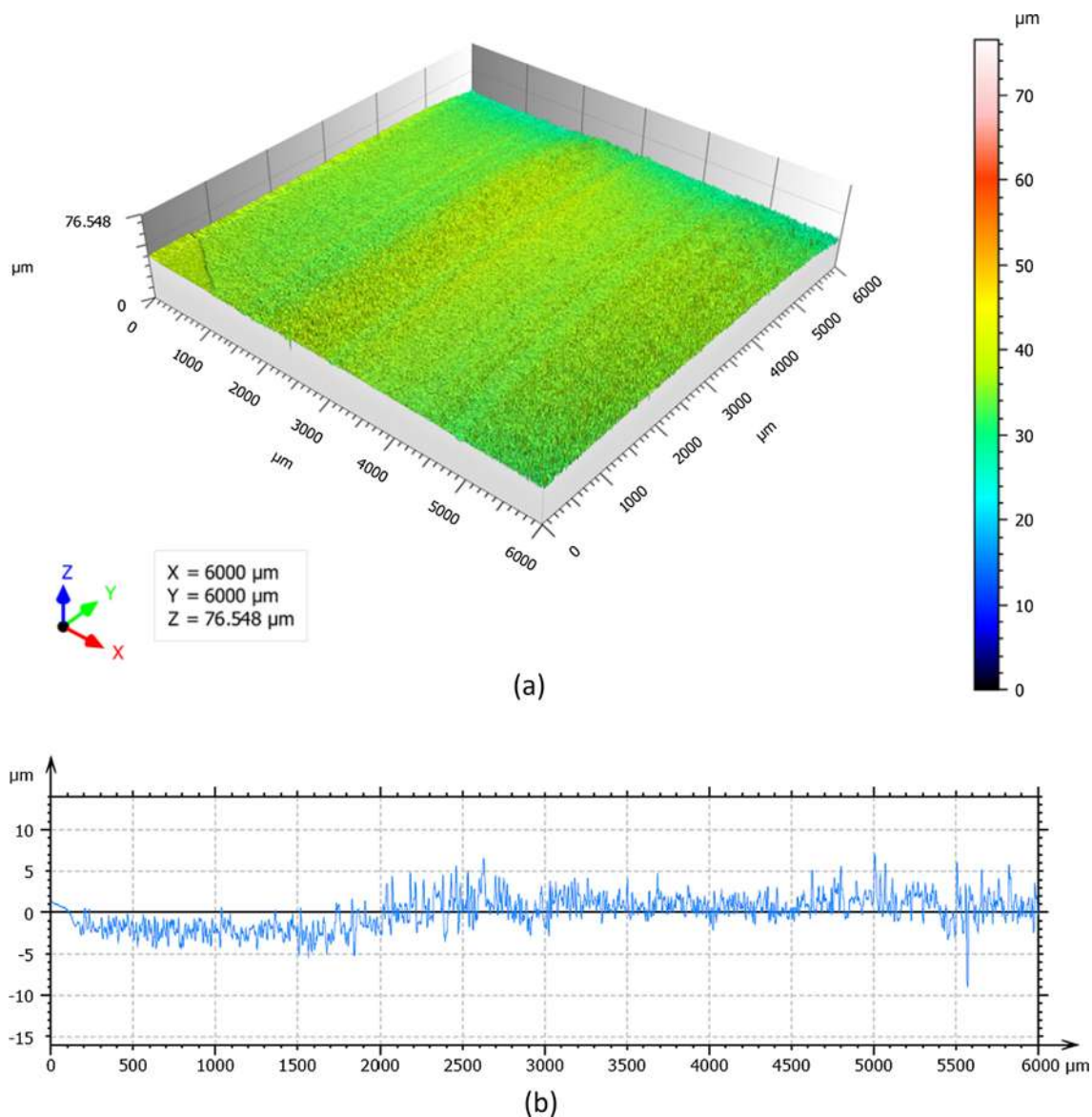


Fig. 2. Profile of malachite surface A: (a) profile height; (b) section analysis.

It is well known that malachite is a hydrophilic mineral, therefore, the contact angle on malachite surface should be small. Fig. 5 shows the contact angle of malachite surface without sodium oleate treatment. The contact angle value of surface A was 28.3°. For surface B and surface C, as soon as the water droplets contact the surface, they spread to form a water film, through which the contact angles were too low to be measured. Müller et al. (2001) also reported that measurements of contact angles below 15° exhibit large error bars. The contact angle results of surface A, B, and C can be explained by the Wenzel model shown in Fig. 6. It is a classical model used to explain the influence of surface roughness on contact angle. Wenzel model considers that surface roughness leads to the increase of liquid-solid contact area. In this case, roughed surface has an actual surface area r times of the ideal surface (perfectly smooth), thus the energy gained in forming the solid-liquid interface is $r(\gamma_{sg} - \gamma_{sl})$, and the energy required to form liquid-gas interface is the same with an ideal surface. Based on the above, Wenzel put forward Wenzel model in 1936 (Wenzel, 1936).

$$\cos\theta_0 = r \frac{(\gamma_{sg} - \gamma_{sl})}{\gamma_{lg}} = r \cos\theta \quad (\text{Wenzel equation})$$

where θ_0 is the contact angle on rough surface, θ is the contact angle on

smooth surface, and r is the ratio between the actual surface areas of a rough surface to the projected area.

Since surface A is the smoothest surface among surface A, B, and C, and the surface is hydrophilic, the contact angle value was 28.3°. While the roughness of surface B and C is much greater than that of surface A, so the values of $\cos\theta$ were higher and the contact angle were smaller, and it is reasonable to expect that the contact angle cannot be measured.

It is well established that sodium oleate is a powerful collector for malachite (Choi et al., 2016). When it adsorbs on malachite surface, it can change the hydrophilic malachite surface to hydrophobic. As shown in Fig. 7, after sodium oleate treatment, the contact angle of surface A, B, and C changed to 113.3°, 122.0°, and 132.8° respectively. The contact angle values increased with the increase of surface roughness. The difference of contact angle on these surfaces can be explained by both the Cassie model and Wenzel model, which are presented in Fig. 8. For “Wenzel state” liquid droplet, it penetrates the “valleys” of the surface, so the ratio between the actual surface areas of a rough surface to the projected area is more than 1. In addition, the malachite surface now is hydrophobic, therefore, the hydrophobicity is increased due to the increment of surface roughness. Cassie and Baxter extended the rough

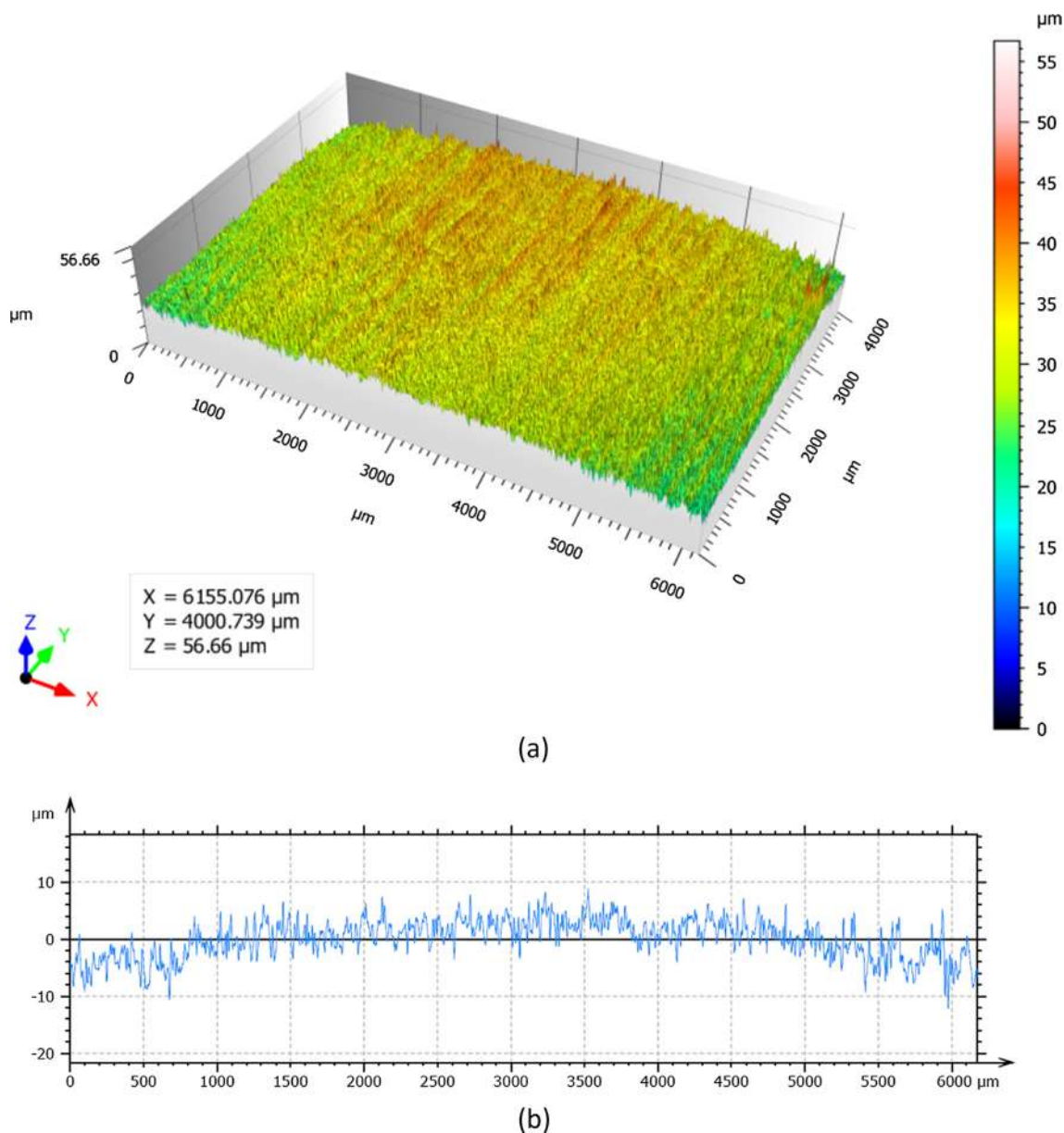


Fig. 3. Profile of malachite surface B: (a) profile height; (b) section analysis.

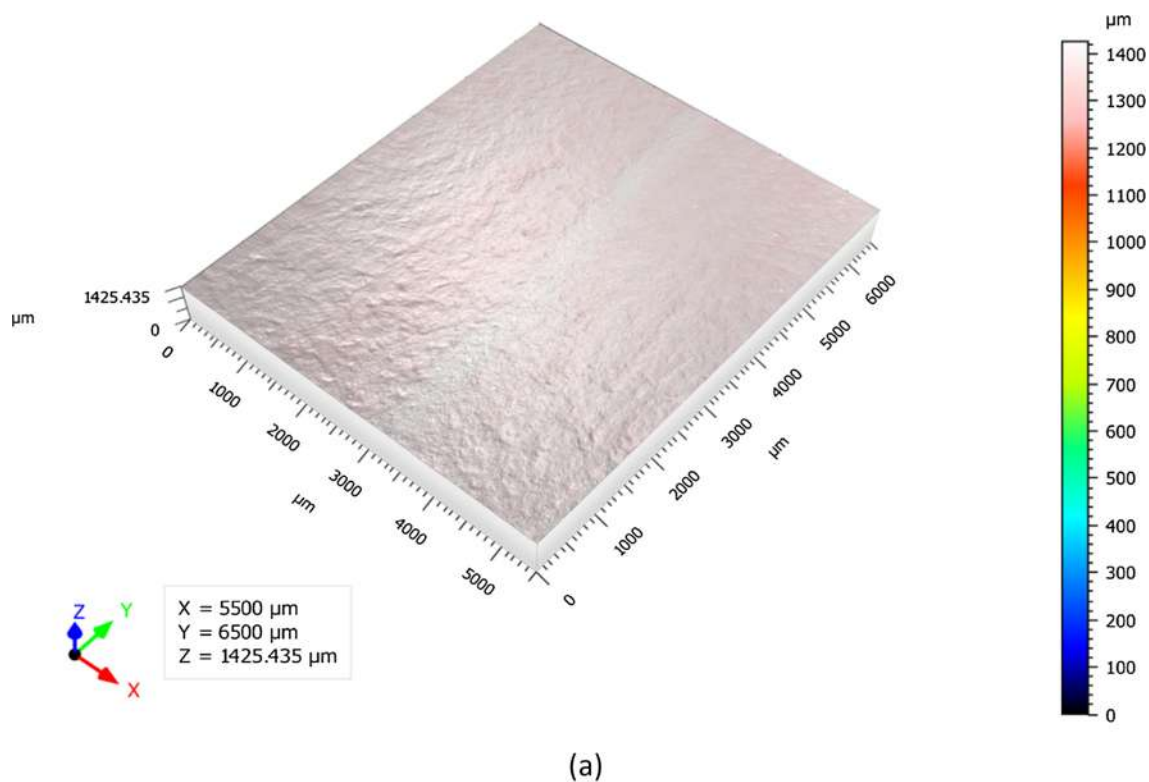
surface to heterogeneous surfaces. The energy gained to form the solid-liquid interface will be $r_1(\gamma_{S1G} - \gamma_{S1L}) + r_2(\gamma_{S2G} - \gamma_{S2L})$ while the energy required to form the liquid-gas interface will remain the same. Therefore, the contact angle can be computed by the Cassie equation (Cassie and Baxter, 1944).

$$\cos\theta_0 = x_1\cos\theta_1 + x_2\cos\theta_2 \quad (\text{Cassie equation})$$

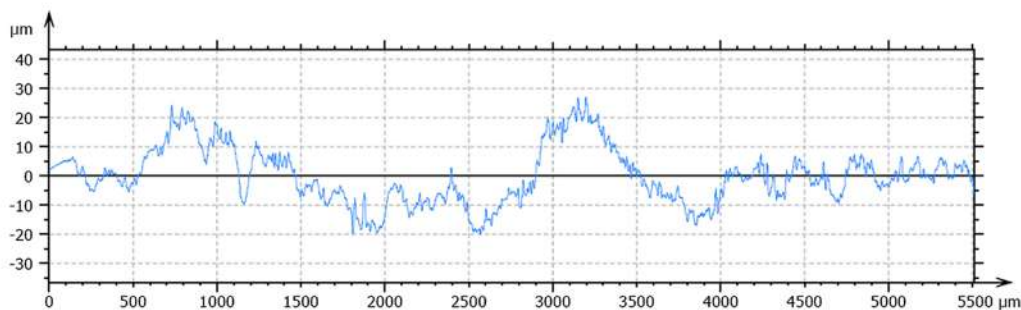
where θ_1 and θ_2 are the contact angles on the two different types of surface, and x_1 and x_2 are the fractional areas of different types of surface. The surface can be an air surface caused by trapping or heterogeneities because of different chemical composition. For “Cassie state” liquid droplet, as shown in Fig. 8c, it sits on top of the surface structure without penetrating the “valleys”, so the air is enclosed and composite surface forms. The advantage of Cassie model over the Wenzel model is that it describes real systems more accurately (Miller et al., 1996). Surface A is the smoothest among surfaces, so the fractional area of the air surface is the smallest and the wetting state is more similar to that presented in Fig. 8a. There are greater air surface percentages with the increase of surface roughness, so the contact angles increased with the increment of surface roughness and the contact

angle increased in order of surface A, B, and C. Another reasonable explanation to the increment of contact angle is that the surface roughness increases the sites for sodium oleate adsorption on the malachite surface, so larger amount of sodium oleate was adsorbed on the surface at the same projected area, resulting in a larger contact angle of malachite surface. In this system, the increment of contact angle may be attributed to the both reasons explained above.

Table 2 presents the specific surface area of malachite samples ground with quartz and montmorillonite measured by the BET method. The specific surface area of malachite ground mixed with quartz is larger than the one with montmorillonite and the values were 1.13 and 0.76 m²/g respectively. The difference between the specific surface areas might be related with the hardness of gangue minerals, which act as grinding media in this study. Quartz, which is of greater hardness, can make more scratches on the malachite surface, so the specific surface area of malachite ground with quartz is larger. It is reported that surface roughness can be computed using the following equation (Rahimi et al., 2012):



(a)



(b)

Fig. 4. Profile of malachite surface C: (a) profile height; (b) section analysis.

Table 1
Roughness parameters of surfaces.

Surface	Ra (μm)	Rq (μm)
Surface A	0.327	0.351
Surface B	1.569	1.951
Surface C	3.620	4.449

$$\lambda = \frac{\rho A_{BET}}{6}$$

where A_{BET} is the BET specific surface area (m^2/g), ρ is the grain density (g/cm^3), D is the average grain diameter (μm), λ is the surface roughness (dimensionless). In this study, the grain density for malachite is the same for both samples, while the grain diameter is almost the same ($-75 + 38 \mu m$). Therefore, the difference of A_{BET} from the two samples indicates that malachite ground with quartz has greater roughness than that ground with montmorillonite.

Recoveries of malachite ground with quartz and montmorillonite in presence of 2×10^{-5} mol/L sodium oleate are plotted in Fig. 9. The malachite recovery remained practically the same in the pH range 7–10. While the recoveries of malachite ground with quartz were around 12% higher than that ground with montmorillonite. In addition, as discussed above, contact angle measurements showed that surface roughness can affect the contact angle values. Therefore, it is



Fig. 5. Contact angle of surface A.



Fig. 6. Wetting state on smooth surface (a) and rough surface (b) of a hydrophilic material (Wenzel model).

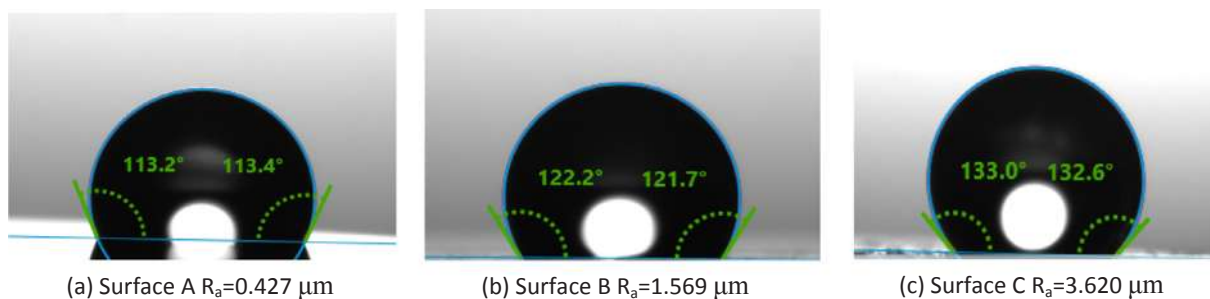


Fig. 7. Contact angle of malachite surface A, B, and C after treatment with 5×10^{-5} mol/L sodium oleate at pH 9.

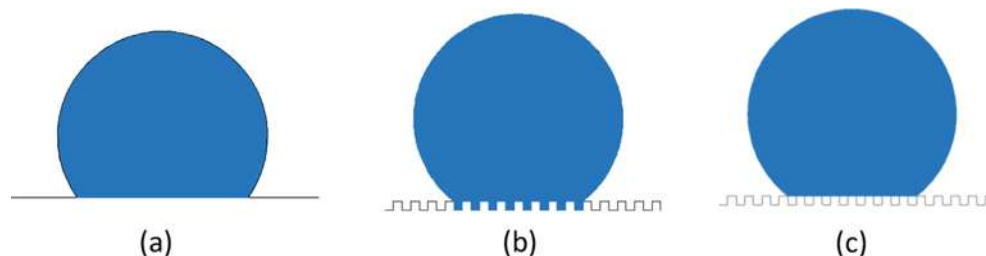


Fig. 8. Wetting state on (a) smooth surface, (b) rough surface (Wenzel model) and (c) rough surface (Cassie model).

Table 2
BET specific surface area of malachite samples ground with different gangue minerals.

Sample	Malachite (quartz)	Malachite (montmorillonite)
Specific surface area (m ² /g)	1.13	0.75

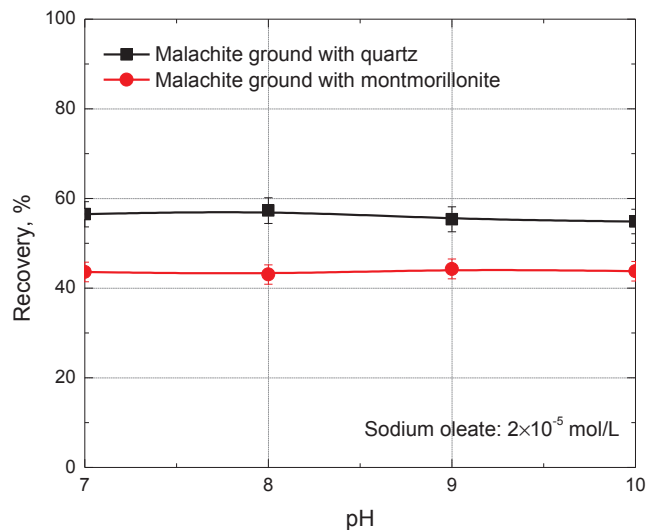


Fig. 9. Recovery of malachite ground with quartz and montmorillonite in the presence of 2×10^{-5} mol/L sodium oleate.

reasonable to conclude that higher roughness of malachite surface leads to larger contact angle after sodium oleate adsorption, as a consequence, the malachite recovery is greater.

4. Conclusion

1. For natural malachite surfaces, the contact angle measurements are in agreement with Wenzel model and the contact angle decreases with the increase of surface roughness. The contact angle measurements of malachite conditioned with 5×10^{-5} mol/L sodium

oleate are in line with Wenzel model and Cassie model, and the contact angle increase with the increase of surface roughness.

2. Particle interactions during comminution can affect the roughness of the mineral surface. Grinding malachite with gangue minerals of greater hardness can make the malachite surface rougher, and therefore, the contact angle is larger after adsorption of collector, resulting in greater malachite recovery.

Acknowledgement

This study was financially supported by the Consejo Nacional de Ciencia y Tecnología (CONACyT) of Mexico under the Grant No. 270186, the Natural Science Foundation of Hubei Province of China under the Grant No. 2016CFA013 and the Wuhan Science and Technology Bureau of China under the Project No. 2016070204020156, for which the authors are grateful. Z. Li would like to thank CONACyT for offering him the scholarship No. 717627 during his PhD studying.

References

Ahmed, M.M., 2010. Effect of comminution on particle shape and surface roughness and their relation to flotation process. *Int. J. Min. Process.* 94 (3–4), 180–191.

Cassie, A.B.D., Baxter, S., 1944. Wettability of porous surfaces. *Trans. Farad. Soc.* 40, 546–551.

Chen, W., Fadeev, A.Y., Hsieh, M.C., Öner, D., Youngblood, J., McCarthy, T.J., 1999. Ultrahydrophobic and ultralyophobic surfaces: some comments and examples. *Langmuir* 15 (10), 3395–3399.

Chen, Y., Xia, W., Xie, G., 2018. Contact angle and induction time of air bubble on flat coal surface of different roughness. *Fuel* 222, 35–41.

Choi, J., Choi, S.Q., Park, K., Han, Y., Kim, H., 2016. Flotation behaviour of malachite in mono- and di-valent salt solutions using sodium oleate as a collector. *Int. J. Min. Process.* 146, 38–45.

Dupuis, A., Yeomans, J.M., 2005. Modeling droplets on superhydrophobic surfaces: equilibrium states and transitions. *Langmuir* 21 (6), 2624–2629.

Hıcıylmaz, C., Ulusoy, U., Bilgen, S., Yekeler, M., 2005. Flotation responses to the morphological properties of particles measured with three-dimensional approach. *Int. J. Min. Process.* 75 (3–4), 229–236.

Hassas, B.V., Caliskan, H., Guven, O., Karakas, F., Cinar, M., Celik, M.S., 2016. Effect of roughness and shape factor on flotation characteristics of glass beads. *Colloid Surface A* 492, 88–99.

Johnson Jr, R.E., Dettre, R.H., 1964. Contact angle hysteresis. III. Study of an idealized heterogeneous surface. *J. Phys. Chem.* 68 (7), 1744–1750.

Miller, J.D., Veeramani, S., Drelich, J., Yalamanchili, M.R., Yamauchi, G., 1996. Effect of roughness as determined by atomic force microscopy on the wetting properties of PTFE thin films. *Polym. Eng. Sci.* 36 (14), 1849–1855.

- Müller, B., Riedel, M., Michel, R., De Paul, S.M., Hofer, R., Heger, D., Grützmacher, D., 2001. Impact of nanometer-scale roughness on contact-angle hysteresis and globulin adsorption. *J. Vac. Sci. Technol. B* 19 (5), 1715–1720.
- Napier-Munn, T., Wills, B.A., 2006. *Wills' Mineral Processing Technology: An Introduction to the Practical Aspects of Ore Treatment and Mineral Recovery*. Elsevier.
- Rahimi, M., Dehghani, F., Rezai, B., Aslani, M.R., 2012. Influence of the roughness and shape of quartz particles on their flotation kinetics. *Int. J. Min. Met. Mater.* 19 (4), 284–289.
- Ulusoy, U., Yekeler, M., 2005. Correlation of the surface roughness of some industrial minerals with their wettability parameters. *Chem. Eng. Process.* 44 (5), 555–563.
- Wenzel, R.N., 1936. Resistance of solid surfaces to wetting by water. *Ind. Eng. Chem.* 28 (8), 988–994.
- Yekeler, M., Ulusoy, U., Hiçyılmaz, C., 2004. Effect of particle shape and roughness of talc mineral ground by different mills on the wettability and floatability. *Powder Technol.* 140 (1–2), 68–78.

Slime coating of kaolinite on chalcopyrite in saline water flotation

Zhi-li Li^{1,2)}, Feng Rao¹⁾, Shao-xian Song²⁾, Yan-mei Li³⁾, and Wen-biao Liu⁴⁾

1) CONACYT Instituto de Investigación en Metalurgíay Materiales, Universidad Michoacana de San Nicolás de Hidalgo, Morelia 58030, México

2) School of Resources and Environmental Engineering, Wuhan University of Technology, Wuhan 430070, China

3) Departamento de Ingeniería en Minas, Metalurgia y Geología, Universidad de Guanajuato, Guanajuato 36020, México

4) Faculty of Land and Resource Engineering, Kunming University of Science and Technology, Kunming 650093, China

(Received: 24 August 2017; revised: 22 November 2017; accepted: 8 December 2017)

Abstract: In saline water flotation, the salinity can cause a distinguishable slime coating of clay minerals on chalcopyrite particles through its effect on their electrical double layers in aqueous solutions. In this work, kaolinite was used as a representative clay mineral for studying slime coating during chalcopyrite flotation. The flotation of chalcopyrite in the presence and absence of kaolinite in tap water, seawater, and gypsum-saturated water and the stability of chalcopyrite and kaolinite particles in slurries are presented. Zeta-potential distributions and scanning electron microscopy images were used to characterize and explain the different slime coating degrees and the different flotation performances. Kaolinite particles induced slime coating on chalcopyrite surfaces and reduced chalcopyrite floatability to the greatest extent when the pH value was in the alkaline range. At 0.24wt% of kaolinite, the chalcopyrite floatability was depressed by more than 10% at alkaline pH levels in tap water. Salinity in seawater and gypsum-saturated water compressed the electrical double layers and resulted in extensive slime coating.

Keywords: chalcopyrite; clay minerals; saline water flotation; slime coating; stability

1. Introduction

With increasing water scarcity and environmental concerns, mining industries are facing pressure to conserve freshwater during mineral processing, particularly flotation [1–3]. Two strategies have been developed to mitigate this problem. The first strategy involves using recycled process water in flotation plants that consume a large proportion of local water resources [4–5]. The second strategy is to use seawater to operate sulfide flotation plants located in arid areas but near the sea (e.g., plants in Australia, Canada, Chile, and Indonesia) [6]. However, both of these strategies increase the salinity in the flotation pulp and affect flotation performance. One of the important effects is that salinity promotes the formation of a slime coating of fine hydrophilic gangue minerals on sulfide-containing minerals. Rao *et al.* [7] reported that salinity enhanced particle–particle (coagulation) and particle–bubble (flotation) interactions by compressing the electrical double layers. Deng *et al.* [8] reported that he-

terocoagulation observed in gypsum-saturated water flotation of zinc sulfide minerals occurred between silica and sphalerite rather than between the precipitated gypsum and sphalerite and that calcium ions were the main cause for the reduced recovery and selectivity of sphalerite. As noted in recent reviews [6–7,9], further studies are required to elucidate the effect of the slime coating in the solution chemistry of saline water flotation of sulfide minerals. In normal (low salinity) flotations, electrostatic attraction has been demonstrated to play a role in the slime coating process [10–12]. However, in saline water flotation, the slime coating might behave differently because the high salinity compresses the electrical double layers of minerals and the hydrolyzed species of multivalent cations specifically adsorb into the Stern layer of clay mineral particles [13].

The flotation of copper sulfide from porphyry copper ore frequently results in slime coating even when fresh water is used because large quantities of fine clay minerals are prevalent in this ore. For example, clay minerals are the main

Corresponding author: Feng Rao E-mail: fengrao@umich.mx

© University of Science and Technology Beijing and Springer-Verlag GmbH Germany, part of Springer Nature 2018

gangue minerals in the Kennecott Utah Copper flotation plant in the Bingham Canyon Mine, which is one of the world's largest open-pit copper mines [14]. In many Chilean porphyry copper mines such as El Salvador, Disputada, Chuquicamata, and El Teniente, copper sulfides of chalcopyrite, chalcocite, enargite, and covellite are processed. Meanwhile, clay minerals such as kaolinite and illite are widespread gangue minerals in these mines [15]. Thus, in the corresponding copper sulfide flotations, although the type and associations of copper sulfide and clay minerals vary widely from one mine/orebody to another, fine clay mineral particles are easily formed during the grinding process. The fine hydrophilic clay particles reduce the flotation rate of copper and increase copper losses in tailings in all cases, mainly through the effect of slime coating on the copper sulfide particles.

In the present work, we characterize the effect of clay mineral slime coating in the saline water flotation of copper sulfides. Kaolinite and chalcopyrite were used as the representative clay mineral and copper sulfide, respectively. Our objective was to better understand the mechanism of slime coating in saline water solutions and to correlate the slime coating to the flotation performance.

2. Experimental

2.1. Materials

High-purity chalcopyrite (CuFeS_2) and kaolinite ($\text{Al}_2\text{Si}_2\text{O}_5(\text{OH})_4$) purchased from Da Hong Shan Mine in Yunnan Province, China, were used in the experiments. The lumps of the chalcopyrite were crushed, hand-sorted, and dry-ground with a mechanical agate mortar and pestle. The sample was then dry screened to collect the $-75 + 38\text{-}\mu\text{m}$ and $-25\text{-}\mu\text{m}$ fractions, of which the coarser fraction was used in flotation tests and turbidity measurements. The finer fraction was further dry-ground and used in zeta-potential distribution measurements. To minimize oxidation, the chalcopyrite sample was sealed in plastic bottles and stored in a freezer at -10°C . The X-ray diffraction (XRD) patterns of the chalcopyrite and kaolinite samples are shown in Fig. 1. The chalcopyrite and kaolinite were both highly pure, with the chalcopyrite containing a trace amount of quartz. The particle size distribution of the kaolinite sample was determined using a Malvern Mastersizer 2000; the 50% cumulative undersize (D_{50}) and the 85% cumulative undersize (D_{85}) were 5.5 and 11.5 μm , respectively (Fig. 2).

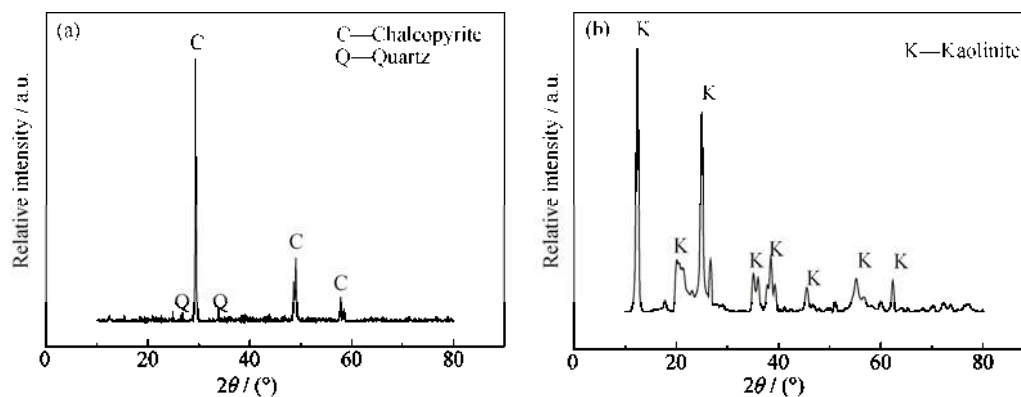


Fig. 1. XRD patterns of the chalcopyrite (a) and kaolinite (b) samples.

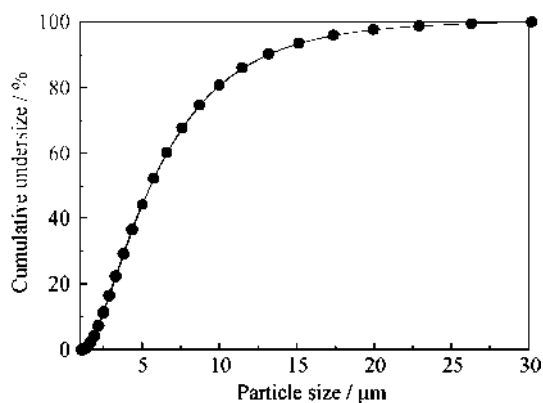


Fig. 2. Particle size distribution of the kaolinite sample.

In this study, tap water, artificial seawater, and gypsum-saturated water were used in flotation experiments. The seawater was prepared by dissolving 35 g API aquarium salt in 1 L of deionized water, as reported elsewhere [16]. The gypsum-saturated water was prepared by dissolving 4 g of calcium sulfate in 1 L of deionized water [8]. The solution was stirred for 1 h and filtered to remove undissolved gypsum. The dissolved gypsum concentration was 2648 ppm (the solubility of gypsum in water is 2400 ppm at 25°C) [17]. ACS-reagent-grade hydrochloric acid (HCl) and sodium hydroxide (NaOH) purchased from Sigma-Aldrich (USA) were used to adjust the pH value. Reagent-grade potassium ethyl xanthate (KEX) and methyl isobutyl carbinol (MIBC)

purchased from Aladdin Industrial, China were used as the collector and frother in flotation tests, respectively. Deionized water (Milli-Q water) with a resistivity of 18.25 M Ω -cm was used in this work.

2.2. Methods

Small-scale flotation tests were conducted using a 100-mL mechanical flotation cell with a 2000 r/min agitation speed. In the tests, chalcopyrite of 3 g (3wt% solid-to-liquid ratio) was mixed with 100 mL of tap water, seawater, or gypsum-saturated water in a Plexiglas cell and the pH level was adjusted to the desired value using HCl or NaOH. In flotations with kaolinite, 90 (0.09wt% solid-to-liquid ratio), 240 (0.24wt%) or 600 (0.60wt%) mg of kaolinite was added to the chalcopyrite slurry. Then, 5×10^{-4} mol/L of KEX and 2×10^{-4} mol/L of MIBC were added and the slurry was conditioned for 5 min and 1 min, respectively. After 3 min of flotation, the concentrate (floated) and tailing (unfloated) products were separately collected, dried, and weighed; the floatability of chalcopyrite was subsequently calculated on the basis of the dry mass of the products.

Slurries of given amounts of chalcopyrite and kaolinite in 100 mL water prepared using the same reagents as those used in the flotation tests were prepared for the turbidity measurements in a Turb 555 IR apparatus with a cylindrical $\phi 28$ mm \times 70 mm cell. The slurries were first settled in a 150-mL cylinder for 15 min, and then 30 mL of the upper solution was transferred for the measurements. Turbidity was used to characterize the stability of the mineral particles in the slurries, where a lower turbidity indicated stronger coagulation.

The zeta-potential distributions of chalcopyrite, kaolinite, and their mixtures were measured with a Malvern Zetasizer Nano ZS90 apparatus equipped with a rectangular quartz electrophoresis cell and a 50-mV laser at a scattering angle of 90°. The zeta-potential distributions were determined by dynamic light scattering and computed from mobility measurements through the Smoluchowski equation [18]. In the measurements, 0.05 g of chalcopyrite ($<5 \mu\text{m}$), kaolinite, or their mixture was prepared in 100 mL of a given type of water and the pH value of the resultant suspension was adjusted to the desired level. The solution was transferred to the cell, and the zeta-potential distribution was recorded at room temperature.

After the flotation experiments, some concentrates or tailings were rinsed with the solution, in which they were suspended (but free of solids), resulting in removal of the slimes not attached to the surfaces. The samples were then

carefully placed on a pin-type mushroom specimen mount and dried at room temperature before the particles were coated with 20-nm-thick gold film. Afterwards, the samples were observed with a Zeiss Ultra Plus scanning electron microscope to characterize the slime coating of kaolinite on the chalcopyrite surface. The instrument was operated at 20 kV and 400 pA, and an attached energy-dispersive X-ray spectroscopy (EDX) apparatus was used to determine the mineral composition.

3. Results and discussion

Fig. 3 shows the flotation of chalcopyrite in tap water without kaolinite and with 0.09wt%, 0.24wt%, and 0.60wt% of kaolinite. Without kaolinite, high chalcopyrite floatability ($>72\%$) was obtained in the pH value range from 4 to 11 because of chemisorption of ethyl xanthate onto chalcopyrite (CuEX) [19]. A slight decrease of floatability was observed in alkaline solutions with pH values from 8 to 11, in good agreement with the results of Liu and Zhang [20], who reported that chalcopyrite floatability decreases when the solution pH value is increased to the very alkaline region. In the presence of 0.09wt% kaolinite, the floatability showed similar behavior as that without kaolinite in pH value range from 4 to 11; however, the floatability was 2% lower. This result suggests that a small amount of kaolinite slightly affects chalcopyrite flotation. In the presence of a medium amount of kaolinite (0.24wt%), chalcopyrite flotation was moderately affected in pH value range from 4 to 6. However, it was greatly affected in the alkaline pH value range, where the floatability decreased by approximately 10%. In the presence of a large amount of kaolinite (0.60wt%), chalcopyrite flotation behavior was similar to that with a medium amount of kaolinite, but the floatability was 2% lower.

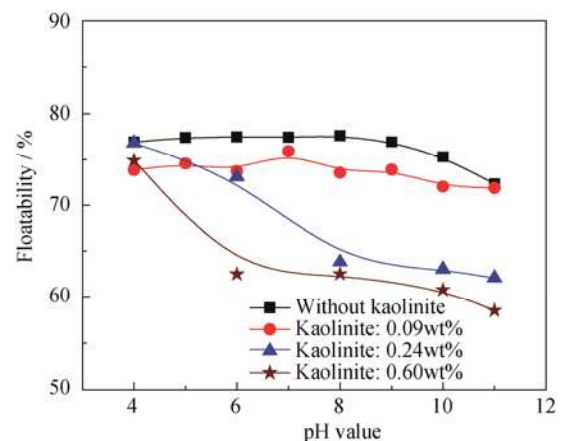


Fig. 3. Flotation of chalcopyrite in tap water with and without kaolinite.

However, at a pH value of 6, the floatability decreased greatly compared with that in the absence of kaolinite. On the basis of these results, the following conclusions can be obtained: (1) the impact of kaolinite on chalcopyrite flotation is higher at alkaline pH levels than at acidic pH levels; (2) a small amount of kaolinite affects chalcopyrite flotation slightly, but this effect increases sharply when the kaolinite amount is increased to a medium level and is maintained in the presence of a large amount of kaolinite; (3) the floatability decreases greatly at a pH value of 6 when a large amount of kaolinite is present.

The low floatability of chalcopyrite might be attributable to slime coating or heterocoagulation of kaolinite on chalcopyrite particles, which can be measured on the basis of the turbidity of the slurry. Fig. 4 presents the turbidity of chalcopyrite and kaolinite slurries in tap water at various pH levels. At pH 5, the turbidity was high, indicating dispersion or low coagulation of the slurry. The turbidity then decreased with increasing pH value, suggesting stronger coagulation at higher pH levels. In the range of $7 \leq \text{pH} \leq 9$, a plateau of turbidity was observed. After this plateau, the turbidity decreased sharply at pH values of 10 and 11, suggesting high coagulation in highly alkaline solutions. Compared with the stability of suspensions with only kaolinite particles, which exhibit coagulation at pH 2.5 and stable

dispersions at $5 \leq \text{pH} \leq 10.5$ [13], these results indicate heterocoagulation or slime coating is the main factor affecting the stability of chalcopyrite and kaolinite slurries. The stability correlated well with the effect of kaolinite on chalcopyrite flotation, where slime coating was high at high pH levels, resulting in low floatability (Fig. 3).

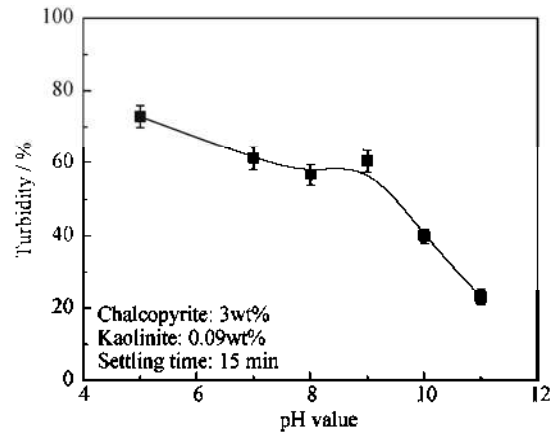


Fig. 4. Sedimentation of chalcopyrite and kaolinite particles in tap water solutions as a function of pH value.

The electrokinetic properties of particles have become an important method in studying the stability of suspensions. Fig. 5 presents the zeta-potential distributions of kaolinite, chalcopyrite, and their mixture at various pH levels. The

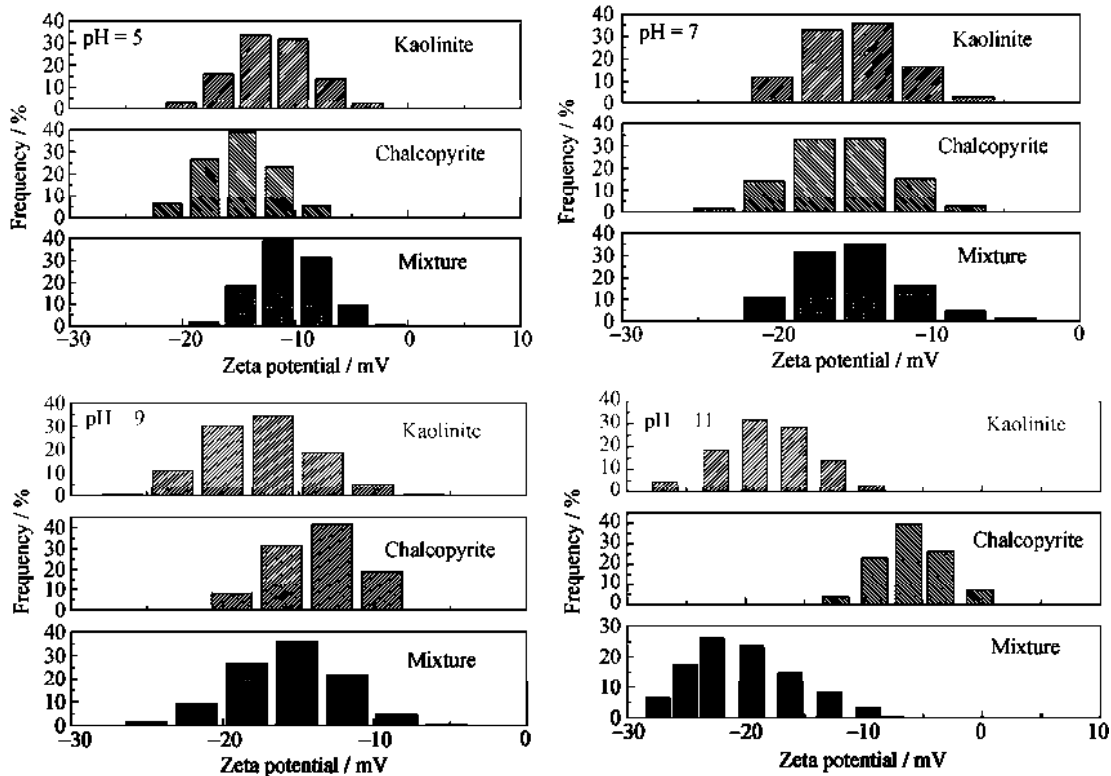


Fig. 5. Zeta-potential distributions of kaolinite, chalcopyrite, and their mixture as a function of pH value.

peak zeta potentials of kaolinite were -13.5 , -13.6 , -16.7 , and -19.2 mV at pH 5, 7, 9, and 11, respectively, which is in accordance with a report that the zeta potential of kaolinite is negative and decreases with increasing pH value [13]. The peak zeta potentials of chalcopyrite were -14.7 , -17.4 , -12.8 , and -6.2 mV at pH 5, 7, 9, and 11, suggesting that the chalcopyrite zeta potential is negative and possesses two high points: one at a pH value less than 5 and one at a pH value greater than 9, consistent with previously reported results [21]. The zeta-potential distributions of the kaolinite and chalcopyrite mixtures were similar to those of chalcopyrite at pH 5 and 7, indicating a low slime coating of kaolinite on chalcopyrite at acidic pH levels. However, they resembled the zeta-potential distributions of kaolinite at alkaline pH levels, indicating high slime coating [22]. For alkaline pH levels, for example, at pH 11, the interaction of the electrical double layers of chalcopyrite and kaolinite is repulsive; however, coagulation occurred because the absolute zeta potential value of chalcopyrite was too low to produce a strong energy barrier between the particles.

According to the DeJaguin–Landau–Verwey–Overbeek (DLVO) theory [23–24], the stability of colloidal dispersions is due to the existence of a potential energy barrier between the particles, which arises from interactions of the electrical double layers and the van der Waals energy. The total potential energy of interaction between the particles (V_T) can be expressed as

$$V_T = V_R + V_A \quad (1)$$

where V_R and V_A are the electrostatic energy and van der Waals energy between the particles, respectively. The potential energy of the electrical double layer interaction between a plate and a sphere particle can be expressed as [25]

$$V_R = \pi \varepsilon_r \varepsilon_0 a \left[(\psi_1^2 + \psi_2^2) \ln \left(\frac{\exp(2\kappa h) + 1}{\exp(2\kappa h) - 1} \right) + 2\psi_1 \psi_2 \ln \left(\frac{\exp(\kappa h) + 1}{\exp(\kappa h) - 1} \right) \right] \quad (2)$$

where ε_0 is the permittivity in vacuum, ε_r is the permittivity of the solvent, a is the particle radius, ψ_1 and ψ_2 are the surface potentials of the sphere and the plate, respectively, and h is the shortest distance between the sphere and the plate. Parameter κ is the Debye reciprocal length and is given by

$$\kappa = \left(\frac{8\pi e^2 CZ^2}{\varepsilon_a k_B T} \right)^{\frac{1}{2}} \quad (3)$$

where e is the charge of the electron (1.602×10^{-19} C), C is the cubic molar concentration of the ion (mol/m^3), Z is the

valence of the ion, T is the absolute temperature (K), ε_a is the permittivity of the particle, and k_B is the Boltzmann constant (1.38×10^{-23} J/K).

The van der Waals energy interaction between a plate and a spherical particle is expressed by [25]

$$V_A = -\frac{A_{123}}{6} \left[\frac{2a(h+a)}{h(h+2a)} + \ln \frac{h}{h+2a} \right] \quad (4)$$

where A_{123} is the Hamaker constant of a plate and a spherical particle in medium 3. And

$$A_{123} \approx (\sqrt{A_{11}} - \sqrt{A_{33}})(\sqrt{A_{22}} - \sqrt{A_{33}}) \quad (5)$$

where A_{11} , A_{22} , and A_{33} are the Hamaker constants of particles 1 and 2 and medium 3 in vacuum, respectively. On the basis of DLVO theory, we calculated the total potential energy of interaction between kaolinite and chalcopyrite particles in aqueous solutions as a function of distance between the particles. The energy barrier was $12k_B T$ at pH 11, which is less than the $15k_B T$ required to inhibit the coagulation of the particles [13,22,26].

Electrical double layers of particles are compressed by salinity in aqueous solutions [7,13,25]. Therefore, the slime coating of kaolinite on the chalcopyrite surface and the flotation of chalcopyrite might exhibit different behaviors in saline water solutions. Fig. 6 shows the flotation of chalcopyrite in seawater without kaolinite and with 0.09wt%, 0.24wt%, and 0.6wt% of kaolinite. In the water without kaolinite, the chalcopyrite floatability maintained approximately 80%, indicating that salinity had little effect on the chalcopyrite floatability. Similar as in tap water, the floatability decreased slightly at pH levels greater than 8. In the presence of 0.09wt% kaolinite, the tendency of floatability at various pH levels resembled that in the absence of kaolinite, whereas the floatability decreased approximately 7%. This decrease was much greater than that of chalcopyrite flotation in tap water (2%) and suggests that a greater slime coating deteriorates chalcopyrite floatability in seawater flotation in the presence of 0.09wt% kaolinite. This behavior might be a consequence of the salinity compressing the electrical double layers of the particles. At 0.24wt% of kaolinite, the floatability decreased sharply in the pH value range from 4 to 6 and maintained a plateau of low floatability (about 61%) in the pH value range from 6 to 11. At 0.60wt% kaolinite, the chalcopyrite floatability exhibited the same tendency as that at 0.24wt% kaolinite but decreased 3%. These results and the flotation results in tap water (Fig. 3) indicate that 0.24wt% kaolinite might result in a “saturated” slime coating of kaolinite on the chalcopyrite particles.

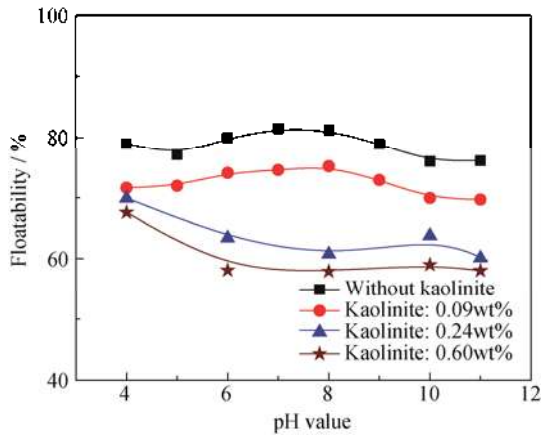


Fig. 6. Flotation of chalcopyrite in seawater without and with kaolinite.

Fig. 7 shows the turbidity of chalcopyrite and kaolinite slurries in seawater at various pH levels. The turbidity at pH 5 was high, indicating dispersion of the suspension. The turbidity then decreased with increasing pH value, which suggests coagulation or formation of a slime coating at higher pH levels. Compared with the plateau of turbidity at $7 \leq \text{pH} \leq 9$ in tap water (Fig. 4), the turbidity decreased continually in seawater. This observation confirms that salinity compresses the electrical double layers and lowers the energy barriers to induce coagulation of kaolinite and chalcopyrite particles at lower pH levels.

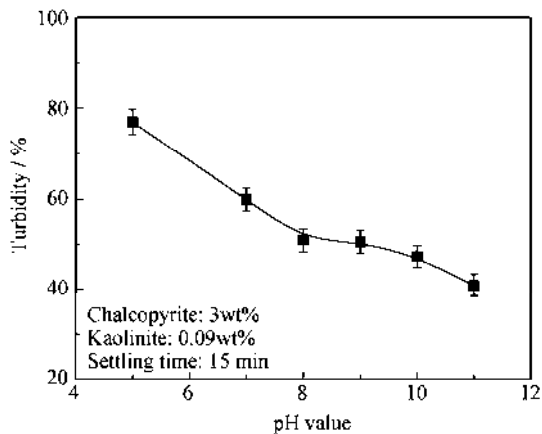


Fig. 7. Sedimentation of chalcopyrite and kaolinite particles in seawater solutions as a function of pH value.

In sulfide mineral flotation practice, the process water with recycled water is usually saturated or supersaturated with gypsum [8]. The salinity of this water differs from that of seawater, which might lead to a distinguishable effect on the slime coating of kaolinite on chalcopyrite. Fig. 8 shows the flotation of chalcopyrite in gypsum-saturated water without kaolinite and with 0.09wt%, 0.24wt%, and 0.60wt% of kaolinite. In the absence of kaolinite, the chalcopyrite

floatability was high at $4 \leq \text{pH} \leq 10$ and then decreased at pH 11. In the presence of 0.09wt% kaolinite, the chalcopyrite floatability decreased approximately 2% from pH 4 to pH 11 compared with that in the absence of kaolinite. In the presence of 0.24wt% of kaolinite, a slight decrease of floatability was noted at pH 4; the floatability then decreased sharply as the pH value was increased to 8. It thereafter maintained a plateau at $8 \leq \text{pH} \leq 11$. In the presence of 0.60wt% kaolinite, the chalcopyrite floatability decreased sharply at $4 \leq \text{pH} \leq 6$, but slightly at $8 \leq \text{pH} \leq 11$ compared with that in the case of 0.24wt% kaolinite, which might be attributable to calcium ions (Ca^{2+}) and hydrolyzed calcium ions ($\text{Ca}(\text{OH})^+$) adsorbing specifically onto kaolinite and inducing extensive slime coating of kaolinite on chalcopyrite. The adsorption of $\text{Ca}(\text{OH})^+$ and Ca^{2+} can reverse the zeta potential of kaolinite, resulting in attractive interaction between electrical double layers of chalcopyrite and kaolinite. The adsorption models of $\text{Ca}(\text{OH})^+$ and Ca^{2+} ions on the surface of kaolinite are shown as follows [13,27–28]:

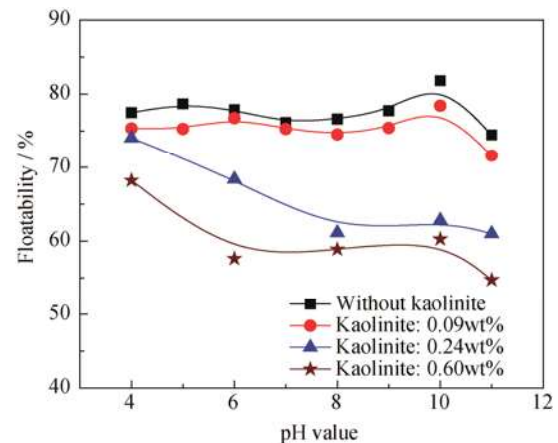
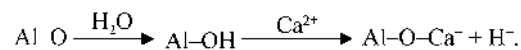
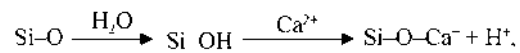
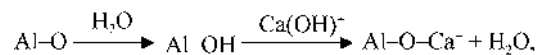
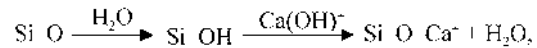


Fig. 8. Flotation of chalcopyrite in gypsum-saturated water with and without kaolinite.

Fig. 9 shows the turbidity of chalcopyrite and kaolinite suspensions in gypsum-saturated water at various pH levels. The turbidity decreased with increasing pH value, indicating that coagulation occurred with increasing pH value. The same as with the suspensions in tap water, a plateau of turbidity at $7 \leq \text{pH} \leq 9$ was observed. Notably, the turbidity in gypsum-saturated water with pH 5 was much lower than that in pH 5 tap water or seawater. This result corresponds

well with the flotation results (0.60wt% kaolinite) and verifies the specific adsorption of Ca^{2+} and hydrolyzed Ca^{2+} onto the kaolinite surface, resulting in the negative surface charge decreasing or reversing, thus inducing coagulation [13].

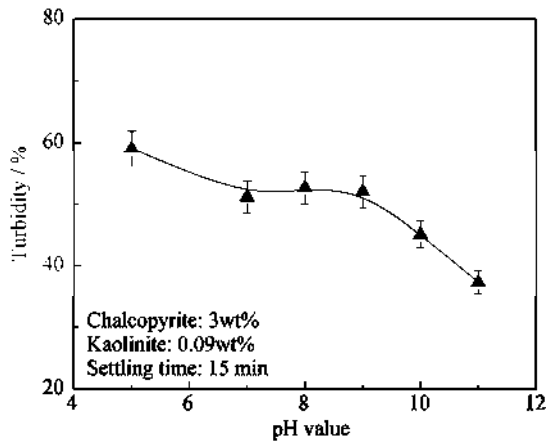


Fig. 9. Sedimentation of chalcopyrite and kaolinite particles in gypsum-saturated solutions as a function of pH value.

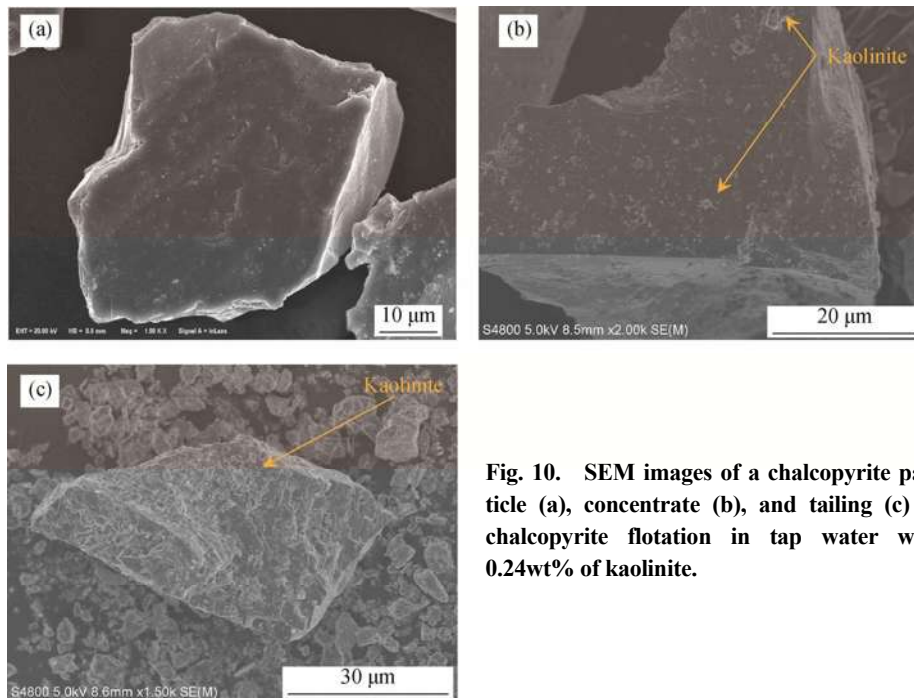


Fig. 10. SEM images of a chalcopyrite particle (a), concentrate (b), and tailing (c) in chalcopyrite flotation in tap water with 0.24wt% of kaolinite.

4. Conclusions

(1) In tap water, seawater, and gypsum-saturated water, the slime coating of kaolinite on chalcopyrite is mostly induced at alkaline pH levels, where the chalcopyrite shows a low negative zeta potential. The chalcopyrite floatability decreases accordingly with increasing slime coating.

(2) With increasing kaolinite content, chalcopyrite floatability decreases. In the presence of 0.24wt% kaolinite, the

Notably, the relationship between the slime coating (kaolinite on chalcopyrite) and the floatability of chalcopyrite is nonlinear because a sufficient coating is required to depress the flotation. As noted in the discussion of the flotation results in tap water, seawater, and gypsum-saturated water, the increase of the kaolinite content from 0.09wt% to 0.24wt% induced a substantial decrease of chalcopyrite floatability in the pH value range of slime coating ($6 \leq \text{pH} \leq 11$). This decrease might be explained by the different degrees of coating of kaolinite on chalcopyrite particles. At 0.09wt% kaolinite, although a slime coating is formed under some specific conditions, the coating of kaolinite is insufficient to prevent flotation of the chalcopyrite particles. Fig. 10 shows scanning electron microscopy (SEM) images of a chalcopyrite particle, concentrate, and tailing corresponding to chalcopyrite flotation in tap water with 0.24wt% of kaolinite. A slime coating is observed on the concentrated chalcopyrite particles, and extensive slime coating is required to depress flotation.

slime coating of kaolinite reaches a “saturated” state on chalcopyrite; thus, the floatability decreases $\geq 10\%$ at pH levels greater than 8 in all three types of water.

(3) Compared with tap water, seawater compresses the electrical double layers of kaolinite and chalcopyrite particles because of its salinity, resulting in extensive slime coating; consequently, the chalcopyrite floatability decreases more greatly (5%) with 0.09wt% kaolinite at alkaline pH levels in seawater flotation. Calcium ions in gyp-

sum-saturated water cause specific adsorption onto kaolinite at $4 \leq \text{pH} \leq 11$, inducing extensive slime coating and reducing chalcopyrite floatability at 0.60wt% kaolinite.

Acknowledgements

This work was financially supported by the Natural Science Foundation of Hubei Province of China (No. 2016CFA013), the Wuhan Science and Technology Bureau of China (No. 2016070204020156), and the Consejo Nacional de Ciencia y Tecnología (CONACYT) of Mexico (No. 270186). Z.L. Li would like to thank the CONACYT for offering him scholarship (No. 717627) during his PhD studying.

References

- [1] M.M. Mekonnen and A.Y. Hoekstra, Four billion people facing severe water scarcity, *Sci. Adv.*, 2(2016), No. 2, art. No. e1500323.
- [2] B. Wang and Y.J. Peng, The effect of saline water on mineral flotation - A critical review, *Miner. Eng.*, 66-68(2014), p. 13.
- [3] L.M. Shengo, S. Gaydardzhiev, and N.M. Kalenga, Assessment of water quality effects on flotation of copper-cobalt oxide ore, *Miner. Eng.*, 65(2014), p. 145.
- [4] A. Azapagic, Developing a framework for sustainable development indicators for the mining and minerals industry, *J. Clean. Prod.*, 12(2004), No. 6, p. 639.
- [5] S. Castro, *Challenges in Flotation of Cu-Mo Sulfide Ores in Sea Water*, J. Drelich ed., Society for Mining, Metallurgy & Exploration (SME), Englewood, 2012, p. 29.
- [6] R.I. Jeldres, L. Forbes, and L.A. Cisternas, Effect of seawater on sulfide ore flotation: A review, *Miner. Process. Extr. Metall. Rev.*, 37(2016), No. 6, p. 369.
- [7] F. Rao, I. Lázaro, and L.A. Ibarra, Solution chemistry of sulphide mineral flotation in recycled water and sea water: a review, *Miner. Process. Extr. Metall.*, 126(2017), No. 3, p. 139.
- [8] M.J. Deng, Q.X. Liu, and Z.H. Xu, Impact of gypsum super-saturated solution on surface properties of silica and sphalerite minerals, *Miner. Eng.*, 46-47(2013), p. 6.
- [9] W.Y. Liu, C.J. Moran, and S. Vink, A review of the effect of water quality on flotation, *Miner. Eng.*, 53(2013), p. 91.
- [10] A.M. Gaudin, D.W. Fuerstenau, and H.L. Miaw, Slime coatings in galena flotation, *CIM Bull.*, 53(1960), p. 960.
- [11] O. Espinoza-Ortega, S. Song, A. Lopez-Valdivieso, F. Galindo-Murillo, and J.L. Reyes-Bahena, Regrinding and floc-flotation of silver sulphide scavenger concentrate, *Miner. Process. Extr. Metall.*, 112(2003), No. 2, p. 90.
- [12] Z.H. Xu, J.J. Liu, J.W. Choung, and Z.A. Zhou, Electrokinetic study of clay interactions with coal in flotation, *Int. J. Miner. Process.*, 68(2003), No. 1-4, p. 183.
- [13] F. Rao, F.J. Ramirez-Acosta, R.J. Sanchez-Leija, S.X. Song, and A. Lopez-Valdivieso, Stability of kaolinite dispersions in the presence of sodium and aluminum ions, *Appl. Clay Sci.*, 51(2011), No. 1-2, p. 38.
- [14] B. Triffett, C. Veloo, B.J.I. Adair, and D. Bradshaw, An investigation of the factors affecting the recovery of molybdenite in the Kennecott Utah Cooper bulk flotation circuit, *Miner. Eng.*, 21(2008), No. 12-14, p. 832.
- [15] S.M. Bulatovic, D.M. Wyslouzil, and C. Kant, Operating practices in the beneficiation of major porphyry copper/molybdenum plants from Chile: Innovated technology and opportunities, a review, *Miner. Eng.*, 11(1998), No. 8, p. 313.
- [16] M. Zhang, Y.J. Peng, and N. Xu, The effect of sea water on copper and gold flotation in the presence of bentonite, *Miner. Eng.*, 77(2015), p. 93.
- [17] A.W. Gardner and E. Glueckauf, Thermodynamic data of the calcium sulphate solution process between 0 and 200°C, *Trans. Faraday Soc.*, 66(1970), p. 1081.
- [18] A. Sze, D. Erickson, L.Q. Ren, and D.Q. Li, Zeta-potential measurement using the Smoluchowski equation and the slope of the current-time relationship in electroosmotic flow, *J. Colloid Interface Sci.*, 261(2003), No. 2, p. 402.
- [19] M.C. Fuerstenau, S. Chander, and R. Woods, *Sulfide Mineral Flotation*, M.C. Fuerstenau, G. Jameson, and R.H. Yoon eds., Society for Mining, Metallurgy & Exploration (SME), Colorado, 2007, p. 425.
- [20] Q. Liu and Y.H. Zhang, Effect of calcium ions and citric acid on the flotation separation of chalcopyrite from galena using dextrin, *Miner. Eng.*, 13(2000), No. 13, p. 1405.
- [21] K.K. Das, Pradip, and K.A. Natarajan, The effect of constituent metal ions on the electrokinetics of chalcopyrite, *J. Colloid Interface Sci.*, 196(1997), No. 1, p. 1.
- [22] T.X. Chen, Y.L. Zhao, and S.X. Song, Electrophoretic mobility study for heterocoagulation of montmorillonite with fluoride in aqueous solutions, *Powder. Technol.*, 309(2017), p. 61.
- [23] B.V. Derjaguin and L. Landau, Theory of the stability of strongly charged lyophobic sols and of the adhesion of strongly charged particles in solutions of electrolytes, *Prog. Surf. Sci.*, 43(1993), No.1-4, p. 30.
- [24] J.T.G. Overbeek and E.J.W. Verwey, *Theory of the Stability of Lyophobic Colloids: The Interaction of Sol Particles Having an Electric Double Layer*, Dover Publications Inc., New York, 1948, p. 66.
- [25] P.C. Hiemenz and R. Rajagopalan, *Principles of Colloid and Surface Chemistry*, CRC press, Florida, 1997, p. 653.
- [26] S. Lu, R. J. Pugh, and E. Forssberg, *Interfacial Separation of Particles*, Elsevier Inc., San Diego, 2005, p. 290.
- [27] F. Rao, S.X. Song, and A. Lopez-Valdivieso, Specific adsorption of chromium species on kaolinite surface, *Miner. Process. Extr. Metall. Rev.*, 33(2012), No. 3, p. 180.
- [28] Y.C. Chemedá, D. Deneele, G.E. Christidis, and G. Ouvrard, Influence of hydrated lime on the surface properties and interaction of kaolinite particles, *Appl. Clay Sci.*, 107(2015), p. 1.